METABOLIC REWIRING IN RESPONSE TO GENETIC AND ENVIRONMENTAL PERTURBATIONS IN CANCER

by

KATY ELIZABETH ROSE HOLLINSHEAD

A thesis submitted to the University of Birmingham for the degree of

DOCTOR OF PHILOSOPHY

School of Cancer Sciences
College of Medical and Dental Sciences
University of Birmingham
September 2016

ABSTRACT

Cancer cells reprogram their metabolism to supply biosynthetic and bioenergetic demands of rapid proliferation. Microenvironmental changes, such as hypoxia, further influence tumour metabolism, driving malignancy. Recent identification of cancer-associated mutations in succinate dehydrogenase (SDH), fumarate hydratase and isocitrate dehydrogenase (IDH) have shown that genetic alterations can directly alter tumour cell metabolism, and may be required for malignant transformation. Mutations in these metabolic enzymes promote tumorigenesis by hijacking the adaptive response to hypoxia. Understanding the metabolic vulnerabilities associated with these mutations may therefore elicit the design of more selective therapies.

Employing a combination of analytical approaches to study metabolism, the research objectives were to characterise metabolic vulnerabilities associated with cells mutated in SDHB and IDH1. Results show that cells deficient in SDH activity maintain proliferation and viability by increasing dependency on pyruvate carboxylase for *de novo* aspartate synthesis. Mutations in IDH1 have a complex role in the metabolic adaptation to hypoxia, partially compromising this hypoxic response, yet also demonstrating aspects of pseudohypoxia, such as increased proline anabolism. This thesis reveals a metabolic vulnerability that could be therapeutically targeted to treat SDH-mutated tumours, and a novel redox-sensitive metabolic pathway, exhibited by both pseudohypoxic SDH and IDH1 mutated tumours, used to retain metabolic plasticity.

DEDICATION

For my parents.

ACKNOWLEDGEMENTS

I thank my supervisor Dr Daniel Tennant for his valued knowledge and mentorship through my PhD training. I am thankful for his support in providing many opportunities to develop both scientifically and professionally, and for continually challenging me to become a better scientist. I acknowledge the current and past members of the Tennant group. In particular, to previous lab members Deborah Williams and Dr Tatiana Volpari for their continued support, kindness and valued friendship. I also thank previous post doctoral researcher Dr Giulio Laurenti and current graduate students Haydn Munford, Kathryn Eales and Robert Murren for their tremendous support in the last few months of my PhD training.

I additionally thank my collaborators Dr Judith Favier, Dr Warwick Dunn, Professor Christian Metallo and Dr Karsten Hiller, along with their respective PhD students and research associates Dr Charlotte Lepoutre-Lussey, Dr William Allwood, Dr Seth Parker and Yannic Nonnenmacher for their training, scientific insight and contributions to my project. For my AstraZeneca collaborators, I thank Dr Filippos Michopoulos and Dr Susan Critchlow. Within the department, I thank David Hodson for his scientific expertise and training, and make a special mention to Dr Christian Ludwig for his invaluable guidance, support, dedicated time and patience. Christian has been a significant part of my PhD training and I hope this will extend to future endeavours.

Lastly, and most importantly, I thank my family for their incredible love and support, sacrifices and unwavering commitment to my success.

Chapter 1 provides a review to the research field and encompasses material from published reviews “Mitochondrial metabolic remodelling in response to genetic and environment perturbations” (Appendix A), “Hypoxia and metabolic adaptation of cancer cells” (Appendix B) and book chapter “Probing Cancer Cell Metabolism Using NMR Spectroscopy” (Appendix C). Chapter 2 is conducted in collaboration with Judith Favier, whose research group were responsible for producing the supporting biology to the NMR analysis, and Christian Metallo, whose research group ran GC-MS samples. This chapter includes material from publication “Loss of succinate dehydrogenase activity results in dependency on pyruvate carboxylation for cellular anabolism” (Appendix D). Chapter 3 has been conducted in collaboration with Warwick Dunn, who performed the metabolomics analysis, Christian Metallo and Karsten Hiller, whose research groups ran GC-MS samples. The last section on pesudohypoxic proline metabolism in IDH1 mutant cells is currently being prepared for submission for publication.

TABLE OF CONTENTS

LIST OF FIGURES

LIST OF TABLES

LIST OF ABBREVIATIONS

∆ex2	Exon 2
2HG	2-hydroxyglutarate
3PG	3-phosphoglycerate
3PHP	3-phosphohydroxypyruvate
A.U.	Arbitrary units
AcCoA	Acetyl coenzyme A
ACO1/2	Aconitase 1/2
ACTB	Beta actin
ACYL	Acetyl CoA citrate lyase
AKT	Serine/threonine protein kinase B
Ala	Alanine
ALDH18A1	Pyyroline-5-carboxylate synthetase
ALKBH	AlkB homolog
AML	Acute myeloid leukemia
AMP	Adenosine monophosphate
ARNT	Aryl hydrocarbon receptor nuclear translocator
ASC	Alanine/serine/cysteine transporter
ASCT1; SLC1A4	Alanine/serine/cysteine transporter 1
ASCT2; SLC1A5	Alanine/serine/cysteine transporter 2
Asn	Asparagine
Asp	Aspartate
BBB	Blood brain barrier
BCAA	Branched chain amino acids
bHLH	Basic helix-loop-helix
BNIP3	BCL2/adenovirus E1B interacting protein 3
BR	Bilirubin
BV	Biliverdin
CA9	Carbonic anhydrase
CCCP	Carbonyl cyaninde m-chlorophenylhydrazone

CCP	Comité de Protection des Personnes
Cit	Citrate
CoA	Coenzyme A
COMETE	Cortico et Médullosurrénale: les Tumeurs Endocrines
COX	Cytochrome c oxidase
cP4H	Collagen prolyl 4-hydroxylases
DMEM	Dulbecco's modified Eagles Medium
DSS	4,4-dimethyl-4-silapentane-1-sulphonic acid
ECM	Extracellular matrix
EGLN	Egl nine homologue
EMT	Epithelial-mesenchymal transition
ETC	Electron transport chain
F6P	Fructose 6-phosphate
FACS	Fluorescence activated cells sorting
FAD(H_2)	Reduced flavin adenine dinucleotide
FAD^+	Flavin adenine dinucleotide
FBS	Foetal bovine serum
FDG-PET	^{18}F-deoxyglucose-positron emission tomography
FH	Fumarate hydratase
FIH	Factor inhibiting HIF
Fum	Fumarate
G3P	Glycerol 3-phosphate
G6P	Glucose 6-phosphate
GAPDH	Glyceraldehyde 3-phosphate dehydrogenase
GBM	Glioblastoma
GC	Gas chromatography
GC-MS	Gas chromatography mass spectrometry
GDH	Glutamate dehydrogenase
GFP	Green fluorescent protein
Glc	Glucose
GLDC	Glycine decarboxylase

Gln	Glutamine
GLS	Glutaminase
GLUD	Glutamate dehydrogenase
GLUT;SLC2A	Glucose transporter family; solute carrier 2
Gly	Glycine
GOT2	Mitochondrial aspartate aminotransferase
GSF	Succinated glutathione
GSH	Reduced glutathione
H_2O_2	Hydrogen peroxide
HBRC	Human Biomaterials Resource Centre
HIFs	Hypoxia-inducible factors
HK	Hexokinase
HLRCC	Hereditary leiomyomatosis and renal cell cancer
HMG-CoA	3-hydroxy-3-methyl-glutaryl-coenzyme A
HMOX1	Haem oxygenase 1
HOG	Human oligodendroglioma
HREs	Hypoxia-response elements
HRP	Horseradish peroxidase
HSQC	Heteronuclear Single Quantum Coherence
IDH1/2/3	Isocitrate dehydrogenase 1/2/3
imCC	Immortalised mouse chromaffin cells
IMP	Inosine monophosphate
Iso	Isocitrate
Jcc	J coupling constant
JmjC	Jumonji C-domain
KEAP1	Kelch-like ECH-associated protein 1
K_M	The Michaelis constant
KO	Knock-out
KRAS	V-Ki-ras2 Kisten rat sarcoma viral oncogene homolog
Lac	Lactate
LAT1; SLC7A5	L-type amino acid transporter 1; solute carrier 7

LDHA/B	Lactate dehydrogenase A/B
LGG	Low-grade glioma
MAF	Mouse adrenal fibroblast
Mal	Malate
MCT1/4	Monocarboxylate transporters 1/4
MDH1/2	Malate dehydrogenase 1/2
ME1/2/3	Malic enzyme 1/2/3
MFA	Metabolic flux analysis
MID	Mass isotopologue distribution
MID	Metabolite isotopomer distribution
MSTFA	N-methyl-N-(trimethylsilyl)trifluoroacetamide
MTBSTFA	*N*-methyl-*N*-(tert-butyldimethylsilyl)trifluoroacetamide)
MYC	v-myc avian myelocytomatosis viral oncogene homolog
NAD^+	Oxidised nicotinamide dinucleotide
NADH	Reduced nicotinamide dinucleotide
$NADP^+$	Oxidised nicotinamide adenine dinucleotide phosphate
NADPH	Reduced nicotinamide adenine dinucleotide phosphate
NEAA	Non-essential amino acids
NMR	Nuclear Magnetic Resonance
NNT	Nicotinamide nucleotide transhydrogenase
NRF2	Nuclear erythroid-related factor 2
OAA	Oxaloacetate
ODDD	Oxygen-dependent degradation domain
P300/CBP	Cyclic AMP responsive element-binding (CREB) protein
P5CDH	Pyrroline 5-carboxylase dehydrogenase
P5CS	Pyrroline 5-carboxylase synthetase
PARP	Poly ADP ribose polymerase
PAS	Per-ARNT-Sim
PBST	1x PBS with 0.05% Tween-20
PC	Pyruvate carboxylase
PCA	Principle component analysis

PCC	Pheochromocytoma
PCK 1/2	Phosphoenolpyruvate carboxykinase
PDAC	Pancreatic ductal adenocarcinoma
PDH	Pyruvate dehydrogenase
PDK1	Pyruvate dehydrogenase kinase 1
PDP1	Pyruvate dehydrogenase phosphatase 1
PEPCK	Phosphoenolpyruvate carboxykinase
PFK	Phosphofructokinase
PGK1	Phosphoglycerate kinase 1
PGL	Paraganglioma
PHDs	HIF prolyl hydroxylases
PHGDH	Phosphoglycerate dehydrogenase
PI3K	Phosphoinositol 3-kinase
PKM/P/L	Pyruvate kinase M/P/L
PLS-DA	Partial least squares discriminate
PMT	Photomultiplier tube
ppm	Parts per million
PPP	Pentose phosphate pathway
Pro	Proline
PRODH	Proline dehydrogenase
PSAT	Phosphoserine aminotransferase
PSPH	Phoshoserine phosphatase
pVHL	Von Hippel-Lindau
PYCR	Pyrroline 5-carboxylase reductase
Pyr	Pyruvate
QC	Quality control
QEHB	Queen Elizabeth Hospital Birmingham NHS Foundation Trust
R5P	Ribose 5-phosphate
RCC	Renal cell carcinoma
RNAi	RNA interference-mediated
ROS	Reactive oxygen species

RT qPCR	Quantitative real time polymerase chain reaction
SAM	S-adenosylmethionine
SAT1; SLC38A1	System A transporters 1
SAT2; SLC38A2	System A transporters 2
SCD	Δ9 stearoyl-CoA desaturase
SDHx	Succinate dehydrogenase A/B/C/D
SDS-PAGE	Sodium dodecyl sulphate polyacrylamide gel electrophoresis
SHMT1/2	Serine hydroxymethyltransferase 1/2
siRNA	Short interfering RNA
SLC25A12	Aspartate-glutamate antiporter
SLC25A13	Aspartate-glutamate antiporter
SRB	Sulfohodamine B
SSP	Serine synthesis pathway
Suc	Succinate
TAD	Terminal activation domain
TBDMCS	Tert-butyldimethylchlorosilane
TBDMS	Tert-butyldimethylsilyl
TCA	Tricarboxylic acid cycle
TCA	Trichloroacetic acid solution
TCGA	The Cancer Genome Atlas
TET	Ten-eleven translocation
THF	Tetrahydrofolate
TIGAR	*TP53*-induced glycolysis and apoptosis regulator
TMCS	Chloro-trimethyl-silane
TMSP	(3-trimethylsilyl)propionic-(2,2,3,3-d4)-acid sodium salt
UHPLC	Ultra-high performance liquid chromatography
WHO	World Health Organisation
WT	Wild-type
αKG	α-ketoglutarate
αKGDH	α-ketoglutarate dehydrogenase

Chapter 1 REVIEW OF THE LITERATURE

Introduction to Cancer Metabolism

Cancers are highly complex heterogeneous diseases, conventionally categorised by cell type or tissue of origin (Greaves & Maley 2012). Recent advances in technology, such as large-scale DNA sequencing (Wong et al. 2011), has further permitted the clustering of cancer into molecular subtypes, which vary in terms of treatment and prognosis. It is becoming increasingly clear from these studies that not only are genomic abnormalities not necessarily confined to cell type, but high levels of phenotypic variability are observed among cells within a single tumour population (Gerlinger et al. 2012; Marusyk et al. 2012). To help comprehend this complexity, certain hallmarks have been proposed as essential for the progression and development of cancer (Hanahan & Weinberg 2000). For example, the reprogramming of energy metabolism is now recognised as 1 of the 10 hallmarks of cancer (Hanahan & Weinberg 2011) and can occur as a direct consequence of various tumour suppressors or oncogenes, where it may be selected or required for malignant transformation. Tumour metabolism is also influenced by changes in the microenvironment, such as the development of hypoxia. Hypoxia is a phenotype common to many cancers, which reprograms tumour metabolism, often resulting in a more malignant and therapy resistant phenotype (Cairns et al. 2011).

Otto Warburg first observed altered tumour metabolism in the 1920's (Warburg 1925; Warburg 1956b). Unlike most normal differentiated cells that use mitochondrial

oxidative phosphorylation to generate much of the ATP required for cellular processes, rapidly proliferating tumour cells were found to consume higher rates of glucose and secrete most of this carbon as lactate rather than oxidising it completely in the mitochondria. This phenotype, described today as the Warburg effect, has since been observed across most tumour types and can be clinically imaged using ^{18}F-deoxyglucose-positron emission tomography (FDG-PET) (Groves et al. 2007). Warburg postulated that the increased rates of glucose consumption was a consequence of impaired oxidative mitochondrial metabolism, and that this mitochondrial dysfunction was a root cause of all cancers (Warburg 1956a). Later observations confirmed that this feature was not unique to cancer cells (Hedeskov 1968; Roos & Loos 1973; Wang et al. 1976; Brand 1985), and indeed defects in oxidative metabolism are not universal to all tumours (Moreno-Sánchez et al. 2007), although frequently observed (Guaragnella et al. 2014; Gaude & Frezza 2014).

Mutations in tumour suppressors and oncogenes are the driving force behind the development of cancer. As changes in metabolism are fundamental to malignant phenotypes, it is therefore not surprising that oncogenic mutations also directly (and indirectly) alter cellular metabolism. For example, activating mutations in the oncogene, phosphoinositol 3-kinase (PI3K), and its downstream effector serine/threonine protein kinase B (AKT), directly stimulate glycolysis by increasing the expression and translocation of glucose transporters to the plasma membrane and activating key glycolytic enzymes such as hexokinase (HK) and phosphofructokinase 2 (PFK-2) (Elstrom 2004; Cairns et al. 2011). The transcription factor p53 also participates in metabolic control and can, in some contexts, act as a

tumour suppressor. For example, p53 decreases glycolytic metabolism through activation of *TP53*-induced glycolysis and apoptosis regulator (TIGAR), which blocks PFK-1 (Bensaad et al. 2006). In addition, glutamine uptake and catabolism is stimulated by the oncogenic transcription factor v-myc avian myelocytomatosis viral oncogene homolog (MYC) through up-regulation of glutamine transporters and glutaminase (Wise et al. 2008; Gao et al. 2009). Mutations in tumour suppressors or oncogenes rarely occur in isolation, where the combination of mutations results in further rewiring of the metabolic network.

Understanding the mechanisms through which specific mutations influence cellular metabolism may reveal metabolic dependencies and/or deficiencies that can be exploited therapeutically. As most oncogenic mutations lead to similar patterns of altered metabolism, targeting the metabolism rather than the oncogene may in some contexts be more successful. In the case for oncogenic mutations in V-Ki-ras2 Kisten rat sarcoma viral oncogene homolog (KRAS), which are the signature event in the progression of ~95% pancreatic ductal adenocarcinoma (PDAC) (Jones et al. 2008; Biankin et al. 2012), no effective treatments to target this protein have reached the clinic to date, owing to therapeutic escape by unforeseen compensatory mechanisms. As mutationally activated KRAS orchestrates a number of metabolic changes; such as reprogrammed glutamine metabolism (Son et al. 2013), increased autophagy (Fujii et al. 2008; Yang et al. 2011; Guo et al. 2011), and macropinocytosis (Commisso et al. 2013), targeting these metabolic pathways may therefore provide more promise in PDAC treatments.

Recently, oncogenic mutations in metabolic enzymes succinate dehydrogenase (SDH), fumarate hydratase (FH) and isocitrate dehydrogenase (IDH) have been identified. Common to all three genes is that they are either situated directly within the mitochondrion (SDH, FH and IDH2) or their metabolic activity directly affects that of the mitochondrion (IDH1). Mutations in such central metabolic enzymes are likely to require extensive metabolic remodelling for efficient cell proliferation and survival. The impact of these oncogenic mutations on tumour metabolism are subject to further discussion in this review and supplemental information can be found in Appendix A.

Cancer Metabolism Supports Anabolism and Cellular Redox

Glucose metabolism

The significant and preferential production of lactate from glucose in the presence of oxygen, known as aerobic glycolysis, is in some respects a less efficient way for highly proliferative cells to make ATP compared to oxidative phosphorylation. While glycolysis produces 2 moles ATP/mole glucose, oxidative phosphorylation can synthesise as much as 38 moles ATP/mole glucose. Although, It has been postulated that glycolytic rates occur at high enough rates to exceed ATP production from oxidative phosphorylation (Guppy et al. 1993; Warburg 1956b), it has been suggested that this increase in glycolysis and subsequent decrease in glucose oxidation facilitates accumulation of glycolytic intermediates required for biosynthesis (Lunt & Vander Heiden 2011). During replication, the cell must double its cellular contents, including nucleotides, proteins, lipids and ATP, to produce two viable daughter cells (Tennant et al. 2010). This increase in biomass involves huge metabolic investment, where in addition to ATP, synthesis of these macromolecules requires carbon and nitrogen (Lunt & Vander Heiden 2011), along with necessary reducing equivalents to maintain redox balance (Sullivan et al. 2015) (Figure 1.1).

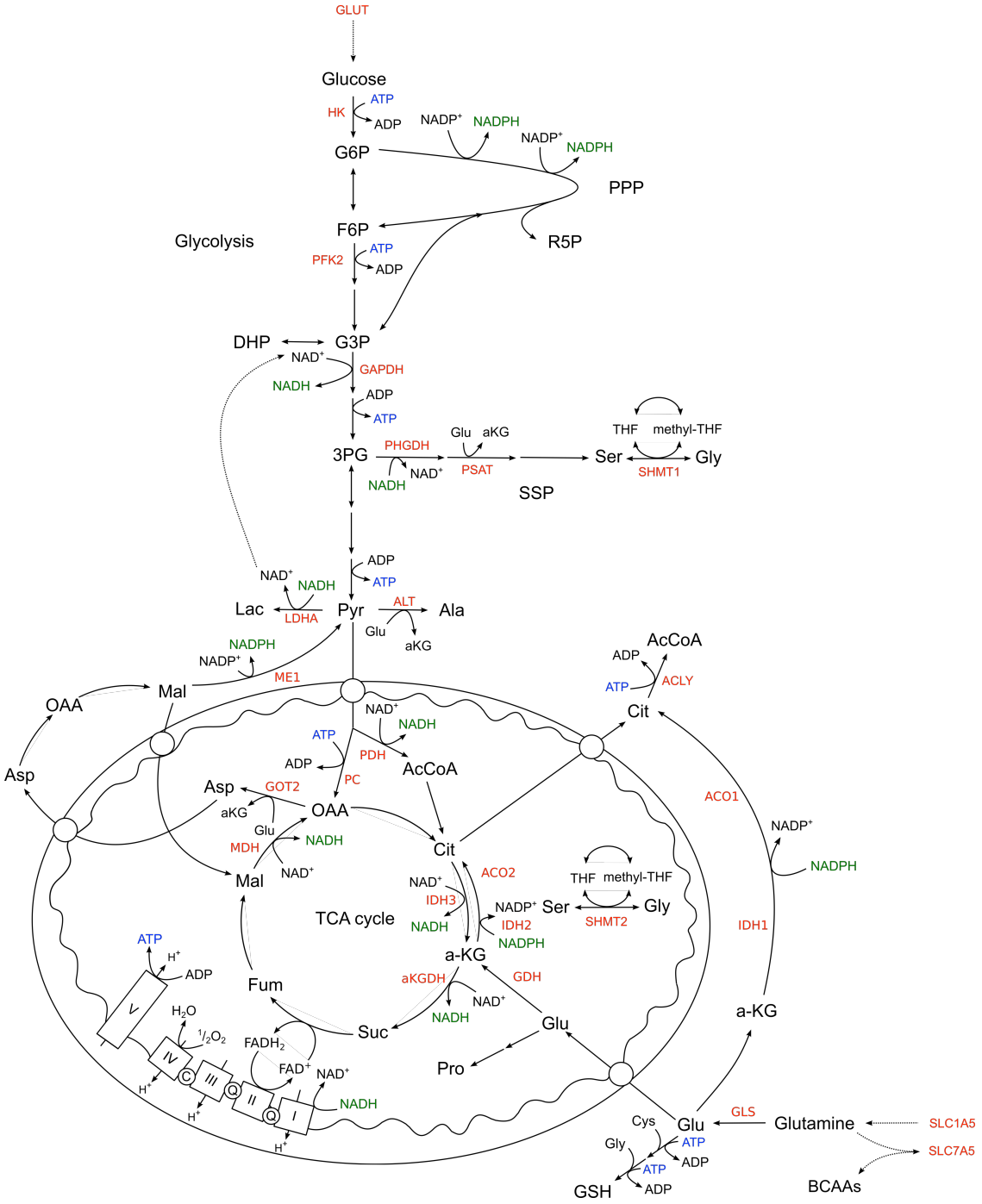

Figure 1.1 Cancer cells reprogram their metabolism support cellular anabolism and redox. The metabolic diagram highlights some of the characterised changes in central carbon metabolism included in the text to support biomass production and maintenance of cellular redox. Key enzymes involved in controlling these pathway activities are shown in red. Abbreviations: ACO 1/2, aconitase 1/2;, AcCoA, acetyl CoA; ACLY, ATP citrate lyase; Ala, alanine; ALT, alanine aminotransferase; Asp, aspartate; BCAAs, branched chain amino acids; Cit, citrate; Cys, cysteine; DHP, dihydroxyphosphate;, F6P, fructose 6-phosphate;

Fum, fumarate; GAPDH, glyceraldehyde 3-phosphate dehydrogenase; G3P, glycerol 3-phosphate; GOT2, aspartate aminotransferase; GSH, reduced glutathione; G6P, glucose 6-phosphate; Glu, glutamate; GLUT, glucose transporter; Gly, glycine; HK, hexokinase; IDH1/2/3, isocitrate dehydrogenase 1/2/3; Lac, lactate; LDHA, lactate dehydrogenase A; Mal, malate; ME1, malic enzyme 1; MDH, malate dehydrogenase; OAA, oxaloacetate; PC, pyruvate carboxylase; PDH, pyruvate dehydrogenase; Pro, proline; Pyr, pyruvate; PHGDH, phosphoglycerate dehydrogenase; PSAT, phosphoserine aminotransferasae; PFK2, phosphofructokinase 2; R5P, ribose 5-phosphate; Suc, succinate; Ser, serine; SHMT1/2, serine hydroxymethyltransferase 1/2; aKG, α-ketoglutarate and aKGDH, α-ketoglutarate dehydrogenase.

Glucose is imported into the cell through a family of plasma membrane transporters (GLUT; *SLC2A*), and is phosphorylated by HK to form glucose 6-phosphate (G6P). During glycolysis, G6P is oxidatively split into 3-carbon molecules, releasing ATP and culminating in the production of pyruvate. G6P can also be fed into the oxidative arm of the pentose phosphate pathway (PPP) to produce reduced nicotinamide adenine dinucleotide phosphate (NADPH) for reductive biosynthetic reactions and/or protection against oxidative stress, and ribose 5-phosphate (R5P) for nucleotide synthesis. R5P is also formed from glycolytic intermediates fructose 6-phopsphate (F6P) and glyceraldehyde 3-phosphate (G3P), which are shunted into the non-oxidative arm of the PPP (Cantor & Sabatini 2012). The lower glycolytic intermediate 3-phosphoglycerate (3PG) can also be shunted into the serine synthesis pathway (SSP), providing carbon for the synthesis of non-essential amino acids (NEAA) serine and glycine required for lipid and nucleotide synthesis (Chaneton et al. 2012).

Glucose-derived pyruvate has a large number of potential fates depending on the metabolic needs of a cell. A significant proportion of pyruvate is used for the

production of lactate by lactate dehydrogenase (LDH), which regenerates oxidised nicotinamide dinucleotide (NAD^+) from reduced nicotinamide dinucleotide (NADH) that can be reused by glyceraldehyde 3-phosphate dehydrogenase (GAPDH) to maintain glycolytic flux (Le et al. 2010). However, it can also be transaminated to produce alanine for protein synthesis. In the mitochondria, pyruvate is oxidised to acetyl coenzyme A (CoA) by pyruvate dehydrogenase (PDH), which then condenses with oxaloacetate to produce citrate. Citrate supports lipid synthesis on export to the cytoplasm and conversion back to acetyl CoA by acetyl CoA citrate lyase (ACLY). The activity of pyruvate carboxylase (PC), a mitochondrial enzyme traditionally involved in gluconeogenesis, can also support nucleotide synthesis, although this anaplerotic reaction does not appear to be universal to all cell types. PC carboxylates pyruvate to form oxaloacetate, which can then be transaminated to aspartate and exported out of the mitochondria for nucleotide synthesis. Equally, it can condense with acetyl CoA to form citrate for lipid synthesis.

Glutamine metabolism

Cancer cells are also highly dependent on glutamine as a source of carbon and nitrogen required to support biosynthesis, energetics and cellular homeostasis to ultimately drive tumour growth (Figure 1.1). Glutamine is imported into the cell through neutral amino acid transporters, such as alanine/serine/cysteine/threonine transporter 2 (ASCT2; *SLC1A5*) (DeBerardinis & Cheng 2010). In the cytosol, imported glutamine can either be used for biosynthesis or exported back out of the cell through antiporters, such as the L-type amino acid transporter (LAT1; *SLC7A5*)

(Nicklin et al. 2009), which extrudes glutamine in exchange for import of branched-chain amino acids (BCAA) such as leucine, required for protein synthesis.

Intracellular glutamine can be converted to glutamate through the loss of an amide group by enzymes involved in nucleotide and hexosamine biosynthesis, or through the action of glutaminases (GLS). Glutamate is then used either as an amino acid, or as an amino donor for the synthesis of nucleotides and NEAAs. The synthesis of NEAAs occurs through the activity of transaminases, which catalyse the transfer of the glutamate amine group to α-ketoacids such as pyruvate, 3PG, OAA and glutamate γ-semialdehyde, to synthesise alanine, serine, aspartate and ornithine, respectively (Wise & Thompson 2010). Serine is a precursor for glycine; ornithine a precursor for arginine; and aspartate a precursor for asparagine biosynthesis. Glutamate is also essential for the biosynthesis of NEAA proline, although proline synthesis occurs in a two-step enzyme-catalysed reduction reaction and does not require the transaminase activity. Glutamate additionally has an important contribution in the synthesis of the antioxidant reduced glutathione (GSH) - a tripeptide produced from cysteine, glutamate and glycine residues, which has a pivotal role in maintaining cellular redox by acting as an electron donor to reduce reactive oxygen species (ROS).

Glutamate can be converted to α-ketoglutarate (αKG) by both transaminase activity, and through the activity of glutamate dehydrogenase (GDH). Glutamine-derived αKG can feed into the TCA cycle to produce energy by supporting the function of the electron transport chain (ETC). In the absence of sufficient glucose oxidation, this

anaplerotic pathway becomes increasingly important for energy production in proliferating cells. Glutamine can therefore be oxidised to support the function of the electron transport chain (ETC). Within the ETC, electrons derived from NADH and reduced flavin adenine dinucleotide ($FADH_2$) are passed through successive electronegative acceptors, losing energy in the process that is used to pump protons across the inner mitochondrial membrane. The final electron acceptor, oxygen, is reduced to water, and the resulting proton gradient is then used to drive the phosphorylation of ADP to form ATP through complex V.

In addition to producing ATP, oxidation of glutamine-derived αKG in the TCA cycle (along with the activity of transaminases), can supply the cell with aspartate, which has a crucial role in purine and pyrimidine biosynthesis to support cell division (Sullivan et al. 2015; Birsoy et al. 2015). Glutamine-derived αKG can also fuel lipid synthesis, and in certain conditions occurs without using oxidative TCA cycle metabolism. Reductive carboxylation of glutamine-derived αKG describes the synthesis of citrate for *de novo* lipogenesis using the reducing potential of NADPH via the enzymes IDH1 and 2, and aconitase (ACO) 1 and 2. Reductive carboxylation was first described in brown adipocytes (Yoo et al. 2008) and has since been shown to occur in hypoxia (Metallo et al. 2011; Wise et al. 2011; Filipp et al. 2012), and in conditions where oxidative phosphorylation machinery is defective (Mullen et al. 2011).

It has been recently recognised that proliferating cells incorporate most of the glutamine they use for biomass for building protein and nucleotides (Hosios et al.

2016). In some tumour cells, a portion of glutamine-derived malate exits the TCA cycle, and through the activity of malic enzyme (ME), produces pyruvate. This is unlikely to be an energy-generating process (DeBerardinis et al. 2007; Son et al. 2013) but used to produce necessary NADPH to support cellular redox and reductive biosynthetic reactions.

Non-essential amino acid metabolism

In addition to changes in glucose and glutamine metabolism, alterations in the requirement for, and synthesis of NEAAs is becoming more appreciated in cancer metabolism, such as increased biosynthesis of serine from glucose (Locasale 2013; Zogg 2014). Serine is a central precursor in folate-mediated one carbon metabolism, generating intermediates that support nucleotide and lipid biosynthesis, redox homeostasis, and epigenetic regulation. Serine is transported into the cell by one of three systems; alanine/serine/cysteine/threonine transporters ASCT1 and ASCT2 (*SLC1A4* and *SLC1A5*, respectively), the system A transporters SAT1 and SAT2 (*SLC38A1* and *SLC38A2*, respectively) and neutral amino acid alanine/serine/cysteine (ASC) transporter system (El-Hattab 2016).

Phosphoglycerate dehydrogenase (PHGDH), the rate limiting step in serine biosynthesis, employs NAD^+ as a cofactor to convert 3PG to 3-phosphohydroxypyruvate (3PHP) and is found to be overexpressed in numerous cancers including melanoma, colorectal and breast cancer (Mullarky et al. 2011; Yoon et al. 2015; Possemato et al. 2011). Interestingly, PHGDH expression has been shown to be up-regulated by MYC (Nilsson et al. 2012). Increased PHGDH activity is

often observed with an increase in the mitochondrial serine hydroxymethyltransferase (SHMT2). This catabolises serine to glycine, thereby supplying one-carbon units that support nucleotide biosynthesis, which yields the production of NAD(P)H, and S-adenosylmethionine (SAM) pools necessary for epigenetic regulation. SHMT2 is also found to be overexpressed in numerous cancers and associated with an adverse outcome (Ye et al. 2014; Lee et al. 2014). In some cases, the availability of serine itself is limiting for cancer cell proliferation (Maddocks et al. 2012), where use of this metabolic pathway has been shown to be regulated by p53 during conditions of serine starvation to promote cell-cycle arrest and replenish GSH stores.

Hypoxia and HIF biology

Hypoxia inducible transcription factors

Owing to the rapid proliferation of cancer cells, the huge metabolic demand for biomass production in tumours can often occur and even result in challenging environments, where the availability of nutrients and oxygen become limiting. Indeed, many cancers are shown to exhibit areas of intratumoural low oxygenation (hypoxia), and are associated with an increased risk of mortality and metastasis (Vaupel et al. 2004). Rapid adaptive responses are therefore induced and required for cell survival and vascularisation of the tumour mass.

Much of the cellular transcriptional response to hypoxia is thought to be mediated by a family of heterodimeric transcription factor complexes known as hypoxia-inducible factors (HIFs). These consist of dynamically regulated α subunits (HIF1α, 2α, 3α) and constitutively active β subunit (HIF1β/aryl hydrocarbon receptor nuclear translocator [ARNT] and ARNT2). In conditions of low oxygen, HIFα subunits stabilise and translocate to the nucleus to heterodimerise with the HIFβ subunit. The heterodimer binds to a co-activator (p300/CBP [cyclic AMP responsive element-binding (CREB) protein]), which de-condenses chromatin to permit the transcription of a number of target genes (Jiang et al. 1996; Schodel et al. 2011) involved in angiogenesis, metabolic adaptation, migration and survival (Liao & Johnson 2007; Luo & Semenza 2011; Semenza 2012).

The majority of HIF transcriptional responses have been attributed to HIF1α and HIF2α, and increased expression of these subunits is associated with a higher risk of mortality in many human cancers (Semenza 2010). The structure of HIF1α and HIF2α consists of an N-terminal basic helix loop helix (bHLH) domain required for DNA binding, a central Per-ARNT-Sim (PAS) domain to facilitate heterodimerisation, and a C-terminal regulatory domain, which recruits transcriptional co-regulatory proteins (Figure 1.2A). The active HIF heterodimer complex initiates transcription by binding to hypoxia-response elements (HREs) containing a conserved 5'-RCGTG-3' core sequence in the promoter or enhancer regions of HIF-regulated genes. HIF is thought to regulate hundreds of genes, with over 500 HIF binding sites have been identified in the human genome (Schödel et al. 2013).

HIF hydroxylases regulate transcriptional activity

HIFα subunits 1 and 2 are co-ordinately regulated by a family of αKG dependent non-haem iron(II)-dioxygenases known as HIF prolyl hydroxylases (PHDs) and factor inhibiting HIF (FIH), the activity of which are dependent on the presence of iron and ascorbate. Three PHD isozymes exist: PHD 1, 2 and 3, are coded for by the Egl nine homologue (EGLN) genes 2, 1 and 3, respectively. PHDs and FIH use one atom of molecular oxygen to hydroxylate prolyl and asparaginyl residues, respectively. The second atom of oxygen is used in the oxidative decarboxylation of αKG to form carbon dioxide and succinate. In the presence of sufficient oxygen, PHDs hydroxylate prolyl residues in the C- and N- terminal of the oxygen-dependent degradation domain (ODDD) of HIFα (Pro 403/564 HIF1α; Pro 405/531 HIF2α) (Figure 1.3A) (Epstein et al. 2001; Bruick 2001). This post-translational modification promotes

recognition by the E3 ubiquitin ligase complex containing the von Hippel-Lindau (pVHL) tumour suppressor protein, targeting HIFα for polyubiquitylation and subsequent proteasomal degradation (Maxwell et al. 2001; Jaakkola et al. 2001). FIH hydroxylates an asparaginyl residue in the C-terminal HIFα transactivation domain (TAD) (Asn 803 HIF1α; Asn 851 HIF2α), which impairs the interaction with coactivator p300 required for full transcriptional activity (Lando 2002; McNeil et al. 2002), therefore regulating HIF activity rather than stability (Figure 1.3A). PHD2 (EGLN1) is considered to be the major HIF1α hydroxylase in normoxia, whereas PHD3 (EGLN3) and PHD1 (EGLN2) are thought to be the major HIF2α hydroxylases (Huang et al. 2002).

The HIF hydroxylases become progressively inactive with a reduction in oxygen tension. Although they have a relatively low affinity for oxygen, their Michaelis constant (K_M) is much higher than the partial pressure of oxygen in tissues, allowing cells to adapt to low oxygen conditions before oxygen is completely absent, which would otherwise result in cell death (Gnaiger et al. 1998). PHDs and FIH enzymes vary in their affinity for oxygen (K_M 100-250 μM for PHDs; 90 μM for FIH), where FIH appears less sensitive to hypoxia and may remain active at lower oxygen tensions (Figure 1.2B) (Koivunen et al. 2004; Ehrismann et al. 2007). This enables differential hypoxic gene sets to be activated in response to varying degrees of hypoxia, thus fine-tuning the magnitude and repertoire of the hypoxic response (Koivunen et al. 2004; Dayan et al. 2006).

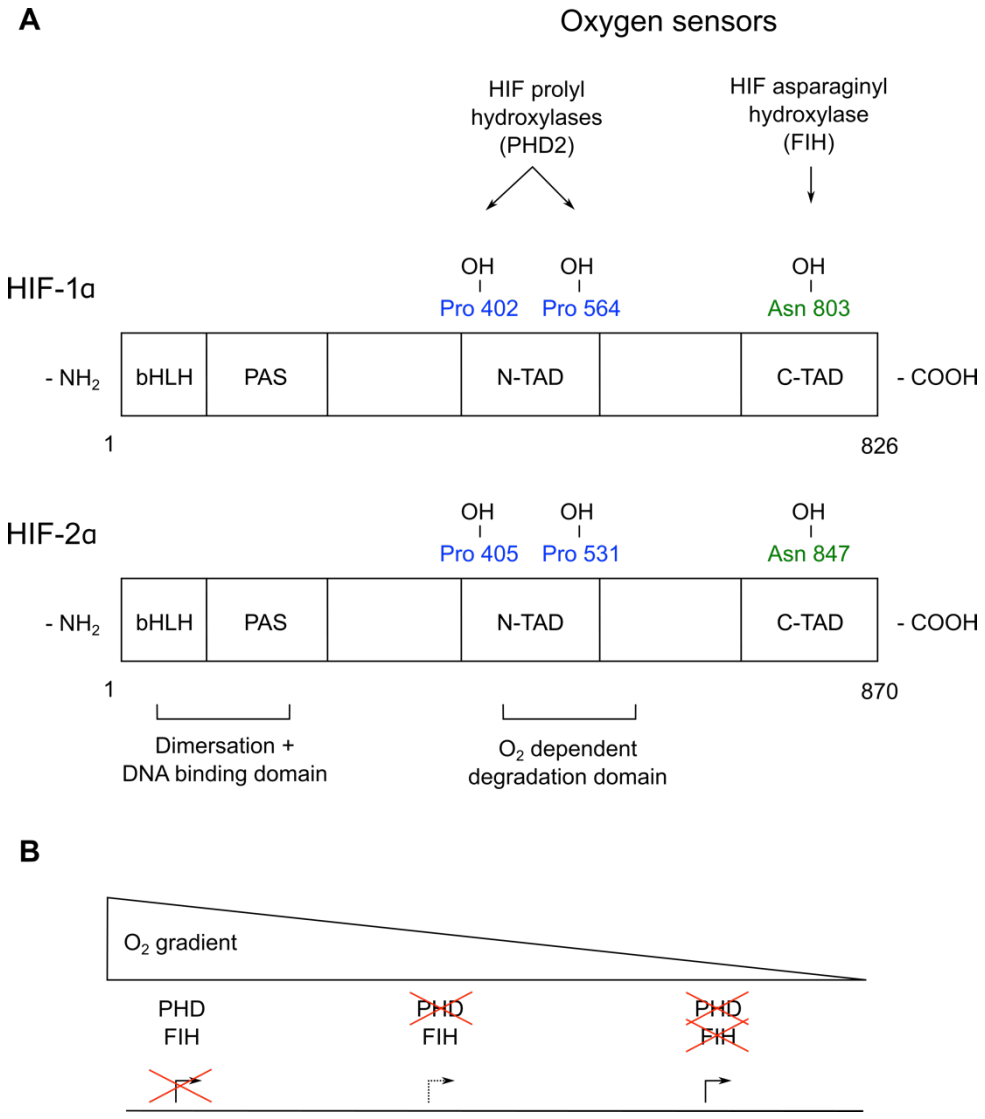

Figure 1.2 Structure and regulation of HIFα. (A) Domain structure of HIF1α and HIF2α showing proline and asparagine residues involved in its regulation by prolyl hydroxylase 2 (PHD2) and factor inducible HIF (FIH). HIFα possesses bHLH and PAS domains that are involved in dimerization with HIF1β and DNA binding. HIFα contains N-TAD and C-TAD where the N-TAD lies within the ODDD. The stability of HIFα is regulated through the ODDD via recognition of the hydroxylation state of the Pro 402 and/or Pro 564 residues on HIF1α, and Pro 405 and/or Pro 531 on HIF2α. PHD2 predominately catalyses this hydroxylation on HIF1α. Hydroxylation of Asn 803 and Asn 847 on HIF1α and HIF2α, respectively, by FIH inhibits activation by preventing binding of transcriptional coactivator p300/CBP. (B) The two TAD domains of HIFα differentially regulate gene expression, depending on gradient of oxygen within a solid tumour as PHDs require higher oxygen levels than FIH for activity. Adapted from Dayan et al. 2006.

Accumulation of mitochondrial ROS is shown to promote HIF activity, where treatment with hydrogen peroxide (H_2O_2) stabilises HIF1α, and cells with non-functional mitochondria (and therefore decreased ROS levels) are unable to stabilise HIF1α in response to hypoxia (Chandel et al. 2000). This likely occurs through oxidation (and therefore inactivation) of the PHD iron(II) catalytic centre to iron(III), overwhelming the reductive capacity of cellular agents such as ascorbate and preventing the hydroxylation-dependent degradation of HIF1α. The activity of HIF hydroxylases are also thought to be modulated through the availability of αKG, where competitive inhibition of the HIF hydroxylases occurs in SDH and FH deficient tumours owing to the accumulation of structurally similar metabolites succinate and fumarate, respectively (Selak et al. 2005; Isaacs et al. 2005). This results in the constitutive activation of hypoxic pathways in the presence of oxygen – a phenomenon known as pseudohypoxia.

HIFα expression profiles

Although the structure and mechanism of regulation for HIF1α and 2α is highly similar, HIF1 and HIF2 are capable of eliciting the transcription of different sets of genes, resulting in a differential response between tumour types (Hu et al. 2003; Sowter et al. 2003; Raval et al. 2005). While expression of HIF1α is ubiquitous: tissue-specific responses to hypoxia are at least partially mediated through restricted expression of HIF2α, which has been shown in cell types such as hepatocytes and endothelial cells (Wiesener 2002). However, it is thought that most cancer cells express both isoforms (Zhong et al. 1999; Talks et al. 2000). HIF3α is the least understood, but is believed to act as a natural antagonist owing to a lack of C-TAD

and capability of binding to HIF1α to prevent transcription activation. Little is known about the impact of HIF3α on hypoxic tumour progression.

Further adjustments to HIF signalling is through differential induction dependent on the type of intratumoural hypoxia. In chronic hypoxia, HIF1α is rapidly increased and stabilised within a few hours, but its expression subsequently decreases. This is likely due to HIF1-mediated increase in PHD2 and PHD3, which could hydroxylate HIF1α resulting in its renewed degradation (Ginouves et al. 2008). HIF2α is thought to be more stabilised in long-term hypoxia than HIF1α, and may therefore play a role in tumour progression under chronic hypoxia (Lin et al. 2011). In contrast to chronic hypoxia, cycling hypoxia results in enhanced activity and stabilisation of HIF1, and is associated with increased metastatic potential and resistance to chemo- and radiotherapy (Dewhirst et al. 2008).

As HIFs are not directly sensitised by oxygen, there are a number of additional factors that can regulate HIF stability. Loss of pVHL function, reported in clear-cell renal cell carcinoma (Latif et al. 1993), results in constitutive HIFα activity in the presence of oxygen, as HIFα is no longer subjected to oxygen-dependent ubiquitylation and degradation (Ratcliffe et al. 1999). Interestingly, it is in this disease context where HIF2α is the primary HIFα isoform responsible for oncogenesis (Kondo et al. 2002; Raval et al. 2005). HIF activity is also regulated by oncogenes and tumour suppressors, for example MYC and p53, where more detail can be found in appendix B.

Hypoxia-induced changes in metabolism and cellular redox

Cytosolic energy compensation

Cells remodel their metabolism in response to hypoxia, a primary goal of which is likely to support oxygen-independent ATP production (Figure 1.3). HIF1 is thought to be the major driver of this adaptation, stimulating increased glycolytic flux in the majority of cell types through the targeted transcription of glucose transporters (GLUT1; *SLC2A1* and GLUT3; *SLC2A3*), and almost all glycolytic enzymes (Tennant et al. 2010). Through up-regulation of the LDH isoform A, HIF1 also supports increased reduction of pyruvate to lactate in hypoxia, required to ensure continued glycolytic flux in the absence of efficient mitochondrial oxidation of NADH (Semenza et al. 1996). LDH is a reversible pentameric complex consisting of variable ratios of the A and B subunit. The resulting isoenzymes differ in their favoured direction of reaction, where LDH1 (5x LDHB) favours lactate oxidation and LDH5 (5x LDHA) favours pyruvate reduction (Cahn et al. 1962; Bishop et al. 1972). The up-regulation of LDHA appears to be a critical hypoxia-induced metabolic alteration, as silencing LDHA in hypoxic breast cancer models has been shown to decrease tumorigenicity (Fantin et al. 2006). Inhibition of LDHA has been shown to increase mitochondrial ROS (Le et al. 2010), induce cell death (Xie et al. 2014) and impair the growth of patient-derived xenografts (Rajeshkumar et al. 2015).

To prevent cytosolic acidification as a result of lactate accumulation, which itself inhibits glycolysis, lactate must be secreted from cells by monocarboxylate transporters (MCTs). In hypoxia, HIF1 mediates the transcription of MCT4 in addition

to Na^+/H^+ exchangers to excrete lactate out of the cell and mediate proton efflux (Ullah et al. 2006; Shimoda et al. 2006). This activity is accompanied by that of another target of HIF1, carbonic anhydrase (CA9). CA9 is a transmembrane protein that regulates intracellular pH by catalysing the reversible conversion of carbon dioxide and water to bicarbonate and H^+, and by importing extracellular bicarbonate into the cytosol. It promotes intracellular alkalinisation required for proliferation, and extracellular acidification required for tumour invasion, metastasis and immune evasion (Švastová et al. 2004; Moellering et al. 2008; Gatenby & Gillies 2008; Parks et al. 2011). Lactate production and excretion through MCT4 by tumour cells has been shown to be taken up by aerobic stromal cells (via MCT1, which is also highly expressed in cancer cells), as an external fuel to regenerate pyruvate for oxidative metabolism, permitting rapid tumour growth in a glucose independent mechanism (Sonveaux et al. 2008).

Mitochondrial regulation of oxygen consumption

In combination with cytosolic changes in glucose metabolism, HIF1 mediates mitochondrial metabolic remodelling on exposure to hypoxic conditions. Carbon entry into the TCA cycle is reduced through the HIF1-induced expression of mitochondrial pyruvate dehydrogenase kinase 1 (PDK1). Active PDK1 phosphorylates the E1α subunit of the PDH complex and inhibits PDH activity (Kim et al. 2006; Papandreou et al. 2006). This indirect mechanism reduces carbon influx into the TCA cycle and further promotes the conversion of pyruvate to lactate. As mitochondrial respiration relies on the availability of oxygen, this metabolic adaptation becomes vital for cell survival in hypoxia by reducing ROS production and stabilising ATP production (Kim

et al. 2006). Such cellular adaptation occurs before oxygen is limiting for mitochondrial respiration, as maximal HIF1 stability is thought to be ~1% O_2, and respiration becomes proportional to oxygen tension at ~0.4 - 0.7% O_2 (Gnaiger et al. 1998) - a protective mechanism consistent with the affinity of HIF hydroxylases for oxygen compared to the partial pressure of oxygen in hypoxic tissues.

As a consequence of the reduction in pyruvate oxidation, loss of PDH activity decreases carbon influx into citrate, thereby altering the citrate to αKG ratio, and is suggested to change the way in which glutamine is metabolised (Fendt et al. 2013; Gameiro et al. 2013). Increased reductive carboxylation of glutamine-derived αKG has been extensively described in hypoxia (Metallo et al. 2011; Wise et al. 2011; Filipp et al. 2012), and in conditions where oxidative phosphorylation machinery is defective (Mullen et al. 2011) for the provision of carbon for anabolic purposes other than oxidative TCA cycle metabolism. IDH1 and ACO1 are cytosolic enzymes involved in the pathway, whereas IDH2 and ACO2 are mitochondrial, forming two pathways with the same activity but distinct localisation. As mitochondrial ACO is susceptible to ROS-mediated inactivation through oxidation of its iron-sulphur centres (Gardner 2002), it would suggest that mitochondrial ACO2 activity is reduced, making IDH2-mediated reductive carboxylation less efficient, and perhaps IDH1 as the major source of reductive carboxylation, consistent with previous reports (Grassian et al. 2014).

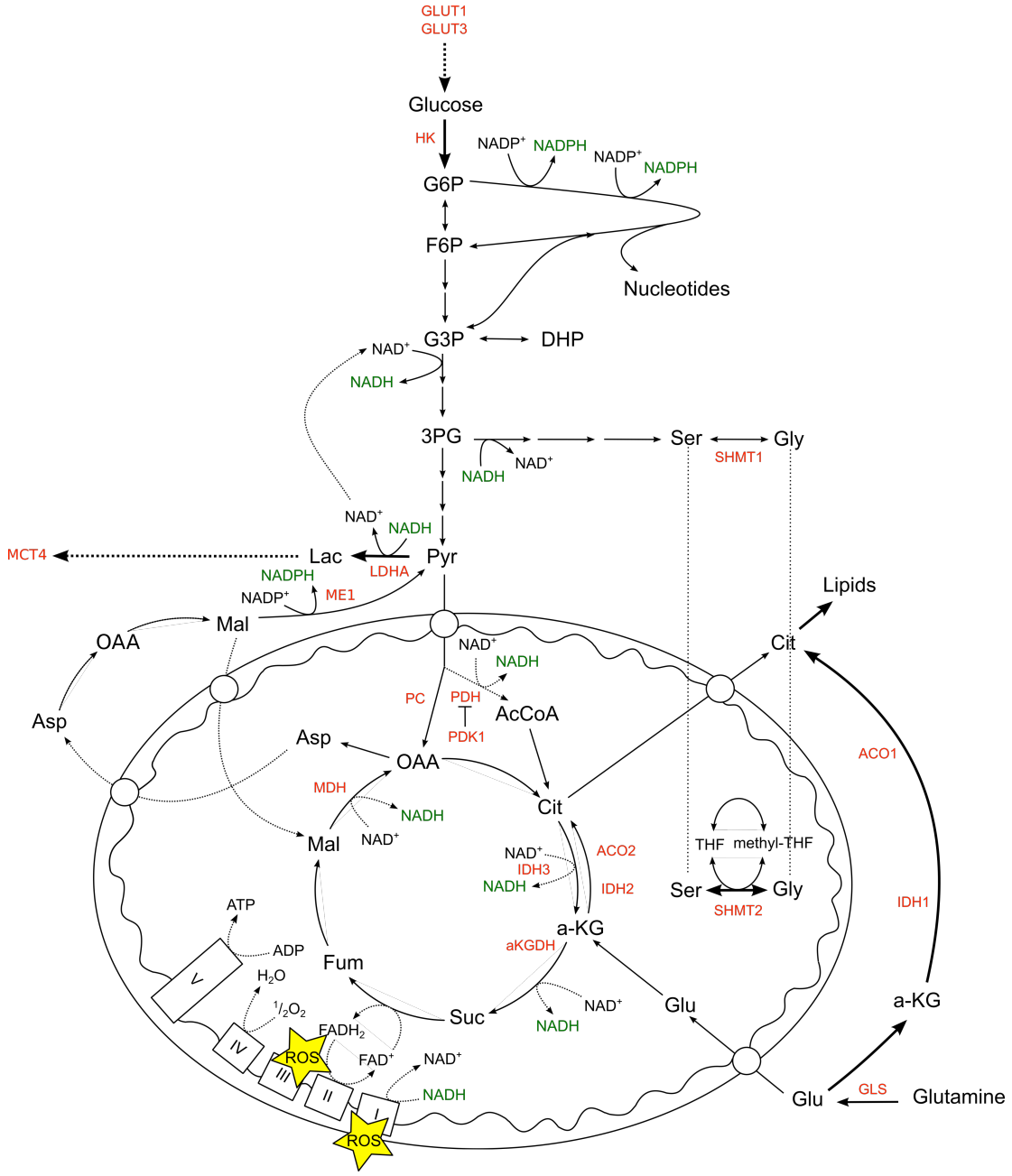

Figure 1.3 Hypoxia-induced changes in metabolism and cellular redox. Some of the metabolic pathways known to have altered activity or importance in hypoxia. Metabolic pathways described in the text are shown, as are the enzymes mentioned shown in red. Thicker lines represent those pathways in which hypoxic cells have been shown to increase flux, or rely more on their activity. Abbreviations: AcCoA, acetyl CoA; ACO1/2, aconitase 1/2; Asp, aspartate; Cit, citrate; DHP, dihydroxyphosphate; Fum, fumarate; G6P, glucose 6-phosphate; G3P, glyceraldhyde 3-phosphate; GLUT1/3, glucose transporter 1/3; Glu, glutamate; GLS, glutaminase; Gly, glycine; HK, hexokinase; IDH1/2/3, isocitrate dehydrogenase 1/2/3; Lac, lactate; LDHA, lactate dehydrogenase A; Mal, malate; MDH,

malate dehydrogenase; ME1, malic enzyme 1; MCT4, monocarboxylate transporter 4; OAA, oxaloacetate; 3PG, 3-phosphoglycerate; PC, pyruvate carboxylate; PDH, pyruvate dehydrogenase; Ser, serine; SHMT1/2, serine hydroxymethyltransferase 1/2; aKG, α-ketoglutarate and aKGDH, α-ketoglutarate dehydrogenase.

HIFs also regulate the expression of subunits of respiratory enzyme complex IV, the complex that transfers electrons to molecular oxygen, by inducing a switch in cytochrome c oxidase (COX) isoform expression from COX4-1 regulatory subunit to COX4-2. HIF1 induces expression of the COX4-2 transcript and the mitochondrial LON protease, which degrades the COX4-1 subunit (Trueblood & Poyton 1988) suggested to optimise respiratory efficiency at low oxygen tensions through more efficient electron transfer by COX-2, reducing mitochondrial ROS production (Waterland et al. 1991; Allen et al. 1995; Burke et al. 1997; Fukuda et al. 2007). This is further enhanced from the HIF1α-mediated decrease in expression of SDH subunit B (Dahia et al. 2005). The resulting decrease in mitochondrial ATP synthesis could promote hypoxia-induced autophagy, a process of "self-catabolism" whereby cytoplasmic organelles are broken down to provide macromolecules for energy generation. To this end, HIF1 induces the expression of BCL2/adenovirus E1B interacting protein 3 (BNIP3), encoding a protein that promotes mitochondrial-selective autophagy to reduce oxidative metabolism (Zhang et al. 2008).

Hypoxic cellular redox changes

Hypoxia directly affects metabolism as a consequence of changes in cellular redox, though the mechanisms for this are not entirely clear. Reduced oxygen availability could elicit changes in mitochondrial redox status that directly increase lactate

production. Under hypoxia, the mitochondrial NADH/NAD^+ ratio is thought to increase owing to slowing of electron transport (through reduced oxygen availability) and consequent reduction in the rate of NADH oxidation (Chance & Williams 1955; Mayevsky 1984). The resulting increased NADH/NAD^+ ratio would inhibit the activity of the TCA cycle dehydrogenases; PDH, IDH3, αKG dehydrogenase (αKGDH) and malate dehydrogenase (MDH). Consequently, mitochondria would be unable to continue to oxidise cytosolic NADH, which in normoxic conditions enters the TCA cycle via the malate-aspartate or glycerol 3-phosphate shuttle. This would then trigger the requirement for increased pyruvate reduction in the cytosol in hypoxia to regenerate NAD^+ for glycolysis. Neither NADH nor NADPH are thought to be able to physically cross the mitochondrial inner membrane. However, in addition to the NADH-active redox shuttles mentioned, mitochondrial nicotinamide nucleotide transhydrogenase (NNT) allows the transfer of reducing potential from NAD^+ to $NADP^+$ and vice versa. Changes in the mitochondrial NADH/NAD^+ ratio in hypoxia could suppress this transfer.

The $NADP^+$/NADPH pyridine redox pair, although relatively low in abundance in most cell types, is critical for maintaining cellular ROS detoxification, allowing the regeneration of GSH. Mitochondrial ROS production is thought to increase in hypoxia (Chandel et al. 1998). The most highly reactive ROS species, the superoxide radical, which is created from the leakage of complex I and III electrons, causes cellular damage through their oxidation of proteins, lipids and DNA. There is an increased demand for reducing equivalents in the mitochondria to maintain genetic stability, protein function, lipid membrane fluidity and cell viability. Some of the enzymes within

the mitochondrial matrix are particularly susceptible to oxidative inactivation: complex I, ACO2 and αKGDH are thought to be the most vulnerable, which results in further loss of TCA cycle activity in hypoxia.

The production of NADPH through the catabolism of serine to glycine removes carbon from glycolytic ATP production. However, this system is also able to cycle reducing potential between the mitochondria and the cytosol through transport of serine and glycine across the mitochondrial membrane, facilitated by the presence of mitochondrial isoforms of the enzymes involved in this pathway. This mechanism may be exploited by hypoxic cells to maintain mitochondrial redox balance and cell survival in hypoxia. Indeed, MYC-transformed cells induce SHMT2 when subjected to hypoxia in a HIF1-dependent manner, which maintains the cellular NADPH/$NADP^+$ ratio, decrease ROS and ultimately avoid cell death (Ye et al. 2014). More recently, SHMT2 and glycine decarboxylase (GLDC), known to prevent the toxic accumulation of glycine in SHMT2 expressing cells, was specifically detected in hypoxic regions of gliomas, thereby providing them with a metabolic advantage under hypoxia (Kim et al. 2015).

Direct regulation of metabolic pathways by oxygen availability

Depleted oxygen levels are also likely to directly limit the activity of some metabolic pathways. For example, cholesterol synthesis is highly oxygen-dependent as eleven molecules of molecular oxygen are consumed by four enzymes during the production of one molecule of cholesterol from acetyl-CoA (Bloch n.d.; Summons et al. 2006). Greatest oxygen consumption during cholesterol biosynthesis occurs in the

demethylation of lanosterol, which consumes nine molecules of molecular oxygen to oxidatively remove three methyl groups. Hypoxic conditions have been shown to decrease the demethylation of lanosterol, resulting in accumulation of sterols and a repression of pathway activity (Song et al. 2005). Adaptive hypoxic signalling pathways are thought to indirectly degrade 3-hydroxy-3-methyl-glutaryl-coenzyme A (HMG-CoA) reductase, the rate-limiting step in cholesterol biosynthesis, mediated through the transcriptional activity of HIF1, to maintain cholesterol homeostasis (Nguyen et al. 2007).

Similarly, the desaturation of fatty acids requires oxygen. Palmitate is a substrate for various elongation and desaturation reactions to accommodate the need for a diversity of fatty acids, of which the most abundant is monounsaturated oleate (C18:1). Oleate is produced from palmitate by elongation to stearate (C18:0) followed by desaturation by Δ9 stearoyl-CoA desaturase (SCD)1 (the rate-limiting enzyme in the production of monounsaturated fatty acids), which requires oxygen as an electron acceptor. A specific ratio of oleate to stearate must be maintained by cells to ensure proper membrane fluidity and thus cell integrity, where an imbalance can induce apoptosis. Hypoxia has been shown to reduce the requirement for *de novo* fatty acid synthesis and desaturation by increasing fatty acid import (Kamphorst et al. 2013).

Mutations of mitochondrial (and associated) metabolic enzymes in cancer

SDH was the first *bona fide* metabolic tumour suppressor identified in paraganglioma (PGL) and pheochromocytoma (PCC) in 2000 (Baysal et al. 2000). The discovery of SDH mutations proved that there are tumours in which Warburg's hypothesis held true. This finding changed our understanding of both basic cell metabolism, and that of cancer. Not only was a fully functional TCA cycle thought to be absolutely required for efficient mammalian cell proliferation, but since Warburg's first observations over 80 years ago, cancer metabolism was typically considered a consequence rather than a cause of cancer. Since this initial discovery, cancer-associated mutations in the mitochondrial and associated metabolic enzymes FH and IDH1 and/or 2 have also been identified.

Inactivating mutations in tumour suppressors SDH and FH have been identified as causative in cancers such as PGL (Baysal et al. 2000; Niemann S 2000; Astuti et al. 2001; Burnichon et al. 2010) and renal cell carcinoma (RCC) (Tomlinson et al. 2002), and result in the significant production of succinate (Selak et al. 2005) and fumarate (Isaacs et al. 2005), respectively. Mutations in IDH however, have been reported in a variety of diverse cancers, including adult gliomas (Parsons et al. 2008; Yan et al. 2009) and acute myelogenous leukemia (AML) (Mardis et al. 2009; Ward et al. 2010), and unlike FH and SDH, are genetic oncogenes. A single hit is only ever observed in IDH and results in loss of wild-type function but also acquires a neomorphic ability to produce (R)-2-hydroxyglutarate (2HG) from αKG (Dang et al. 2009). Mutations in IDH are believed to be early genetic events, but are insufficient to induce transformation

on their own (Watanabe, Nobusawa, et al. 2009; Watanabe, Vital, et al. 2009; Masato Sasaki et al. 2012; Chaturvedi et al. 2013).

Owing to the structural similarities to αKG, the production and accumulation of oncometabolites succinate, fumarate and (R)-2HG target αKG-dependent dioxygenases in cancer, resulting in the competitive inhibition of numerous αKG-dependent hydroxylases (Selak et al. 2005; Isaacs et al. 2005; Xu et al. 2011; Xiao et al. 2012). They have therefore all been reported to cause global epigenetic remodelling and interact with the HIF system. In the case of SDH and FH mutations, these unequivocally result in HIFα stabilisation and the subsequent development of pseudohypoxia (Selak et al. 2005), whereas with IDH1 and IDH2 the case is less clear (Yang et al. 2013).

Succinate Dehydrogenase

SDH is a highly conserved, heterotetrameric complex, where all the subunits are encoded entirely by the nuclear genome. The two hydrophilic subunits, subunit A and B protrude into the mitochondrial matrix. SDHA contains a covalently attached flavin adenine dinucleotide (FAD^+) cofactor and provides the succinate-binding site. Iron-sulphur subunit B tethers catalytic A to hydrophobic subunits C and D, which act as an anchor in the inner mitochondrial membrane and also produce the binding site for ubiquinone (Bardella, Pollard, et al. 2011). SDH catalyses the 2-electron oxidation of succinate to fumarate in the TCA cycle with the subsequent transfer of electrons yielding ubiquinol from ubiquinone. As an integral component in the mitochondrial respiratory chain and the TCA cycle, SDH has a dual function in energy production, contributing to both mitochondrial membrane potential and ATP synthesis. Interestingly, complex II is the only complex in the ETC that does not pump protons. Unlike many TCA cycle enzymes, SDH is unique to the mitochondrion and has no existing isoforms, making the mitochondrion the major source of succinate.

Mutations in SDHD were the first to be identified as causative in patients with hereditary PGL and subsequently in PCC (Baysal et al. 2000). Since this initial discovery, mutations in all the other subunits constituting the SDH complex have been identified in the same syndrome - SDHB and SDHC, and more recently SDHA - as well as the required assembly factor SDHAF2, which encodes the protein found to be responsible for covalent attachment of FAD^+ into catalytic SDHA (Burnichon et al. 2010; Astuti et al. 2001; Niemann S 2000; Baysal et al. 2000; Hao et al. 2009).

Mutations identified in all the SDH subunits may not be entirely intuitive, owing to the different structure and function exhibit by each SDH subunit.

PCC and PGL are neuroendocrine tumours arising from chromaffin cells of the adrenal medulla and paraganglia of the autonomous nervous system, respectively. They are mainly benign, but 10% of PCCs and up to 40% PGLs become malignant with a 5-year survival rate below 50% (Castro-Vega et al. 2015). PGL and PCC are relatively rare with an annual incidence of 1 or 2 per 1 million, respectively (Baysal 2008). Interestingly, PCC/PGLs exhibit remarkable genetic determinism, where at least 12 susceptibility genes have been identified (Dahia 2014). These mutations present in both familiar and apparently sporadic PGL/PCC where up to 40% of affected patients carry a germline mutation in one of these genes and the remaining ~60% are thought to be sporadic. SDH mutations have also been reported in other tumour types including gastrointestinal stromal tumours, RCCs and neuroblastoma (Janeway et al. 2011; Ricketts et al. 2008; Schimke et al. 2010).

SDH mutations are heterozygous germline mutations, where loss of protein function results from a ‘second hit’ or loss of the wild-type allele, resulting in neoplastic transformation (Gottlieb & Tomlinson 2005). Loss of any SDH subunit results in full loss of dehydrogenase activity and a complete block in the TCA cycle, where accumulation of succinate occurs at millimolar concentrations (Gimenez-Roqueplo et al. 2001; Gimenez-Roqueplo et al. 2002; Douwes Dekker et al. 2003; Selak et al. 2005; Pollard 2005; Hao et al. 2009; Burnichon et al. 2010). Interestingly, it is mutations in SDHB that predispose to a more malignant and aggressive phenotype,

and are associated with a poorer prognosis (Gimenez-Roqueplo et al. 2003; Amar et al. 2007; Boedeker et al. 2007). It is unknown why only mutations in SDHB lead to this clinical observation, highlighting a incomplete understanding of SDH function.

Reports to date have shown that succinate accumulation owing to a loss of SDH activity, imparts inhibition of all αKG-dependent dioxygenases studied to date. This includes histone and DNA demethylases, and results in a hypermethylated phenotype of the chromatin, which is thought to promote cell migration and is interestingly increased in cells deficient in *Sdhb* (Xiao et al. 2012; Letouzé et al. 2013). Loss of SDH has also been reported to activate HIFs at normal oxygen tension through the inhibition of αKG-dependent PHDs, giving HIF1 and 2 stabilisation in the presence of oxygen (Selak et al. 2005; Briere 2005). This elicits changes in metabolism to a more 'hypoxic-like' state through HIF transcriptional activation of downstream targets, driving increased glycolysis regardless of oxygen tension. This is suggested to be the primary mechanism of tumour progression as inhibition of HIFα expression in tumour cells with stable SDHB knockdown reduced their growth as xenografts (Guzy et al. 2008). It has been additionally suggested that SDH-deficient mitochondria may generate more superoxide owing to a block in electron flow (Yankovskaya 2003), which would result in further PHD inactivation.

Fumarate Hydratase

Like SDH, FH is also a *bona fide* tumour suppressor gene, inactivation of which is causative in hereditary leiomyomatosis and renal cell cancer (HLRCC) (Tomlinson et al. 2002). Patients inherit one defective copy of the gene, and following loss of heterozygousity, develop leiomyomas of the skin and uterus, along with aggressive RCC (Tomlinson et al. 2002; Gottlieb & Tomlinson 2005). The aggressiveness of RCC leads to early metastasis (Grubb et al. 2007), similar to that observed in SDHB deficient tumours. There is evidence to suggest that FH deficiency may also contribute to the development of breast and bladder tumours (Lehtonen 2006).

FH is a homotetrameric enzyme that catalyses the stereospecific and reversible hydration of fumarate to malate in the TCA cycle. Malate can then either be oxidised to oxaloacetate by MDH to generate NADH, or oxidatively decarboxylated to pyruvate by ME to form NADPH. Mitochondrial and cytosolic isoforms of FH exist, differing only in the translation start site used. Mutations in the *FH* gene may be missense, frameshift or deletion and are detected in 90% of HLRCC families (Kuwada et al. 2014).

Loss of the remaining wild-type allele in FH mutants gives rise to a complete deficit of enzyme activity and block in TCA cycle activity. This instigates the accumulation of fumarate, which like succinate, competitively inhibits αKG dioxygenases and results in a hypermethylated phenotype and a pseudohypoxic response through HIF1α stabilisation (Isaacs et al. 2005; Xiao et al. 2012). Loss of FH activity has been shown to result in significant metabolic reprogramming, which is essential for continued cell

viability (Figure 1.4). In addition to increased aerobic glycolysis emanating from HIF1α stabilisation, loss of FH activity has also been shown to increase glutamine-dependent reductive carboxylation (Mullen et al. 2011). As fumarate is not only an intermediate of the TCA cycle, but also a product of the urea cycle, the accumulation of cytosolic fumarate stemming from FH loss, causes reversal of the urea cycle, whereby argininosuccinate lyase reverses its usual activity, converting fumarate to argininosuccinate. This has the effect of making FH-deficient cells metabolically sensitive to arginine depletion (Zheng et al. 2013; Adam et al. 2013).

It was initially proposed that stabilisation of HIF was required for tumour formation (Isaacs et al. 2005; Pollard 2005), but genetic deletion of HIFs did not prevent cyst formation in *Fh*-deficient mice (Adam et al. 2011). It has since been suggested that the transcription factor nuclear erythroid-related factor 2 (NRF2) is the primary driver in oncogenesis. As an electrophilic metabolite, fumarate has been shown to spontaneously (albeit slowly) react and form covalent bonds with free sulphydryl groups in cysteine residues – a process known as succination, and a phenotype observed in *Fh*-deficient mice and HLRCC patients (Bardella, El-Bahrawy, et al. 2011). Succination of Kelch-like ECH-associated protein 1 (KEAP1), an E3 ubiquitin ligase and an inhibitor of NRF2, prevents the interaction between KEAP1 and NRF2, resulting in nuclear translocation of NRF2 and activation and expression of antioxidant genes (Adam et al. 2011; Ooi et al. 2011), which could further promote tumourigenesis by supporting ROS detoxification. Fumarate-dependent succination, rather than ROS-induced oxidation of KEAP1, is thought to be the dominant mechanism for NRF2 activation in this system.

Haem oxygenase 1 (HMOX1), the first enzyme involved in haem degradation, is a well characterised NRF2 target gene, which has been shown to be synthetic lethal with FH deficiency (Frezza et al. 2011), further supporting NRF2 as a major contributor to pathogenesis. Accumulation of TCA cycle intermediate succinyl CoA from glutamine, permits the synthesis and degradation of haem in the mitochondrial matrix, allowing partial mitochondrial NADH production and release of biliverdin and bilirubin, both of which have been suggested as antioxidants (Robertson & Fridovich 1982; Galliani et al. 1985). Interestingly, in this study, both PC and SDH are predicted to be synthetic lethal with FH deficiency, though no definitive experimental evidence exists to support this yet.

The accumulation of fumarate has also been demonstrated to directly bond with the antioxidant GSH *in vitro* and *in vivo*, producing the novel metabolite succinated glutathione (GSF). GSF acts as an alternative substrate for glutathione reductase, resulting in a decreased NADPH/$NADP^+$ ratio, reduced detoxification of mitochondrial ROS, HIF1 activation and oxidative stress (Sudarshan et al. 2009; Sullivan et al. 2013). The oxidative stress induced by GSH succination is necessary and sufficient to elicit cellular senescence in non-transformed cells (Zheng et al. 2015). Ablation of cellular senescence results in the transformation of benign renal cysts into a hyperplastic lesion, suggesting that fumarate-induced senescence needs to be bypassed for the initiation of renal cancers in HLRCC. Succination also inhibits ACO2 activity, at three cysteine residues required for iron-sulphur cluster binding, further

truncating the cycle (Ternette et al. 2013). How this inhibition of aconitase affects reductive carboxylation remains unclear.

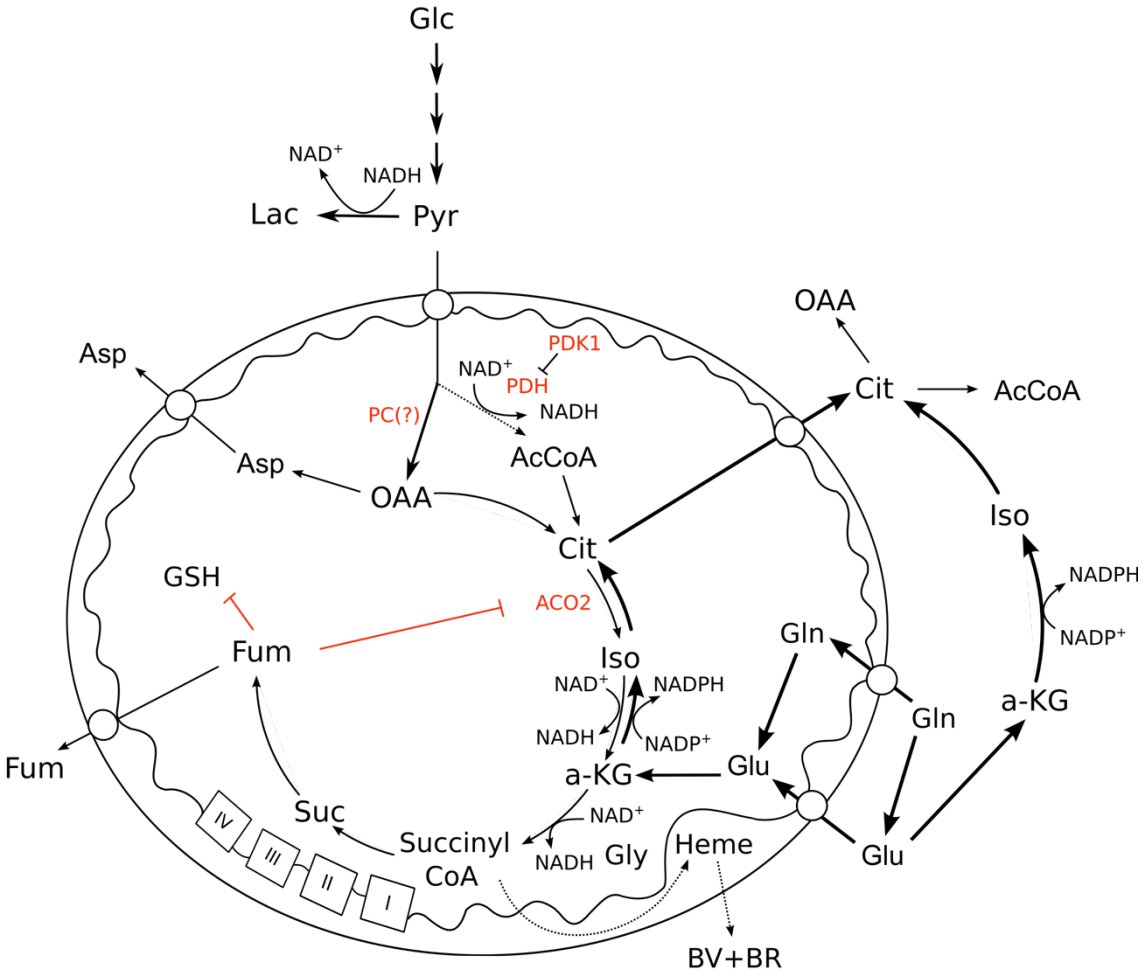

Figure 1.4 Metabolic remodelling in cancers with mutated fumarate hydratase. Known metabolic pathways that have been shown in tumours or cells containing mutations in fumarate hydratase are shown. Likely pathways that are not yet confirmed are marked with '?'. Abbreviations: AcCoA, acetyl CoA; ACO2, mitochondrial aconitase; a-KG; α-ketoglutarate; Asp, aspartate; BR, bilirubin; BV, biliverdin; Cit, citrate; Fum, fumarate; Glc, glucose; Gln, glutamine; Glu, glutamate; GSH, reduced glutathione; Gly, glycine; Iso, isocitrate; Lac, lactate; OAA, oxaloacetate; PC, pyruvate carboxylase; PDH, pyruvate dehydrogenase; PDK1, pyruvate dehydrogenase kinase 1; Pyr, pyruvate; Suc, succinate.

Isocitrate Dehydrogenase

Recurrent somatic mutations in IDH1 were first identified in 2008, when The Cancer Genome Atlas (TCGA) conducted a genome-wide study characterising genetic abnormalities driving glioblastoma (GBM) pathogenesis. Since this initial study, a total of 149 tumours have been analysed, where 12% of tumours display recurrent somatic heterozygous missense mutations in *IDH1* (Parsons et al. 2008). These mutations rarely present in primary GBMs but occur in the majority of secondary GBMs. Secondary GBMs evolve from lower-grade glioma, typically observed in younger patients (Ohgaki & Kleihues 2007), but are histologically identical to primary tumours. Deep sequencing further revealed that mutated IDH1 and IDH2 (although to a lesser extent) are highly prevalent in low-grade gliomas (LGG) (>70% grade II), including grade II-III oligodendrogliomas and/or oligoastrocytomas and grade III astrocytomas (Balss et al. 2008). They present in younger patients, with a median age of 33.2 years (compared to 55.3 years for wild-type IDH), and confer a survival advantage of 3.8 years (in comparison to 1.1 years for wild-type IDH) (Parsons et al. 2008). It is unknown whether the IDH1 status alone contributes to this, or characteristics of secondary GBM. Interestingly, it has been suggested that IDH1 mutant tumours are associated with higher rates of total surgical resection (Beiko et al. 2014).

IDH enzymes catalyse the oxidative decarboxylation of isocitrate to αKG and carbon dioxide. Five IDH genes (1, 2, 3A/B/G) in the nuclear genome encode the three IDH isoforms (1, 2 and 3) expressed by eukaryotic cells (Dalziel 1980). IDH1 and 2 are reversible, $NADP^+$/NADPH dependent homodimers, where interconversion of

isocitrate and αKG occur in the cytosol and mitochondria, respectively. These isoforms are highly homologous with ~70% sequence identity, almost identical quaternary structures and two identical enzyme active sites per homodimer (Xu et al. 2004; Ceccarelli 2002). Cytosolic NADPH production by IDH1 is thought to be important for limiting cellular oxidative damage (Kim et al. 2007) and is also required as a reducing agent in lipid synthesis (van Roermund 1998). Although, both IDH1 and 2 are capable of reductive carboxylation, IDH1 may be primarily involved in hypoxia-mediated reductive carboxylation for *de novo* lipid synthesis. IDH3 is an irreversible NAD^+-dependent heterodimer, both genetically and structural unrelated to IDH isoforms 1 and 2. IDH3 is primarily responsible for mitochondrial isocitrate oxidation and therefore regulating oxidative phosphorylation and redox homeostasis. Interestingly, IDH3 is the only isoform not yet linked to cancer progression.

All reported IDH1 mutations have a single-point mutation in an arginine residue located in the enzyme active site at codon 132. The most common heterozygous missense mutation found in IDH1, occurring in ~90% of IDH1 mutated gliomas, is the substitution of the arginine residue with histidine (R132H) (Parsons et al., 2008, Yan et al., 2009b, Gravendeel et al., 2010). The remaining R132 mutations observed result in a substitution of arginine with cysteine, glycine, serine, leucine and glutamine substitutions (Pusch et al. 2014; Molenaar et al. 2014). The number and variety of amino acid substitutions may suggest that it is the replacement of arginine that confers a tumour-supportive activity, rather than the incorporation of a new residue. However, the frequency of the R132H mutations argue that there may be a selective pressure, which could be explained by reports demonstrating that R132H is

associated with the lowest production of (R)-2HG (Ward et al. 2013) to potentially avoid cellular toxicity (Pusch et al. 2014). Interestingly, the R132C mutation occurs more frequently in astrocytoma than oligodendroglioma, suggesting that the type of IDH1 mutation may correlate to the histological types of glioma (Gravendeel et al. 2009). Consistent with this, is the finding that different genetic alterations follow the IDH1 mutation, where IDH1 mutated astrocytomas exhibit loss of p53, and IDH1 mutated oligodendrogliomas exhibit co-deletion of chromosome 1p and 19q (Wakimoto et al. 2014).

Mutations in IDH1 and 2 are thought to be mutually exclusive (Yan et al. 2009), suggesting that either isoform is sufficient to confer growth or survival advantages. Unlike glioma, mutations in IDH2 are much more prevalent in AML than IDH1 mutations (15-33% as compared to 9%) (Mardis et al. 2009). It is unknown why this is the case, but perhaps suggests the role of mutant IDH is context dependent. Mutations in IDH2 in gliomas occur at a much lower frequency (0-6%) than IDH1 in a paralogous amino acid residues R140 and R172, which are most commonly substituted with lysine (Yan et al. 2009). R132 and R172 in IDH1, and R140 and R172 in IDH2 are key residues in IDH activity as they form hydrogen bonds with the α-carboxyl and β-carboxyl groups of isocitrate to facilitate isocitrate binding in the enzyme active site (Xu et al. 2004; Dang et al. 2009). Mutations in these residues reduce binding affinity for isocitrate and increase binding affinity for NADPH, resulting in the reduction of αKG by NADPH and the release of the (R) enantiomer 2HG (Rendina et al. 2013). Although (R)-2HG is physiological, produced by αKG reductase enzymes and oxidised back to αKG by 2HG dehydrogenases (Struys,

2006), cellular concentrations of (R)-2HG accumulate to extremely high millimolar (<35 mM) concentrations, disrupting a number of cellular functions (Dang et al. 2009).

The production of (R)-2HG requires heterozygosity, as homozygous IDH1 mutations have been shown to significantly reduce the production of (R)-2HG (Jin et al. 2013), with a K_M that is approximately 11-fold lower (Brooks et al. 2014). Wild-type IDH1 either increases the enzymatic activity of mutant IDH1 towards αKG by inducing a different conformational state, or the wild-type allele produces the αKG required for mutant IDH activity and subsequent (R)-2HG production. The latter would result in a redox neutral process and permit both increased and more stable (R)-2HG production.

Owing to the structural similarity between 2HG and αKG, the effect of IDH mutations on the αKG-dependent dioxygenase family of enzymes has also been studied. Much like SDH- and FH- mutated tumours, IDH mutations have been shown to exhibit a hypermethylated phenotype through competitive inhibition of the ten-eleven translocation (TET) family of DNA demethylases and members of the Jumonji C-domain (JmjC) histone demethylases (Figueroa et al. 2010; Xu et al. 2011; Koivunen et al. 2012; S et al. 2012) resulting in global epigenetic modifications.

Unlike SDH and FH mutations however, the effect of (R)-2HG on PHD activity has been the subject of some controversy. An initial report demonstrated that (R)-2HG production in IDH1 mutant U87 glioma cells inhibits HIF degradation owing to lack of

proline hydroxylation, and occurs as a result of loss of wild-type activity and decreased production of αKG (Zhao et al. 2009). A subsequent study confirmed increased 2HG production in IDH mutants and suggested (R)-2HG could cause competitive inhibition of αKG-dependent PHDs, thus providing an alternative reason for increased HIF (Dang et al. 2009). Consistent with these findings are both increased HIF protein levels and transcription of target genes in the brain cells of IDH1 mutant mice (M. Sasaki et al. 2012).

In contrast, (R)-2HG in human astrocytes expressing IDH1 R132H was later shown to act as an agonist or co-substrate for PHD activation, resulting in reduced HIF expression and increased proliferation (Koivunen et al. 2012). In an enantiomer specific manner, (R)-2HG was shown to act as a co-substrate by the non-enzymatic oxidisation of 2HG into αKG, to provide a source of normal substrate at a level sufficient to support PHD2 catalysis, which is ultimately decarboxylated to succinate during the hydroxylation reaction (Tarhonskaya et al. 2014). Analysis of IDH mutant astrocytomas in the TCGA data set confirmed reduced HIF activity using a previously defined HIF-responsive gene expression signature (Nickols et al. 2007; Verhaak et al. 2010).

A subset of IDH mutant tumours from a cohort of 120 human gliomas showed HIF1α overexpression localised to areas of necrosis only (Williams et al. 2011). These findings may support the IDH mutant mouse model (M. Sasaki et al. 2012), which was associated with haemorrhage and high perinatal mortality. The role of (R)-2HG in hypoxia biology may be context dependent and influenced by the disease

environment. It should be noted that the blunted HIF response observed by Koivunen et al. was at a given level of hypoxia (7.5% O_2), whereas the previous studies were all conducted in normoxia. It is likely that different oxygen tensions shift the inhibitory or activation potential of (R)-2HG, with a differential effect on each member of the dioxygenase family.

In addition to the biological effects of (R)-2HG production in IDH1 mutants, the effects of a mutation in IDH1 itself, or a change in redox as a result of the IDH mutation may have intriguing effects in hypoxia. Cancer cells become more dependent on reductive glutamine metabolism in hypoxia, likely mediated by IDH1 (Metallo et al. 2011; Wise et al. 2011). Given the hypoxic nature of gliomas, and the preference for mutations in IDH1, there may be a requirement for IDH2 wild-type activity in hypoxic IDH1 mutant gliomas. However, IDH1 mutated cells, unlike their wild-type counterparts, are thought to retain oxidative TCA cycle metabolism in hypoxia (Grassian et al. 2014). If the consumption of oxygen in hypoxic IDH1 mutant cells is sustained, this would create a challenging environment, further exacerbating hypoxic conditions to form areas of necrosis. The lack of mitochondrial adaptation to low oxygen may account for the improved survival observed in patients harbouring gliomas with mutated IDH1.

Collagen maturation and stability also requires post translation modification through the activity of PHDs (Myllyharju 2004). PHD enzymes hydroxylate proline residues on type IV collagen for formation of the collagen triple helix, which contributes to the integrity of the blood brain barrier (BBB). In the animal models described earlier, mice were found to have higher levels of immature type IV collagen (M. Sasaki et al.

2012). 2HG may therefore cause defects in collagen protein maturation and breakdown the BBB owing to 2HG-mediated inhibition of collagen prolyl and lysyl hydroxylases (M. Sasaki et al. 2012; Poschl 2004). Interestingly, mutations in collagen synthesising genes have been associated with IDH mutation in non-central nervous system tumours (Tarpey et al. 2013) and RNA expression array analysis of mutant IDH1 xenograft tumours identified alterations in type IV collagen expression (Rohle et al. 2013).

Methods to decipher cancer metabolism

Metabolomics

Progress in the field of cancer metabolism has largely been facilitated by the development of analytical techniques such as chromatography, mass spectrometry (MS) and nuclear magnetic resonance (NMR) spectroscopy. The study of the metabolome encompasses a phenotype that reflects changes in the genome, transcriptome and proteome. Metabolomics describes a broad and sensitive approach that provides relative intra- or extracellular metabolite levels present in a given biological sample, particularly effective for investigating metabolic changes between different states or conditions. It can be used to reveal disease biomarkers, that may be useful for diagnosis, prognosis and assessing treatment outcome. An untargeted metabolomics analysis studies hundreds (as is the case for NMR) to thousands (as is the case for MS) of metabolites with limited prior information regarding sample composition. This type of data analysis lends well to generating a biological hypothesis. Targeted studies, on the other hand, are typically conducted after a hypothesis has been generated, and tends to involve the analysis of a number of functionally related metabolites.

Isotopic tracing

The metabolomics approach offers limited mechanistic information, as concentration changes could be indicative of altered activity of connected consuming or producing reactions (Buescher et al. 2015). Nor does this approach provide information regarding flux or pathway directionality, as an increase in metabolite levels could be

indicative of increased activity of metabolite-producing reactions or decreased activity of metabolite-consuming reactions (Fendt et al. 2010). In addition, a given metabolite can be produced by a number of intersecting pathways, for example, glutamate is involved in 55 known pathways and approximately 200 reactions (Fan et al. 2012). Methods that therefore allow interrogation of pathway usage, or determine flux through it, are often more useful. These methods rely on the use of naturally occurring metabolites, enriched in a relatively rare heavy isotope. One of the most frequently used is ^{13}C, which is particularly effective considering the prevalence of carbon-containing metabolites in mammalian cells. As this isotope possesses a non-integer spin and a different mass, metabolic tracers or their products enriched in ^{13}C can be traced using both NMR and MS-based methods, respectively.

To perform these analysis, up to 100% ^{13}C-enriched tracers (such as glucose or glutamine) are added to the culture media of cells. Metabolism of the tracer results in increasingly ^{13}C-enriched downstream metabolites until a steady state is reached and is highly dependent on the system and metabolic pathway being studied. The metabolic tracer, whether it is the metabolite itself or its isotopic labelling position, provides information on differential pathway activities, and should therefore be dictated by the biological question, for example, [1,2-$^{13}C_2$]-glucose is thought to reveal most information of glycolysis and PPP activity (Metallo et al. 2009).

In many cases, the direct interpretation of labelling patterns within a metabolite is sufficient to provide information on relative pathway activities. Qualitative changes in

pathway contributions and nutrient contribution to the production of different metabolites can also be inferred from this type of analysis. This direct interpretation is known as isotope tracer analysis. Metabolic flux analysis (MFA) refers to labelling patterns in intracellular metabolites resulting from a particular tracer, combined with cellular uptake and excretion rates, and an almost complete understanding of the biochemical reaction network to computationally estimate metabolic fluxes. This provides information on flux magnitudes but is however, much more time and data intensive.

NMR Spectroscopy

NMR spectroscopy is highly reproducible and provides accurate absolute quantification of metabolite concentrations with little inter-experiment variation. It can exploit the physical properties of any non-zero spin nuclei, which include spin-half nuclei such as ^{1}H, ^{15}N, ^{31}P as well as ^{13}C. NMR spectroscopy is a powerful technique for the elucidation of structures at the molecular level, and for this reason, is capable of distinguishing positional ^{13}C enrichment (isotopomers). This enables the determination of labelling patterns in intracellular metabolites which have the same number of ^{13}C nuclei present, but differ in position, and can provide more accurate conclusions on pathway activity. As the sample does not interact directly with the instrument, sample alteration or damage is avoided. The major limitation of NMR is poor sensitivity, compared to other analytical techniques such as MS, where high concentrations of metabolites are required for reliable detection and quantification.

1D ^{1}H NMR is the simplest and most sensitive NMR method. In a 1D ^{1}H spectrum, the signal intensity (the area under each signal) is directly proportional to the number

of ^{1}H nuclei contributing to the signal, making this approach useful for metabolite quantification. As no prior assumption of metabolite composition is required for analysis, this method can also be useful for untargeted studies. However, in biological mixtures such as body fluids, tissues and cell extracts, the 1D ^{1}H spectrum can become highly crowded. As each proton within a metabolite resonates at a specific frequency, depending upon its chemical environment, and biological mixtures can contain hundreds of metabolites, this can make identification and quantification difficult.

Improvements in metabolite overlap within a spectrum is achieved by the introduction of a second dimension such as 2D Heteronuclear Single Quantum Coherence (HSQC) spectroscopy. This spectroscopy correlates the resonance frequencies of ^{1}H and ^{13}C that are directly bound, where each ^{1}H-^{13}C pair gives rise to a signal at the proton chemical shift in the horizontal (direct) and the ^{13}C chemical shift in the vertical (indirect) dimension. ^{13}C-incorporation is determined by analysing signal splitting, or multiplet analysis, in a given metabolite, which arises from simultaneous ^{13}C incorporation into neighbouring carbon nuclei. In combination with quantification of metabolite concentrations from analysis of 1D ^{1}H NMR spectra, HSQC spectroscopy can determinate intracellular fluxes, determining the rate of substrate conversion per cell (metabolite amount converted/cell/time).

HSQC spectra need to be acquired at high resolution to accurately interpret signal splitting/multiplets, which results in long and often impractical acquisition times. Non-uniform sampling can be employed to overcome this, where only a subset of

increments are sampled, and the remaining is reconstructed using algorithms such as compressed sensing (Stanek & Koźmiński 2010; Kazimierczuk & Orekhov 2011; Hyberts et al. 2007). However, this requires substantial computational capacity. Despite the introduction of a second dimension, this approach is still limited by sensitivity, where the label incorporation analysis can only focus on metabolites that are present in sufficient abundance. Further details of other NMR spectroscopy methods can be found in appendix C.

Mass Spectrometry

In comparison to NMR, MS is highly sensitive, with quick-scanning times, high mass resolution and mass accuracy, facilitating rapid and accurate metabolite identification. Ion fragment detection by MS follows chromatographic separation. Gas chromatography mass spectrometry (GC-MS) is a widely used and well established technique implemented for isotopic tracing and metabolomics. Prior to chromatographic separation and detection, GC-MS requires the derivatisation of metabolites by chemical modification. This involves the addition of molecular groups comprised of C, H, N, O and Si atoms to polar functional groups within metabolites to promote vaporisation at GC temperatures and chromatographic separation. This limits GC-MS to volatile compounds and small mass metabolites, which lends itself well to targeted studies. As interference with the sample affects reproducibility, and derivatisation efficiency can vary greatly between metabolites (Koek et al. 2006), GC-MS requires the use of internal and external standards.

In MS, the mass isotopologue distribution (MID) is analysed, which refers to the shift in mass of a metabolite that occurs due to the incorporation of isotopes, making MS only able to differentiate metabolites that differ in isotope composition (isotopologues). MIDs describe the fractional abundance of each isotoplogue normalised to the sum of all possible isotopologues. MS can identify isotopomers in specific cases of tandem MS (Choi et al. 2012; Antoniewicz 2013), or the analysis of multiple fragments (Antoniewicz et al. 2011). Although analysis of isotopomers provides more accurate conclusions on pathway activity, MIDs can be sufficient in some cases to draw conclusions on nutrient contributions regarding known pathway activities. Importantly, MS requires to correct for the presence of naturally occurring isotopes (Fernandez et al. 1996; Yuan et al. 2008).

Thesis aims

Cancer cells alter their metabolism to make sufficient energy to support replication, support the anabolic demands of macromolecular biosynthesis, and maintain cellular redox homeostasis to maintain high rates of proliferation. Hypoxia is a well-described phenotype of most cancers, driving many aspects of malignancy, which further remodels metabolism to fine tune the balance between biosynthesis and bioenergetics. Moreover, many cancers hijack the adaptive response to hypoxia to promote tumorigenesis. Further understanding of the significant metabolic plasticity demonstrated by cancer cells, and how metabolism changes in response to hypoxic stimuli, may therefore elicit the design of new selective therapies.

This thesis aims to investigate using primarily NMR spectroscopy and GC-MS based methods, how cancer-associated mutations in metabolic enzymes SDH and IDH reprogram mitochondrial metabolism to facilitate tumour growth and development. More specifically, we intend to identify how cells deficient of SDHB activity maintain proliferation and viability in PCC/PGL, and investigate how mutations in IDH1 affect the metabolic adaptation to hypoxia in glioma progression. In addressing these questions, we aim to further understand how metabolic perturbations are induced by hypoxia, how mutations in these enzymes control mitochondrial metabolism, and what this could mean for the biology of the cancers in which these mutations are observed.

Chapter 2 *SDHB*-DEFICIENT CELLS RELY ON PYRUVATE CARBOXYLASE FOR ASPARTATE BIOSYNTHESIS

Introduction

Despite being the first metabolic *bona fide* tumour suppressor identified in the TCA cycle, the direct molecular mechanisms of SDH dysfunction remain uncharacterised. Given the importance of the TCA cycle in supplying reducing potential for oxidative phosphorylation during ATP synthesis, and for providing anabolic substrates for cell growth, the means by which cells proliferate in the absence of a fully functional TCA cycle, and how this resulting phenotype is capable of sustaining oncogenic transformation, remains unknown. A previous steady-state metabolic profile analysis performed on SDH-mutated tumours (unpublished work from Judith Favier's research group) provided metabolic changes, useful for biochemical identification and tumour stratification, but did not however permit the analysis of biochemical fluxes necessary for proliferation. Therefore, to define SDH-mutated metabolism, with the potential aim to identify cancer-specific metabolic vulnerabilities, the use of stable isotope labelling approaches were employed.

Until recently, RNA interference-mediated (RNAi) approaches have been used to silence SDH subunits, permitting what may be only a partial understanding of the biological effect of SDH deficiency (Selak et al. 2005; Guzy et al. 2008; Xiao et al. 2012). As a complete loss of SDH activity is not achieved using RNAi, residual enzyme activity remains, potentially limiting data interpretation. Furthermore, the only *in vitro* models reported to date have successfully deleted subunit B of the SDH

complex (Letouzé et al. 2013; Cardaci et al. 2015). We therefore sought to investigate how cells deleted in SDHB remodel their metabolism in order to maintain proliferation and viability using PGL/PCC as a genetically relevant tumour model.

Results

Sdhb deletion induces complete block in TCA cycle and drives an aerobic glycolysis phenotype

To define the metabolism of SDH deficient cells, two physiologically relevant *in vitro* models, carrying deletions in SDH subunit B, were employed in the study. This included the previously described *Sdhb* knock-out (KO) immortalised mouse chromaffin cell (imCC) model (*Sdhb* KO clone 6 and clone 8) (Letouzé et al. 2013) and a novel *Sdhb* KO mouse adrenal fibroblast (MAF) model. Confirmation of *Sdhb* deletion in the novel MAF cell line is shown in Figure 2.1A, which resulted in a complete loss in protein expression of SDHB but unchanged SDHA levels (Figure 2.1B). Loss of *Sdhb* in both cell models resulted in a complete block of TCA cycle activity, as demonstrated by high steady-state concentrations of intracellular and extracellular succinate (Figure 2.1C and 2.1D, respectively).

To investigate the overall metabolic changes associated with *Sdhb* deficiency, the culture media was firstly assessed from both cell line models using NMR spectroscopy. Extracellular lactate concentrations in *Sdhb* KO cells were increased compared to wild-type (Figure 2.2A), indicative of an increase in glycolytic metabolism. When cell lines were incubated with [1,2-$^{13}C_2$]-glucose for 24 hours, increased concentrations of labelled lactate, in addition to unlabelled, were observed in the culture media, suggesting that *Sdhb* loss drives Warburg-like bioenergetic features of aerobic glycolysis (Figure 2.2B). This enhanced glycolytic flux is

consistent with the pseudohypoxic phenotype previously reported in SDH deficient cells (Selak et al. 2005; Briere 2005).

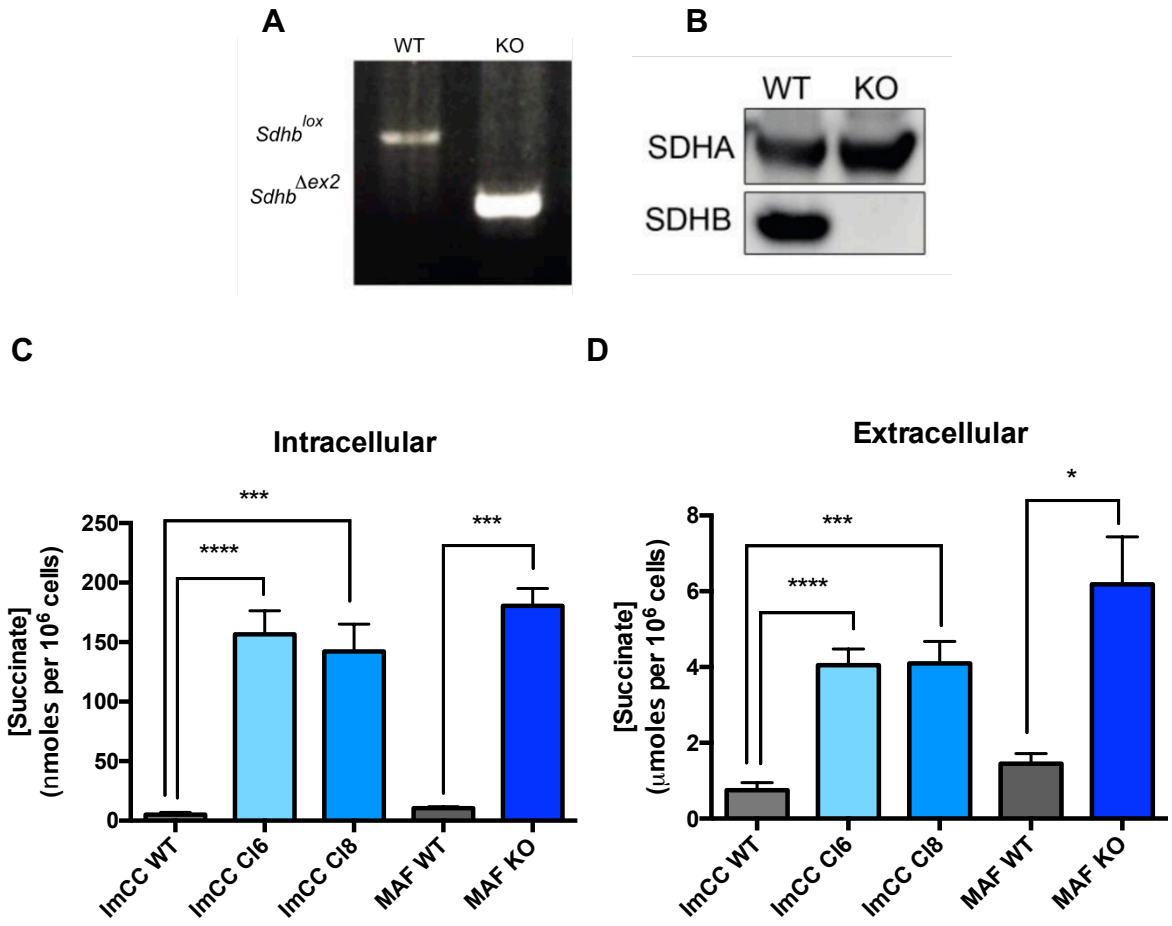

Figure 2.1 *Sdhb* deficient cells confirm a block in SDH activity. (A) Genotyping of the MAF KO cell line shows homozygous deletion of *Sdhb* exon 2 (Δex2) resulting in (B) complete loss of SDHB protein expression. $Sdhb^{lox}$ represents the targeting vector with full length endogenous *Sdhb* exon 2 flanked by loxP sites. *Sdhb* is deleted by Cre-mediated recombination ($Sdhb^{\Delta ex2}$). Suppression of exon 2 leads to a premature stop codon resulting in the translation of a truncated protein. Steady-state concentrations of succinate are increased in (C) cells and (D) culture medium from *Sdhb* KO imCC and MAF cells, as quantified by 1D ^{1}H-NMR spectroscopy. Data is mean +/- S.E.M and representative of at least three biological replicates. Significance determined using two-tailed unpaired student's t-test. Data (A) and (B) are produced by Judith Favier's research group.

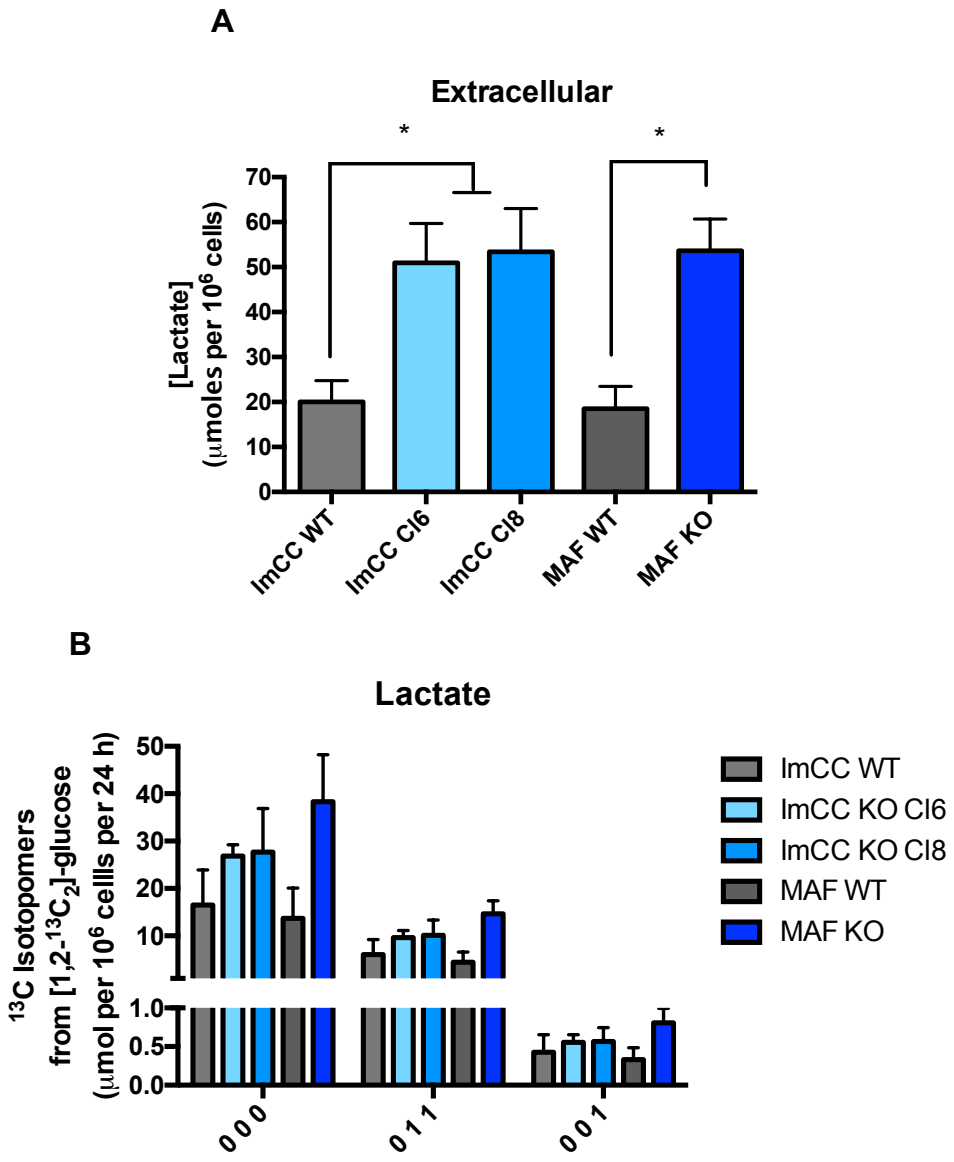

Figure 2.2 *Sdhb* deficient cells exhibit an aerobic glycolysis phenotype. *Sdhb* KO ImCC and MAF cells exhibit increased extracellular lactate concentrations as determined using 1D,^{1}H-NMR Spectroscopy (A). 24 h incubation with [1,2-$^{13}C_2$]-glucose in *Sdhb* KO ImCC and MAF cells reveals increased ^{13}C labelled and unlabelled (0 0 0) lactate concentrations in the cell culture medium (B), indicative of increased rates of glycolysis. [2,3-$^{13}C_2$]- lactate (0 1 1) and [3-$^{13}C_1$]-lactate (0 0 1) arise from glycolytic and PPP activity, respectively. Increased ^{13}C incorporation in [3-$^{13}C_1$]-lactate in *Sdhb* KO cells suggests increased PPP activity compared to wild-type.

Sdhb deficient cells exhibit altered pyruvate metabolism

Given the pseudohypoxic phenotype described in cells deficient in SDH activity, differential glucose metabolism between wild-type and *Sdhb* KO cells was firstly assessed. Once in the mitochondria, pyruvate, the end-product of glycolysis, can either be oxidatively decarboxylated by PDH to form acetyl CoA, or carboxylated by PC to form oxaloacetate. Further metabolism of acetyl CoA and/or oxaloacetate by the TCA cycle results in the synthesis of αKG, which can be transaminated to form glutamate. The position of ^{13}C atoms within glutamate can therefore be used as a read-out of relative activities of PC ([2,3-$^{13}C_2$]- glutamate) and PDH ([4,5-$^{13}C_2$]-glutamate). NMR can be employed to investigate positional ^{13}C incorporation by analysing simultaneous ^{13}C incorporation into neighbouring carbon atoms (^{13}C-^{13}C couplings) within a given metabolite. NMR is therefore useful to deconvolute isotopomer mixtures such as the example above from [1,2-$^{13}C_2$]-glucose. A brief explanation of multiplet analysis by 2D ^{1}H,^{13}C-NMR spectroscopy using glutamate to differentiate PDH and PC activity by is highlighted in Figure 2.3.

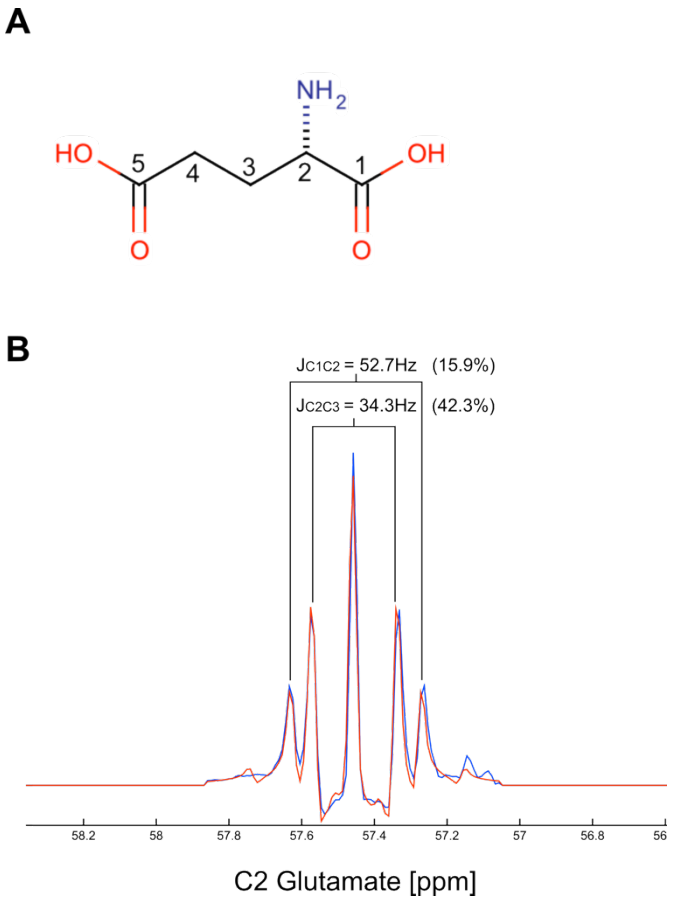

Figure 2.3 Example multiplet analysis using glutamate to differentiate relative pathway activity. 2D $^{1}H,^{13}C$-HSQC NMR analysis of ^{13}C incorporation into glutamate from [1,2-$^{13}C_2$]-glucose can be used to assess relative flux through the activity of PDH and PC. The chemical structure of glutamate (A) is shown, along with the multiplet of C2 glutamate (B). The quantum mechanical simulation of the nuclear spin system (red line) is fitted to the experimental data (blue line). C2 can provide labelling information on adjacent carbons, which dictates the splitting of the multiplet. In the example multiplet, two doublets are observed corresponding to [1,2-$^{13}C_2$]- and [2,3-$^{13}C_2$]-glutamate. The doublets are differentiated by the J coupling constant (Jcc), which itself is dictated by the functional groups attached to the adjacent carbon. For example, [1,2-$^{13}C_2$]-glutamate has a larger coupling constant than [2,3-$^{13}C_2$]-glutamate owing to the attached COOH functional group. The percentage contribution of each multiplet therefore provides relative information on the pathway activity, where [1,2-$^{13}C_2$]-glutamate corresponds to two rounds of TCA cycle resulting from PDH activity and [2,3-$^{13}C_2$]-glutamate is formed directly from PC activity.

Figure 2.3 Example multiplet analysis using glutamate to differentiate relative pathway activity, *continued*. Spectra (C) for ImCC and MAF *Sdhb* KO cell lines are normalised to cell number. Wild-type samples show a small percentage contribution for [2,3-$^{13}C_2$]-glutamate (large C3 middle peak) but a large [1,2-$^{13}C_2$]-glutamate (small C2 middle peak). The opposite is true for SDH deficient cells. [4,5-$^{13}C_2$]-glutamate labelling in C4 is present in all samples but the contribution is significantly less in SDH deficient cells. It is assumed here that the middle peak is natural abundance only (i.e. unlabelled, and therefore only possible to get labelling in [4,5-$^{13}C_2$]-glutamate – this is not strictly true but the percentage contribution of C3 in lactate and alanine from [1,2-$^{13}C_2$]-glucose in negligible).

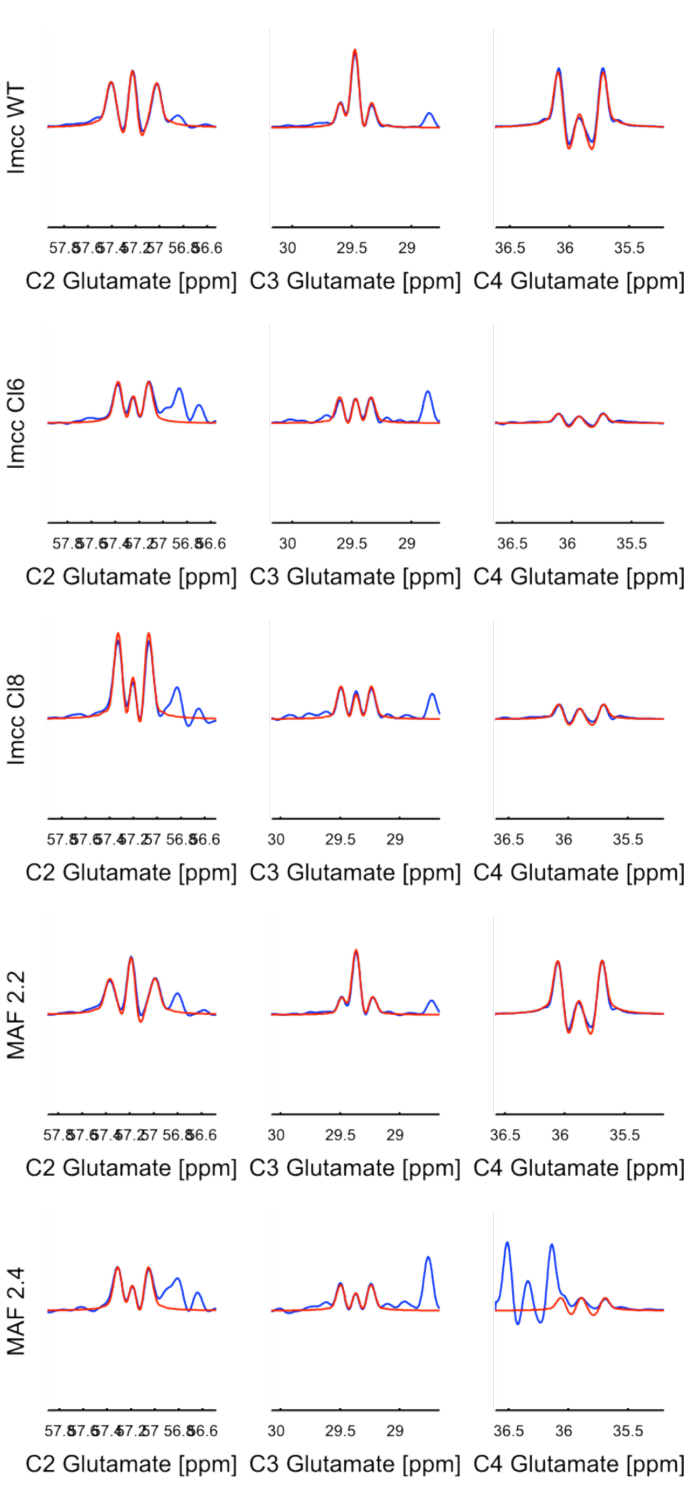

Analysis of glutamate after cells were labelled with [1,2-$^{13}C_2$]-glucose for 24 hours revealed differential isotopomer distributions between wild-type and *Sdhb* KO cells (Figure 2.4A). In wild-type cells, [4,5-$^{13}C_2$]-glutamate was the major isotopomer observed, consistent with oxidative decarboxylation of pyruvate by PDH. An additional round of TCA cycle activity was also observed through the identification of [1,2-$^{13}C_2$]-glutamate in wild-type cells, and its absence in *Sdhb* KO cells owing to the previously stated block in TCA cycle activity. The labelling schematic for wild-type cells is illustrated in Figure 2.4B. In *Sdhb* KO cells, however, the relative contribution of [4,5-$^{13}C_2$]-glutamate was reduced by ~50%, and instead a considerable percentage of [2,3-$^{13}C_2$]-glutamate was detected, representing the incorporation of labelled oxaloacetate into the TCA cycle. The same isotopomer distributions in glutamate were also reflected in the media (Figure 2.4C). Collectively, these data suggest that in *Sdhb* KO cells, there is an increase in oxaloacetate synthesis from pyruvate, likely through the activity of PC, which compensates for the reduction in pyruvate oxidation (Figure 2.4D). This mechanism, which presumably occurs as a result of HIF1α stabilisation and subsequent transcriptional activation of PDK1 to inhibit PDH activity, may provide necessary carbon for continued cellular anabolism in *Sdhb* KO cells.

The isotopomers of aspartate, a direct metabolite produced through the transamination of oxaloacetate, confirmed the switch in pyruvate oxidation to carboxylation in *Sdhb* KO cells (Figure 2.4E). Although wild-type cells were observed to synthesise [1,2-$^{13}C_2$]-/[3,4-$^{13}C_2$]-aspartate through oxidative TCA cycle activity, these isotopomers were absent in SDH-deficient cells and a significant increase (~10

fold) in [2,3-$^{13}C_2$]-aspartate synthesised from PC-derived oxaloacetate was detected. This observation, along with the fact that mitochondrial aspartate production from oxidative TCA metabolism is absent in *Sdhb* KO cells, led to the hypothesis that oxaloacetate produced by PC was used primarily for aspartate synthesis, and this biosynthetic pathway may be essential for proliferation of *Sdhb* KO cells.

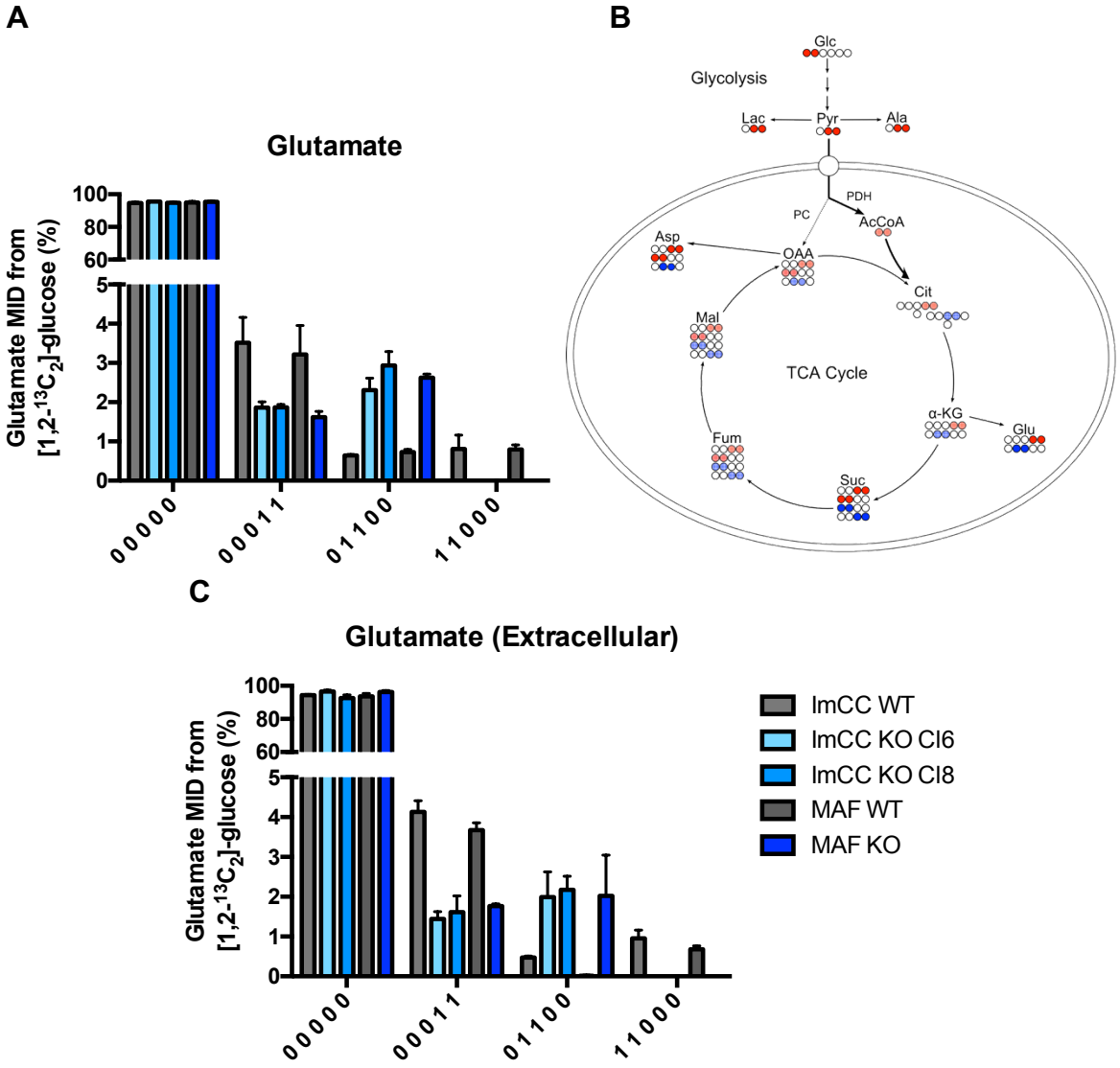

Figure 2.4 Loss of *Sdhb* results in increased pyruvate carboxylation. 2D ^{1}H,^{13}C-NMR spectroscopy analysis of resulting ^{13}C incorporation from [1,2-$^{13}C_2$]-glucose into glutamate (A). Diagram (B) describes the incorporation of carbon from glucose through PDH (red) and PC (blue) activity into wild-type *Sdhb* cells. The same ^{13}C label incorporation in glutamate is also reflected in the culture media (C).

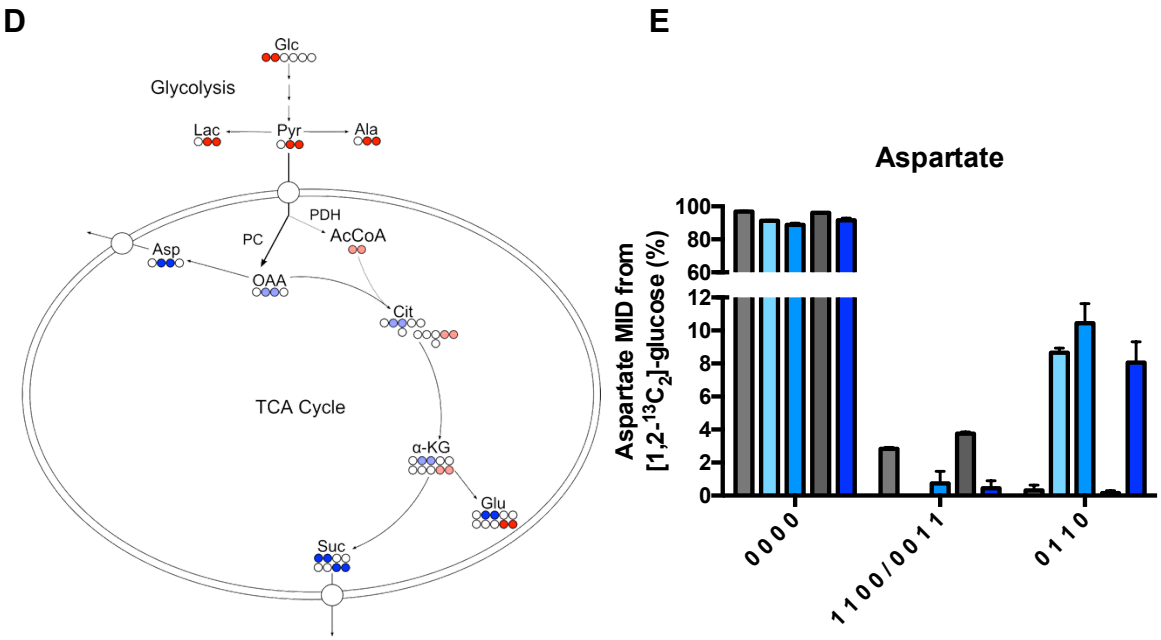

Figure 2.4 Loss of *Sdhb* results in increased pyruvate carboxylation, *continued*. Reduction in the relative abundance of the [4,5-$^{13}C_2$]-glutamate and increase in [2,3-$^{13}C_2$]-glutamate isotopomers in *Sdhb* KO cells suggest an increase in PC activity and relative decrease in PDH activity, as exemplified in diagram (D). This is confirmed by the change in metabolite isotopomer distribution (MID) in aspartate from cell extracts towards [2,3-$^{13}C_2$]-aspartate (E). Note that MID for NMR data refer to metabolite isotopomer distributions (not mass isotopologue distribution). Coloured circles on each diagram represent carbons that are ^{13}C labelled and white circles represent carbons that are ^{12}C. Translucent circles represent those metabolites that are not detectable by NMR due to low abundance. Data is mean +/- S.E.M from three biological replicates. Abbreviations in metabolic diagrams: AcCoA, acetyl CoA; Ala, alanine; Asp, aspartate; Cit, citrate; Glc, glucose; Gln, glutamine; α-KG, α-ketoglutarate; Lac, lactate; OAA, oxaloacetate; PC, pyruvate carboxylase; PDH, pyruvate dehydrogenase; Pyr, pyruvate.

Aspartate synthesis is dependent on pyruvate carboxylase activity in *Sdhb* deficient cells

As the NMR isotopomer analysis of glutamate and aspartate suggested *Sdhb* KO cells depend upon mitochondrial PC activity, PC protein expression was assessed and shown to be increased in *Sdhb* KO imCC cells (Figure 2.5A) and in SDH-mutated PCC (Figure 2.5B), further highlighting the potential importance of PC activity in the metabolism on SDH mutant cells and tissues.

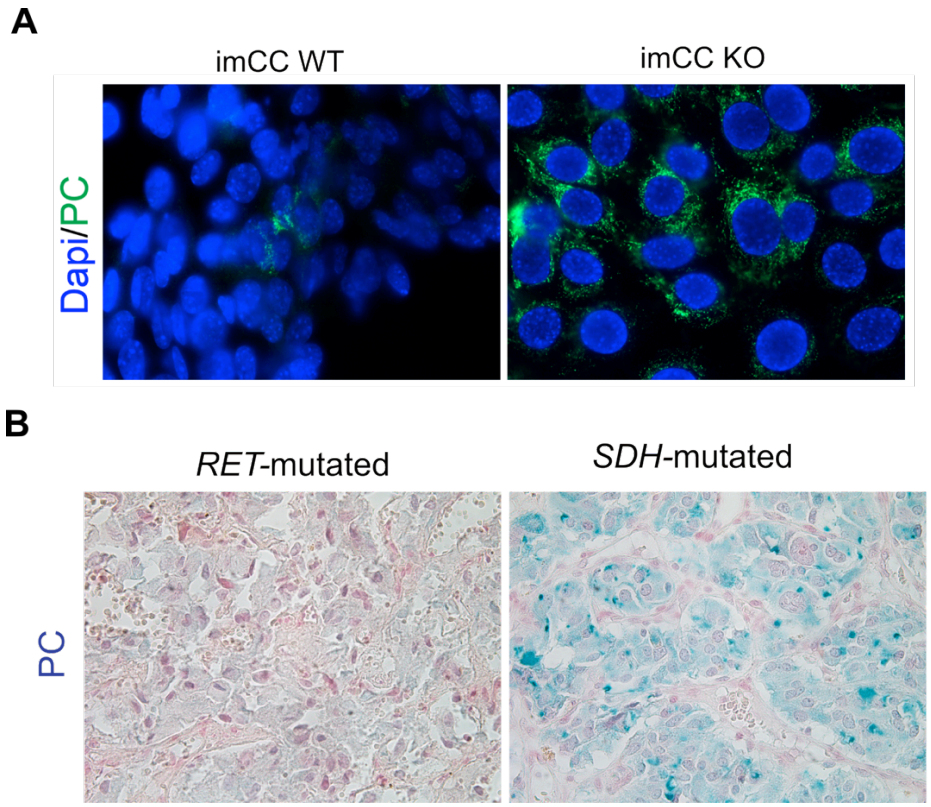

Figure 2.5 SDH deficient cells and tumours increase expression of pyruvate carboxylase. (A) PC protein expression is increased in imCC *Sdhb* KO cells compared to wild-type controls. (B) SDH-mutated PCC shows extensive up-regulated PC protein expression compared with non SDH-mutated PCC harbouring a RET mutation. Scale bar, 50 μm. Data produced from Judith Favier's research group.

As aspartate has a pivotal role in cellular anabolism to support nucleotide and protein synthesis, and aspartate synthesis in *Sdhb* KO cells is shown to be PC dependent, we predicted that loss of PC activity in *Sdhb* KO cells would affect proliferation and/or survival. Knock-down of PC in the imCC cell model was validated using two independent short interfering RNA (siRNA) sequences, achieving significant reduction in PC mRNA (Figure 2.6A) and protein expression (Figure 2.6B). Absence of PC had no effect in wild-type cells (Figure 2.6C) but a significant decline in proliferation and viability was observed in the *Sdhb* KO cells (Figure 2.6D). This confirmed the essential role of PC in *Sdhb* KO cell growth and survival. Identifying PC as an essential gene for SDH-deficient but not wild-type cells, unveiled a metabolic vulnerability that could be exploited for potential treatment.

As the proliferation of *Sdhb* KO cells requires the mitochondrial production of aspartate through PC activity, aspartate must be made available for cytosolic biosynthetic processes, and therefore requires export across the inner mitochondrial membrane. The aspartate-glutamate antiporter (SLC25A13) is one example transporter used to export aspartate into the cytosol. Indeed, expression of SLC25A13 was increased in imCC KO cell lines (Figure 2.7A) and shown to be significantly and specifically up-regulated in SDH-deficient tumours (Figure 2.7B).

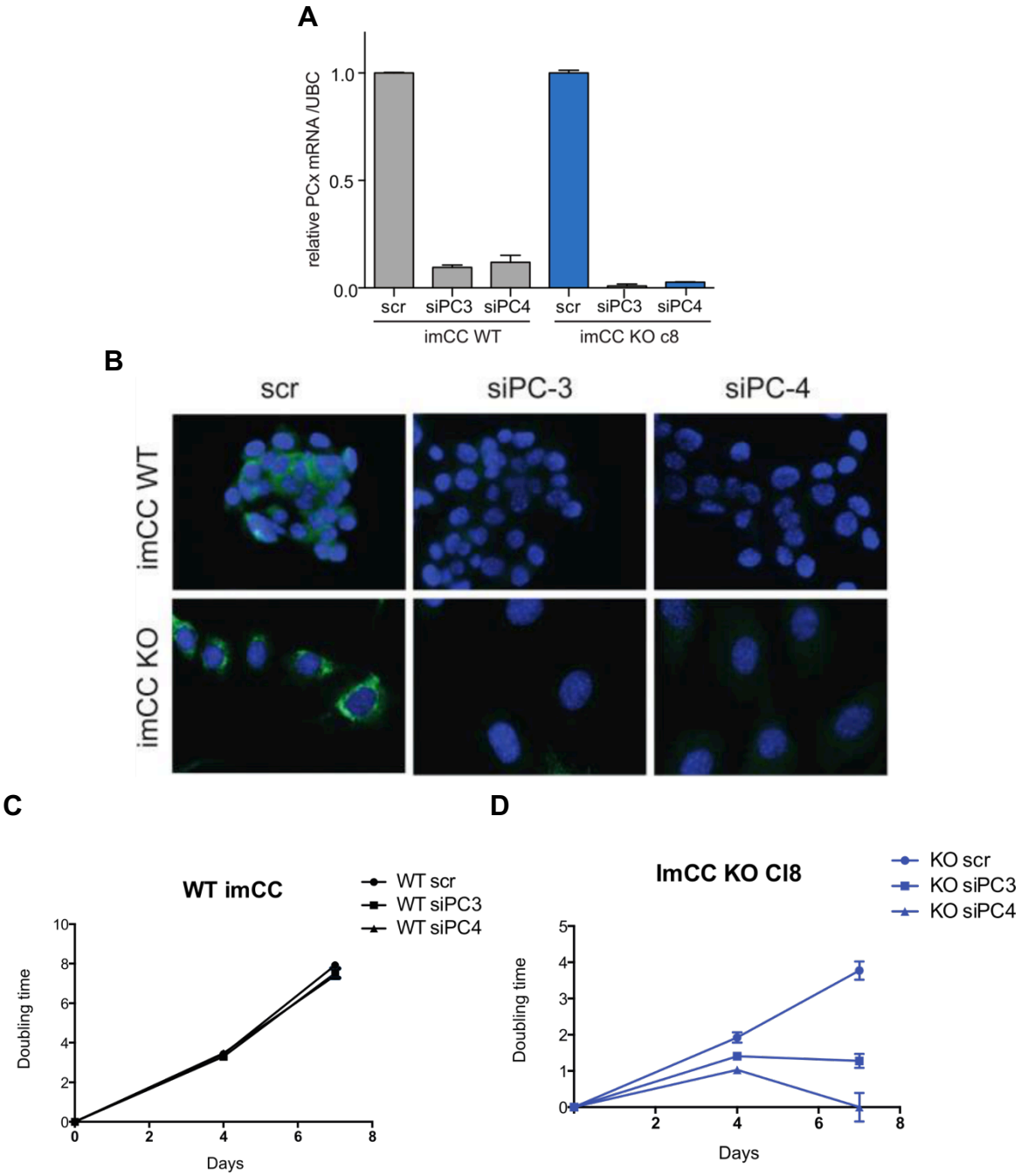

Figure 2.6 Expression of pyruvate carboxylase is essential for the proliferation of *Sdhb* deficient cells. Successful knockdown of PC protein and mRNA expression in both the wild-type (WT) and *Sdhb* KO clone 8 assessed by (A) RT-PCR and (B) immunofluorescence. Reduction in the expression of PC using two independent siRNA sequences, siPC #3 and #4, results in (A) unaffected proliferation of wild-type cells and (B) a significant reduction in proliferation of SDH deficient cells. Data produced from Judith Favier's research group.

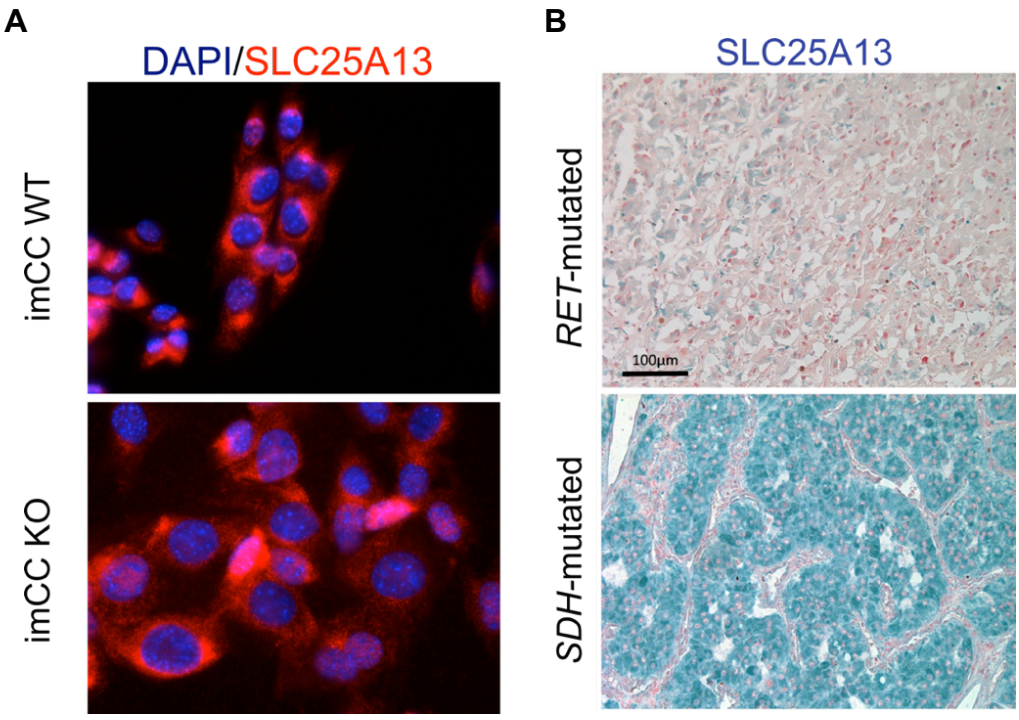

Figure 2.7 Increased expression of glutamate/aspartate antiporter SLC25A13 in SDH deficient cells and tumours. Increased protein expression of the glutamate-aspartate antiporter SLC25A13 is shown in (A) imCC KO cells and (B) SDHB-mutated PCC, by immunofluorescence and immunohistochemistry, respectively. Scale bar, 100 µm. Data produced from Judith Favier's research group.

Cultured cells are entirely reliant on endogenous aspartate synthesis for growth, as aspartate is not present in the culture medium DMEM. When cultured with exogenous [U-$^{13}C_4$]-aspartate, *Sdhb* KO cells were found to import (Figure 2.8A) and metabolise (Figure 2.8B) significantly more exogenous aspartate than their wild-type counterparts. These observations support the notion that *Sdhb* KO cells have an increased dependence on aspartate, as a result of a truncated TCA cycle.

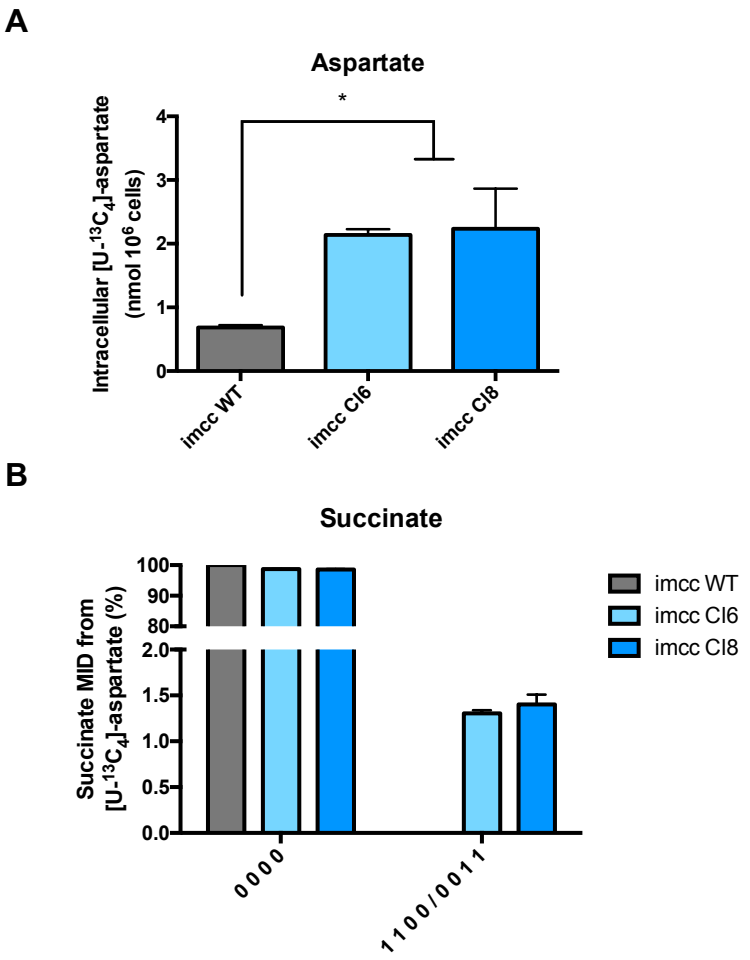

Figure 2.8 *Sdhb* deficient cells have increased dependence on aspartate. (A) ImCC KO cells Cl6 and Cl8 demonstrate increased uptake of extracellular aspartate when incubated with 0.1 mM [U-$^{13}C_4$]-aspartate for 48 h compared to wild-type, which is further metabolised intracellularly, as evident from isotopomer distrubution of succinate (B), and is consistent with a increased requirement for aspartate to support proliferation in SDH-deficient cells. Owing to the symmetrical nature of succinate, [1,2-$^{13}C_2$]-and [3,4-$^{13}C_2$]-isotopomers cannot be distinguished using NMR spectroscopy and are therefore reported as a single combined value. Data is mean +/- S.E.M from three biological replicates. Significance determined using an ordinary one-way ANOVA.

Sdhb deficient cells elicit reductive glutamine metabolism but is insufficient to refill the depleted metabolite pools

As a considerable amount of glucose carbon is directed towards mitochondrial aspartate biosynthesis mediated by PC in *Sdhb* KO cells, we next sought to investigate whether glutamine, an alternative carbon source to glucose, could be used for the synthesis of cytosolic aspartate through reductive glutamine metabolism. Glutamine is an important source of carbon for *de novo* nucleotide biosynthesis and the synthesis of almost all NEAAs. In common with other systems where oxidative TCA cycle metabolism is perturbed, there may be an increased reliance on reductive carboxylation for cellular anabolism (Mullen et al. 2011). To investigate this, cells were incubated with [U-$^{13}C_5$]-glutamine for 24 hours and the resulting polar extracts from the cells and culture media were obtained and analysed for ^{13}C incorporation into metabolites.

^{13}C labelled carbon nuclei from glutamine were significantly enriched in malate and aspartate isotopomers in wild-type imCC cells, consistent with oxidative ([U-$^{13}C_4$]- and [1,2-$^{13}C_2$]-/[3,4-$^{13}C_2$]-) and reductive ([1,2,3-$^{13}C_3$]-/[2,3,4-$^{13}C_3$]-) glutamine metabolism (Figure 2.9A and B, respectively). Analysis of the isotopomer distribution in lactate synthesised from [U-$^{13}C_5$]-glutamine, although significantly less than glucose (~50-fold), confirmed the presence of oxidative glutamine metabolism ([U-$^{13}C_3$]- and [1,2-$^{13}C_2$]-) in the wild-type cells only (Figure 2.9C). However, identification of [2,3-$^{13}C_2$]-lactate in both wild-type and *Sdhb* KO cells supported the activity of

reductive glutamine metabolism, exemplified in labelling schemes Figure 2.9D and 2.9E.

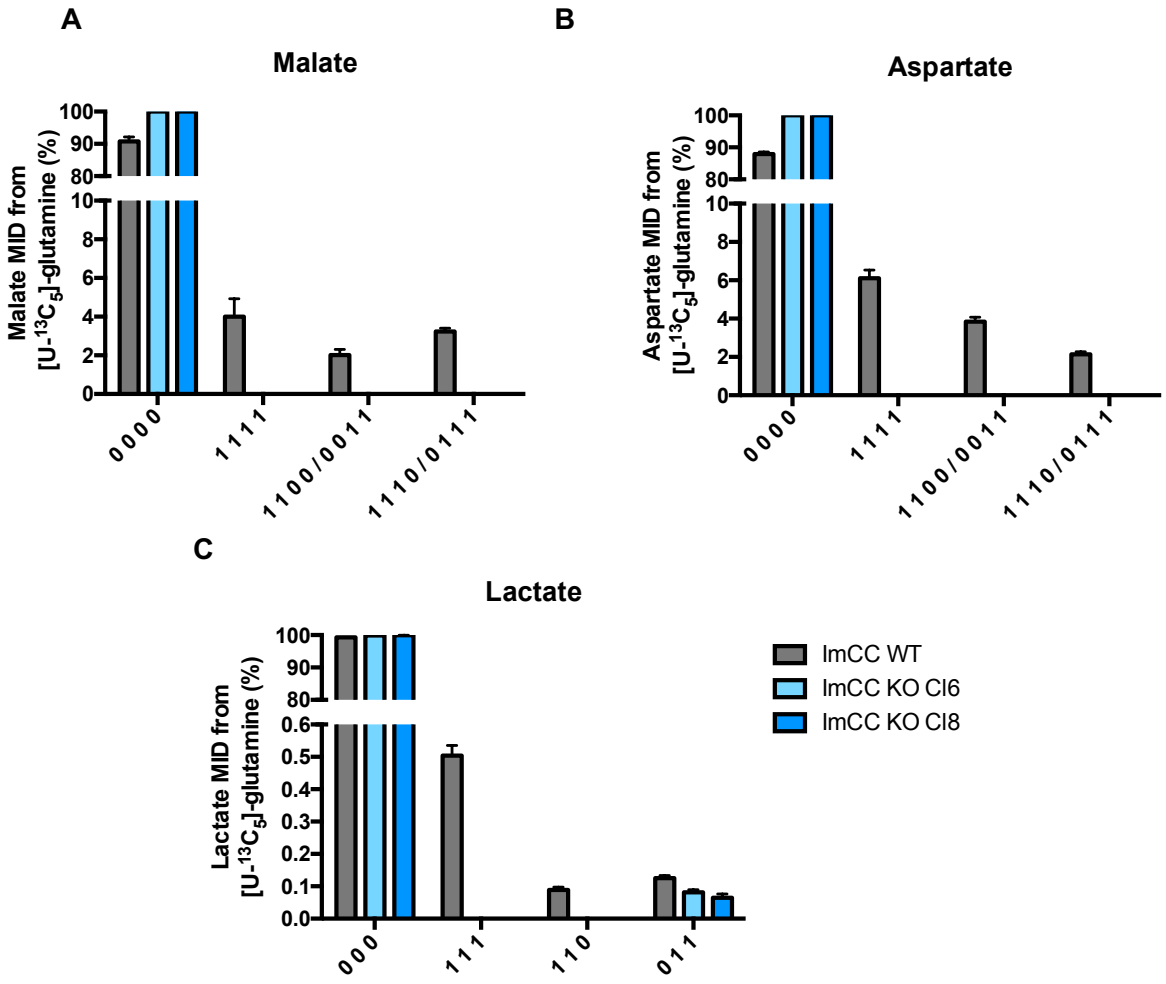

Figure 2.9 SDH deficient cells exhibit dysfunctional glutamine metabolism. Glutamine metabolism leads to incorporation of ^{13}C from [U-$^{13}C_5$]-glutamine into (A) malate and (B) aspartate in ImCC WT cells only, as analysed by NMR spectroscopy. However, no isotopomers were detected in *Sdhb* KO cells suggesting a lack of reductive glutamine metabolism in addition to oxidative glutamine metabolism. Isotopomer distributions in (C) lactate confirm the presence of reductive glutamine metabolism in both wild-type and *Sdhb* KO cells by the identification of [2,3-$^{13}C_2$]-lactate. Data is mean +/- S.E.M from three biological replicates.

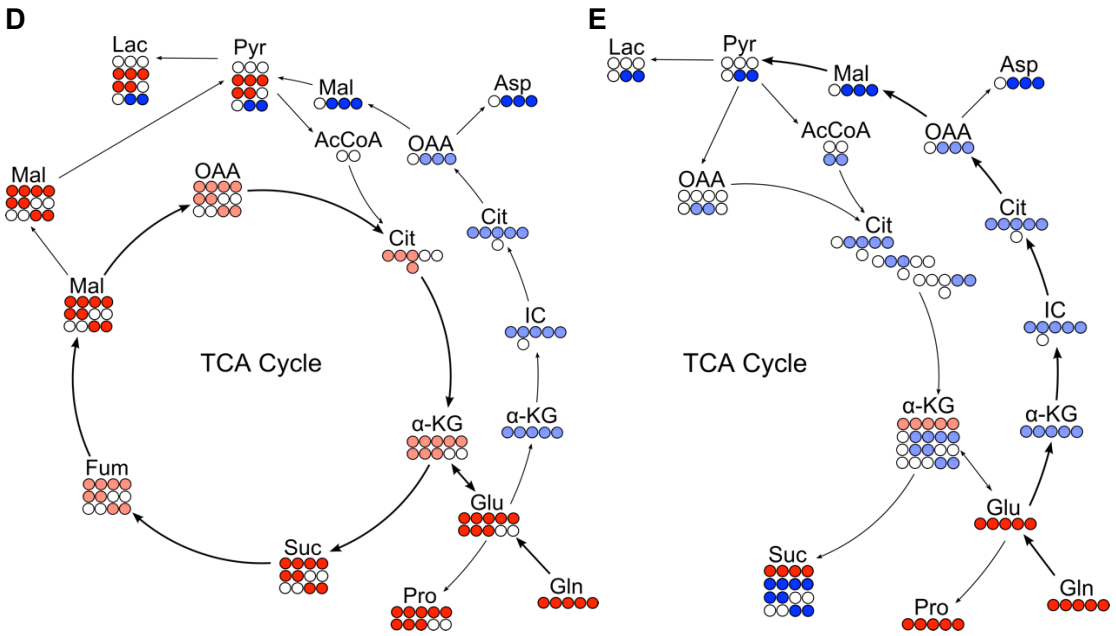

Figure 2.9 SDH deficient cells exhibit dysfunctional glutamine metabolism, *continued*. Diagrammatic representation of the oxidative (red) and reductive (blue) metabolism of glutamine in wild-type (D) and ImCC and MAF *Sdhb* KO (E) cells. Abbreviations in metabolic diagrams: AcCoA, acetyl CoA; Asp, aspartate; Cit, citrate; Gln, glutamine; IC, isocitrate; α-KG, α-ketoglutarate; Lac, lactate; Mal, malate; OAA, oxaloacetate; Pro, proline; PC, pyruvate carboxylase; PDH, pyruvate dehydrogenase; Pyr, pyruvate; Suc, succinate.

To investigate whether the enzymes involved in reductive glutamine metabolism supported this activity (Figure 2.10A), a transcriptional analysis was performed, which suggested increased expression of cytosolic reductive glutamine enzyme activity in *Sdhb* KO cells (Figure 2.10B).

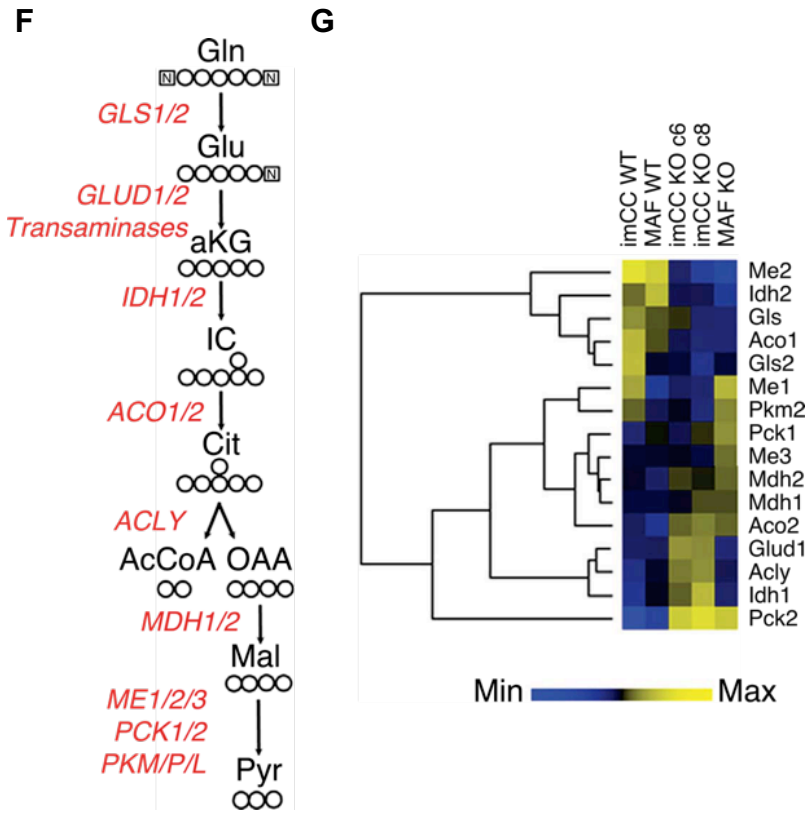

Figure 2.10 SDH deficient cells increase expression of enzymes involved in reductive glutamine metabolism. The enzymes involved in the reductive metabolism of glutamine (A) are differentially expressed in SDH-deficient cells (B). Noticeably, most enzymes with cytosolic reductase activity are up-regulated, whereas most with mitochondrial-localised reductive activity are down-regulated. Data is produced from Judith Favier's research group. Abbreviations: ACLY, ATP citrate lyase; ACO1/2, aconitase 1/2; GLS, glutaminase; GLUD1/2, glutamate dehydrogenase; IDH1/2, isocitrate dehydrogenase 1/2; ME1/2/3, malic enzyme 1/2/3; MDH1/2, malate dehydrogenase 1/2; PCK1/2, phosphoenolpyruvate carboxykinase; and PKM/P/L, pyruvate kinase M/P/L.

In case the absence of observable label incorporation into aspartate and malate in *Sdhb* KO cells was due to the lack of sensitivity of the NMR approach, cell samples were incubated with [U-$^{13}C_5$]-glutamine for longer incubation times of 72 hours and extracted for GC-MS analysis. Owing to very low steady-state concentrations, neither

labelling in malate, aspartate or citrate could be identified by GC-MS (Figure 2.11A, 2.11B and 2.11C, respectively). The low steady-state concentrations of malate and aspartate were consistent with previous findings from the metabolomics analysis performed on SDH-mutated PCC (Figure 2.21D and 2.21E, respectively). However, isotopologues of fumarate confirmed increased proportions of M+3 in *Sdhb* KO cells from [U-$^{13}C_5$]-glutamine, which is consistent with the presence of reductive carboxylation (Figure 2.12A).

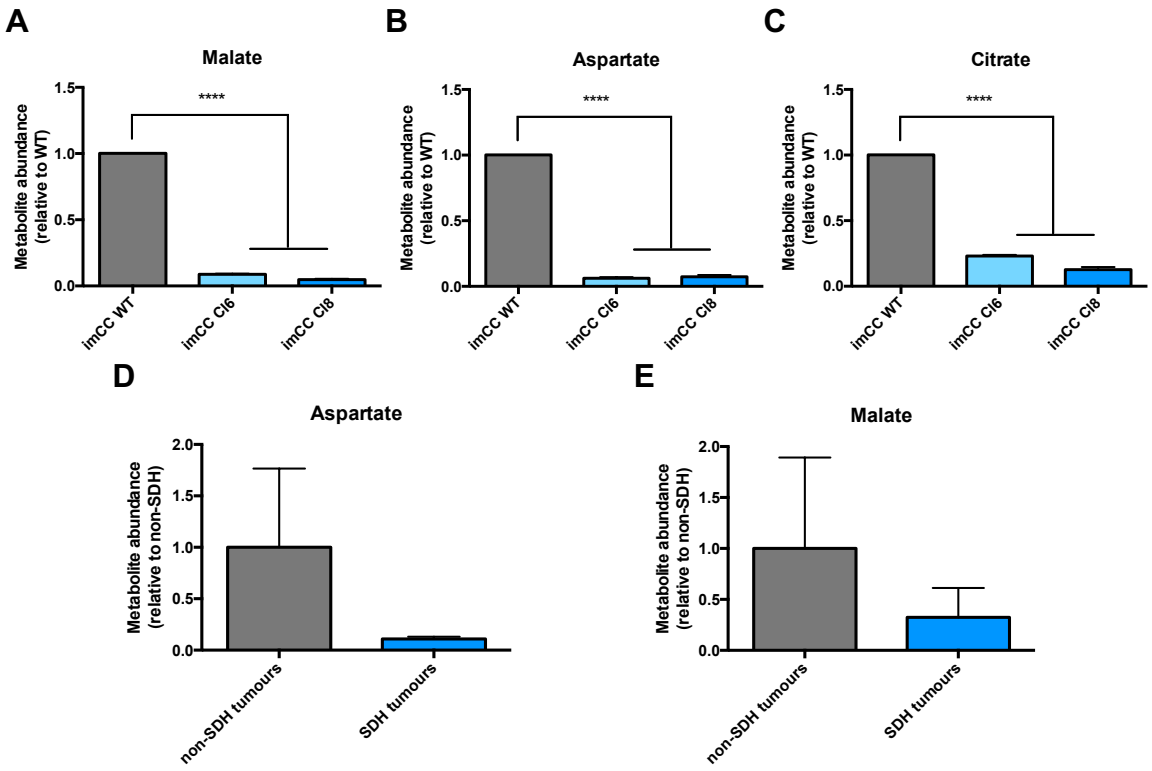

Figure 2.11 GC-MS data confirms depleted amino acid pools as a consequence of a truncated TCA cycle. ImCC incubation with [U-$^{13}C_5$]-glutamine for 72 h confirms a lack of labelling in metabolites malate (A), aspartate (B) or citrate (C), owing to low intracellular concentrations, which is additionally observed in SDH-mutated tumours (D) and (E). Data is mean +/- S.D. Statistical significance determined using ordinary one-way ANOVA. Metabolite abundance determined by normalising ion counts to norvaline and calculating relative to wild-type.

An additional observation, was the substantial ^{13}C incorporation into glutamate (Figure 2.12B) and succinate (Figure 2.12C) from [U-$^{13}C_5$]-glutamine in *Sdhb* KO cells. Increased expression of SLC25A13 (Fig 2.7), for transport of mitochondrial aspartate across the inner mitochondrial membrane to support biosynthetic purposes, may additionally contribute to the increase of flux into glutamate.

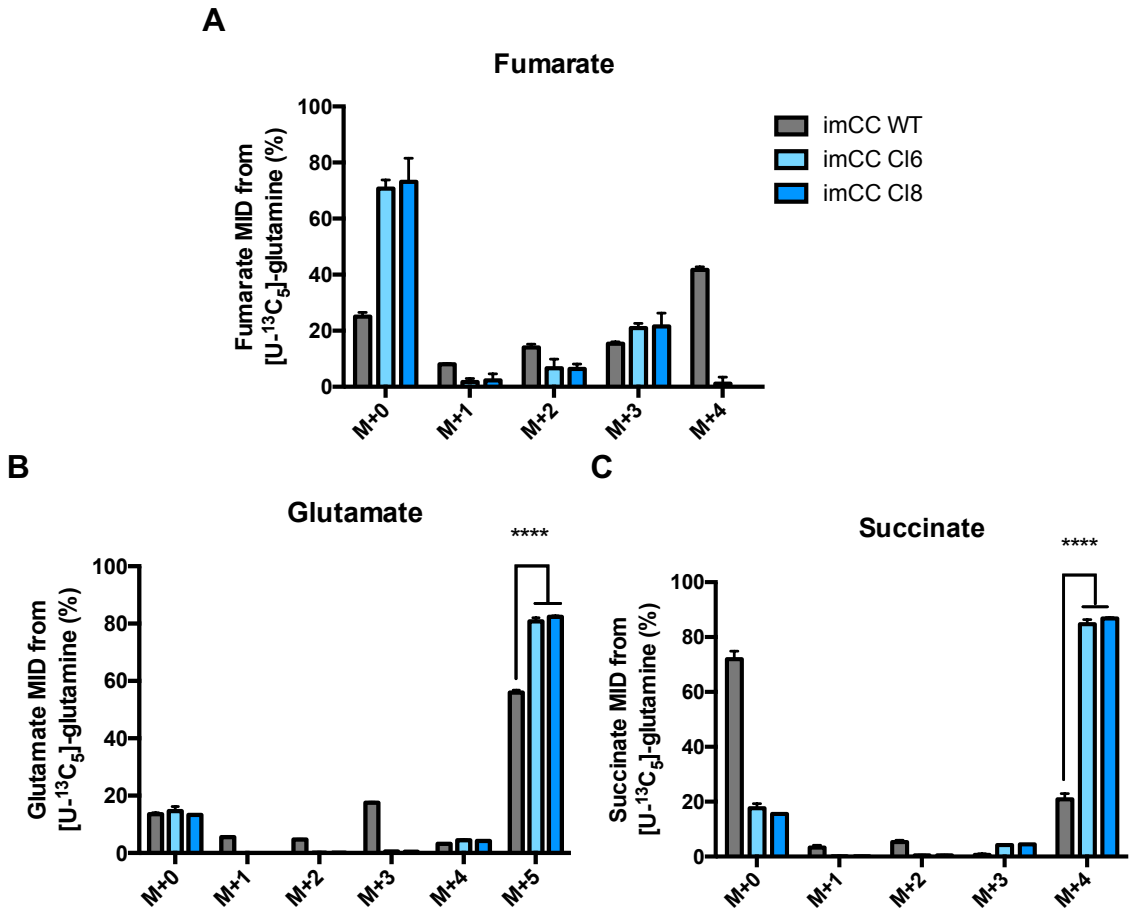

Figure 2.12 GC-MS data confirms the presence of reductive carboxylation. The presence of reductive carboxylation in *Sdhb* KO is confirmed by virtue of (A) increased M+3 fumarate. As PC activity is high, the labelling in M+3 fumarate from reductive carboxylation is likely diluted by mitochondrial fumarate from glucose. High M+5 glutamate (B) and M+4 succinate (C) from [U-$^{13}C_5$]-glutamine in KO cells suggest decreased oxidative IDH flux. Note that all GC-MS data shows the mass isotopolgues distribution (MID) from [U-$^{13}C_5$]-glutamine, presented mean +/- SD and performed in technical triplicate. Statistical significance determined using ordinary one-way ANOVA.

Non-essential amino acid metabolism is highly perturbed in *Sdhb* deficient cells

In addition to differential ^{13}C incorporation into NEAAs aspartate and glutamate, analysis of ^{13}C incorporation into serine and proline revealed potential differences in their usage or synthesis between wild-type and *Sdhb* KO cells. An increase in [2,3-$^{13}C_2$]-serine was observed from [1,2-$^{13}C_2$]-glucose (Figure 2.13A), in parallel with a decrease in steady-state serine concentrations (Figure 2.13B) in *Sdhb* imCC KO cells and SDH-mutated PCC (Figure 2.13C), suggesting a change in the rate of serine synthesis and use.

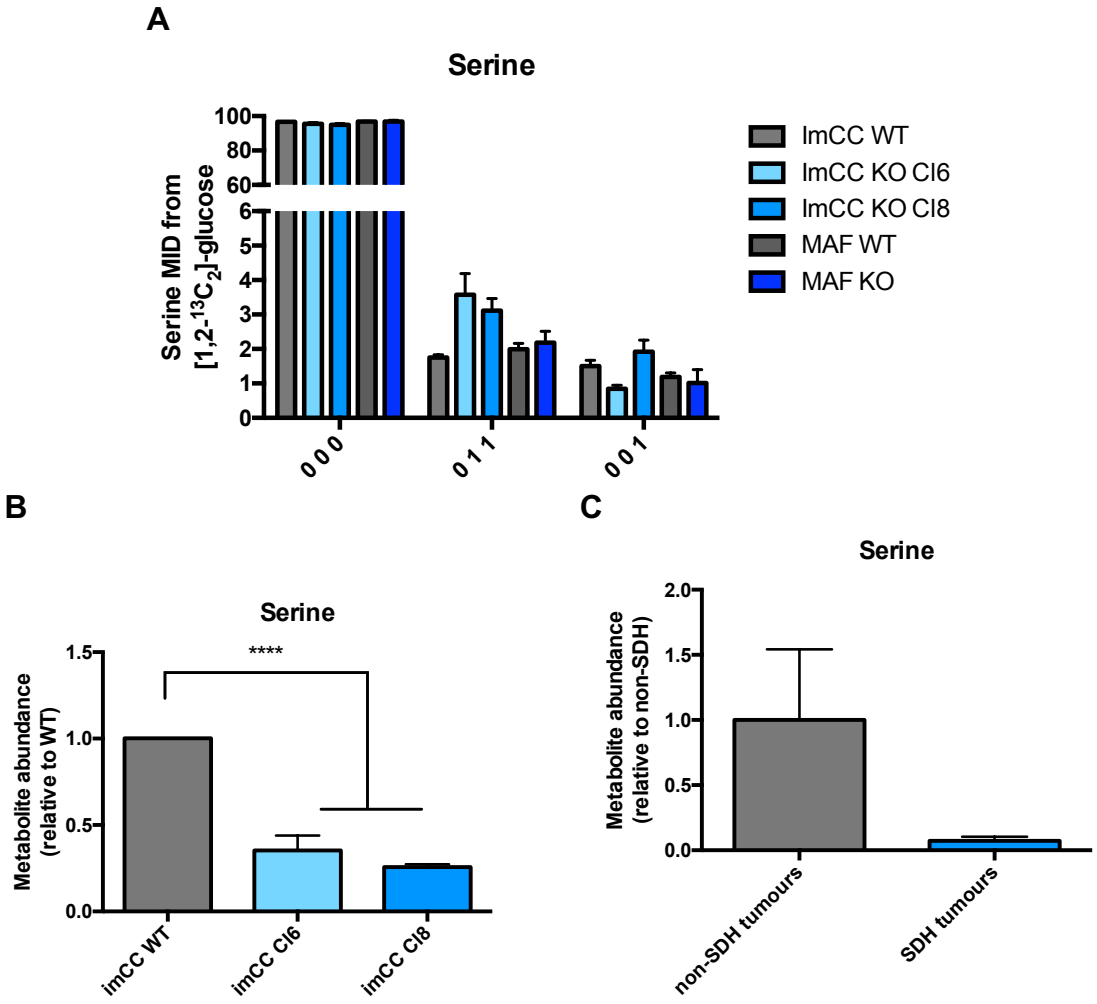

Figure 2.13 Loss of SDH activity increases usage of the serine synthesis pathway. Increased ^{13}C incorporation is observed into [2,3-$^{13}C_2$]- and [3-$^{13}C_1$]-serine isotopomers after 24 h incubation with [1,2-$^{13}C_2$]-glucose, as identified by 2D ^{1}H,^{13}C-NMR spectroscopy (A). [3-$^{13}C_1$]-serine arises through activity of PPP. Data is mean +/- S.E.M from three biological replicates. Decreased steady-state values were observed in *Sdhb* KO imCC cells (B) and tumours (C) by GC-MS where data is mean +/- S.D from three technical triplicates. Significance determined using ordinary one-way ANOVA. Data suggestive of increased production and usage of serine.

This was supported by the increased expression of a number of enzymes involved in serine biosynthetic pathway (Figure 2.14A) in SDH-mutated tumours (Figure 2.14B)

and *Sdhb* KO cells (Figure 2.14C). Most noticeably, mitochondrial SHMT2 transcripts were significantly up-regulated in SDH mutated tumours.

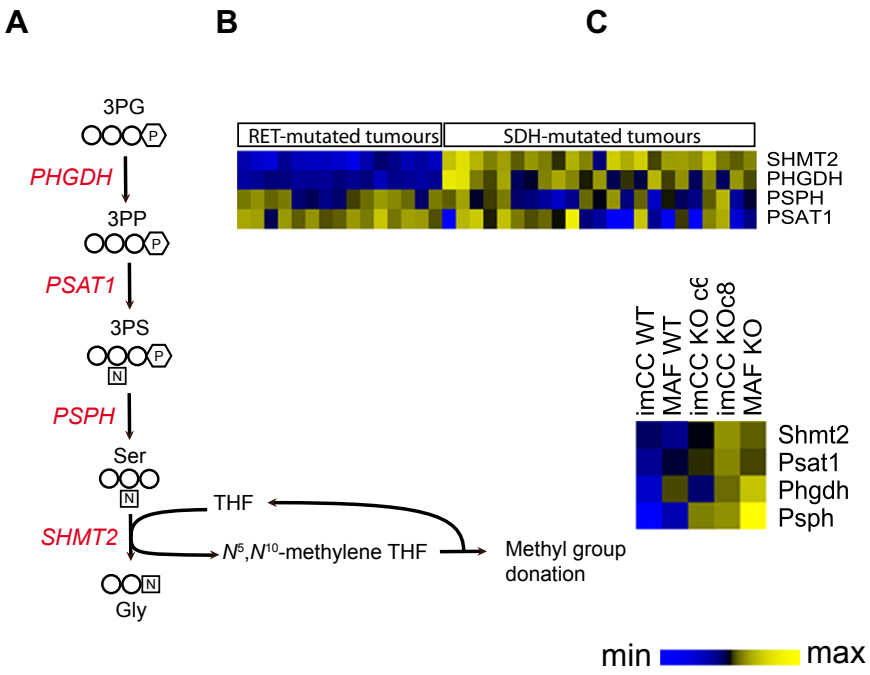

Figure 2.14 Loss of SDH increases expression of enzymes involved in the serine synthesis pathway. Expression of the serine biosynthetic enzymes (A) was assessed, and confirms an increase in expression if SDH-mutated tumours (B) and *Sdhb* KO cells (C), where SHMT2 was most noticeably increased in SDH-mutated tumours. Data is produced from Judith Favier's research group. Abbreviations: PHGDH, phosphoglycerate dehydrogenase; PSAT1, phosphoserine aminotransferase 1; PSPH, phosphoserine phosphatase; SHMT2, serine hydroxymethyltransferase 2 and THF, tetrahydrofolate.

Increased expression and activity of this enzyme is consistent with increased glycine concentrations in both SDH deficient cells (Figure 2.15A) and tumours (Figure 2.15B). Collectively, the data suggests that *Sdhb* KO cells significantly increase the synthesis of serine and its subsequent catabolism potentially to support anabolism, redox or epigenetic regulation.

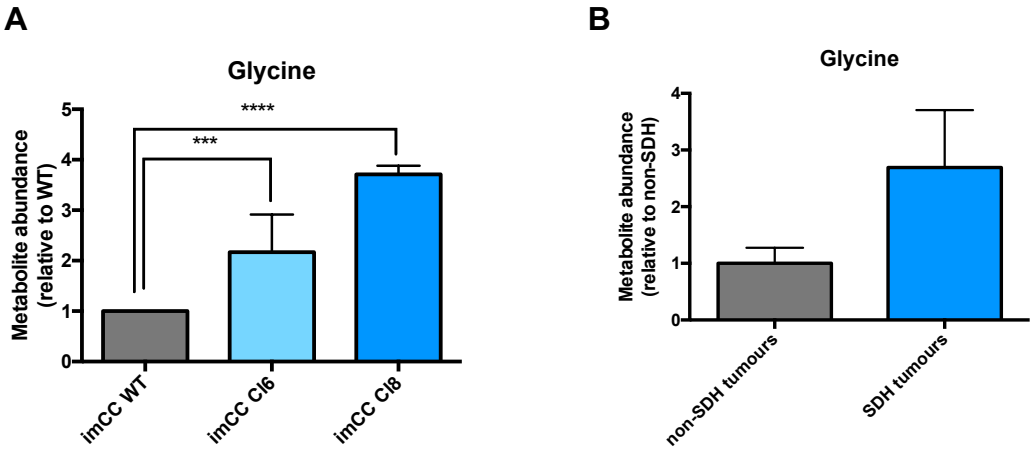

Figure 2.15 Increased glycine concentrations support increased usage of the serine synthesis pathway. Increased glycine concentrations in both cells (E) and tumours (F) confirmed an increase in pathway usage. Data is mean +/- S.D from three technical triplicates. Significance determined using ordinary one-way ANOVA.

Proline, one of the major amino acids synthesised from glutamine, revealed different isotopomer distributions between wild-type and *Sdhb* KO cells from the analysis of both [1,2-$^{13}C_2$]-glucose and [U-$^{13}C_5$]-glutamine polar extracts. While both [U-$^{13}C_5$]- and [1,2,3-$^{13}C_3$]-proline isotopologues from [U-$^{13}C_5$]-glutamine were found in wild-type cells, only [U-$^{13}C_5$]-proline was detected in *Sdhb* KO cells and was found to be increased (approximately 5% over 24 hours) (Figure 2.16A). This is consistent with the ^{13}C labelled proline exported into the medium (Figure 2.16B), where almost three times the amount of proline (both labelled and unlabelled) was exported in *Sdhb* KO cells. Steady-state proline concentrations reflect this observation, where increased proline was determined in *Sdhb* KO cells (Figure 2.16C) (although this was inconsistent between the clones) and SDH-deficient tumours (Figure 2.16D).

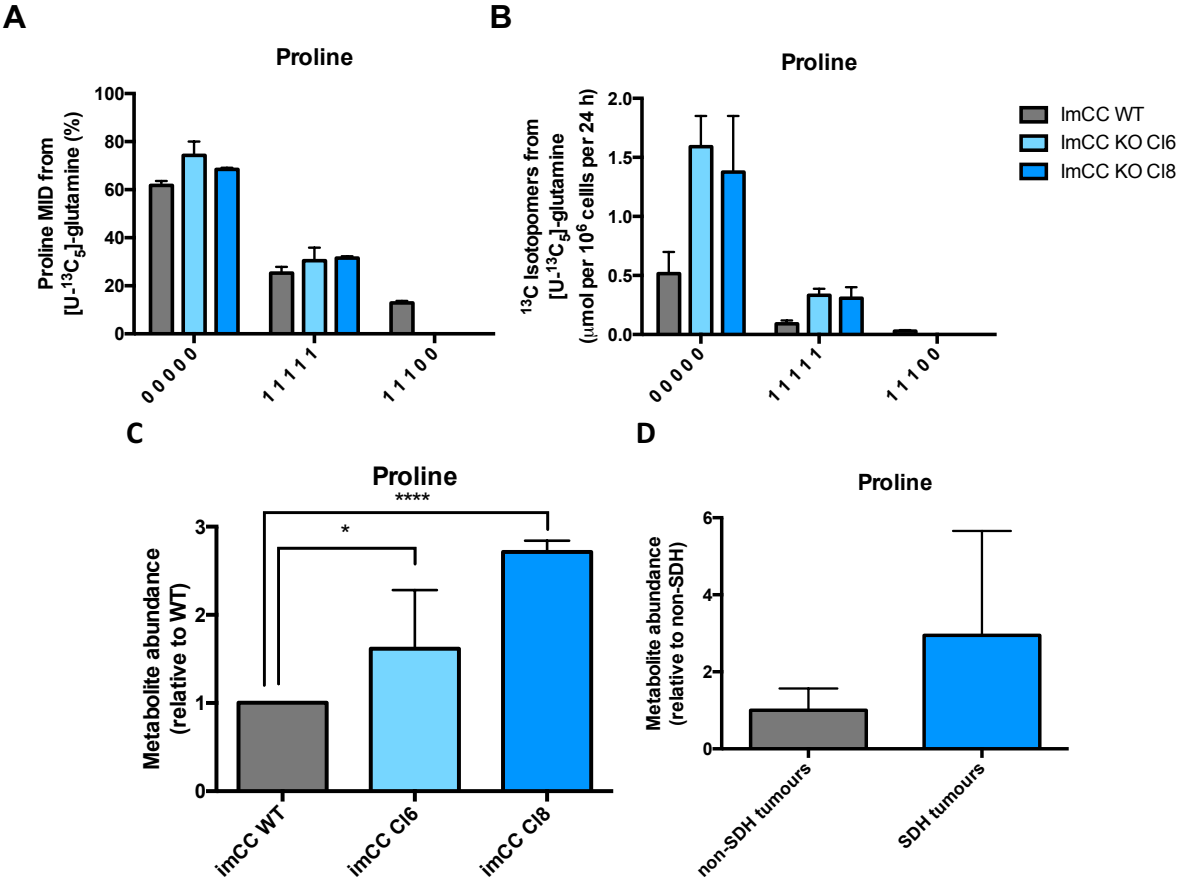

Figure 2.16 Loss of SDH activity increases glutamine-derived proline biosynthesis and extracellular export. Proline biosynthesis from glutamine (A) shows an increase in [U-$^{13}C_5$]-proline in imCC *Sdhb* KO cells and no [1,2,3-$^{13}C_3$]-proline owing to the block in TCA cycle activity. Significant amounts of proline (both labelled and unlabelled) are exported into the medium of imCC *Sdhb* (B). Data are mean +/- S.E.M from three biological replicates. Proline concentrations are increased in cells (C) although not consistent between clones, and in tumours (D). Data are mean +/- S.D from technical triplicates. Significance determined using unpaired student's t-test.

In addition, there was significant up-regulation in gene expression of pyrroline 5-carboxylase reductase 1 (PYCR1), the principle enzyme responsible for the reduction of pyrroline 5-carboxylate into proline, in *Sdhb* KO cells and SDH-mutated tumours (Figure 2.17), supporting the observed increase in glutamine-derived proline biosynthesis.

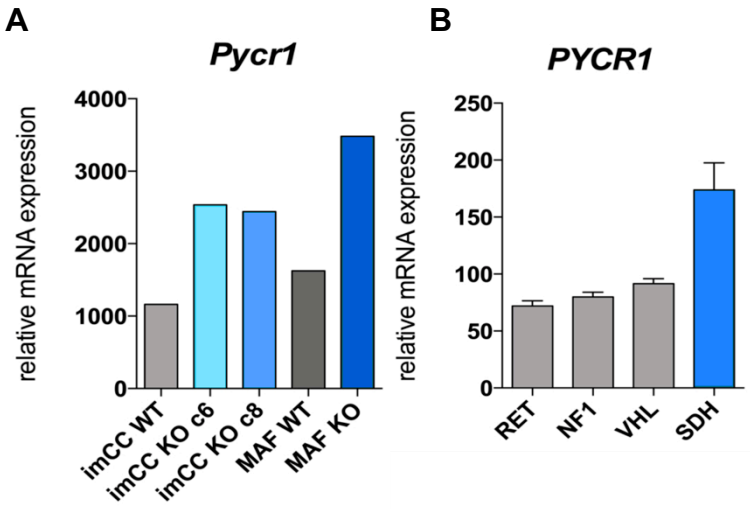

Figure 2.17 Loss of SDH activity increases glutamine-derived proline biosynthesis and extracellular export. The observed increase in glutamine-derived proline biosynthesis is supported by the increase in gene expression of pyrroline-5-carboxylate 1 (PYCR1) – the rate limiting step in proline biosynthesis – in *Sdhb* deficient cells (A) and SDH-mutated tumours (B). Data from Judith Favier's research group.

No isotopomers of proline were identified from [1,2-$^{13}C_2$]-glucose in *Sdhb* KO cells (Figure 2.18A), presumably as a considerable amount of glucose carbon is directed towards aspartate synthesis through the activity of PC. GC-MS data confirmed a decrease in labelling from glucose (Figure 2.18B), which was in accordance to that of glutamate (Figure 2.18C).

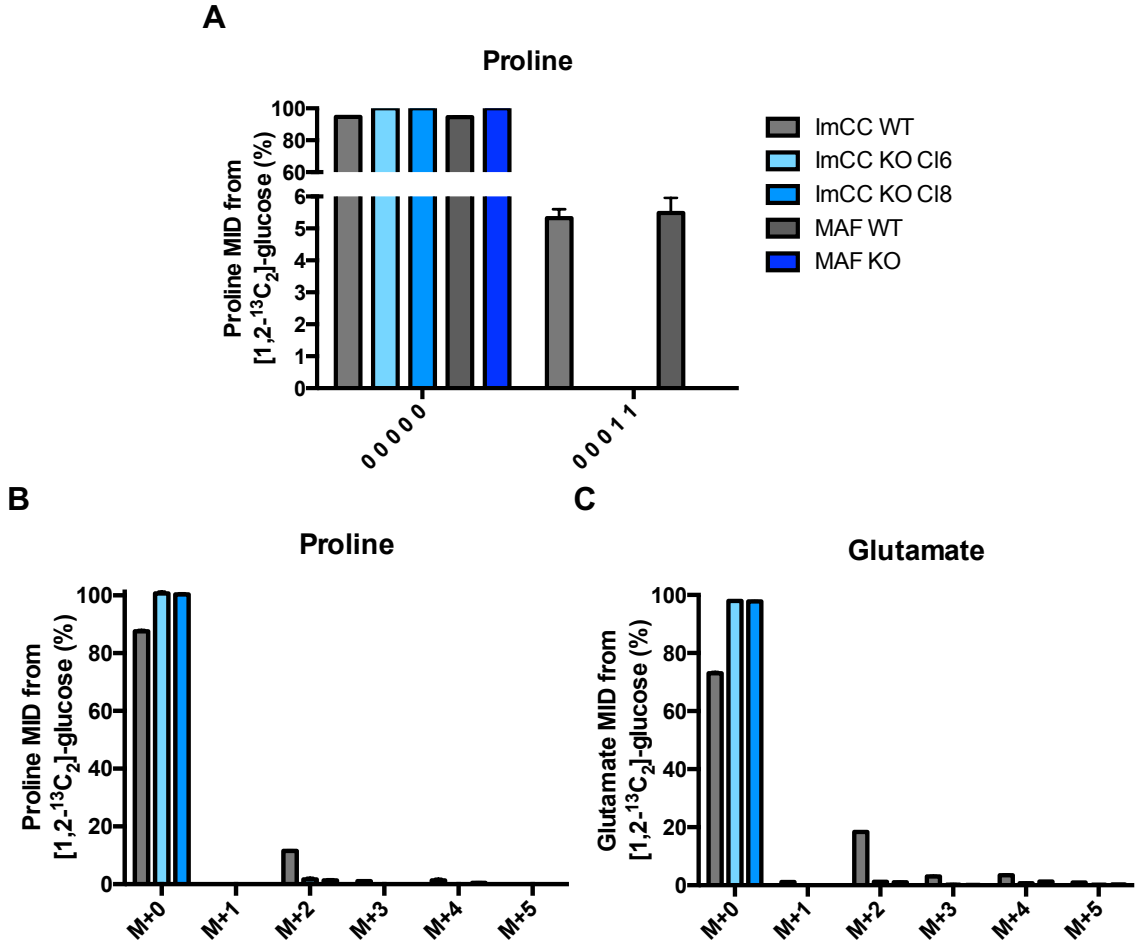

Figure 2.18 Increased proline biosynthesis from glucose is not observed in *Sdhb* deficient cells. Proline is not detected in *Sdhb* KO cells after 24 h incubation with [1,2-$^{13}C_2$]-glucose by NMR spectroscopy (A) or GC-MS (B), which is also supported by the mass isotopologue distribution (MID) of glutamate (C). NMR data is mean +/- S.E.M from three biological replicates, whereas GC-MS data is mean +/- S.D from three technical replicates.

Our results suggest that the majority of proline is synthesised from glutamine in *Sdhb* KO cells, and the increased synthesis of proline is likely to exceed biomass production as it is exported in significant proportions into the culture medium.

Discussion

PGL/PCC presents an ideal genetic model to study how cancer cells deficient in SDH activity reprogram mitochondrial metabolism to sustain proliferation. Inactivation of SDH and loss of mitochondrial function *per se*, along with the subsequent development of a pseudohypoxic phenotype as a result of succinate accumulation has been well established. However, the direct effects of metabolic transformation owing to a loss in SDH activity were as yet uncharacterised.

The metabolic tracer studies demonstrate that there is considerable metabolic rewiring of mitochondrial pathways, as a result of a truncated TCA cycle. *Sdhb* deficient cells increase PC-dependent carboxylation of pyruvate to synthesise oxaloacetate for the production of aspartate (Figure 2.4). These findings are consistent with recent publications using a primary *Sdhb*-ablated epithelial kidney cell line (Cardaci et al. 2015). As inhibition of this biosynthetic pathway results in a loss of proliferation and viability, it is clear that SDH-deficient cells are highly dependent on mitochondrial aspartate production. Aspartate is a major precursor for protein and nucleotide biosynthesis, as well as the synthesis of NEAAs arginine and asparagine. As aspartate is among one of the least abundant amino acids circulating in human plasma (Mayers & Vander Heiden 2015), and is inefficiently transported into most mammalian cells (Birsoy et al. 2015), *de novo* synthesis is required for cell growth and proliferation. The loss of metabolic plasticity means that PC-mediated aspartate biosynthesis is likely to determine the anabolic and proliferative state of the cell. This

cellular vulnerability therefore presents as an ideal way to therapeutically target these tumours.

Traditionally a gluconeogenic enzyme, PC is expressed in a tissue-dependent manner, where greatest expression occurs in the liver and kidney. It uses a covalently attached biotin cofactor to catalyse the ATP-dependent carboxylation of pyruvate to oxaloacetate in the presence of magnesium and is allosterically regulated by levels of acetyl CoA and aspartate. Acetyl CoA enhances the rate of biotin carboxylation and therefore positively regulates PC activity, whereas aspartate is thought to inhibit PC activity by repressing the PYC1 promoter (Jitrapakdee et al. 2008). As the induction of PC activity is not universal to all hypoxic tissues, it may therefore be induced by the low intracellular levels of aspartate as identified in SDH deficient cells (Figure 2.11B) and tissues (Figure 2.11D) rather than the direct development of “pseudohypoxia” itself.

For aspartate to be used for biosynthetic purposes in the cytosol, it must be exported out of the mitochondria. Our results suggest that the expression of the aspartate-glutamate antiporter SLC25A13 is increased with SDHB deficiency (Figure 2.7). SLC25A13 is one of two solute carrier family 25 transporters responsible for exporting mitochondrial aspartate into the cytosol. Unlike SLC25A13, which is widely expressed, with greatest expression in the liver, SLC25A12 is found mainly in heart, skeletal muscle and brain (Del Arco et al. 2000; Palmieri et al. 2001). Use of either aspartate-glutamate transporter would further import glutamate into the mitochondria,

which would partially be removed through the increased activity of mitochondrial aspartate aminotransferase (GOT2) to convert PC-derived oxaloacetate to aspartate.

In *Sdhb* deficient cells, which exhibit reduced PDH activity (Figure 2.4A), and therefore reduced acetyl CoA production from glucose, it may be possible that an alternative pool of mitochondrial acetyl CoA exists. This could be produced from an external source such as β-oxidation, which would yield numerous reducing equivalents in the mitochondria to drive ATP production under normal SDH function. Alternatively, *Sdhb* deficient cells could utilise reductive glutamine metabolism to produce citrate, thereby bypassing the activity of citrate synthase. Despite evidence to support the presence of reductive glutamine metabolism in *Sdhb* deficient cells (Figure 2.9C, 2.10, 2.12A), activity of this pathway appears to be so rapid that metabolite steady-state levels remain low, and therefore do not fully compensate for the lack of oxidative TCA cycle activity. The absence of detectable ^{13}C incorporation in malate, aspartate and citrate from [U-$^{13}C_5$]-glutamine resulted in a suspected lack of sensitivity in the NMR approach, and the need for the use of GC-MS to take advantage of its enhanced sensitivity. Although, findings using GC-MS were consistent with the NMR results, with none of the above metabolites detected. Activity of this pathway is unlikely to exceed the reliance of *Sdhb* deficient cells on mitochondrial PC activity for endogenous aspartate synthesis.

In the absence of SDH activity, there is likely to be an increase in glutamate carbon and nitrogen within the mitochondria, owing to both a block in TCA cycle activity and as a result of increased aspartate export by GOT2. Increased biosynthesis of proline

from glutamine may provide a means to remove excess glutamate from the mitochondrion. As mitochondrial proline biosynthesis from glutamine is a highly redox-regulated pathway that requires the use of 2 NAD(P)H, increased use of this pathway may also be an important way in which these cells support cellular redox homeostasis. Increased NADH/NAD^+ is likely to occur as a result of decreased ETC function, as is thought to be the case for hypoxic cells. Increased use of this pathway could remove excess NADH from the mitochondrion, in addition to glutamate. The most striking observation regarding proline however, was its high extracellular export in *Sdhb* deficient cells (Figure 2.16B). Our results suggest that proline is produced in amounts exceeding biomass requirements and secretion may act to remove excess NADH and glutamate in *Sdhb* deficient cells.

Like lactate, proline export may have a functional role within a larger system of metabolic cooperation and symbiosis between tumour cells and the microenvironment (Nakajima & Van Houten 2013). In addition to regulating redox, extracellular export of proline could also be used by surrounding stromal cells as a source of energy. This “two compartment” model of tumour metabolism may further stimulate tumour proliferation and metastasis, as reported in breast cancer cells and their neighbouring fibroblasts (Martinez-Outschoorn et al. 2011; Sotgia et al. 2011) and ovarian cancer cells and their neighbouring adipocytes (Nieman et al. 2011). Interestingly, PYCR1 has been identified as a major driver of metastatic invasive breast carcinoma (Possemato et al. 2011).

As collagen in the extracellular matrix (ECM) is primarily comprised of proline residues, extracellular export of proline could support increased collagen synthesis. Interestingly, a key step in collagen production is to ensure correct folding and secretion by the hydroxylation of proline residues catalysed by collagen prolyl 4-hydroxylases (cP4H). It has been recently shown in hypoxic breast cancer cells that HIF1 activates the transcription of genes encoding cP4Hs, which are critical for collagen deposition and promotes cancer cell alignment resulting in enhanced invasion and metastasis (Gilkes et al. 2013). Owing to the pseudohypoxic phenotype reported in SDH deficient tumours, it may be interesting to see whether SDH deficient tumours do indeed accumulate collagen deposits, and whether this contributes to the invasive and metastatic phenotype reported in the majority (50-97%) of SDHB mutated tumours (Fliedner et al., 2010).

Our metabolomics, transcriptomics and isotope tracing analyses suggest that *Sdhb* deficient cells increase *de novo* serine synthesis and catabolism from glucose. It is unlikely that the low steady-state concentrations of serine (Figure 2.13B and 2.13C) in *Sdhb* deficient cells are due to decreased or dysfunctional serine uptake from the culture medium, as the numerous serine antiporters that exist for extracellular serine uptake are thought to be active even at steady-state (DeNicola et al. 2015). In addition, it has been shown that cells with PHGDH amplification, as appears to be the case for SDH-mutated tumours (Figure 2.14B) and cells (Figure 2.14C), require flux through the SSP even when serine is available (Possemato et al. 2011). Usage of this metabolic pathway could be increased in *Sdhb* KO cells to sustain nucleotide synthesis and/or mitochondrial NAD(P)H production in the absence of a fully

functional TCA cycle. It could also be up-regulated to provide methyl groups required for biosynthesis, or even DNA and histone methylation, which is consistent with the hypermethylation profile observed in this tumour type (Letouzé et al. 2013).

Previous studies have identified the importance of serine catabolism for supporting redox homeostasis in hypoxia (Ye et al. 2014). The high expression of mitochondrial SHMT2 identified in SDH-mutated tumours (Figure 2.14B) and cells (Figure 2.14C) indicates a potential requirement of mitochondrial NADPH production from serine catabolism to support redox homeostasis. Reports have shown that loss of SDHB leads to increased mitochondrial ROS production (Guzy et al. 2008), which may therefore create an increased demand for NADPH. The increase in PPP activity observed by virtue of an increase in [3-$^{13}C_1$]-lactate from [1,2-$^{13}C_2$]-glucose (Figure 1.2C) in the culture media of *Sdhb* deficient cells, along with the detection of [2,3-$^{13}C_2$]-lactate production from [U-$^{13}C_5$]-glutamine (Figure 1.9C) using the activity of cytosolic ME1, may be evidence of this putative increase in NADPH production. It could be possible that our results for increased serine synthesis and catabolism also support this putative increase in NADPH demand.

It is becoming increasingly clear that the TCA cycle is not necessarily a cycle, but a series of linear reactions required by the cell for biosynthetic demands. The integration of diverse carbon sources and conversion of one carbon source to another in mitochondria means that the cells do not completely rely on exogenous nutrient sources for cell proliferation and repair. Collectively, these data provide insight into how the reprogramming of mitochondrial aspartate biosynthesis through

the activity of PC could be exploited to mitigate the growth of SDH-deficient tumours (Figure 2.19).

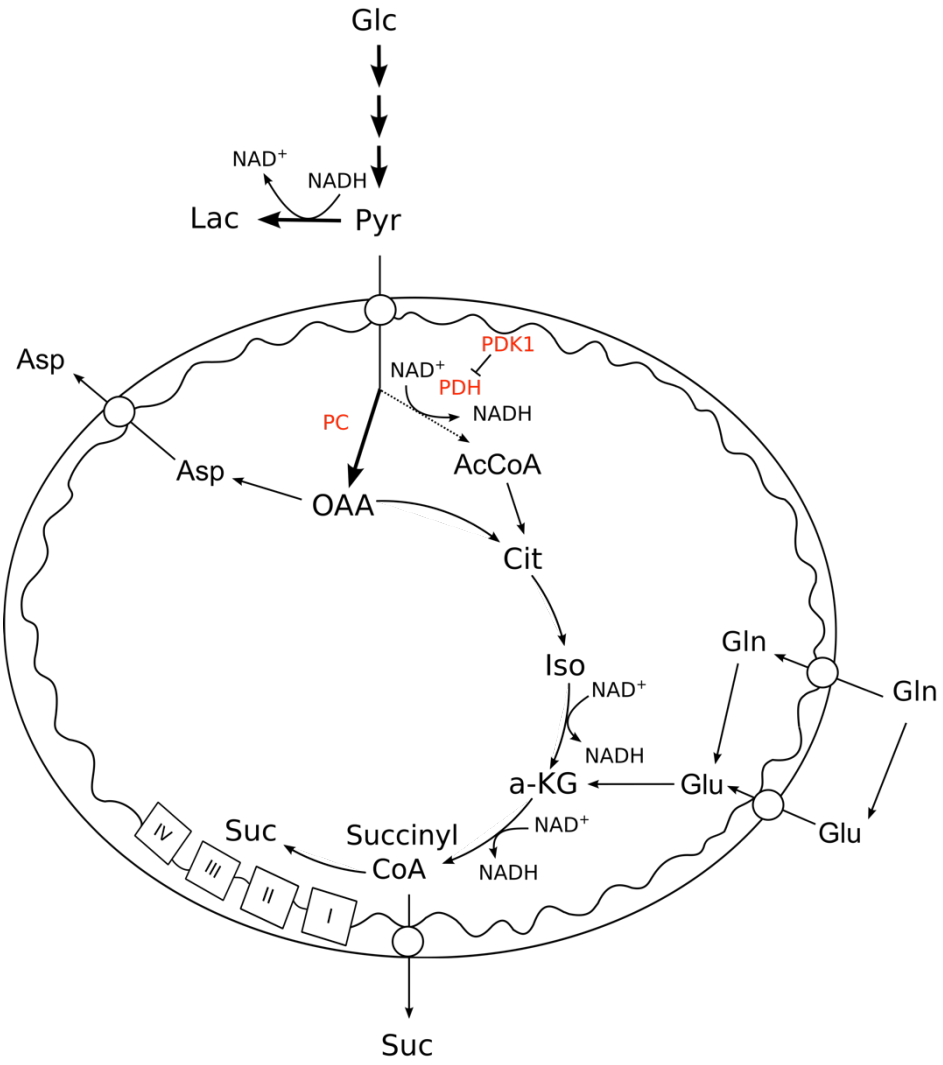

Figure 2.19 Summary of succinate dehydrogenase deficient cell metabolism. As a result of a truncated TCA cycle, SDH deficient cells increase PC-mediated aspartate biosynthesis, which is essential for proliferation and viability. Abbreviations: AcCoA, acetyl CoA; Asp, aspartate; Cit, citrate, Glc, glucose; Glu, glutamate; Gln, glutamine; Iso, isocitrate; a-KG, α-ketoglutarate; Lac, lactate, OAA, oxaloacetate; Pyr, pyruvate; PC, pyruvate carboxylase; PDH, pyruvate dehydrogenase; PDK1, pyruvate dehydrogenase kinase 1 and Suc, succinate.

Experimental Procedures

Patient Information

In collaboration with Judith Favier

Tumour samples were collected prospectively by the French 'Cortico et Médullosurrénale: les Tumeurs Endocrines' (COMETE) network and ethical approval for the study was obtained from the institutional review board [Comité de Protection des Personnes (CPP) Ile de France III, June 2012]. Written informed consent for the sample collection and subsequent analyses was obtained from all patients. The procedures used for PCC/PGL diagnosis were in accordance with both internal and international clinical practice guidelines (Plouin PF, Gimenez-Roqueplo AP n.d.; Lenders et al. 2014).

Diagnosis was confirmed by histology in each case. A total of 202 consecutive cases of PCC/PGL, recruited over 15 years (1993-2008), were included in the study. Fresh tumour samples collected during surgery were immediately frozen and stored in liquid nitrogen until processing. Formalin-fixed paraffin-embedded tissues were used for immunohistochemical analyses.

Cell Lines

Immortalised mouse chromaffin cells (imCC) and mouse adrenal fibroblast cells (MAF) were kindly donated by Dr Judith Favier and cultured in GIBCO® high glucose DMEM (Dulbecco's modified Eagles Medium) containing 2 mM GlutaMAX and 1 mM pyruvate (ThermoFisher Scientific, 10569044), supplemented with 10% FBS (foetal

bovine serum) (Thermo Fisher Scientific, 10270-106) (Letouzé et al. 2013; Lussey-Lepoutre et al. 2015).

Cell lines were maintained using standard procedures in a 37°C humidified incubator, 5% CO_2 and regularly tested and excluded for mycoplasma contamination using PCR Mycoplasma Test kit I/C (PromKine, PK-CA91-1048).

Gene expression data

In collaboration with Judith Favier

Gene expression profiles of 186 PPC/PGL tumours available from a previous study were genotyped for the presence or the absence of germline and somatic mutations in well-known PCC/PGL susceptibility genes (Burnichon et al. 2011). In total, 23 SDHx, 38 VHL, 30 NF1, 14 RET, 1 TMEM127, 3 MAX, 6 HRAS, 3 MET, 65 sporadic, 1 NF1/MET, 1 RET/HRAS and 1 TP53/CDKN2A/MET were identified (Castro-Vega et al. 2015). HG-U133 Plus 2.0 Affymetrix GeneChip data from this previous study are available online as ArrayExpress entry E-MTAB-733 (http://www.ebi.ac.uk/arrayexpress/) (Castro-Vega et al. 2015).

Gene expression profiles of imCC and MAF cell lines were assessed in duplicates using the GeneChip® Mouse Gene 1.0 ST Array. Data are available as ArrayExpress entry E-MTAB-3403.

Immunohistochemistry

In collaboration with Judith Favier

6 µM sections cut from 27 paraffin-embedded tumour samples were mounted on SuperFrost® Plus slides (ThermoFisher Scientific, 10143560). The following

antibodies and a standard procedure were used for immunohistochemistry40 with Histogreen as a chromogen:

Table 2.1 Antibodies employed for Immunohistochemistry staining of pyruvate carboxylase and the aspartate-glutamate transporter

Antibodies	Supplier	Product Code	Dilution	Antigen Retrieval
Anti-PC	Abcam	Ab115579	1:100	Boil slides in Tris-EDTA buffer (pH 9.0)
Anti-SCL25A13	Abcam	Ab156010	1:50	Boil slides in citrate buffer (pH 6.0)

Images were acquired with a Leica DM400B microscope with Leica Application Suite software version 2.8.1, and a Leica DFC420C camera (Leica).

RNA Silencing

In collaboration with Judith Favier

To assess the knockdown in expression of PC, 5 x 10^4 cells were seeded onto 12-well plates in standard culture conditions. After 24 h, cells were transfected following manufacturer's instructions with 150 ng of Silencer Select Pre-designed siRNA against PC (Thermo Fisher, siRNA references s71354 and s71355) or Silencer Select negative control (Thermo Fisher, 4390843) using Lipofectamine® RNAiMax reagent (Thermo Fisher, 13778) as described by the manufacturer. 48 h post transfection, cells were passaged and efficiency of gene extinction was evaluated by immunofluorescence and RT-qPCR. Passaged cells were re-transfected 24 h later to maintain long-term extinction.

Quantitative real-time PCR

In collaboration with Judith Favier

Total RNA was extracted using the mini RNeasy kit (Qiagen, 74104) according to manufacturer's protocol. 500 ng RNA per sample was subjected to reverse transcription (RT) using the iScript cDNA Synthesis Kit (Bio-Rad, 1708890). qPCR (SybrGreen) was performed with 10 ng of cDNA preparation and the iTaq Universal SYBR Green Supermix (Bio-Rad, 172-5120) in a CFX96 Real Time PCR machine (Bio-Rad). The following primers and probes were used:

Table 2.2 Primers for pyruvate carboxylase isoforms 1 and 2

#	Primer	Sequence	Target	Isoform	Exon	Species	Application
206	Pcx-E13_F1	GATCCTGCTGTTCCTGTGGT	Pcx	1 and 2	ex13 (isoform1) or ex12 (isoform2)	Mouse	qPCR (SybrGreen)
207	Pcx-E14_R1	TAGGGCGCAATCTTTTTGAG	Pcx	1 and 2	ex14 (isoform1) or ex13 (isoform2)	Mouse	qPCR (SybrGreen)

The expression of PC in each sample was normalised to Ubiquitin C as housekeeping gene. Comparative analysis across samples was calculated using the $2^{-\Delta\Delta CT}$ method.

Immunofluorescence

In collaboration with Judith Favier

Cells were seeded at 5 x 10^4 onto glass coverslips (Thermo Scientific, 1014355) and left overnight. Cells were washed in 1x PBS and fixed for 20 min in ice-cold paraformaldehyde 4% and permeabilised and blocked in 1% BSA, 0.1% Triton for 30 min. The following antibodies were used:

Table 2.3 Antibodies against pyruvate carboxylase employed in immunofluorescence microscopy

Primary antibody	Anti-PCB antibody	Abcam	Ab110314	1:100	Overnight incubation at 4^{o}C
Secondary antibody	Alexa Fluor 488 Goat anti-mouse IgG	Invitrogen	A28175	1:2000	1 h incubation at room temperature in the dark

Slides were mounted in Vectashield® mounting medium with DAPI, and acquisitions were performed using Axioimager ZI Zeiss, with apotome system.

Proliferation

In collaboration with Judith Favier

Cells were seeded at 5 x 10^4 onto 6-well plates under standard culture conditions. Cell were transfected 24 h post seeding as described and passaged until confluence was reached on 10 cm dishes. Growth curves were established by counting cells every 48 h post transfection for a total of 8 days. Experiments were performed three times in duplicate.

NMR Spectroscopy

6 × 10^6 ImCC and MAF cells were plated onto two 15 cm dishes and cultured in standard medium for 24 h, where it was then replaced with fresh DMEM (no glucose) supplemented with 1 mM sodium pyruvate and 10 mM [1,2-$^{13}C_2$]- D-glucose (Sigma-Aldrich, 453188), or DMEM (high glucose with pyruvate and no glutamine) supplemented with 2 mM [U-$^{13}C_5$]-L-glutamine (Sigma-Aldrich, 605166) for 24 h. For aspartate labelling, cells were cultured in standard medium supplemented with 0.1 mM [U-$^{13}C_4$]-L-aspartate (Sigma-Aldrich, 604852) for 48 h.

Cells were washed with ice-cold PBS and scraped in a pre-chilled acetonitrile-methanol-water (55:35:10) solution. The cell lysates were vortexed for 15 min at 4°C and immediately centrifuged at 15,000 x *g* for 15 min at 0°C. The polar fraction was aliquoted and evaporated to dryness using a SpeedVac concentrator for 5 h at 30°C. For the metabolomic extraction of conditioned media, 600 µl of an acetonitrile-methanol (60:40) solution was added to 200 µl of cell media, and then processed as described above. Extraction was performed on 3 different cultures for each labelling experiments.

Dried samples were resuspended in 60 µL 100 mM sodium phosphate buffer containing 500 µM TMSP [(3-trimethylsilyl)propionic-(2,2,3,3-d4)-acid sodium salt] and 10% D_2O, pH 7.0. Samples were vortexed, sonicated (5-15 min) and centrifuged briefly (x2), before transferred to 1.7mm NMR tubes using an automatic Gilson 215 Liquid Handler (Bruker Biospin).

1D-^{1}H NMR spectra and 2D-^{1}H,^{13}C-HSQC NMR spectra were acquired using a 600-MHz Bruker Avance III spectrometer (Bruker Biospin, UK) with a TCI 1.7 mm z-PFG cryogenic probe at 300 K. Spectral widths were set to 7,812.5 and 24,155 Hz for the ^{1}H and ^{13}C dimensions, respectively. 16,384 complex data points were acquired for the 1D-^{1}H NMR spectra and 512 complex data points were acquired for the ^{1}H dimension of 2D-^{1}H,^{13}C-HSQC NMR spectra. An exponentially weighted non-uniform sampling scheme was used for the indirect dimension. Here, 30% of 8,192 complex data points (2,458) were acquired. 128 transients were recorded for the 1D-^{1}H NMR spectra with a relaxation delay of 4 s, and two transients were recorded for the 2D-^{1}H,^{13}C-HSQC NMR spectra with a relaxation delay of 1.5 s. Each sample was automatically tuned, matched and then shimmed (1D-TopShim) to a TMSP line width

of <2 Hz prior to acquisition of the first spectrum. Total experiment time was ~15 min per sample for 1D-^{1}H NMR spectra and 4.5 h per sample for 2D-^{1}H,^{13}C-HSQC NMR spectra. 1D-^{1}H NMR spectra were processed using the MATLAB-based MetaboLab software (Ludwig & Günther 2011). All 1D data sets were zero-filled to 131,072 data points before Fourier Transformation. The chemical shift was calibrated by referencing the TMSP signal to 0 p.p.m. 1D spectra were manually phase corrected. Baseline correction was achieved using a spline function (Ludwig & Günther 2011). 1D-^{1}H NMR spectra were exported into Bruker format for metabolite identification and concentration determination using Chenomx 7.0 (ChenomxINC). 2D-^{1}H,^{13}C-HSQC NMR spectra were reconstructed using compressed sensing in the MDDNMR and NMRpipe software (Delaglio et al. 1995; Kazimierczuk & Orekhov 2011; Orekhov & Jaravine 2011). The final spectrum size was 1,024 real data points for the ^{1}H dimension and 16,384 real data points for the ^{13}C dimension. Analysis was performed using MetaboLab and pyGamma software was used in multiplet simulations (Smith et al. 1994). The methyl group of lactate was used to calibrate the chemical shift based on its assignment in the human metabolome database (Wishart et al. 2013).

Cell GC-MS

In collaboration with Christian Metallo

Cells were seeded onto 6-well plates and cultured in standard medium for 24 h. Media was then replaced by DMEM (high glucose with pyruvate, no glutamine) supplemented with 2 mM [U-$^{13}C_5$]-L-glutamine (Sigma-Aldrich, 605166) for 72 h.

At the conclusion of tracer experiments, culture media was aspirated and cells washed twice with 0.9% NaCl solution. Cellular metabolites were extracted in

methanol (-20°C): water (4°C): chloroform (-20°C), where 1 µg/well DL-norvaline (Sigma-Aldrich, N7502) was employed as internal standard in the polar fraction. Samples were vortexed at 4°C for 30 min and subsequently centrifuged at 14,000 x *g* for 15 min at 4°C. The polar fraction was aliquoted and dried by speed vacuum concentration at 2,000 RPM for 4 h at 30°C.

Derivatisation of polar metabolites has been previously described (Metallo et al. 2011; Lewis et al. 2014). Briefly, polar metabolites were derivatised to form methoxine-TBDMS (tert-butyldimethylsilyl) derivatives by incubation with 2% methoxyamine hydrochloride (Sigma-Aldrich, 226904) dissolved in Pierce™ pyridine (Thermo Fisher Scientific, 25104) at 37°C for 1-1.5 h followed by addition of MTBSTFA (*N*-methyl-*N*-(tert-butyldimethylsilyl)trifluoroacetamide) with 1% TBDMCS (tert-butyldimethylchlorosilane) (Sigma-Aldrich, 375934) incubated at 37°C for 30-60 min.

Derivatised polar samples were analysed by GC-MS using an Agilent 7890B gas chromatograph equipped with a 30 m DB-35MS capillary column (30 m x 0.25 mm i.d. x 0.25 µm) connected to an Agilent 5977A mass spectrometer. MIDs were determined by integrating metabolite ion fragments and corrected for natural abundance as previously described (Fernandez et al. 1996).

Metabolite ion counts were normalised to norvaline and isoleucine ion counts to normalise for varying derivatisation efficiency and cell number, respectively.

Tissue Triple Quadrupole GC-MS/MS

In collaboration with Judith Favier

Six snap-frozen tumour samples (1 SDHD, 2 SDHB, 2 NFI and 1 MAX-mutated) and six imCC samples (three WT and three KO) were processed by organic extraction with ethylacetate, derivatisation with N,O-bis(trimethylsilyl) trifluoroacetamide with 1% trimethylchlorosilane, and analysed by tandem mass GC on a GC-MS triple quadrupole (Scion TQ, Bruker Daltonics). Analytes were identified by retention time and mass spectrum in selected reaction monitoring mode based on standard spectral reference libraries.

Statistical Analysis

Samples sizes and reproducibility for each figure are denoted in the figure legends. Unless otherwise noted, all experiments are representative of at least three biologically independent experiments performed in technical triplicate, where error bars represent mean +/- S.E.M. Statistical significance was determined by either a one-way ANOVA or two-tailed Student's t-test using GraphPad Prism 6, where *P < 0.05; **P < 0.01; and ***P < 0.001.

Chapter 3 IDH1 MUTATIONS EXHIBIT PSEUDOHYPOXIC PROLINE METABOLISM

Introduction

Cytosolic IDH1 catalyses the reversible $NADP^+$-dependent oxidative decarboxylation of isocitrate to α-ketoglutarate (αKG). Recurrent heterozygous missense mutations in the IDH1 gene have been reported in the majority of LGGs and secondary GBMs, where they clinically present in younger patients and are associated with an improved prognosis (Parsons et al. 2008). Missense IDH1 mutations occur in the arginine residue at codon 132 (R132), which is most commonly replaced by a histidine residue (R132H) (Parsons et al., 2008, Yan et al., 2009b, Gravendeel et al., 2010) and results in a change of substrate specificity. Instead of the $NADP^+$-coupled oxidation of isocitrate to αKG, αKG is reduced to form the oncometabolite (R)-2HG, employing NADPH as a cofactor (Dang et al. 2009). The majority of studies have concentrated on the biological effects from the significant production of (R)-2HG, which has been shown to inhibit a number of αKG dependent dioxygenases, inducing changes in DNA and histone methylation (Turcan et al. 2012; Lu et al. 2012; Chowdhury et al. 2011; Figueroa et al. 2010) as well as collagen folding and maturation (M. Sasaki et al. 2012).

Similar to other cancer-associated mutations in mitochondrial metabolic enzymes, IDH mutations have been shown to perturb regulation of the HIF system. While mutations in SDH and FH unequivocally result in HIFα stabilisation and the activation

of hypoxic pathways despite the presence of oxygen, it is not yet conclusive whether IDH mutations promote (Zhao et al. 2009) or suppress (Koivunen et al. 2012) HIFα stabilisation, and may be context or cell-specific. Given the highly hypoxic nature of gliomas (Evans 2004; Collingridge et al. 1999; Søndergaard et al. 2002), where mutations in IDH1 are "selected" for, along with the defined role of wild-type IDH1 in hypoxic reductive carboxylation for *de novo* lipogenesis (Metallo et al. 2011; Wise et al. 2011), it remains unclear as to how mutations in IDH1 metabolically affect glioma progression. This is likely to be important, as not only does hypoxia itself alter redox, but altered substrate specificity by virtue of the IDH mutation also predisposes IDH mutated cells to a change in cellular redox. Employing tissue and IDH1 R132H cell models, we therefore sought through metabolomics methodologies and stable isotope tracers, to investigate how the metabolism of cells harbouring an IDH1 mutation differ to wild-type, and to address the potential interplay between hypoxia and mutant IDH1.

Results

IDH1 mutant gliomas are metabolically distinct from wild-type

To assess whether gliomas with mutated IDH1 exhibit a metabolism different to those with wild-type IDH1, an untargeted mass spectrometry analysis was performed on 25 tumour biopsy samples. The non-polar and polar fractions were analysed by ultra-high performance liquid chromatography (UHPLC) and GC-MS, respectively, and principle component analysis (PCA) was performed for each analytical platform. PCA is an unsupervised multivariate method, that compresses data to investigate biological significance, and naturally separates the data based on biological variance. Tumour tissue samples that are highly clustered therefore represent biologically similar tumour types, and those tumour samples that are segregated represent biologically distinct tumour types.

Figure 3.1 shows the acquired PCA plot (panel A) and sample number (panel B) for the analysis of the tumour samples by GC-MS, wherein each sample number corresponds to a different patient tumour sample. Tumour samples 4 and 12 were visibly segregated from the remaining tumour samples, distinguishing these samples as metabolically different, along with further clustering of two other subgroups in the remaining IDH1 wild-type tumour samples. Importantly, the QC samples were highly clustered, verifying the conditions of analysis. Reference to patient data confirmed the presence of mutant IDH1 in tumour samples 4 and 12 by immunohistochemistry, thus establishing this metabolomics methodology as a valid approach for segregating tumours based on IDH status. As segregation of IDH1 status was identified by the

analysis of the polar fraction by GC-MS, it is also evident that the IDH1 mutations significantly affect intracellular metabolism.

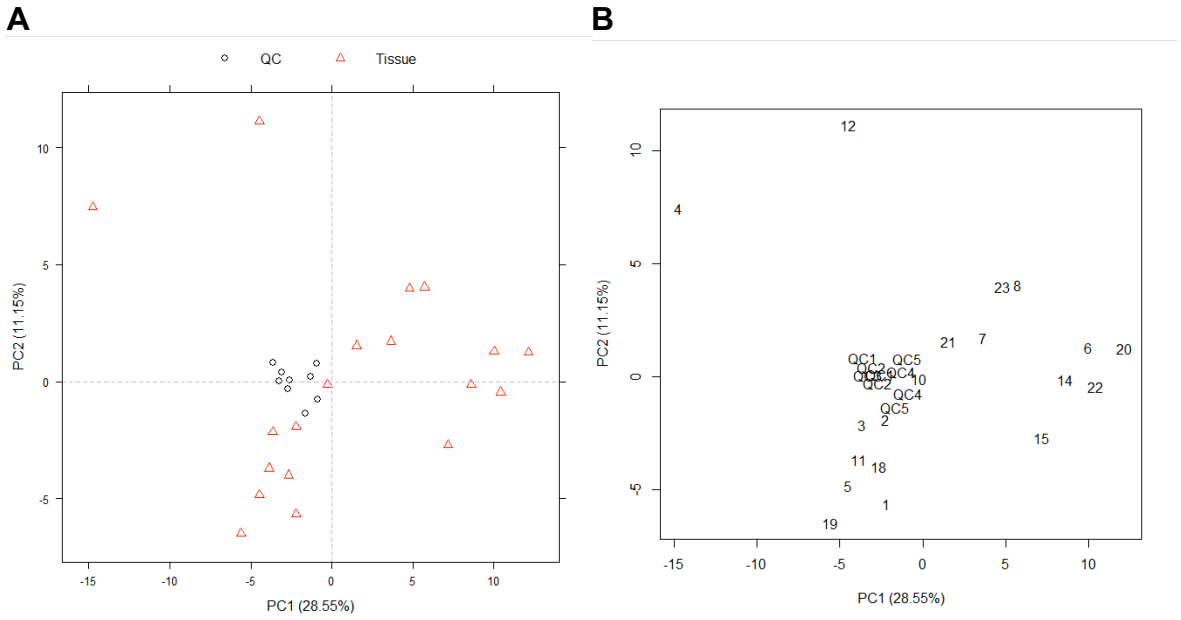

Figure 3.1 Tissue GC-MS segregates gliomas based on IDH1 status. (A) PCA and (B) sample number obtained for tissue GC-MS, which shows the segregation of tumour tissues (red triangles) and clustering of quality control (QC) samples (black circles). PC1 is the principle component with the most variation, and thus has a higher percentage compared to PC2. The PCA shows significant segregation of two IDH mutated tumour tissues, corresponding to patient tumour samples 4 and 12, from the remaining samples. The high biological variability is further illustrated by high clustering of Quality Control (QC) samples. Analysis performed by Warwick Dunn.

To better understand the alterations in tumour metabolism elicited by mutations in IDH1, metabolites responsible for the segregation of samples were identified by calculating the fold difference between the two IDH1 mutant tumours and the remaining wild-type tissue samples, where they were filtered for consistent changes of greater than 20% (Figure 3.2). As expected, the greatest change observed was elevation of 2HG, which was elevated at 117 and 43 fold in patient number 4 and 12,

respectively. In addition, amino acids, organic acids and glycolytic intermediates were detected, suggesting diverse metabolic differences between wild-type and mutant IDH1 tumours.

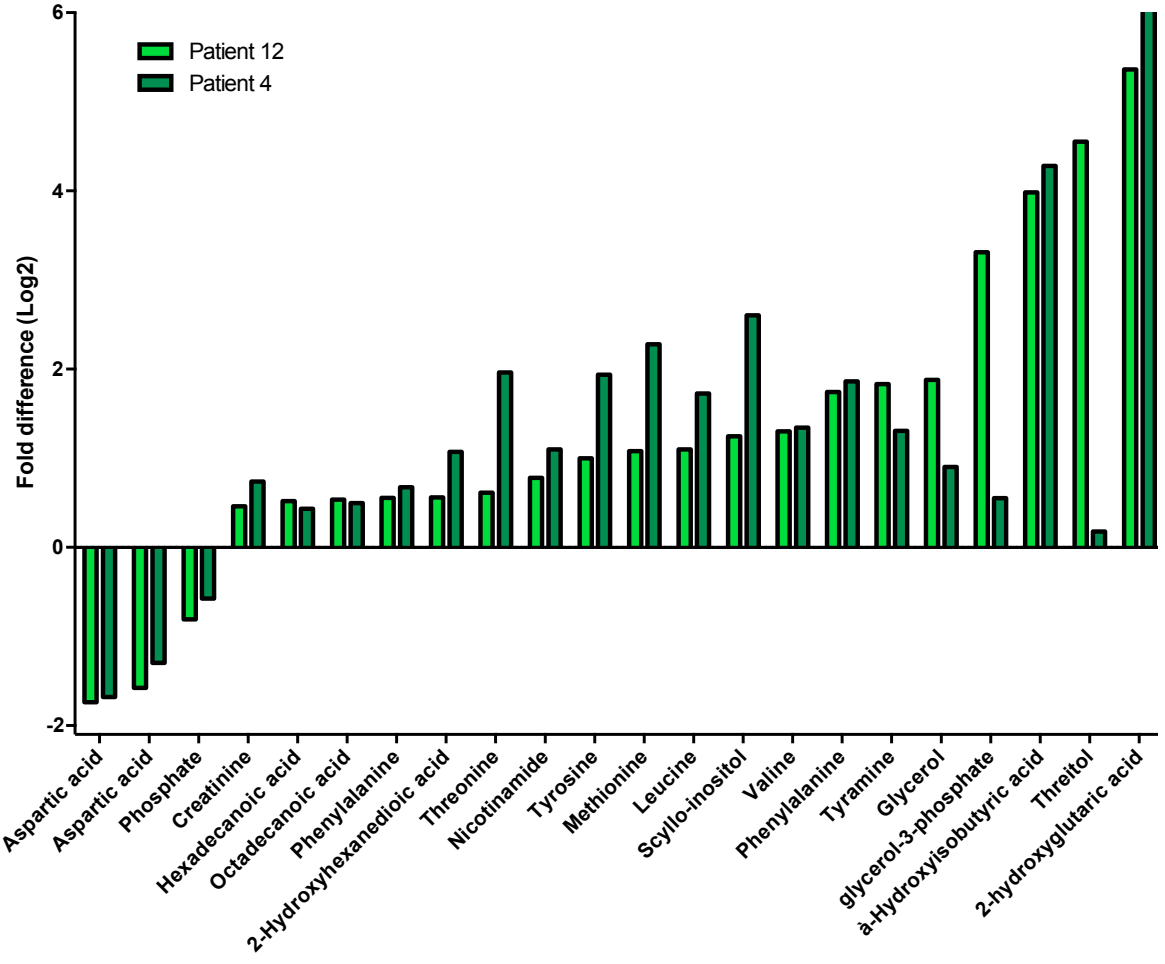

Figure 3.2 Metabolites responsible for the segregation of gliomas based on IDH1 status. Metabolites responsible for the segregation between IDH1 mutant and wild-type tumour samples were calculated, where the fold difference between IDH1 mutated patient 4 and 12 tumour samples and remaining wild-type tumour samples were calculated and filtered for consistent changes of >20% in both the IDH1 mutant samples. Those metabolites indicated twice represent the detection of different fragments.

IDH1 mutated cells do not metabolically adapt to hypoxia

The significant production of (R)-2HG in IDH mutant tumours has an ambiguous role in HIF biology, with reports claiming that (R)-2HG either causes competition inhibition (Zhao et al. 2009), or acts as a co-substrate (Koivunen et al. 2012), for the activity of PHDs. Furthermore, the importance of wild-type IDH1 function has been shown in hypoxic tumour metabolic remodelling for the provision of carbon in lipid synthesis (Metallo et al. 2011). As HIF is a major regulator of metabolism, and mutations in IDH1 would be predicted to affect hypoxic metabolic remodelling, we therefore sought to investigate the metabolic response of IDH1 mutated cells to conditions of low oxygen. To characterise the hypoxic metabolic phenotype of IDH1 mutant-expressing cells, an untargeted GC-MS analysis was employed using a U87 glioma cell line stably transfected with either wild-type IDH1 or IDH1 bearing the R132H mutation. Cells were exposed to normoxia or hypoxia for 24 hours, defined as 21% and 1% O_2 respectively, before extraction and analysis of the polar fraction, from which PCA was performed.

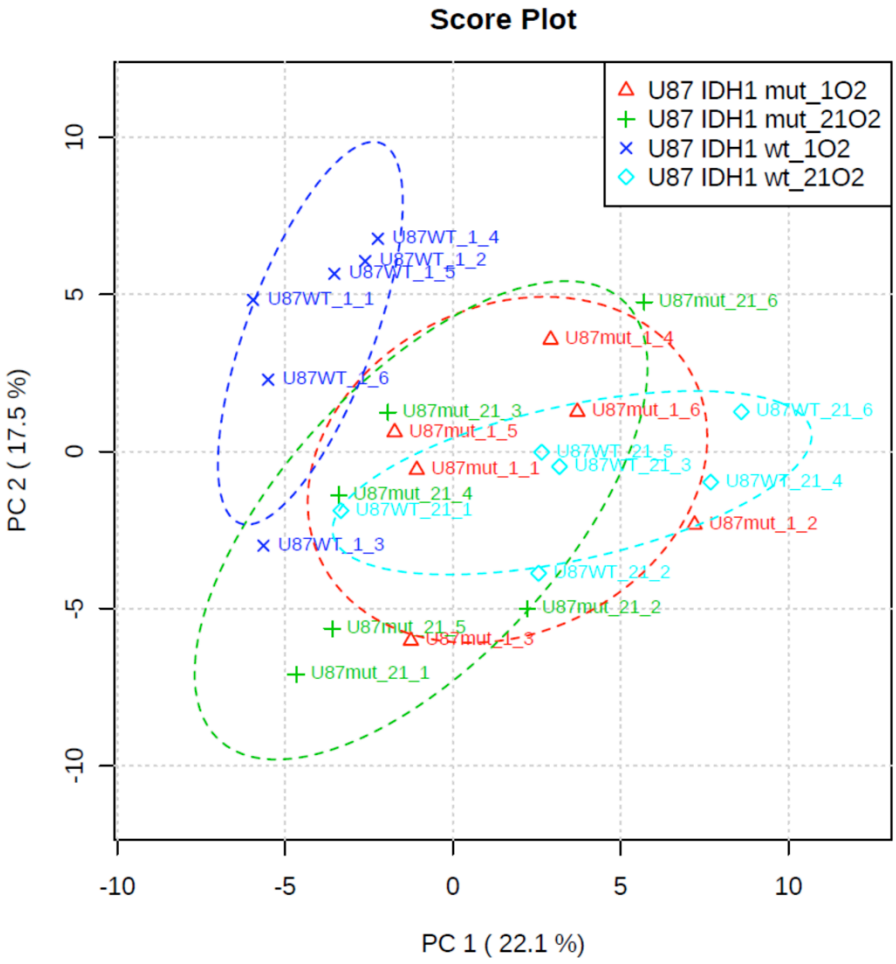

Figure 3.3 IDH1 R132H are metabolically clustered in hypoxia. PCA shows segregation of U87 IDH1 wild-type cell samples in normoxia (21% O_2) (light blue diamond) and hypoxia (1% O_2) (dark blue crosses), and clustering of U87 IDH1 R132H cell samples in normoxia (21% O_2) (green pluses) and hypoxia (1% O_2) (red triangles) where the segregated ellipses (dashed lines) are representative of 75% confidence intervals (n=6 technical triplicate per sample). Analysis performed by Warwick Dunn.

The PCA plot shown in Figure 3.3. shows clear segregation of normoxic U87 IDH1 wild-type cell samples from hypoxic U87 IDH1 wild-type cell samples. As stabilisation of the HIF transcription factors during hypoxia results in the increased transcription of a number of metabolic target genes, this therefore suggests that wild-type IDH1 cell samples undergo extensive hypoxic metabolic reprogramming in response to low

oxygen. However, U87 IDH1 R132H cell samples are highly clustered, regardless of oxygen tension, suggesting that the presence of the IDH1 R132H mutation inhibits this adaptation. We hypothesised that this effect could either occur as a result of a pre-established “pseudohypoxic” phenotype through HIF stabilisation, or through an inability to metabolically adapt to hypoxia.

The ellipse indicating the 75% confidence interval for IDH1 R132H samples overlapped with normoxic IDH1 wild-type U87 cells (Figure 3.3), implying a lack of metabolic adaptation to hypoxia. However, when expression of HIF was examined, a partial stabilisation was observed in IDH1 R132H U87 glioma cells in normoxia, and in IDH1 wild-type cells when pre-treated with 5 mM (R)-2HG for 48 hours, although the level of stabilisation was not similar to that observed in hypoxia (Figure 3.4A). This partial stabilisation of HIF might be expected to lead to a pseudohypoxic metabolic phenotype, rather than the inability to metabolically adapt to hypoxia, as observed in Figure 3.3. It was therefore investigated whether the observed stabilisation of HIF was sufficient to elicit a transcriptional response. Analysis of well-characterised HIF1 metabolic target genes, pyruvate dehydrogenase kinase 1 (PDK1), phosphoglycerate kinase 1 (PGK1), lactate dehydrogenase A (LDHA) and the facultative glucose transporter 1 (SLC2A1, also known as GLUT1) showed that there was indeed a partial transcriptional response in IDH1 mutant cells, that could be downstream of HIF1α. However, the increase in target gene expression was not uniform across all target genes examined. While PDK1 was up-regulated in IDH1 R132H cells to levels similar to that of hypoxic IDH1 wild-type cells (Figure 3.4B),

only a modest increase was observed in the other target genes in the same conditions (Figure 3.4C, D, E).

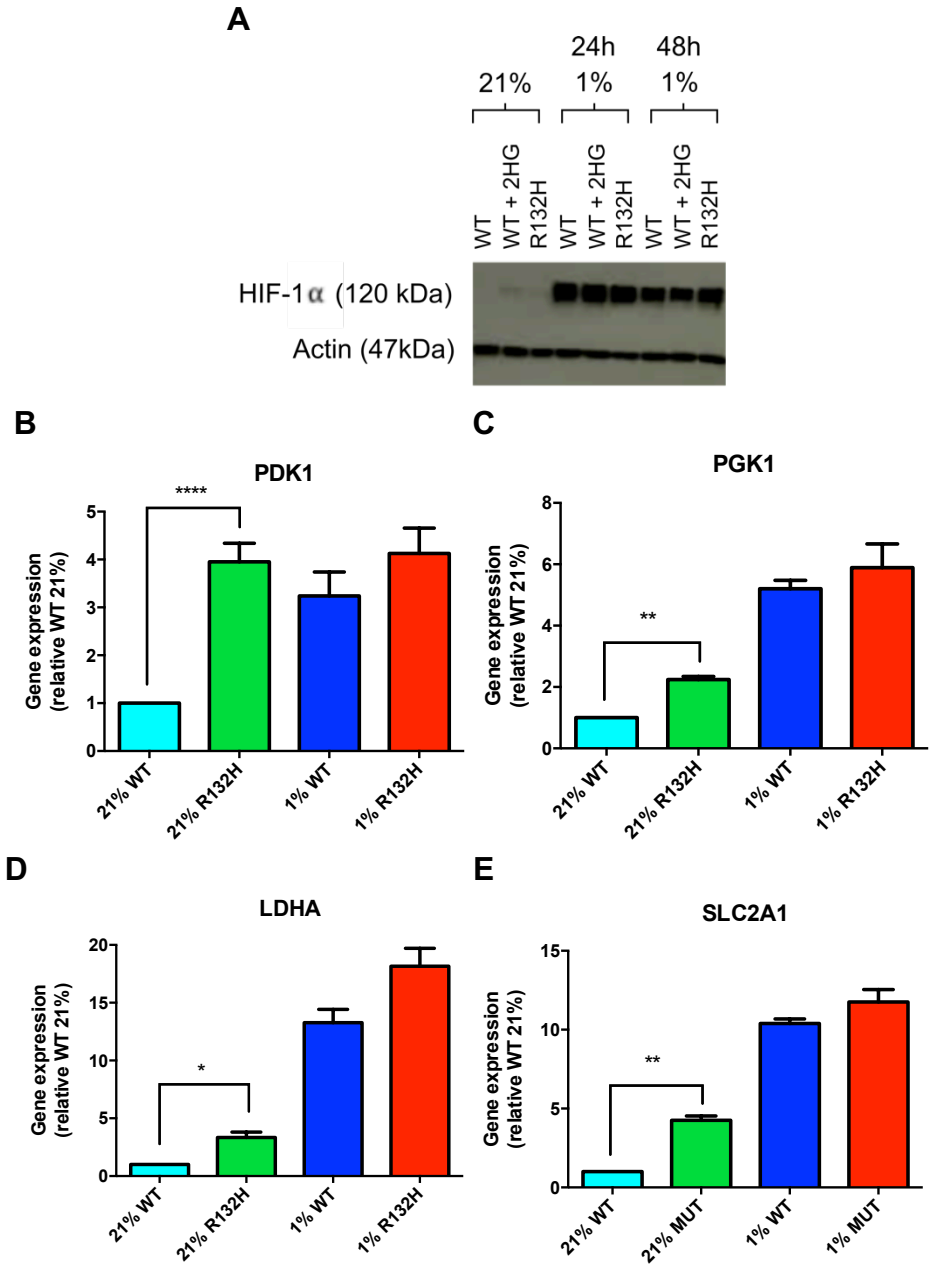

Figure 3.4 IDH1 R132H cells exhibit partial stabilisation of HIF1α. (A) Partial stabilisation of HIF1α protein in normoxia in IDH1 R132H and IDH1 wild-type + 5 mM (R)-2HG U87 glioma cells, along with a corresponding transcriptional increase in HIF1α target genes (B) PDK1, (C) PGK1, (D) LDHA and (E) SLC2A1. RT-qPCR performed in technical triplicate, with at least four biological replicates. Statistical significance determined using unpaired student's t-test with Welch's correction.

To clarify the nature of the metabolic alteration (or lack of it) induced by hypoxia in IDH1 mutant cells, the metabolites responsible for the observed segregation in the PCA plot (Figure 3.3) were identified by calculating the fold difference between statistically significant metabolites in each sample class (Figure 3.5). Comparison of IDH1 wild-type cells in normoxia and hypoxia produced a comprehensive list of hypoxia-inducible metabolic changes (Figure 3.5A), consisting of changes in intermediates of glycolysis (e.g. sugar derivatives) and the TCA cycle (e.g. malate and aspartate). Additional alterations were identified in the levels of some NEAAs, including alanine, glycine, glutamate and proline. Interestingly, differences in BCAAs valine, leucine and isoleucine were detected. These decreased in hypoxia, which is consistent with recent publications to suggest that wild-type IDH1 tumours catabolise BCAAs in hypoxia to aid tumour progression (Tönjes et al. 2013). In comparison with wild-type cells, IDH1 R132H-expressing cells exhibited very few metabolic changes in hypoxia, where only sugar derivatives, aspartate and malate were detected (Figure 3.5B).

Few metabolic changes were also observed between wild-type and R132H IDH1 cells in normoxic conditions (Figure 3.5C), including the increase in BCAAs observed in wild-type IDH1, and decrease in malate and aspartate observed in R132H IDH1 U87 cells. The greatest change was the expected production of 2HG in IDH1 R132H cells (Figure 3.5C). Consistent with the inability of IDH1 R132H cells to adapt to hypoxia, more statistically significant metabolites were differentially detected between wild-type and mutant IDH1 in hypoxia (Figure 3.5D), than in normoxia (Figure 3.5C). The metabolites identified as being different between IDH1 wild-type and mutant cells

in hypoxia include glycolytic intermediates (sugar derivatives, glycerol-3-phosphate and pyruvate) and NEAAs (aspartate, glutamate, glycine, and alanine). Many of these metabolic changes were similar to those observed between normoxic and hypoxic IDH1 wild-type cells (Figure 3.5A). Redox sensitive changes in nicotinamide – a precursor to NAD(P^+) synthesis in the cell - were consistently detected in both tissue (Figure 3.2) and cell models (Figure 3.5A and 3.5D), and found to be increased in IDH1 mutant tumours and hypoxic wild-type IDH1 cells.

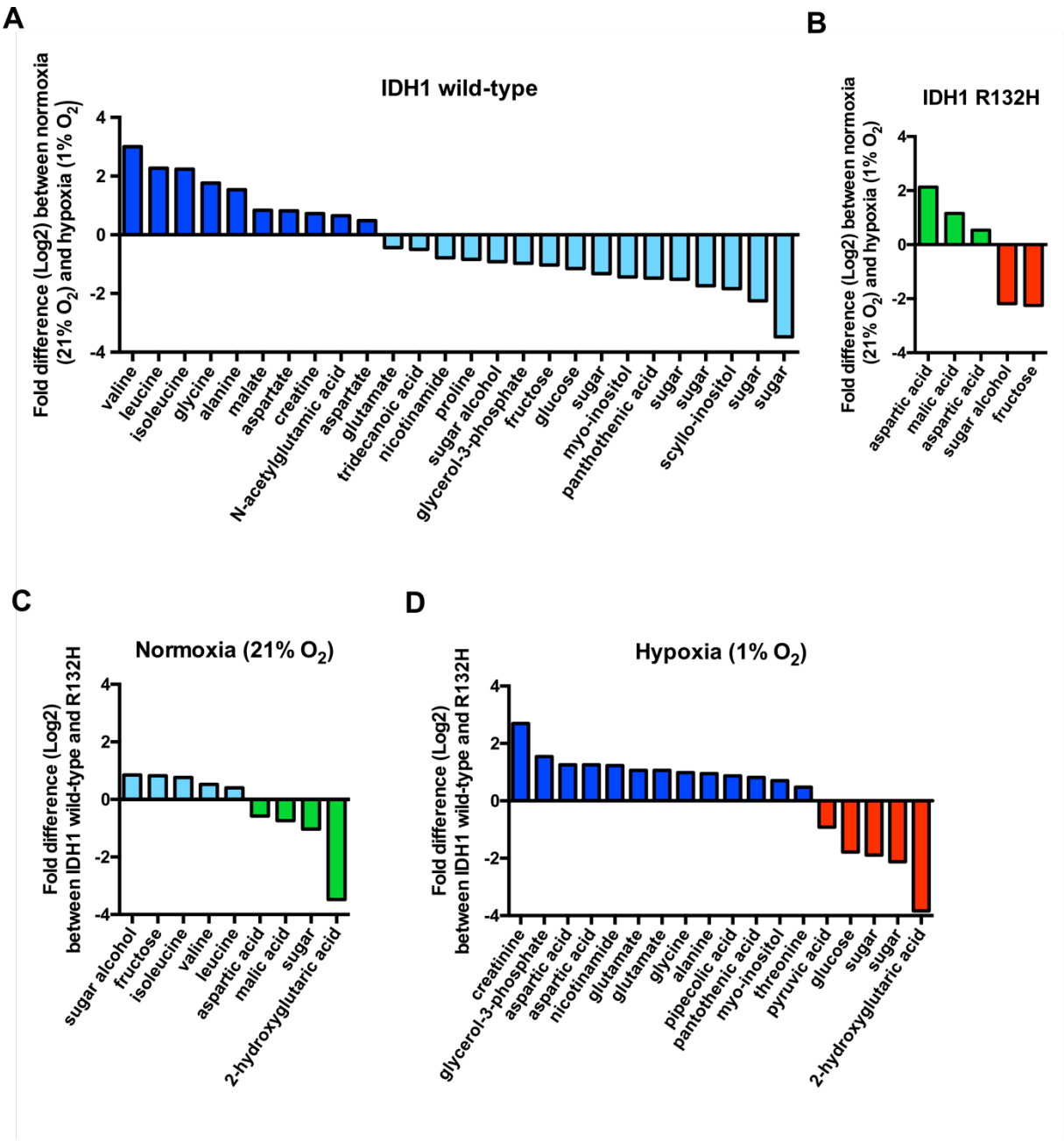

Figure 3.5 Metabolites responsible for the segregation between IDH1 status and oxygen tension. Fold difference in significant metabolites between normoxia (21% O_2) and hypoxia (1% O_2) in IDH1 wild-type (A) and IDH1 mutant (B) cell samples and between IDH1 wild-type and mutant in normoxic (21% O_2) (C) and hypoxic (1% O_2) (D) conditions identified by GC-MS (n=6 technical replicates in total). Those metabolites indicated twice represent the detection of different fragments.

The data above therefore show that IDH1 R132H U87 glioma cells exhibit very few metabolic changes in response to low oxygen. As this would be expected to impact their ability to maintain or adapt their phenotype in hypoxia, we wanted to assess their growth characteristics in hypoxia. The normoxic proliferation of U87 IDH1 R132H-expressing cells was observed to be slower than that of U87 IDH1 wild-type cells (Figure 3.6), consistent with previously reported data (Bralten et al. 2011). As expected, the growth of wild-type cells was indeed markedly reduced in hypoxia (~50% decrease; Figure 3.6). However, the hypoxic growth rate for mutant cells did not differ to that observed in normoxia until day 3 (72 hours), where there was a consistent marked decline in cell number, indicating that these cells are unable to continue to proliferate in chronic hypoxia (Figure 3.6). Therefore, despite an initial growth advantage, lack of metabolic adaptation appears to render IDH1 mutant cells more sensitive to long periods of hypoxic stress and consequently become unable to maintain proliferation.

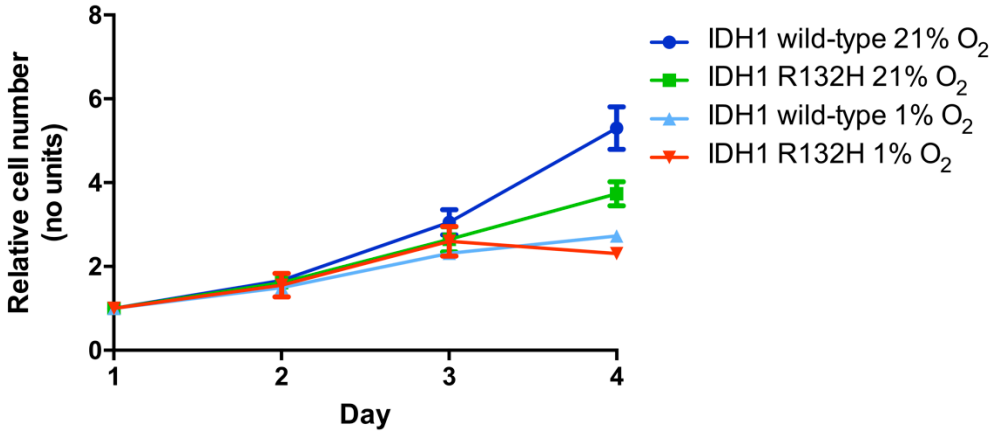

Figure 3.6 U87 hypoxic growth curve. Proliferation assay of U87 IDH1 wild-type and U87 IDH1 R132H cell samples in normoxia (21% O_2) and hypoxia (1% O_2). Cell counts were determined over a time course of 4 days (96 h) (n=3 technical replicates per day, n=5 biological replicates in total).

Cells with mutated IDH1 sustain oxidative reactions in hypoxia

Whilst being an untargeted tool, and therefore useful for gaining an overview of a system, the metabolomic approach offers limited mechanistic information regarding pathway activity. To improve our understanding of some of the metabolic differences outlined above, we performed a targeted metabolic tracer analysis using stable isotope-enriched carbon sources, and employed a cell line derived from a low-grade human oligodendroglioma (HOG) as a more biologically relevant model, infected to stably overexpress wild-type or R132H mutant IDH1 by lentivirus (Reitman et al. 2011). Since the majority of metabolites detected in the metabolomics approach indicated changes in central carbon metabolism, cells were incubated for 24 hours with [U-$^{13}C_6$]-glucose and [U-$^{13}C_5$]-glutamine to probe metabolic differences between IDH1 wild-type and mutant cells during the metabolic adaptation to hypoxia. The resulting polar extracts were analysed for ^{13}C incorporation by GC-MS.

Production of (R)-2HG in the IDH1 R132H HOG cell model was confirmed (Figure 3.7A), and shown to increase in hypoxia, consistent with previous reports (Wise et al. 2011). Pyruvate is an important metabolite, being the end-point of glycolysis, as it represents a key metabolic node and a major entry point to the TCA cycle. Changes in ^{13}C incorporation into this metabolite can therefore reveal important information regarding the metabolic state of the cell (Figure 3.7B). Figure 3.7 shows the comparison between the percentage ^{13}C incorporation into pyruvate and its products lactate and alanine after incubating cells for 24 hours with [U-$^{13}C_6$]-glucose. Increased ^{13}C incorporation in lactate was observed when both cell lines were

exposed to hypoxia, suggesting that the majority of lactate is produced from glucose in hypoxic conditions (Figure 3.7C). In comparison to lactate, ~50% less ^{13}C incorporation was detected in alanine (Figure 3.7D). As the majority of lactate is produced in the cytosol, and the majority of alanine is produced in the mitochondria (Adeva et al. 2013; Vacanti et al. 2014; Yang et al. 2014; Groen et al. 1982), this observation would suggest that the enrichment of the cytosolic and mitochondrial pools of pyruvate from glucose are different, whereby the majority of cytosolic pyruvate to support lactate production is derived from [U-$^{13}C_6$]-glucose. The mitochondrial pool of pyruvate is consequently generated from glucose and another source, most likely through glutamine-derived malate. Analysis of ^{13}C incorporation into pyruvate revealed significantly reduced ^{13}C incorporation into pyruvate in hypoxia, particularly in the IDH1 R132H HOG cells (Figure 3.7E), inferring reduced glycolytic carbon entry into the mitochondrion in hypoxia, as expected, and potentially an increase in the supply of alternative sources of mitochondrial pyruvate in IDH1 mutant cells under conditions of low oxygen.

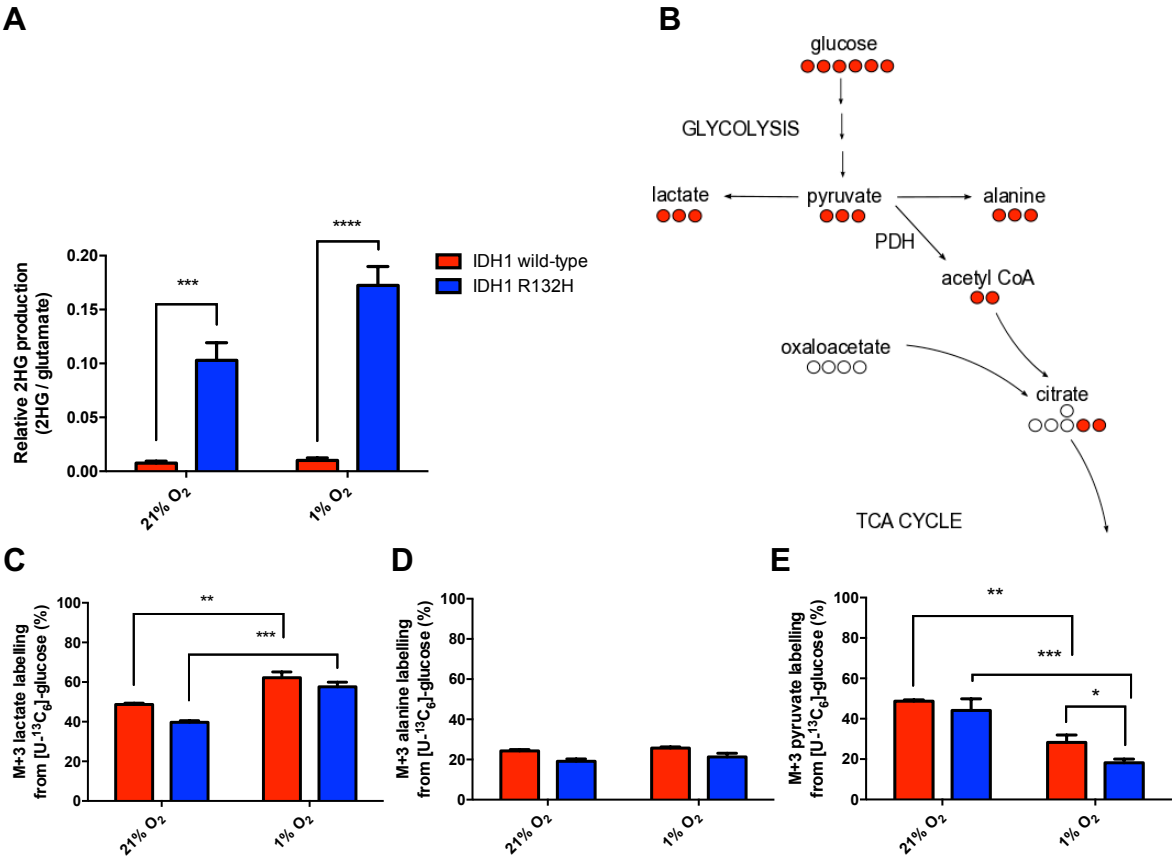

Figure 3.7 IDH1 mutant cells exhibit altered pyruvate metabolism. (A) Confirmation of 2HG production in HOG IDH1 R132H cell model. The ratio of 2HG/glutamate is used to show the substantial increase in 2HG production in IDH1 R132H HOG cells. Typically, the ratio of 2HG to αKG is used (as αKG has the same labelling pattern as 2HG) or norvaline. However, αKG was not present in detectable amounts in these samples and norvaline does not account for differences in cell number. (B) Schematic of the pyruvate nodes, showing differential ^{13}C incorporation into (C) lactate, (D) alanine and (E) pyruvate. Data is in technical triplicate, mean +/- S.D. Significance determined using two-tailed unpaired student's t-test.

When pyruvate enters the mitochondria, it can either be oxidatively decarboxylated by PDH to produce acetyl CoA, or carboxylated by PC to form oxaloacetate. As carbons in citrate arise from both oxaloacetate and acetyl CoA, the mass isotopologue distribution (MID) of citrate can reveal differences regarding the relative activity of PDH and PC using [U-$^{13}C_6$]-glucose (Figure 3.8A). Although minimal

changes were observed between cell types in normoxic conditions (Figure 3.8B), in hypoxia, IDH1 R132H HOG cells preserved a high contribution of the M+2 isotopologue to the overall pool, indicative of retained PDH activity (Figure 3.8C). In contrast, wild-type IDH1 HOG cells exhibited almost 50% less M+2 and increased proportions of the M+3 isotopologue, consistent with the expected decrease in pyruvate oxidation during hypoxia and a subsequent increase in mitochondrial PC activity for continued TCA cycle anaplerosis (Figure 3.8C). Sustained PDH activity in IDH1 mutant cells was further exemplified when comparing the relative PDH activity by calculating the ratio of M+2 citrate/M+3 alanine (Figure 3.8D), whereby M+3 alanine represents the labelling of the mitochondrial pyruvate pool.

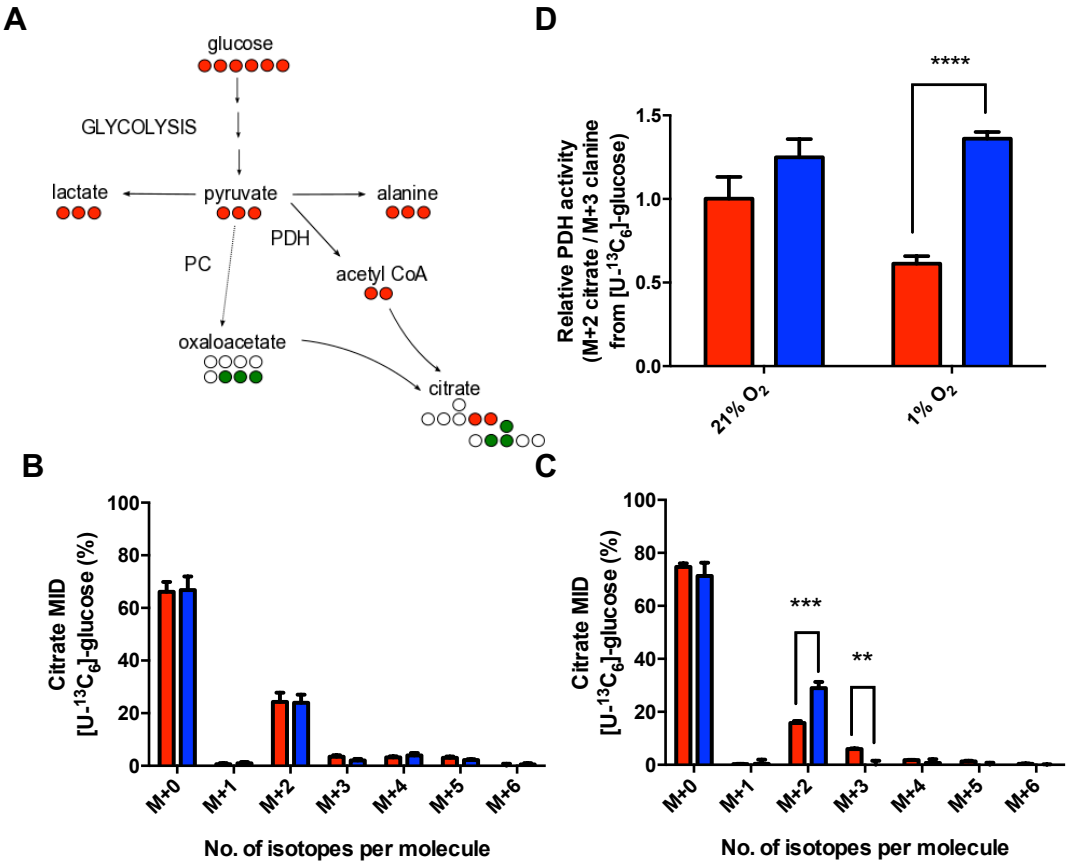

Figure 3.8 IDH1 R132H cells sustain the activity of pyruvate dehydrogenase in hypoxia. (A) Schematic to describe mitochondrial pyruvate metabolism by analysing the mass isotopologue distribution (MID) of citrate, where M+0, M+1, M+2 etc. mass isotopologues correspond to ion fragments containing 0, 1, 2 ^{13}C atoms, respectively. Pyruvate oxidation by PDH results in M+2 citrate from [U-$^{13}C_6$]-glucose. This is observed in both wild-type and mutant IDH1 cells in normoxia (B). As PDH activity is reduced in hypoxia through the HIF1α-mediated transcriptional activation of PDK1, an increase in PC activity can occur, resulting in the carboxylation of pyruvate to oxaloacetate and giving rise to M+3 citrate (C). This is observed in wild-type IDH1 cells only, suggesting that HIF1α transcriptional activity is compromised in IDH1 R132H cells. M+4 and M+5 citrate are formed from a second round of TCA cycle activity from M+2 and M+3 citrate, respectively. (D) The ratio of M+2 citrate to M+3 alanine is used to further illustrate this metabolic difference, as a readout of PDH-derived citrate from mitochondrial pyruvate. Data is performed in technical triplicate, mean +/- S.D. Statistical significance determined using two-tailed unpaired Student's t-test.

HIF-induced up-regulation of PDK1 in hypoxia results in the phosphorylation and inactivation of PDH, yet our findings from the metabolic tracer analysis using [U-$^{13}C_6$]-glucose suggested that IDH1 R132H cells sustain PDH activity in conditions of low oxygen. Therefore, our data suggest that HIF1α transcriptional activity could be compromised in IDH1 R132H cells in hypoxia. Despite this, a degree of HIF1α stabilisation and transcriptional up-regulation of PDK1 was observed in IDH1 R132H cells (Figure 3.9A and B), which is increasingly evident at lower oxygen tensions and is consistent with findings from the IDH1 U87 glioma model (Figure 3.4), although transcriptional activation appears to occur to a lesser extent. Interestingly, analysis of HIFα subunit stabilisation in IDH1 R132H HOGs showed increased HIF1α stabilisation and blunted HIF2α stabilisation, implying differential regulation in the HIF hydroxylases (Figure 3.9A).

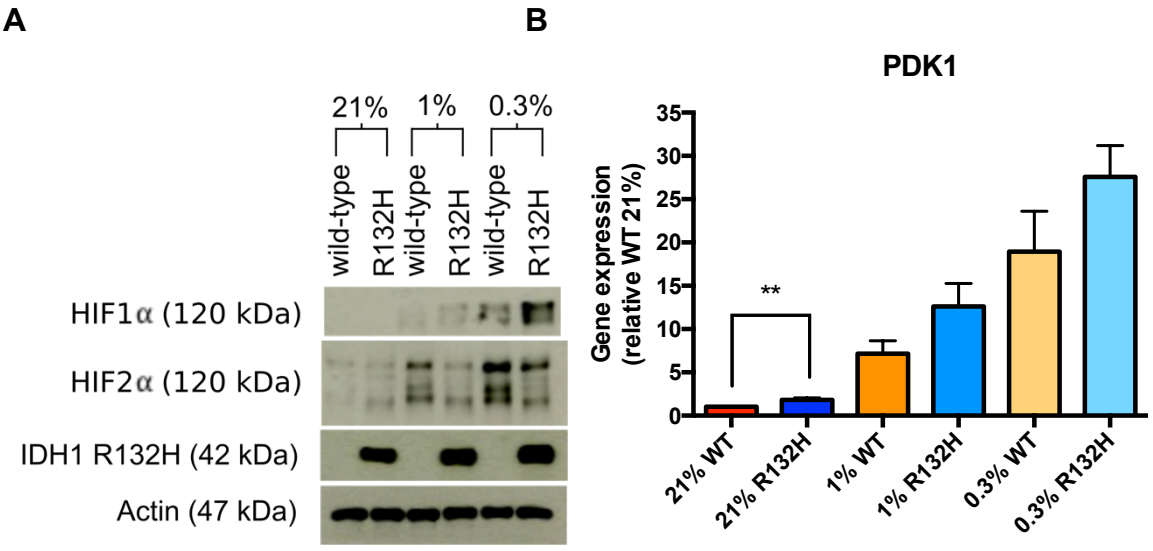

Figure 3.9 Partial HIF1α stabilisation and transcriptional activity. (A) Increased HIF1α protein stabilisation and blunted HIF2α protein stabilisation is observed in IDH1 R132H cells, which is particularly emphasised at lower oxygen tensions of 0.3% O_2, along with (B) increased transcriptional expression of HIF1α target gene PDK1. Data is mean +/- S.E.M. Statistical significance determined using unpaired student's t-test.

Analysis of differential ^{13}C incorporation from glucose in IDH1 wild-type and R132H mutant cells in the metabolic adaptation to hypoxia indicated perturbed central carbon metabolism in IDH1 mutant cells, particularly in the mitochondrial metabolites. Glutamine is the other major carbon source to glucose, supplying carbons into the TCA cycle in most if not all proliferating cells. To investigate the metabolism of glutamine in both IDH1 wild-type and mutant cells in hypoxia, cells were incubated for 24 hours with [U-$^{13}C_5$]-glutamine. Assessment of ^{13}C label incorporation in citrate can be used to determine the relative extent of oxidative and reductive glutamine metabolism (Figure 3.10A). Minimal changes in ^{13}C label incorporation were observed between cells expressing wild-type IDH1 or the R132H mutant when comparing the citrate MID in normoxia (Figure 3.10B). Both cell lines predominately exhibit M+4 and M+2 isotopologues, indicative of one and two rounds of glutamine oxidation through TCA cycle activity, respectively. However, significant changes were observed in ^{13}C incorporation into citrate in hypoxia (Figure 3.10C). Unlike mutant IDH1 HOG cells, which exhibit no difference in ^{13}C incorporation in hypoxia, wild-type IDH1 cells showed an increase in the proportion of M+5 citrate, consistent with the reductive carboxylation of glutamine-derived αKG as previously reported in hypoxic cells to support *de novo* lipogenesis (Metallo et al. 2011; Wise et al. 2011). This metabolic change is further exemplified by plotting the ratio of M+3/M+4 aspartate (Figure 3.10D) as a measure of relative reductive/oxidative glutamine metabolism, where M+3 aspartate is derived from M+5 citrate through the activity of ATP citrate lyase (Figure 3.10A).

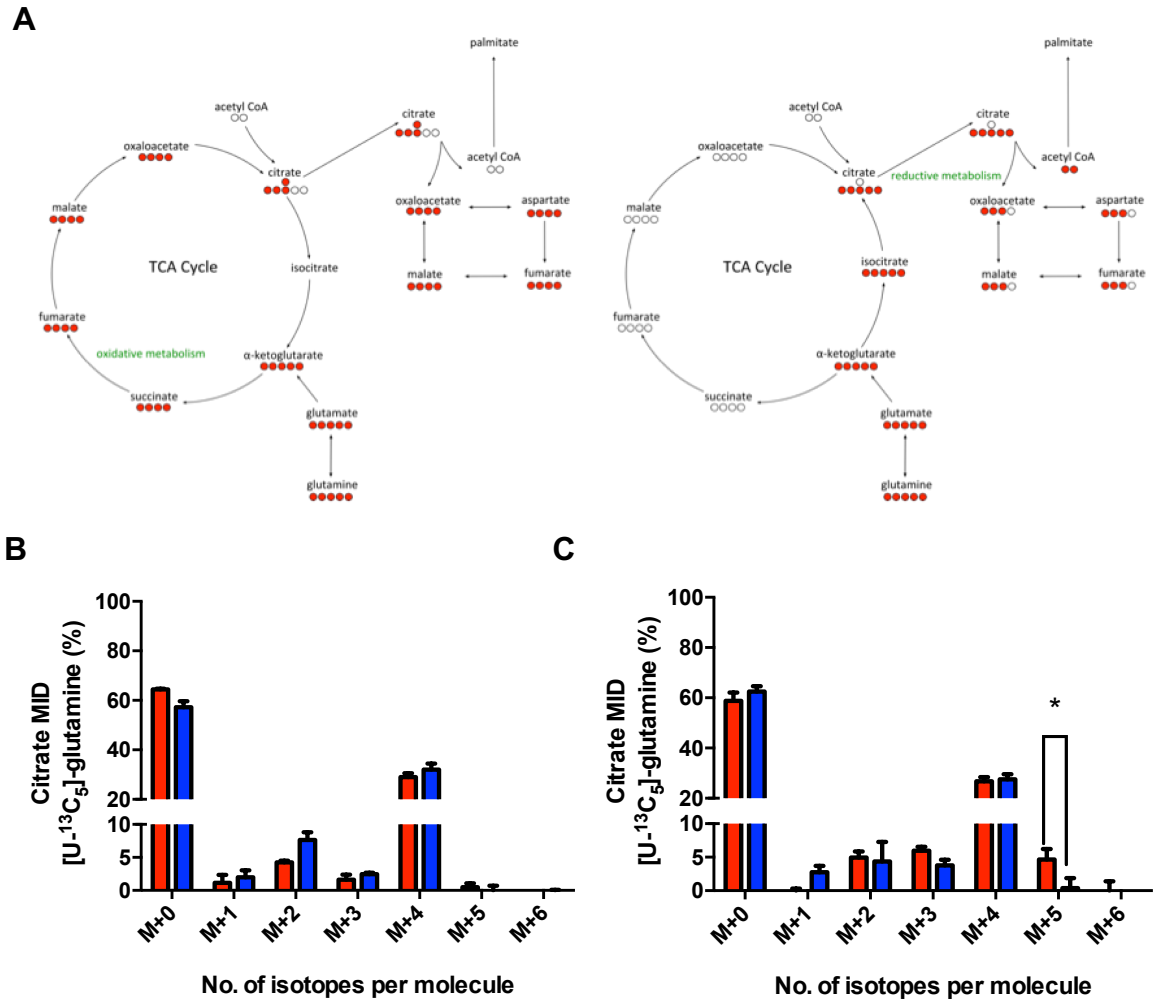

Figure 3.10 IDH1 mutants have compromised hypoxic reductive glutamine. Comparison of the MID in citrate employing a [U-$^{13}C_5$]-glutamine tracer to assess the relative contributions of oxidative and reductive TCA activity. In normoxia, glutamine-derived αKG undergoes oxidative TCA metabolism producing M+4 citrate from M+4 TCA cycle intermediates. In hypoxia, cells increase their reliance on reductive carboxylation of glutamine-derived αKG producing M+5 citrate and M+3 aspartate (A). No differences are observed in the citrate MID in normoxia (B), but in hypoxia, only IDH1 wild-type cells exhibit an increase in M+5 citrate (C), suggesting that IDH1 R132H cells do not increase their reliance on reductive glutamine metabolism in hypoxia.

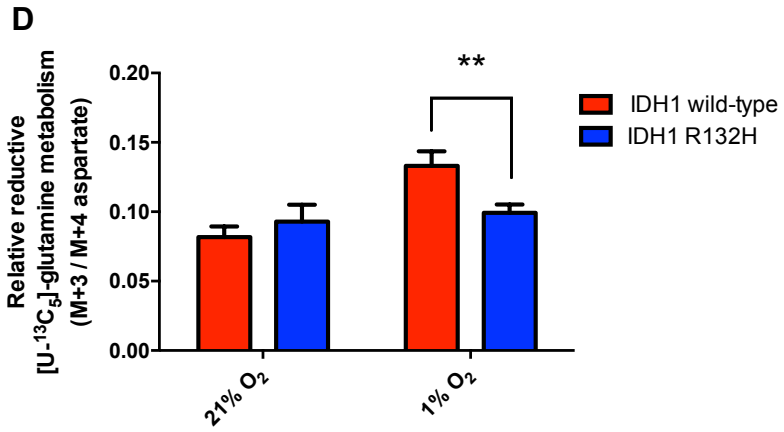

Figure 3.10 - IDH1 mutants have compromised hypoxic reductive glutamine, *continued*. This metabolic change is further exemplified by calculating the ratio of M+3/M+4 aspartate as a measure of reductive/oxidative glutamine metabolism (D). Experiments performed in technical triplicate, data is mean +/- S.D. Significance determined using two-tailed unpaired Student's t-test.

As reductive glutamine metabolism does not appear to be induced in hypoxic IDH1 R132H-expressing cells, oxidative metabolism of this amino acid was assessed, using the ratio of uniformly ^{13}C labelled succinate and fumarate to glutamate. Wild-type IDH1 cells present a relative increase in M+4 succinate (Figure 3.11A), along with a corresponding decrease in M+4 fumarate in hypoxia (Figure 3.11B), indicative of decreased complex II activity and most likely as a result of decreased respiration. However, lack of a hypoxia-induced shift in this ratio in IDH1 R132H cells infer that they sustain oxidative metabolism in hypoxia unlike their wild-type counterparts, which is again consistent with previously reported data (Leonardi et al. 2012; Grassian et al. 2014). This data suggests that the decreased label incorporation observed in pyruvate from [U-$^{13}C_6$]-glucose in hypoxic IDH1 R132H cells compared to wild-type cells (Figure 3.7E) is likely to be a product of the continued oxidation of glutamine and synthesis of pyruvate from glutamine-derived malate. Collectively, our

results indicate that IDH1 mutations may compromise the capacity of the cell to undergo reductive glutamine metabolism, and continue to sustain oxidative metabolism despite the low oxygen conditions.

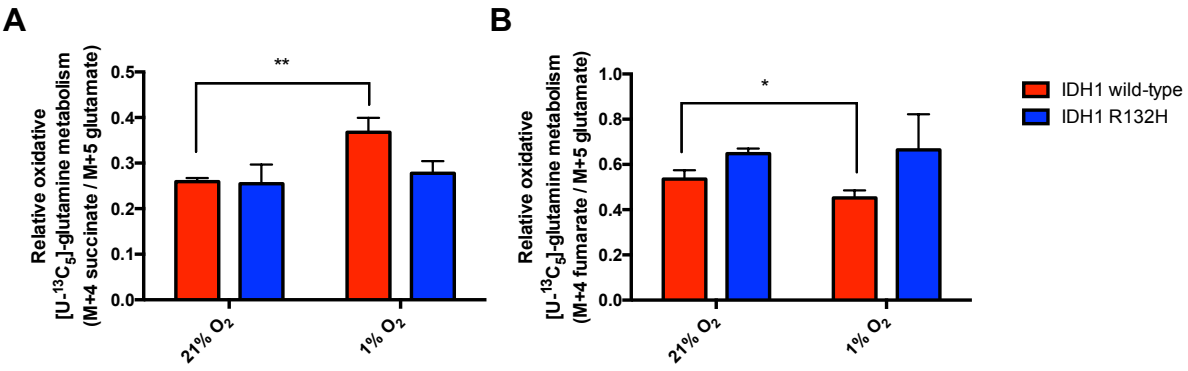

Figure 3.11 IDH1 mutants sustain oxidative TCA metabolism in hypoxia. Consistent with the lack of reductive carboxylation in IDH1 R132H HOG cells is sustained oxidative metabolism, where no relative increase in ^{13}C incorporation in succinate (A) or subsequent decrease in fumarate (B) was observed from [U-$^{13}C_5$]-glutamine. Data is presented M+4/M+5 glutamine to account for differences in anaplerosis. Experiments performed in technical triplicate. Data is mean +/- S.D. Statistical significance determined using two-tailed unpaired Student's t-test.

The sustained activity of PDH and oxidative glutamine metabolism exhibited by IDH1 mutant cells in hypoxia suggest that the presence of the IDH1 R132H mutation compromises the metabolic adaptation to hypoxia, despite partial HIF1α stabilisation and transcriptional activity. As (R)-2HG production from IDH1 mutant cells has been reported to competitively inhibit numerous αKG-dependent enzymes (Zhao et al. 2009; Xu et al. 2011; Turcan et al. 2012; Lu et al. 2012), the lack of metabolic adaptation to HIF-target genes could imply potential inhibition of protein synthesis, as translational activity has been recently shown regulated by αKG-dependent hydroxylases (Zhuang et al. 2015).

IDH1 mutants exhibit pseudohypoxic proline metabolism

Contrary to the number of metabolic findings that argue mutant IDH1 cells do not metabolically adapt to hypoxia, there was one observed phenotype to suggest that mutant IDH1 cells may display aspects of "pseudohypoxia". Using a [U-$^{13}C_5$]-glutamine tracer for 24 hours, our results revealed that hypoxia significantly increases glutamine-derived proline biosynthesis in wild-type IDH1 cells (Figure 3.12A). Proline is one of many NEAAs synthesised from glutamine (Figure 3.12B). In comparison to wild-type IDH1 cells, the presence of the IDH1 R132H mutation, significantly increased ^{13}C incorporation from glutamine into proline in both normoxic and hypoxic oxygen tensions (Figure 3.12A), with normoxic levels in IDH1 R132H cells being analogous to that of wild-type expressing hypoxic cells.

Steady-state concentrations of intracellular proline, as determined by 1D ^{1}H NMR spectroscopy, support the observed increase in proline biosynthesis at oxygen tensions as low as 0.3% (Figure 3.12C). Approximately twice the amount of proline was observed in IDH1 R132H HOG cells compared to wild-type in normoxic conditions. Analysis of the culture media confirmed the export of glutamine-derived proline out of the cell (Figure 3.12D), which is predicted to permit continued intracellular proline synthesis, as the activity of the last enzyme involved in this pathway is strongly product inhibited by proline (De Ingeniis et al. 2012). Increased export of glutamine-derived proline was observed in the media of hypoxic wild-type cells when compared to their normoxic controls and mutant IDH1 HOG cells in

normoxia (Figure 3.12D). These data suggest that IDH1 mutant cells synthesise and excrete proline in a manner similar to that of hypoxic wild-type IDH1 cells.

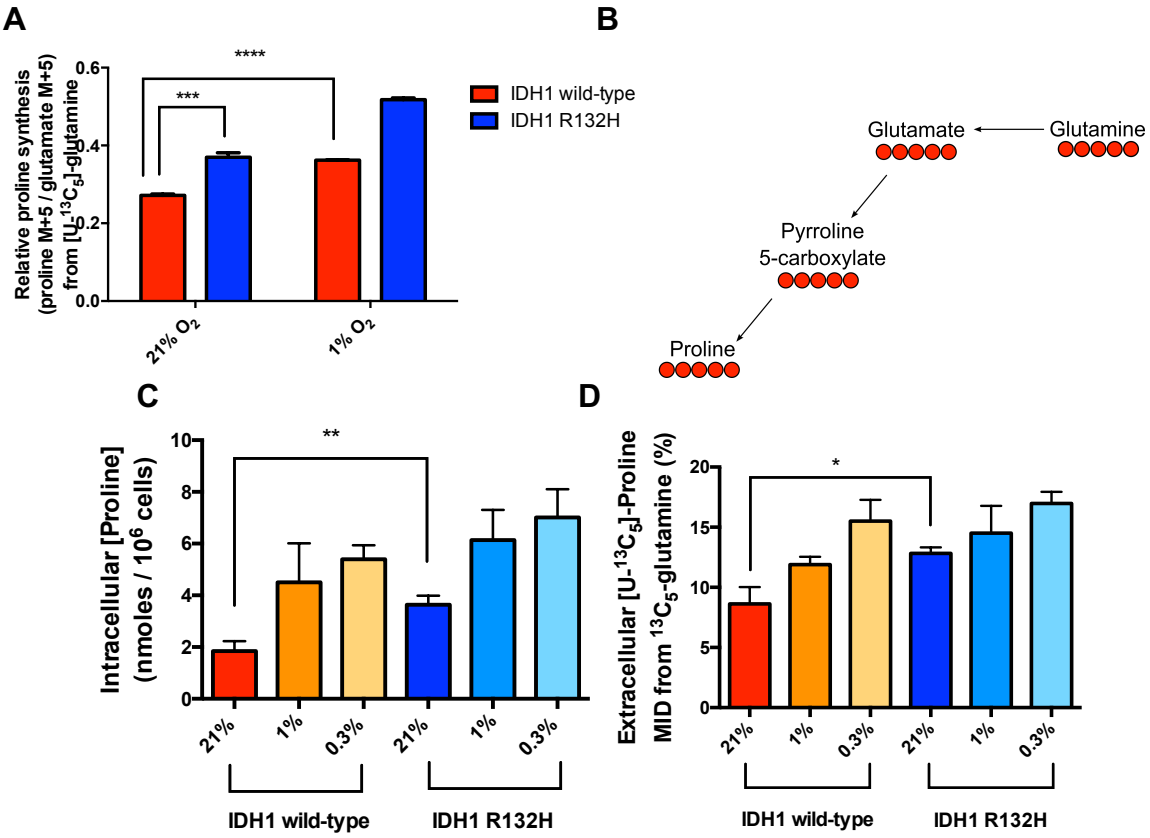

Figure 3.12 IDH1 R132H HOG cells exhibit hypoxic-like proline metabolism. Proline biosynthesis from [U-$^{13}C_5$]-glutamine increases in hypoxia in IDH1 wild-type cells and is increased in IDH1 R132H cells at normal oxygen tensions compared to wild-type as identified by GC-MS (A) Data is presented M+5 glutamate/M+5 proline to account for differences in anaplerosis. Experiments performed in technical triplicate. Data is mean +/- S.D. The majority of proline in synthesised from glutamine, where M+5 glutamine gives rise to M+5 proline (B). Intracellular steady-state concentrations of proline, as determined by 1D ^{1}H-NMR Spectroscopy, reflect this increase in pathway usage (C) (n=6 biological replicates, data is mean +/- S.E.M). (D) [U-$^{13}C_5$]-proline is exported out of the cell, where increased ^{13}C incorporation from [U-$^{13}C_5$]-glutamine is observed in hypoxia (1% and 0.3% O_2) and in IDH1 R132H HOG cells in normoxia. Experiments performed in biological replicate. Data is mean +/- S.E.M. Significance determined using two-tailed unpaired Student's t-test for all graphs.

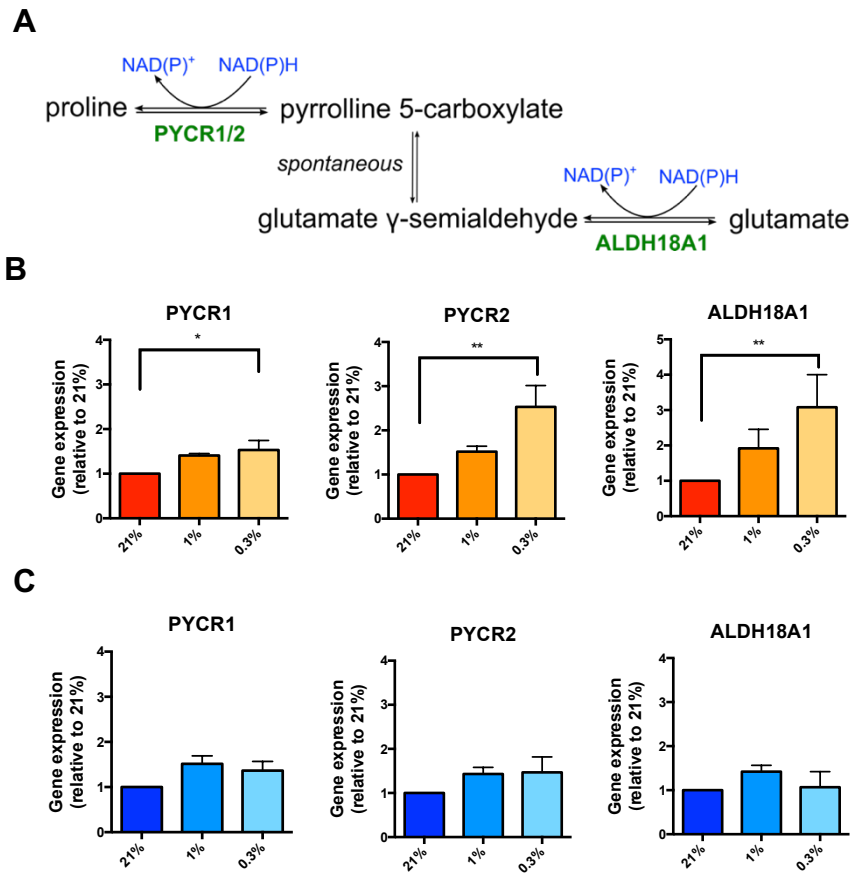

Figure 3.13 IDH1 mutant cells exhibit a blunted transcriptional increase in the proline biosynthetic eyzymes. Gene expression of enzymes involved in the biosynthetic pathway (A) are increased in wild-type IDH1 HOG cells (B) but blunted in IDH1 R132H HOG cells (C). Experiments performed in technical and biological triplicate. Data is mean +/- S.E.M. Significance determined by one-way ANOVA.

As metabolic pathway activity can be altered by enzyme expression, relative expression of the enzymes shown to be involved in mitochondrial proline biosynthesis from glutamine: pyrroline-5-carboxylate synthetase (ALDH18A1), pyrroline carboxylate reductase 1 (PYCR1) and 2 (PYCR2) (Figure 3.13A), were assessed (De Ingeniis et al. 2012). Consistent with the observed increase in glutamine-derived proline biosynthesis in IDH1 wild-type cells in response to low oxygen, expression of the proline biosynthetic enzymes were increased in hypoxia

(Figure 3.13B), where PYCR2 and ALDH18A1 were the most responsive. However, IDH1 R132H HOG cells exhibit a blunted transcriptional response for all three transcripts (Figure 3.13C). Importantly, the increase in hypoxic gene expression was not reflected at the protein level, where no significant difference between IDH1 status or exposure to low oxygen tension (24 hours at 1% or 0.3% O_2) was detected (Figure 3.14A). This reasons that observed changes in proline synthesis are unlikely to be due to altered expression of the biosynthetic enzymes.

As previously described, IDH1 mutations result in the accumulation of the oncometabolite, (R)-2HG, shown to be the direct mediator of a number of reported phenotypes in cells and tissues bearing the IDH1 mutation. To investigate whether the proline synthetic phenotype was also due to (R)-2HG accumulation, IDH1 wild-type cells were treated with (R)-2HG for 48 hours prior to [U-$^{13}C_5$]-glutamine addition. Despite the build-up of intracellular 2HG in IDH1 wild-type cells after treatment, no change in proline concentration was observed (Figure 3.15B), suggesting that the R132H IDH1 mutation elicits this metabolic phenotype through an alternative mechanism, likely to occur through a change in redox owing to the presence of the IDH1 R132H mutation.

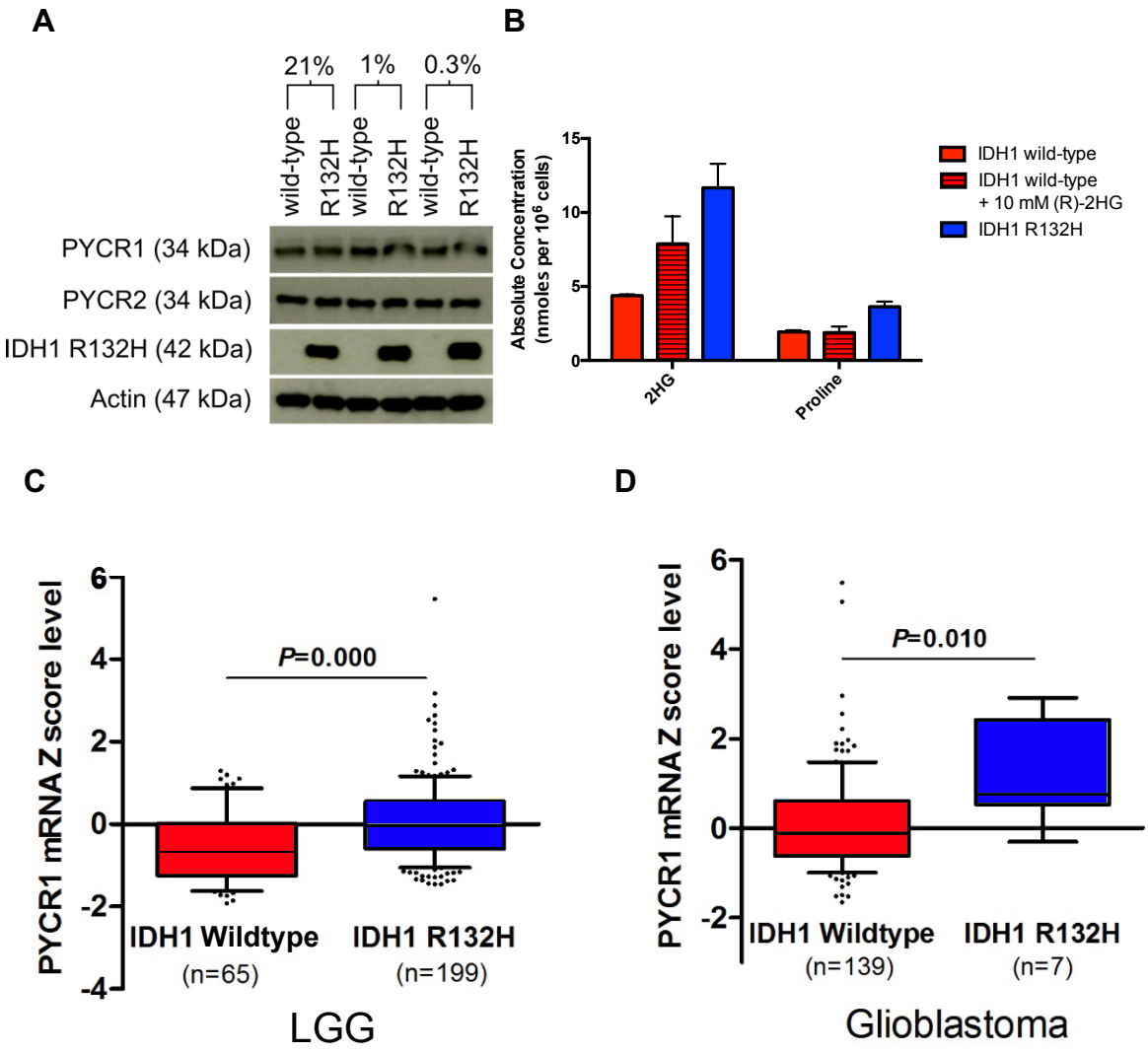

Figure 3.14 Increased PYCR1 gene expression may support the increase in proline biosynthesis displayed in IDH1 mutants. Immunoblot analysis confirms no difference in PYCR1 or PYCR2 protein expression between oxygen tension, or IDH1 status (A). The increase in glutamine-derived proline biosynthesis in IDH1 R132H HOG cells is unlikely to result from (R)-2HG production (B). Experiments performed in biological triplicate. Data is mean +/- S.E.M. PYCR1 gene expression is increased in IDH1 mutated LGG (C) and GBMs (D) (data extracted from TCGA cbioportal).

IDH1 mutations are observed in the majority of LGGs and secondary GBM (Parsons et al. 2008). Despite no significant difference in the gene expression of any of the biosynthetic enzymes between wild-type and mutant IDH1 status *in vitro*, *in vivo*

analysis of PYCR1 gene expression was significantly increased in IDH1 mutant LGGs (Figure 3.15C) and GBMs (Figure 3.15D).

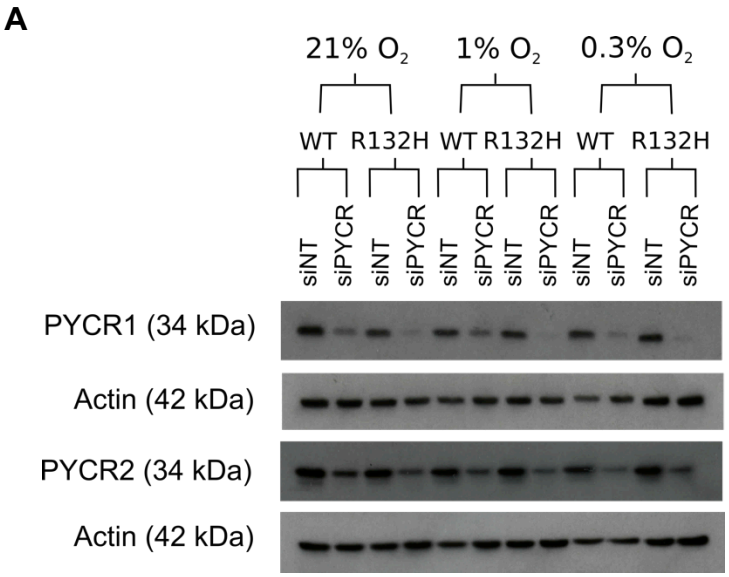

Figure 3.15 Successful knock down of PYCR isoforms. Successful knock down of PYCR isoforms 1 and 2 protein was validated for all experimental conditions (A). Immunoblotting demonstrates protein knock down 48 h post transfection.

To investigate the biological function of increased proline biosynthesis from glutamine in mutant IDH1 R132H cells, knock down of the rate-limiting step - PYCR enzyme isoforms 1 and 2 by siRNA was validated and achieved for all experimental conditions (Figure 3.15A). Knockdown of both isoforms reduced label incorporation from [U-$^{13}C_5$]-glutamine to proline, where knockdown of PYCR1 appeared to have the most significant effect regardless of oxygen tension (Figure 3.16A). The effect of PYCR2 knock down on ^{13}C incorporation had a greater effect in hypoxia (Figure 3.16B), consistent with the observed transcriptional increase in PYCR2 gene expression in response to low oxygen (Figure 3.13B). Knockdown of either PYCR1 or 2 decreased intracellular steady-state concentrations of proline by at least 50% in

IDH1 wild-type and mutant-expressing cells (Figure 3.16C), concluding that the majority of proline in these cells is synthesised by these two isozymes.

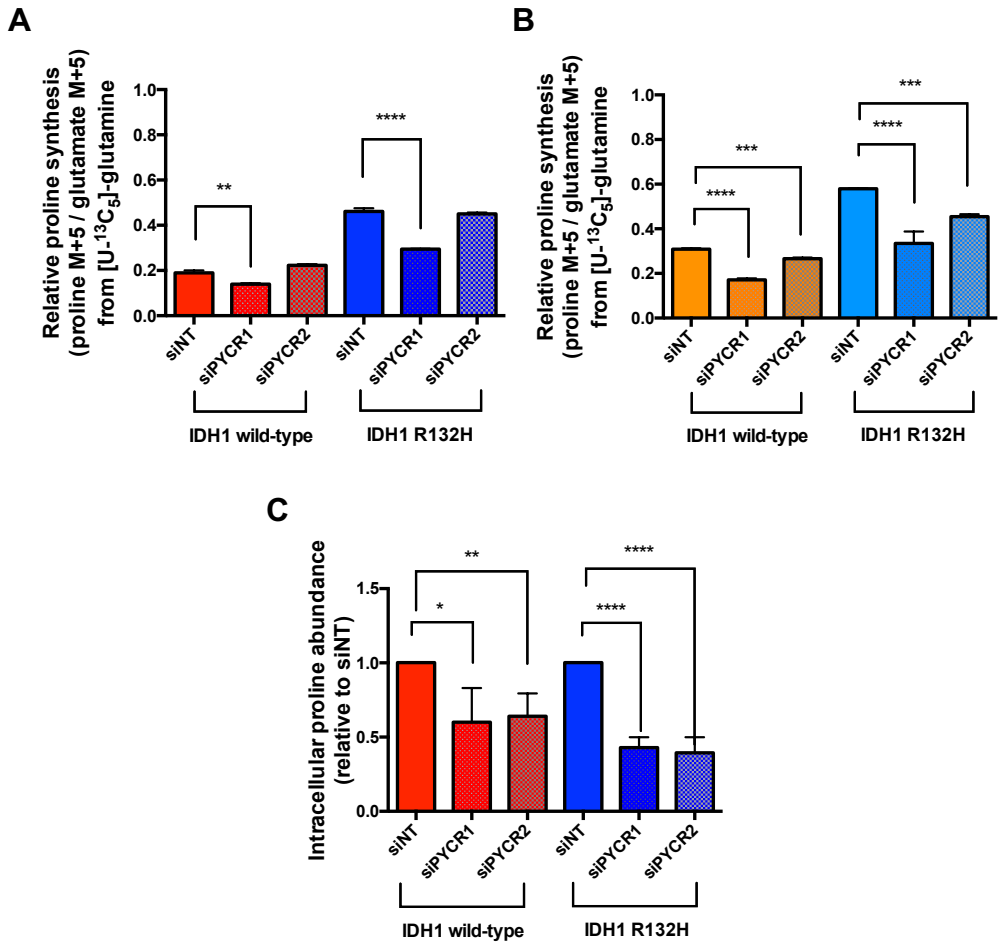

Figure 3.16 PYCR knockdown reduces proline biosynthesis. Knockdown of PYCR isoforms decrease ^{13}C label incorporation from [U-$^{13}C_5$]-glutamine in normoxia (A) and hypoxia (B), where siPYCR1 has the most significant effect. Decreased steady-state concentrations of intracellular proline also confirm knockdown (C). All data is mean +/- S.D, performed in technical triplicate and analysed by GC-MS. Metabolite abundance was normalised to d6-glutaric acid and cell number, and then calculated relative to wild-type. Significance determined using two-tailed unpaired Student's t-test.

Increased proline biosynthesis maintains redox plasticity

As the synthesis of proline from glutamate is a highly redox regulated pathway, requiring 2 molecules of NAD(P)H (Figure 3.13A), it was hypothesised that increased proline biosynthesis may be an important means by which cells and tumours bearing an IDH1 mutation regulate cellular redox state. Previous reports suggested that IDH1 mutant cells may have higher levels of oxidative stress than IDH1 wild-type cells (Gilbert et al. 2014). To test whether the pathway consumed NADPH, and therefore induced this phenotype, cells were treated with H_2O_2 and assessed for viability after 24 hours. No difference was observed between the two cell lines, suggesting that this pathway is unlikely to be consuming NADPH. Independent knock down of PYCR1 and 2 before treatment with H_2O_2, would increase resistance to oxidative stress-mediated cell death if the pathway were NADPH dependent. Again, no differences were detected (Figure 3.17). These data are consistent with reports that PYCR1 and 2 exhibit a higher specific activity in the presence of NADH compared to NADPH in melanoma cells (De Ingeniis et al. 2012).

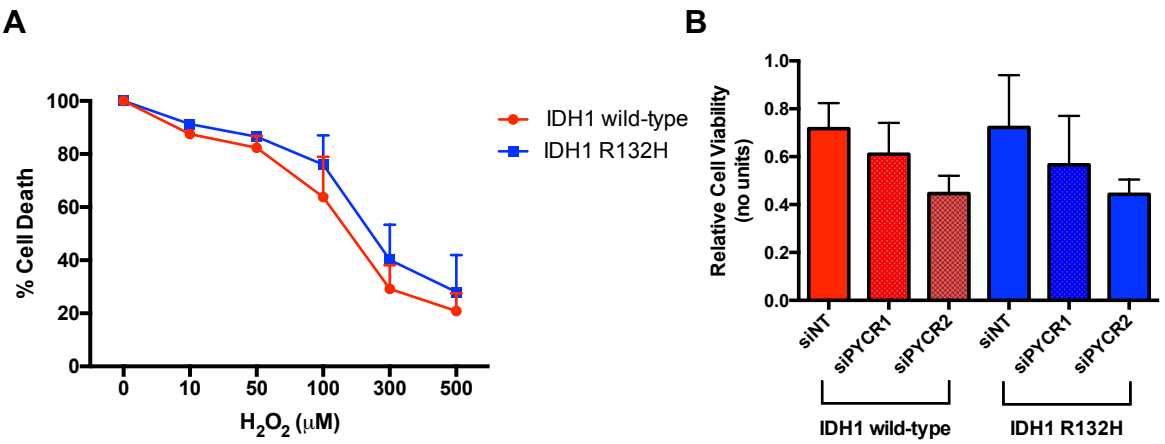

Figure 3.17 Increased mitochondrial proline biosynthesis is unlikely to consume NADPH. (A) Dose-response curves to compare and determine IC50 of H_2O_2 in wild-type and R132H IDH1 cells, as determined by SRB assay. (B) SRB assay confirmed no significant difference in relative cell viability between wild-type and R132H IDH1 HOG cells in response to treatment with 100 μM H_2O_2. All experiments performed in biological and technical triplicate. H_2O_2 treated cells are normalised to untreated for each condition. Data is mean +/- S.E.M.

The majority of mitochondrial NADH is produced by dehydrogenases (PDH, IDH3, MDH and αKGDH) to supply electrons to the electron transport chain. If increased proline biosynthesis from glutamine were to consume NADH, then knockdown of PYCR1 or 2 would be expected to increase the ratio of NADH/NAD^+ and result in an increase in NADH oxidation by complex I. Confocal microscopy was used to assess cellular levels of NAD(P)H (not $NAD(P)^+$), as the reduced forms of these molecules autofluoresce when excited with ultra-violet light (Chance & Baltscheffsky 1958). NADH is the major autofluorescent signal in cells (Avi-Dor et al. 1962), hence confocal microscopy real-time imaging of NADH has been widely employed to detect changes in NADH oxidation as a read-out of mitochondrial respiration (Mayevsky 1984; Mayevsky & Rogatsky 2006). To better evaluate the maximum and minimum

NADH levels in the mitochondria, NADH oxidation was blocked with rotenone, an inhibitor of complex I, and mitochondria were uncoupled using carbonyl cyanide m-chlorophenylhydrazone (CCCP) to stimulate maximal NADH oxidation (Figure 3.18A, B, C, D).

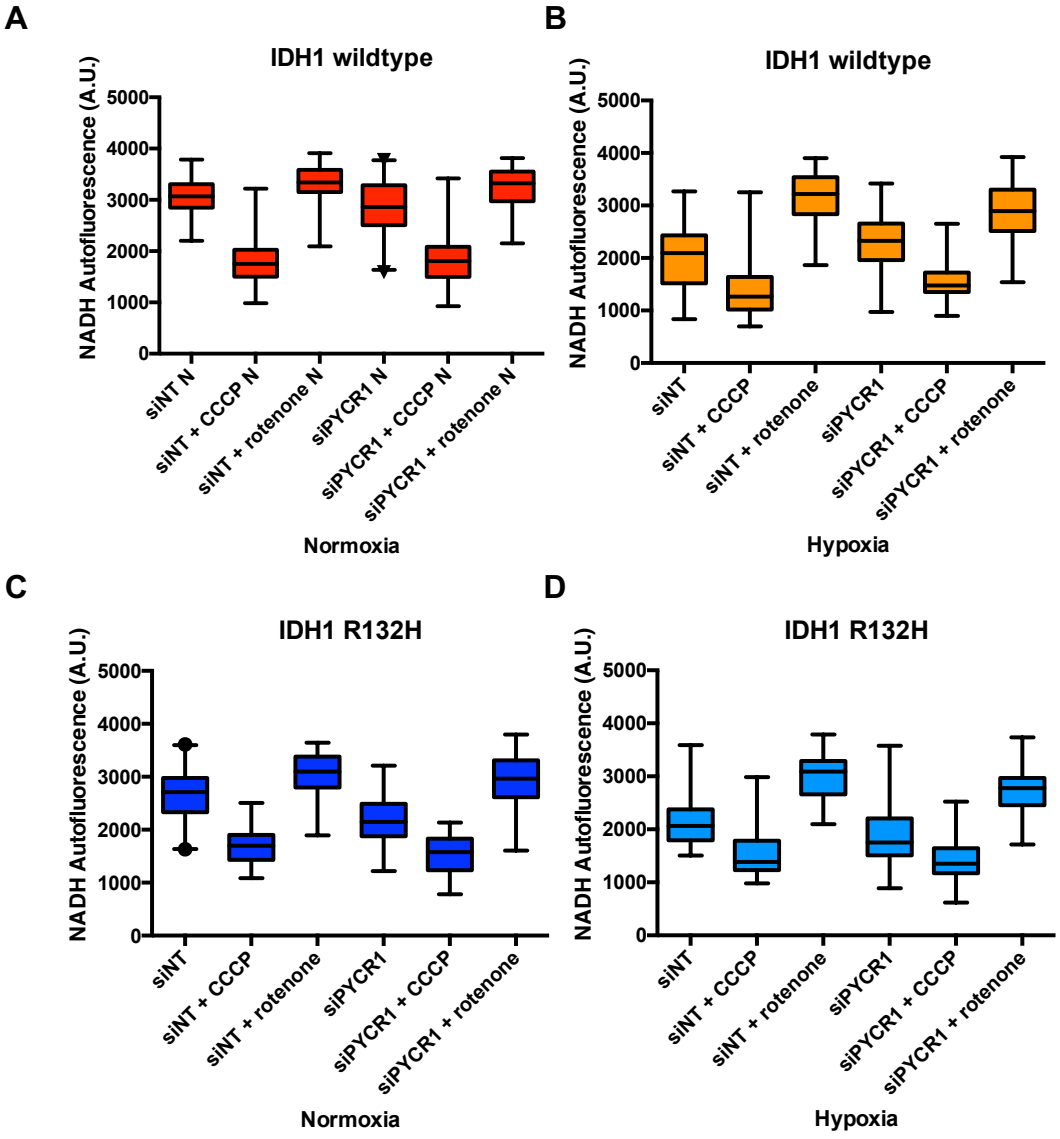

Figure 3.18 Knockdown of PYCR increases NADH availability in IDH1 R132H cells. NADH autofluorescence for IDH1 wild-type cells in normoxia (A) and hypoxia (B) and IDH1 R132H cells in normoxia (C) and hypoxia (D). Addition of CCCP (20 μM) uncouples respiration resulting in depleted mitochondrial NADH, whereas addition of rotenone (60 μM) inhibits complex I resulting in increased NADH autofluorescence.

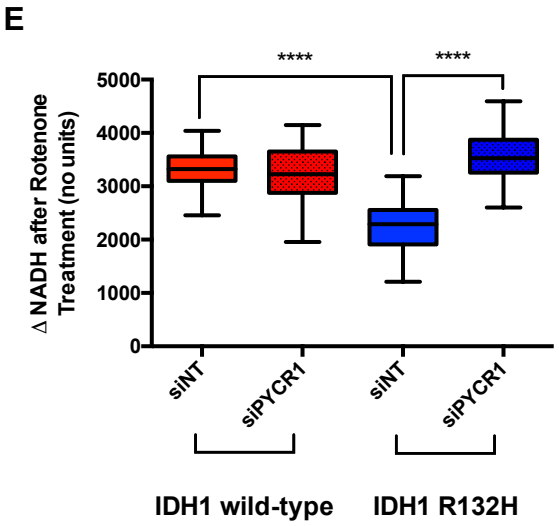

Figure 3.18 – Knockdown of PYCR increases NADH availability in IDH1 R132H cells, *continued*. Minimal changes in basal NADH are observed between normoxia and hypoxia. Rotenone addition in hypoxia increases NADH levels to that of rotenone-treated normoxic cell samples. (E) Knockdown of siPYCR1 has no effect on wild-type IDH1 cells but increases NADH levels in IDH1 R132H HOG cells, suggesting that proline synthesis consumes mitochondrial NADH that would otherwise be available for oxidation by complex I. Data subtracted from CCCP, treated subtracted from untreated. Mean is +/- SD, Significance determined using one-way ANOVA.

After normalising NADH levels to basal (CCCP-induced), the change in NADH level following rotenone treatment was assessed as a measure of the proportion of mitochondrial NADH oxidised through complex I activity. No change was observed in NADH levels on knockdown of PYCR1 in IDH1 wild-type cells. However, a significant increase in NADH was observed in IDH1 R132H cells (Figure 3.18E), suggesting that loss of PYCR1 activity results in complex I being responsible for oxidising a greater proportion of the mitochondrial NADH. This suggests that the increase in glutamine-derived proline biosynthesis in IDH1 R132H cells in normoxia uses mitochondrial NADH that would otherwise be available for oxidation by complex I. Interestingly, comparison of NADH levels between wild-type and IDH1 R132H cells revealed

significantly less NADH in IDH1 R132H cells, but were restored to levels similar to that of IDH1 wild-type cells on knockdown of PYCR1 (Figure 3.18E). This may reason that the increased proline biosynthesis observed in IDH1 R132H cells in normoxia oxidises a considerable proportion of mitochondrial NADH.

Based on the results presented in Figure 3.18, it was hypothesised that proline synthesis in IDH1 R132H cells was responsible for oxidation of a significant proportion of mitochondrial NADH in normoxia, and knockdown of PYCR1 or 2 would increase the availability of NADH for electron transfer in the ETC, thereby increasing oxygen consumption. To investigate this, the rate of oxygen consumption was measured using a Clarke-type oxygen electrode. Comparable oxygen consumption rates were observed between wild-type and IDH1 R132H-expressing cells in both U87 (Figure 3.19A) and HOG (Figure 3.19B) cell models. Consistent with our NADH autofluorescence results, knockdown of both PYCR1 and 2 had no effect on oxygen consumption in IDH1 wild-type cells (Figure 3.19C). However, the rate of oxygen consumption was significantly increased in IDH1 R132H HOG cells when either PYCR1 or 2 were knocked down (Figure 3.19D) This indicates that proline biosynthesis oxidises significant NADH in IDH1 mutant-expressing cells, reducing the requirement of these cells to consume oxygen, and perhaps making more oxygen available for other cellular processes.

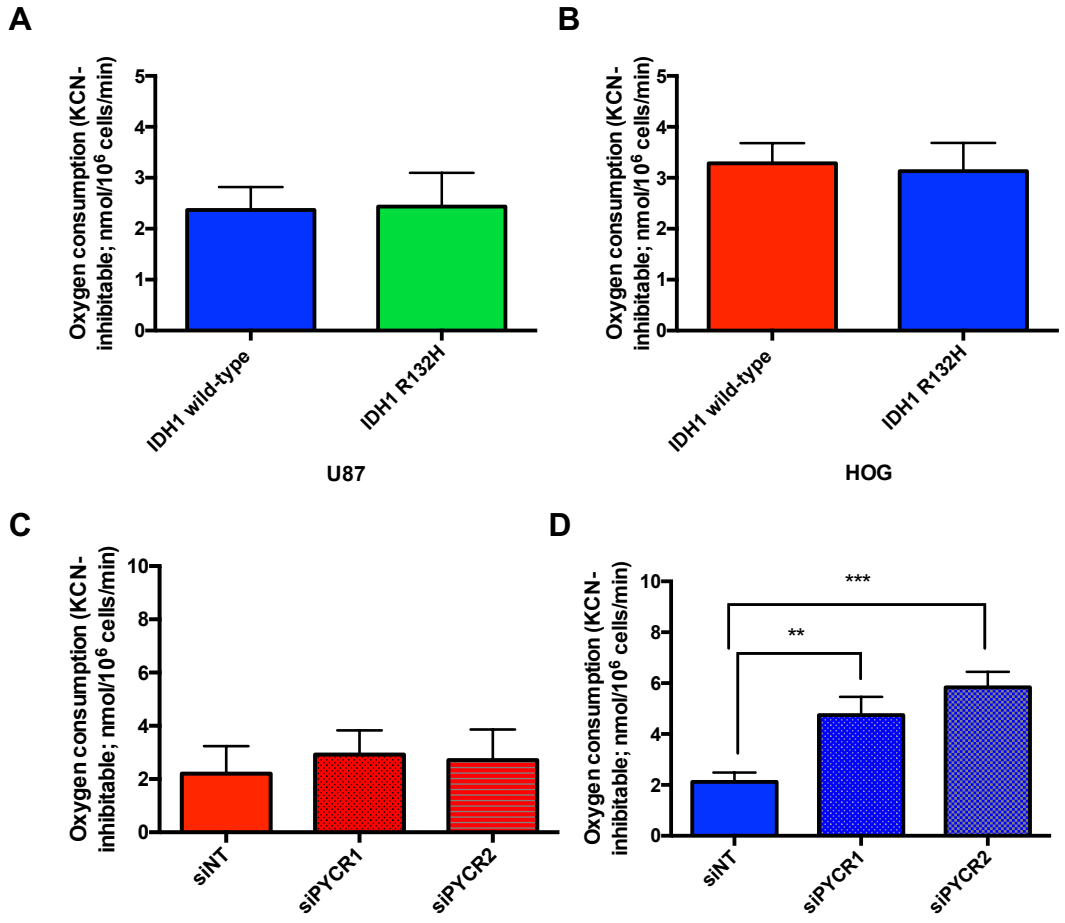

Figure 3.19 Knockdown of PYCR increases NADH availability for oxygen consumption in IDH1 mutant cells. No difference is observed in oxygen consumption measurements between IDH1 status in either (A) U87 or (B) HOG cell models in normoxia. Knockdown of PYCR 1 and 2 have no effect in oxygen consumption in (C) IDH1 wild-type HOG cells but resulted in a significant increase in oxygen consumption in (D) IDH1 R132H HOG cells. Experiments performed in technical triplicate. Data is mean +/- S.D. Significance determined using one-way ANOVA.

Oxidation of NADH in the mitochondria by a non-ETC reaction, such as proline biosynthesis would provide cells the means to continue TCA cycle dehydrogenase activity, producing anabolic substrates for continued proliferation in the presence of ETC inhibitors, such as rotenone. Indeed, wild-type cells were more sensitive to sub-maximal concentrations of rotenone than mutant IDH1 cells, and this sensitivity

decreased when wild-type cells were exposed to hypoxia (Figure 3.20B). Collectively, our findings support the concept that increased proline biosynthesis occurs in response to a change of cellular redox elicited by cells expressing the IDH1 R132H mutation or those in hypoxia. This alteration in mitochondrial activity may be used as a means of regulating mitochondrial redox state, removing the dependency of NADH oxidation on oxygen availability, and permitting continued proliferation in an oxygen sparing mechanism.

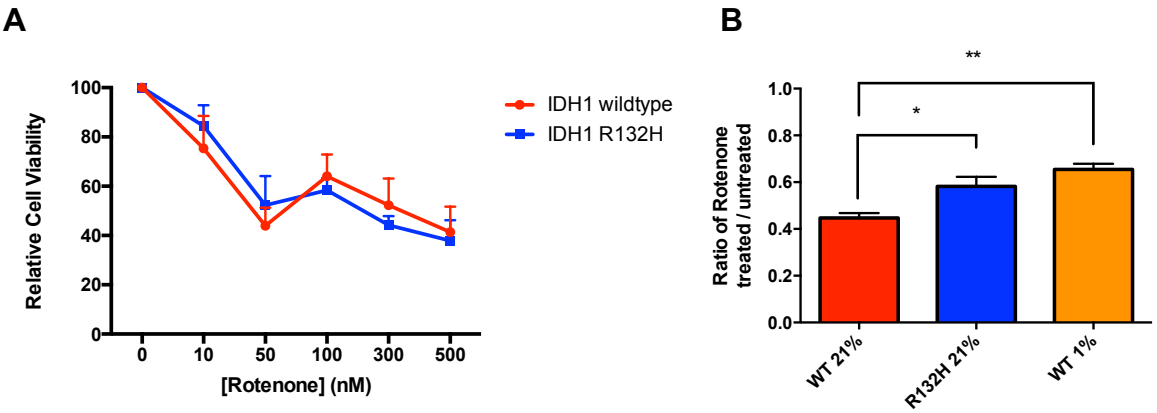

Figure 3.20 IDH1 mutants are less sensitive to complex I inhibition. (A) Dose-response curves to compare and determine IC50 of rotenone in wild-type and R132H IDH1 cells, as determined by SRB assay. (B) IDH1 R132H HOG cells are less sensitive to complex I inhibition when treated with 50 nM rotenone for 72 h, as determined using SRB assay. Data performed in technical and biological triplicate, presented as mean +/- S.E.M. Significance determined using an unpaired student's t-test.

Discussion

Although mutant IDH1 gliomas are clinically and biologically distinct to those expressing wild-type IDH1, unravelling the mechanisms behind this is challenging. The nature of the interplay between IDH1 mutations and hypoxia on glioma biology and tumour progression remains somewhat elusive. Our results have shown that IDH1 mutant gliomas are metabolically distinct to those with wild-type IDH1 (Figure 3.1 and 3.2), and mutations in IDH1 compromise the metabolic adaptation to hypoxia (Figure 3.3), despite observable HIF1α stabilisation (Figure 3.4A and 3.9A). When exposed to conditions of low oxygen, IDH1 R132H U87 glioma cells did not exhibit the same degree of metabolic adaptation as observed for wild-type cells (Figure 3.3). Given the overlapping metabolic profile of IDH1 R132H cells with that of normoxic IDH1 wild-type cells (rather than hypoxic wild-type IDH1 cells) in the PCA plot (Figure 3.3), and the greater number of metabolic differences identified between IDH1 mutant-expressing cells in both oxygen tensions when compared to hypoxic wild-type IDH1 cells (Figure 3.5), our metabolomic data perhaps more strongly suggest that IDH1 mutant cells compromise the metabolic adaptation to hypoxia. Indeed, sustained activity of PDH (Figure 3.8C and 3.8D) and oxidative glutamine metabolism (Figure 3.11) in IDH1 mutant cells in hypoxia, as identified by ^{13}C labelling approaches, suggest that these cells are unable to undergo a complete metabolic adaptation to hypoxia. Consistent with this theory, was the observation that IDH1 mutant cells initially maintain proliferation in hypoxia but become more sensitive to hypoxic stress over longer periods of time (Figure 3.6).

There is overlap in the statistically significant metabolites responsible for the segregation of wild-type and mutant IDH1 from the metabolomics analysis of glioma tissue and U87 cell samples. This confirms that the cell model used is biologically relevant, and would be important should novel therapeutic approaches be designed using our results. Many of the metabolic differences identified in tissues and cells reveal differences in glycolytic intermediates, organic acid and amino acids – but also include redox sensitive changes. Nicotinamide is a redox sensitive change that was consistently detected, where it is found to be increased in IDH1 mutant tumour tissues (Figure 3.2) and hypoxic IDH1 wild-type cells (Figure 3.5A and 3.5D). Changes in nicotinamide is indicative of altered NAD^+ metabolism, as it is not only a precursor for $NAD(P)^+$ synthesis, but is also a product of de-acetylation through the activity of NAD^+-dependent sirtuins, and/or a product of poly ADP ribose polymerase (PARP) activity. Interestingly, recent reports have suggested that IDH enzymes inhibit alkylated DNA repair enzyme alkB homolog (ALKBH) through the production of (R)-2HG leading to DNA damage and sensitisation to alkylating agents (Wang et al. 2015). This would result in high DNA damage that could increase PARP activity, utilising (and potentially depleting) NAD^+ as a substrate, and regenerating nicotinamide. This report could explain the increased nicotinamide observed, and may contribute to the susceptibility of IDH1 mutant cancers to NAD^+ depletion (Tateishi et al. 2015).

The significant production of (R)-2HG in IDH1 mutant cells results in partial HIF1α stabilisation and transactivation of target genes in both cell line models studied (Figure 3.4 and 3.9), indicative of a pseudohypoxic phenotype common to those

observed in SDH and FH deficient cells and tumours. The discrepancies in the extent of HIF-target gene transactivation (Figure 3.4) suggest differences in their regulation, which could be accounted for by the spectrum of effects HIF signalling has depending on its level of stabilisation. Alternatively, these differences may emanate from changes beyond the HIF/hypoxic response elicited in the IDH1 mutant cells. For example, owing to the effects of mutant IDH1 on cellular epigenetics, or other transcription factors.

Despite an increase in the mRNA of PDK1, the regulatory kinase for PDH (Figure 3.4B and 3.9B), no decrease in PDH activity was observed in our metabolic studies (Figure 3.8). This infers that either the increased PDK1 mRNA is not reflected at the increased protein expression level, or a compensatory increase in the PDH phosphatase 1 (PDP1) allows IDH1 mutant cells to retain PDH activity. If RNAi approaches were employed, it may be possible to understand whether the differential response in HIF target genes is due to the activity of HIF or by the activity of a different transcription factor. Nuclear localisation of HIF, or chromatin immunoprecipitation studies may provide additional evidence to prove whether HIF is transcriptionally active and binds to the PDK1 promoter.

HIF1 α stabilisation is not reflected in the metabolic profile, as IDH1 mutant cells are shown to sustain PDH and oxidative glutamine metabolism in hypoxia. It may therefore be possible that 2HG produced by IDH1 mutant-expressing cells directly alters mRNA translation. αKG-dependent hydroxylases belong to a large family of oxygenase enzymes whose activities are still emerging. Translational hydroxylases

involved in protein synthesis are becoming increasingly recognised as an important level of gene expression control. To date, three αKG oxygenases have been identified as ribosomal protein hydroxylases: OGFOD1, MINA53 and NO66 (Ge et al. 2012; Loenarz et al. 2014; Singleton et al. 2014). The biological consequences of these hydroxylation events remain to be defined. However, MINA53 and NO66 are thought to be involved in regulating growth and proliferation (Tsuneoka et al. 2002; Sinha et al. 2010). One possible explanation for the partial HIF1α stabilisation and transcriptional activity in IDH1 mutant cells, without evidence of metabolic adaptation, may be due to the competitive inhibition of αKG-dependent translational hydroxylases by the significant production of (R)-2HG, resulting in a block in protein translation of HIF1α targets.

Intriguingly, our results also indicate that HIF1α and 2α are differentially stabilised in IDH1 R132H and wild-type HOG cells (Figure 3.9A), indicating that different HIF prolyl hydroxylases are affected to different degrees by the production of (R)-2HG. Increased expression of HIF1α suggests inhibition of PHD2 activity (Berra 2003), yet the blunted expression of HIF2α observed in IDH1 R132H cells is indicative that PHD1 or PHD3 activity is maintained (Appelhoff et al. 2004). HIF1 and HIF2 are capable of eliciting the transcription of different sets of genes, for examples Ca9 and PHD3, wherein the former is predominantly HIF1 regulated and the latter HIF2 regulated, resulting in a differential response between tumour types (Hu et al. 2003; Sowter et al. 2003; Raval et al. 2005). At this stage, it is unclear what the biological implications are for this differential HIF regulation in mutant and wild-type IDH1 tumours.

Our results further suggest that increased proline biosynthesis from glutamine appears to be a hypoxia-inducible metabolic pathway (Figure 3.12). Increased proline is observed in the metabolomics approach in IDH1 wild-type U87 glioma cells when exposed to hypoxia (Figure 3.5A), supporting further evidence that proline biosynthesis increases in hypoxia. In addition to the significant production of (R)-2HG in cells expressing mutant IDH1, it is likely that the change in activity results in an alteration in cellular redox state (Dang et al. 2009). Proline biosynthesis from glutamine, a highly redox-dependent pathway, is significantly increased in IDH1 mutant cells regardless of oxygen tension (Figure 3.12). This suggests that IDH1 mutant cells demonstrate increased proline metabolism, similar to that of hypoxic wild-type IDH1 cells. Our results indicate that proline biosynthesis can be used by cells as a means to modulate or maintain cellular redox, and in an IDH1-mutant background is independent of 2HG production (Figure 3.14B). Increased proline biosynthesis is found to decouple TCA cycle activity from the ETC by reducing NADH-mediated electron donation to complex I of the respiratory chain (Figure 3.18E), and is observed through the reduced sensitivity to complex I inhibitors (Figure 3.20C), and the increased oxygen consumption on inhibition of proline synthesis (Figure 3.19D). By providing an alternative mechanism for oxidation of mitochondrial NADH, reduced electron flux through the ETC may yield lower ROS generation, and decrease oxygen consumption by the mitochondria, perhaps making oxygen more available for other metabolic or biological processes. Interestingly, PYCR1 has been previously linked to regulation of mitochondrial complex I, mediated through an interaction with regulatory protein DJ-1, where knockdown of DJ-1 and PYCR1 reduced cell viability under conditions of oxidative stress (Yasuda et al. 2013). Such

an adaptive redox mechanism could provide a way in which cells regulate oxidative metabolism, and therefore oxidative stress in hypoxia (Figure 3.21).

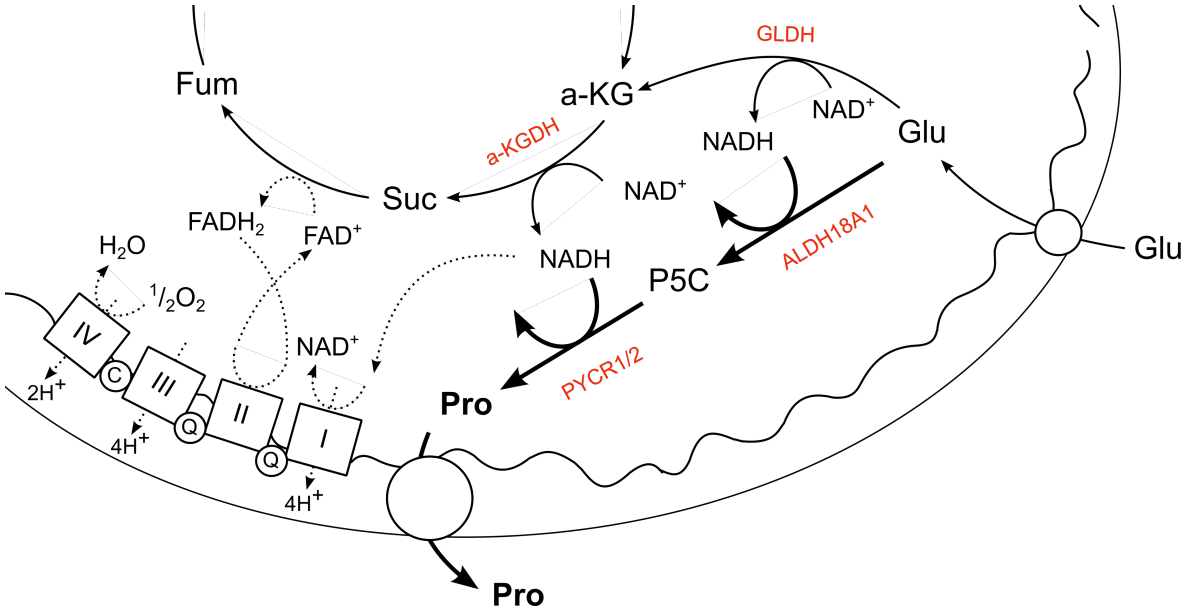

Figure 3.21 IDH1 mutations exhibit pseudohypoxic proline metabolism. IDH1 mutations increased glutamine derived proline biosynthesis to retain redox plasticity by reducing electron donation to complex I of the ETC. Abbreviations: ALDH18A1, pyyroline-5-carboxylate synthetase; Fum, fumarate; Glu, glutamate; GLDH, glutamate dehydrogenase; a-KG, α-ketoglutarate; a-KGDH, α-ketoglutarate dehydrogenase; Pro, proline; P5C, pyrroline 5-carboxylate; PYCR1/2, pyyroline carboxylate reductase 1/2 and Suc, succinate.

Overall, it would appear that IDH1 mutant cells exhibit a “semi-pseudohypoxic” state. This results from a lack of adaptation to hypoxia, whereby cells maintain oxidative reactions in the absence of oxygen, yet also exhibit hypoxic-like features, such as increased glutamine-derived proline biosynthesis in normal oxygen tensions (pseudohypoxic proline metabolism). Although the data are not entirely clear, it might be inferred that sustained normoxic phenotypes occur as a result of blunted HIF transcriptional activity, yet the hypoxic phenotypes occur as a result of hypoxic-like redox changes elicited from the presence of the IDH1 mutation. How this benefits the

progression of the tumour is unknown. It could be hypothesised that this facilitates rapid metabolic plasticity to fluctuating regions of varying oxygen tension and occurs from the unstable and chaotic organisation of the tumour-associated neovasculature. But, this metabolic plasticity is unsustainable for longer periods of hypoxia, consistent with the improved prognosis associated with IDH1 mutant gliomas.

Experimental Procedures

Patient information

The use of patient material was approved by HBRC (Human Biomaterials Resource Centre), HTA Research License number 12358, reference for ethical approval 09/H1010/75 (North West 5 Research Ethics Committee – Haydock Park). GBM samples were collected with informed consent from patients at the Queen Elizabeth Hospital Birmingham (QEHB) NHS Foundation Trust between 2011 and 2012. Immediately following surgical resection, tumour samples were flash frozen and stored in liquid nitrogen. All histological diagnoses were confirmed by the Pathology department at the QEHB and graded according to 2007 World Health Organisation (WHO) classification (Louis et al. 2007).

Cell Lines

U87 glioma cell line stably transfected with green fluorescent protein (GFP)-tagged IDH1 wild-type or R132H mutant were kindly donated by Dr. Pim J. French (Bralten et al. 2011). Cells were routinely cultured in DMEM with 10% FBS and 2 mM glutamine (all Hyclone Thermo Scientific; SH30081, SV30180.03, and 25030081, respectively).

U87 glioma cell lines were re-selected for the presence of the construct by fluorescence activated cells sorting (FACS) to isolate the cells expressing the highest GFP levels. For one week following FACS, medium was supplemented to a final concentration of 200 units/mL penicillin, 200 µg/mL streptomycin (Thermo Fisher, 1688253) and 50 µg/mL gentamicin (Sigma-Aldrich, G1397).

A cell line derived from a grade III human oligodendroglioma infected with either wild-type or mutant IDH1 (R132H) by lentivirus, was kindly donated by Professor Hai Yan (Reitman et al. 2011). Both HOG IDH1 wild-type and R132H cell lines were cultured in high glucose DMEM (Sigma-Aldrich, D5796) supplemented with 10% FBS (Hyclone Thermo Scientific, SV30180.03).

Cell lines were maintained using standard procedures in a 37^{o}C humidified incubator, 5% CO_2 and regularly tested and excluded for mycoplasma contamination using EZ-PCR Mycoplasma Test Kit, (Geneflow, K1-0210).

Proliferation

U87 IDH1 wild-type and R132H cells were seeded at 5 x 10^4 cells in 6-well plates and left overnight to adhere to the plate surface under standard conditions. Relevant plates were transferred to Don Whitley H35 Hypoxystation set at 1% O_2, where the media was changed on all wells of all plates. Cell counts were performed 24 h, 48 h, 72 h and 96 h using Invitrogen Automated Cell Countess®^{TM} (Thermo Fisher, C10227).

RNA and Protein Analysis

Cells were seeded at 1 x 10^5 onto 6-well plates and left for 24 h. Relevant plates were transferred to Don Whitley H35 Hypoxystations set at 1% and 0.3% O_2, and left for a further 24 h before lysed for protein and RNA to assess gene expression.

Quantitative real-time PCR

Total RNA was extracted using the RNeasy Mini Kit (Qiagen, 74104) according to the manufacturer's protocol. 1 µg RNA per sample was subjected to reverse transcription using Promega Reverse Transcriptase kits (MMLV-RT, M1701, or AMV-RT, A3500). 10 µL of the resulting cDNA was used with TaqMan® gene expression master mix (AB, 4369016) for quantitative real-time PCR using AB 7500 Real Time PCR System. The following primers and probes were purchased from Thermo Fisher Scientific:

Table 3.1 HIF target genes for quantitative real-time PCR

Gene Target	Product Code
LDHA	(Hs00855332_g1)
PGK1	(Hs00943178_g1)
PDK1	(Hs00176853_m1)
SLC2A1	(Hs00892681_m1)
PYCR1	(Hs01048016_m1)
PYCR2	(Hs01016460_gH)
ALDH18A1	(Hs00913261_m1)

The expression of all genes targets were normalised to beta actin (ACTB) as housekeeping gene. Comparative analysis across samples was calculated using the $2^{-\Delta\Delta CT}$ method.

Immunoblotting

Cells were washed with 1x PBS and lysed directly into 100 µL 1x Laemmli buffer (Sigma-Aldrich, S3401-1VL), heated at 100^{o}C for 10 min, and loaded on polyacrylamide gels for SDS-PAGE (sodium dodecyl sulphate polyacrylamide gel electrophoresis). Proteins were separated under reducing denaturing conditions, using the mini-PROTEAN Tetra System (BIO-RAD), and transferred electrophoretically onto 0.1 µm nitrocellulose membrane (GE Healthcare,

10600000) at 100 V for 75-90 min. Blots were blocked in 1x PBS with 0.05% Tween-20 (PBST) buffer containing 5% (w/v) non-fat skimmed dry milk powder (Marvel) for 1 h, and then incubated with the specific primary antibody of interest (table below) diluted in blocking buffer at 4^{o}C overnight (excluding anti-β-actin, which was incubated for 1.5 h at room temperature). All antibodies were diluted in 5% milk with the exception of HIF1α, which was diluted in 1% milk. Membranes were washed three times in PBST and incubated with the relevant horseradish peroxidase (HRP)-conjugated secondary antibody diluted in 5% milk for 1 h at room temperature. Membranes were washed three times and developed using EZ-ECL enhanced chemiluminescence detection kit (BI, 20-500-120). Luminescence was visualised using Amersham Hyperfilm^{TM} (GE HealthCare, 28906836), which was subsequently developed (SRX 101A Konica Minolta). All western blots are representative of at least two experiments unless otherwise indicated.

Table 3.2 Primary antibodies employed for immunoblotting

Primary Antibody	Company	Product Code	Species	Dilution	Mw
Anti-β-actin	Sigma	A4700	Mouse	1:4000	42 kDa
Anti-IDH1 R132H	Dianova	DIA-H09	Mouse	1:500	48 kDa
Anti-HIF1α	BD Biosciences, UK	610959	Mouse	1:500	120 kDa
Anti-HIF2α	Novus Biologicals	NB100-122	Mouse	1:500	120 kDa
Anti-PYCR1	Proteintech	13108-1-AP	Rabbit	1:5000	34 kDa
Anti-PYCR2	Proteintech	17146-1-AP	Rabbit	1:1000	34 kDa

Table 3.3 Secondary antibodies employed for immunoblotting

Secondary Antibody	Company	Product Code	Dilution
Anti-mouse	Cell Signalling	#7076	1:4000
Anti-rabbit	Cell Signalling	#7074	1:4000

RNA Silencing

To assess the knockdown in expression of PYCR1 and PYCR2, cells were seeded at 8 x 10^4 onto 12-well plates in standard culture conditions. After 24 h, cells were transfected following manufacturer's instructions with non-targeting RNA (siNT) and siRNA targeting PYCR1 (siPYCR1) and PYCR2 (siPYCR2) (Dharmacon ON-TARGETplus human siRNA; D-001810-10, L-012349-00 and L-016646-00, respectively) at 25 nM using DharmaFECT 1 transfection reagent (Thermo Fisher Scientific, T2001-01).

24 h, 48 h and 72 h post transfection, cells were lysed for protein to evaluate efficiency of gene knockdown. All transfections were carried out 24 h post seeding and all experiments were subsequently terminated approximately 48 h from transfection.

NAD(P)H Autofluorescence

HOG cells were seeded at 0.2 x 10^5 onto 8-well chamber slides (Thistle Scientific, IB-80826) under standard culture conditions and transfected 24 h later with targeting and non-targeting siRNA against PYCR1 before NAD(P)H imaging 48 h later using a Zeiss UV Axiovert confocal autofluorescence captured at l = 285-470 nm using a photomultiplier tube (PMT) (1024 x 1024 pixels; 12-bit). CCCP 20 µM (Sigma-Aldrich, C2759) and rotenone 60 µM (Sigma-Aldrich, R8875) were added to each well to achieve basal and maximal NAD(P)H autofluorescence, respectively. User-blinded offline analysis was performed using Fiji software (http://fiji.sc/) and 48-126 random visual fields were considered per experimental condition. To prevent re-oxygenation

of hypoxic samples, slices were sealed with parafilm and imaged within 15 min of removal from 1% O_2.

Oxygen Consumption Measurements

Cells were seeded at 2 x 10^5 onto 6-well plates in standard culture conditions and were transfected 24 h later with targeting siRNA against PYCR1 and PYCR2. Oxygen consumption measurements were made using a Clark-type oxygen electrode (Oxytherm, Hansatech Instruments, Norfolk, UK) that measures oxygen concentration in a sealed chamber. The cells were harvested and resuspended in complete media. 4 x 10^5 cells in 300 µl were added to the electrode chamber and the oxygen consumption rate was measured over a 5 min period using Oxygraph software (http://www.hansatech-instruments.com/). Cells were kept in suspension using a stirring bar and the chamber temperature was maintained at 37°C through the use of a solid-state heating block. After recording for 5 min, KCN 700 µM (Sigma-Aldrich, 60178) was added to the electrode chamber to inhibit cellular respiration and the oxygen consumption was measured for a further 3 min.

The final respiration rate was obtained by subtracting the oxygen consumption rate in presence of KCN to the oxygen consumption rate in the absence of KCN.

SRB assay

Cells were fixed in 20% (v/v) ice-cold trichloroacetic acid solution (TCA) (Sigma-Aldrich, T0699) for 30 min at 4°C. Plate wells were washed with water and once dry, intracellular protein was stained using 0.4% (w/v) sulfohodamine B (SRB) (Sigma-Aldrich, 230162) in 1% acetic acid for 10 min at room temperature. After washing with

1% acetic acid to reduce non-specific staining, SRB was dissolved in 50 mM Tris/HCl pH 8.8 once dry. 100 µL/well was aliquoted for quantification by absorbance at 495 nm on FLUOstar Omega (BMG LabTech).

Final sample absorbance values were determined by calculating the mean blank-corrected absorbance for each replicate, where 50 mM Tris/HCl pH 8.8 alone was used as the blank.

Hydrogen Peroxide

HOG cells were seeded at 4 x 10^4 onto 24-well plates in standard culture conditions and incubated for 24 h. Cells were dosed with H_2O_2 concentrations of 10, 50, 100, 300 and 500 µM and incubated for 24 h to determine the IC50 before fixing using the SRB method.

The effect of H_2O_2 treatment on cell viability was assessed by dosing the above plate format with 100 µM H_2O_2 24 h post transfection using targeting siRNA against PYCR1 and PYCR2. Cells were treated with H_2O_2 for 24h before fixing using the SRB method.

Rotenone

HOG cells were seeded at 4 x 10^4 onto 24-well plates in standard culture conditions and incubated for 24 h. Cells were dosed with rotenone concentrations of 10, 50, 100, 300 and 500 nM to determine the IC50 and incubated for 24 h before fixing using the SRB method.

The effect of rotenone treatment on proliferation was assessed by dosing the above plate format with 10 nM and 50 nM rotenone 24 h post seeding in normoxia and

hypoxia (1% O_2). Cells were incubated with rotenone for 24, 48 and 72 h. At each time-point, cells were fixed, stained and analysed using the SRB method.

Metabolomics

In collaboration with Warwick Dunn

Tissue: ~50 mg (+/-10 mg) tumour tissue was weighed and homogenised using Precellys®24 at 6,800 Hz for 2 x 30 s cycles. Metabolites were extracted in 850 µL methanol (-20^{o}C): chloroform (-20^{o}C) (1:1) and shaken for 10 min at 4^{o}C, before placed on ice for 10 min. 425 µL pre-chilled water was added and left on ice for a further 10 min, before centrifugation at 13,500 x *g* for 15 min. The "sample weight normalised" volume of polar and non-polar extract phase was calculated using the following formulae:

"Sample weight normalised volume" = (maximum volume/ minimum weight sample) x sample weight.

QC samples were prepared by mixing 'sample weight normalised' volumes for each sample. Polar extracts were dried by speed vacuum concentration for 5 h at 35^{o}C. Non-polar extracts dried under nitrogen gas stream.

Cell: U87 IDH1 wild-type and R132H cells were seeded at 1 x 10^6 in standard culture conditions and left overnight. Relevant cell plates were transferred to Don Whitley Hypoxystation set at 1% O_2 the following day and subjected to 24 h of normoxia or hypoxia (n=6 per sample class). Cells were washed x3 with ice-cold 1x PBS and scraped in pre-chilled methanol (-20^{o}C), chloroform (-20^{o}C) and water (4^{o}C) in 1:1:1 ratio. Cell lysates were vortexed for 15 min at 4^{o}C and immediately centrifuged at 15,000 x *g* for 15 min at 4^{o}C. The total recoverable volume (550 µL) of the polar

extract (after removal of aliquots for QC) was split for analysis by GC-MS. Polar extracts were dried by speed vacuum concentration for 6 h at 30°C.

GC-MS: Dried polar extracts were derivatised by adding 50 μL of 20 mg/mL solution of methoxylamine in pyridine, vortex mixing and heating at 60°C for 30 min. 50 μL of N-methyl-N-trifluoroacetamide was added followed by vortex mixing and heating at 60°C for 30 min. 20 μL retention index marker solution (1 mg/mL C_{10}, C_{12}, C_{15}, C_{19}, C_{22} n-alkanes) was added prior to centrifugation. The resulting supernatant was transferred to GC-MS vials for analysis.

Derivatised polar samples were analysed by GC-MS using an Agilent 6890 gas chromatograph (Agilent Technologies, Stockport, U.K.) coupled to a LECO Pegasus III (Leco Corp., St. Joseph, MO) electron ionisation time-of-flight mass spectrometry (EI-TOF-MS) in a randomised sample order for analysis. Following a derivitisation blank, QC samples were analysed for the first two injections and every fourth and fifth injection respectively. The GC-MS parameters have been previously described (Dunn et al., 2011).

Data were pre-processed using the ChromaTOF v3.25 software package and metabolites assigned, as described in (Armitage et al. 2015). Data were normalised to total peak area for each sample followed by statistical analysis applying non-parametric Mann Whitney U tests or Kruskal-Wallis test. PCA analysis Partial Least Squares Discriminate (PLS-DA) in the freely available package MetaboAnalyst (Xia et al., 2012).

Isotope Tracing

Basic formulation DMEM media (Sigma, D5030) was supplemented with the relevant tracer [U-$^{13}C_6$]-D-glucose (Sigma, 389374) or [U-$^{13}C_5$]-L-glutamine (Sigma, 605166) at 10 mM and 2 mM respectively, along with the same concentration of corresponding unlabelled glutamine and glucose. All tracing experiments were conducted for 24 h and commenced 24 h post seeding.

NMR Spectroscopy

4 x 10^6 HOG cells were plated onto 15 cm dishes and cultured in standard medium overnight. Relevant cell plates were transferred to Don Whitley Hypoxystations (set at both 1% and 0.3% O_2) the following morning. Media was replaced with basic formulation DMEM (Sigma-Aldrich, D5030) supplemented with 10% FBS, 10 mM [U-$^{13}C_6$]-D-glucose (Sigma-Aldrich, 389374) or 2mM [U-$^{13}C_5$]-L-glutamine (Sigma-Aldrich, 605166) for a further 24 h before extraction.

Cells were washed x3 with ice-cold 0.9% saline solution and scraped in 1.2 mL pre-chilled methanol (-20^{o}C), water (4^{o}C) and chloroform (-20^{o}C) in a 1:1:1 ratio. Cell lysates were vortexed for 15 min at 4^{o}C and immediately centrifuged at 15,000 x *g* for 15 min at 4^{o}C. The polar fraction was aliquoted and evaporated to dryness using a SpeedVac concentrator for 5h at 30^{o}C. Extraction was performed on three different cultures for each labelling experiment.

Dried samples were resuspended in 60 µL of 100 mM sodium phosphate buffer containing 500 µM DSS (4,4-dimethyl-4-silapentane-1-sulphonic acid) and 2 mM Imidazole, 10% D_2O, pH 7.0. Samples were vortexed, sonicated (5-15 min) and

centrifuged briefly, before transferred to 1.7 mm NMR tubes using an automated Gilson 215 Liquid Handler (Bruker Biospin).

1D-^{1}H NMR spectra and 2D-^{1}H,^{13}C-HSQC NMR spectra were acquired using a 600-MHz Bruker Avance III spectrometer (Bruker Biospin, UK) with a TCI 1.7 mm z-PFG cryogenic probe at 300 K. Spectral widths were set to 7,812.5 and 24,155 Hz for the ^{1}H and ^{13}C dimensions, respectively. 16,384 complex data points were acquired for the 1D-NMR spectra and 512 complex data points were acquired for the ^{1}H dimension of 2D-^{1}H,^{13}C-HSQC NMR spectra. An exponentially weighted non-uniform sampling scheme was used for the indirect dimension. Here, 30% of 8,192 complex data points (2,458) were acquired. 128 transients were recorded for the 1D-NMR spectra with a relaxation delay of 4 s, and two transients were recorded for the 2D-^{1}H,^{13}C-HSQC NMR spectra with a relaxation delay of 1.5 s. Each sample was automatically tuned, matched and then shimmed (1D-TopShim) to a DSS line width of <2 Hz prior to acquisition of the first spectrum. Total experiment time was ~15 min per sample for 1D-^{1}H NMR spectra and 4.5 h per sample for 2D-^{1}H,^{13}C-HSQC NMR spectra. 1D-^{1}H NMR spectra were processed using the MATLAB-based MetaboLab software (Ludwig & Günther 2011). All 1D data sets were zero-filled to 131,072 data points before Fourier Transformation. The chemical shift was calibrated by referencing the DSS signal to 0 p.p.m. 1D-spectra were manually phase corrected. Baseline correction was achieved using a spline function (Ludwig & Günther 2011). 1D-^{1}H NMR spectra were exported into Bruker format for metabolite identification and concentration determination using Chenomx 7.0 (ChenomxINC). 2D-^{1}H,^{13}C-HSQC NMR spectra were reconstructed using compressed sensing in the MDDNMR and NMRpipe software (Delaglio et al. 1995; Kazimierczuk & Orekhov 2011; Orekhov &

Jaravine 2011). The final spectrum size was 1,024 real data points for the ^{1}H dimension and 16,384 real data points for the ^{13}C dimension. Analysis was performed using MetaboLab and pyGamma software was used in multiplet simulations (Smith et al. 1994). The methyl group of lactate was used to calibrate the chemical shift based on its assignment in the human metabolome database (Wishart et al. 2013).

GC-MS

GC-MS analysis in collaboration with Christian Metallo

HOG cells were seeded at 1 x 10^5 in 6-well plates and cultured in standard medium overnight. Hypoxic plates were transferred to Don Whitley Hypoxystation set at 1% O_2 the following morning. 24 h post seeding, cells were cultured for a further 24 h, in either normoxia and hypoxia, in glucose or glutamine free DMEM (Sigma-Aldrich, D5030) containing 10% FBS and supplemented with the appropriate tracer - 10mM [U-$^{13}C_6$]-D-glucose (Sigma-Aldrich, 389374) or 2mM [U-$^{13}C_5$]-L-glutamine (Sigma-Aldrich, 605166).

At the conclusion of tracer experiments, culture media was aspirated and cells washed twice with 0.9% NaCl saline solution. Cellular metabolites were extracted in methanol (-20^{o}C): water (4^{o}C): chloroform (-20^{o}C), where 1 µg/well DL-norvaline (Sigma-Aldrich, N7502) was employed as internal standard in the polar fraction. Samples were vortexed at 4^{o}C for 30 min and subsequently centrifuged at 14,000 x *g* for 15 min at 4^{o}C. The polar fraction was aliquoted and dried by speed vacuum concentration at 2,000 RPM for 4h at 30^{o}C.

Polar metabolites were derivatised to form methoxine-TBDMS derivatives by incubation with 2% methoxyamine hydrochloride (Sigma-Aldrich, 226904) dissolved

in Pierce^{TM} pyridine (Thermo Fisher Scientific, 25104) at 37^{o}C for 1-1.5 h followed by addition of MTBSTFA with 1% TBDMCS (Sigma-Aldrich, 375934) incubated at 37^{o}C for 30-60 min (Metallo et al. 2011)(Lewis et al. 2014).

Derivatised polar samples were analysed by GC-MS using an Agilent 7890B gas chromatograph equipped with a 30 m DB-35MS capillary column (30 m x 0.25 mm internal diameter x 0.25 µm) connected to an Agilent 5977A mass spectrometer. MIDs were determined by integrating metabolite ion fragments and corrected for natural abundance (Fernandez et al. 1996).

Metabolite ion counts were normalised to norvaline and cell number to normalise for varying derivatisation efficiency and varying metabolite concentrations, respectively.

GC-MS analysis in collaboration with Karsten Hiller

HOG cells were seeded at 2 x 10^5 onto 6-well plates in standard culture conditions. After 24 h, cells were transfected with 25 nM non-targeting RNA (siNT) and siRNA targeting PYCR1 (siPYCR1) and PYCR2 (siPYCR2). After overnight incubation, relevant plates were transferred to hypoxia (1 % and 0.3% O_2), where 24 h post transfection, media was changed to basic formulation DMEM (Sigma-Aldrich, D5030) containing 10% FBS and supplemented with 2mM [U-$^{13}C_5$]-L-glutamine (Sigma-Aldrich, 605166) for a further 24 h.

At the conclusion of tracer experiments, culture media was aspirated and cells washed twice with ice-cold 0.9% NaCl solution. Cellular metabolites were extracted in methanol (-20^{o}C): water (4^{o}C) containing 1 µg/mL d6-glutaric acid (C/D/N ISOTOPES INC, D-5227): chloroform (-20^{o}C). Extracts were shaken at 1,400 rpm for 20 min at 4^{o}C and centrifuged at 16,000 x *g* for 5 min at 4^{o}C. The polar fraction was aliquoted

and evaporated in GC glass vials under vacuum at -4^{o}C using a refrigerated CentriVap Concentrator (Labconco).

Metabolite derivatisation was performed using an Agilent autosampler. Dried polar metabolites were dissolved in 2% methoxyamine hydrochloride (Sigma-Aldrich, 226904) dissolved in pyridine (Thermo Fisher Scientific, 25104) at 45^{o}C. After 1 h, an equal volume of MSTFA (N-methyl-N-(trimethylsilyl)trifluoroacetamide) + 1% TMCS (chloro-trimethyl-silane) (ThermoFisher Scientific, TS-48915) was added and metabolites were incubated for 30 min at 45^{o}C.

Derivatised polar extracts were analysed by GC-MS using an Agilent 6890 gas chromatograph equipped with a 30 m DB-35MS capillary column (30 m x 0.25 mm internal diameter x 0.25 µm). The gas chromatograph was connected to an Agilent 5975C mass spectrometer. For MID determination, spectra were corrected for natural isotope abundance. Data processing from raw spectra to MID correction and determination was performed using MetaboliteDetector software (Hiller et al. 2009). Metabolite ion counts were normalised to d6-glutaric acid and cell number to normalise for varying derivatisation and varying metabolite concentrations, respectively.

Statistical Analysis

Samples sizes and reproducibility for each figure are denoted in the figure legends. Unless otherwise noted, all experiments are representative of at least three biologically independent experiments performed in technical triplicate. All error bars represent mean +/- S.E.M. Statistical significance was determined by either a one-

way ANOVA or two-tailed Student's t-test using GraphPad Prism 6, where *P < 0.05; **P < 0.01; and ***P < 0.001.

Chapter 4 DISCUSSION

Cancer cells reprogram their energy metabolism to enable rapid proliferation and to adapt to changes in their microenvironment. The identification of mutations in metabolic enzymes SDH, FH and IDH have not only shown that malignant transformation can occur as a direct result to changes in normal metabolism, but have emphasised the importance of hypoxia-induced metabolic reprogramming in driving this malignancy. Further understanding of how mutations in SDH, FH and IDH control metabolism, and how metabolism changes in response to hypoxic stimuli, may therefore elicit the design of new selective therapies.

The research presented highlights novel mechanisms whereby cancer cells with mutations in metabolic enzymes SDH and IDH rewire their metabolism to support both the demands of cellular anabolism and the maintenance of redox homeostasis for proliferation and viability. In particular, it reveals a metabolic vulnerability relevant in SDH-deficient cells that could be efficacious for the treatment of other tumours harbouring these mutations. It additionally characterises a novel, redox-sensitive metabolic pathway common to both pseudohypoxic IDH1 and SDHB mutated cells that plays a critical role in maintaining metabolic plasticity.

Pyruvate carboxylase is a metabolic vulnerability associated with SDH deficiency

A key question this thesis addresses is how cells deficient in SDHB maintain proliferation and viability in PGL/PCC. Our published results (see Appendix - D)(Lussey-Lepoutre et al. 2015), along with another recent publication (Cardaci et al.

2015), demonstrate that loss of SDH activity results in an increased dependency on PC for endogenous aspartate synthesis. With limited means by which these cells can make aspartate in the absence of a fully functional TCA cycle, the proliferation-driven demand for aspartate exceeds supply. Aspartate is required for the synthesis of two major classes of macromolecules: proteins and polynucleosides. In addition to its obvious contribution to protein synthesis, it is required for the *de novo* synthesis of arginine and asparagine, the conversion of inosine monophosphate (IMP) to adenosine monophosphate (AMP) in *de novo* purine synthesis and the carbon backbone for *de novo* pyrimidine synthesis. Owing to a block in TCA cycle activity, PC-mediated aspartate biosynthesis is likely to determine the anabolic and proliferative state of the cell. Dysregulation of PC activity has been shown to extend to other disease areas, such as renal cancer (Cardaci et al. 2015), non-small lung cancer (Sellers et al. 2015) and diabetes (Kumashiro et al. 2013), and may be compatible with mutations in other TCA cycle intermediates, as predicted to be the case with loss of FH activity (Frezza et al. 2011).

Inhibiting PC-mediated *de novo* aspartate biosynthesis in SDH-mutated tumours

Increased PC activity highlights a metabolic vulnerability specific to SDH-mutated tumours and thus represents a valid therapeutic target. PC is an enzyme that is amenable to a number of different approaches for inhibitor design. Examples include; disrupting the interaction with biotin, use of carboxyphosphate or ATP analogues, employing pyruvate structural analogues, or decreasing the availability of positive allosteric regulators such as acetyl CoA (Jitrapakdee et al. 2008). However, a

problem with all the above drug design approaches is the ubiquitous nature of PC, leading to theoretical selectivity arguments with other metabolic pathways, and resulting in numerous off-target effects. This makes PC in itself a difficult therapeutic target. As SDH deficient tumours are dependent upon endogenous production of aspartate for nucleotide synthesis, it could be feasible to target other aspects of the aspartate biosynthetic pathway. Our results demonstrate that SDH-mutated PCC also significantly up-regulates expression of the glutamate-aspartate antiporter, as well as the transaminase responsible for converting oxaloacetate to aspartate in the mitochondria (GOT2) (data not shown). The low levels of aspartate detected in SDH-mutated tumours, may imply that mild inhibition of aspartate aminotransferases, such as GOT2, may be more effective in limiting proliferation.

Increased malignancy of mutations in SDHB and use of the serine synthesis pathway

The potential phenotypic similarities and differences in cancer cells harbouring mutations in other SDH subunits has not yet been investigated. Furthermore, results do not yet indicate why mutations in SDHB are associated with increased malignancy when compared to other SDHx mutated tumours. The basis for increased malignancy with loss of SDHB has previously been speculated by several groups. One of the few studies to examine the differential effects of deficiencies in the various SDH subunits suggested that RNAi-mediated reduction in the expression of SDHB led to increased mitochondrial ROS production (Guzy et al. 2008) and is perhaps is the basis for increased malignancy associated with mutated SDHB tumours. A subsequent study reported significantly greater hypermethylation in SDHB tumours when compared to

mutations in other SDH subunits, resulting in greater epigenetic silencing of genes involved in neuroendocrine differentiation and epithelial-mesenchymal transition (EMT) (Letouzé et al. 2013). It therefore poses an interesting speculation as to whether mutations in other SDH subunits show the same increase in *de novo* serine synthesis from glucose and subsequent catabolism, as high activity within this pathway has been recently associated with metastasis (Piskounova et al. 2015), and could be used to support the demand for mitochondrial NADPH and/or one-carbon groups for DNA and histone methylation.

Proline biosynthesis maintains cellular redox plasticity in tumours

A significant finding consistent for both SDH and IDH1 mutations was the increased biosynthesis of proline from glutamine, which also appeared to be a feature of hypoxic cells. The catabolism of glucose and glutamine in cancer cells is used not only for cellular anabolism, but also to maintain redox homeostasis. Well-characterised examples of metabolic pathways that support cellular redox include i) increased lactate production to regenerate NAD^+, which is reused by GAPDH to sustain glycolysis, cytosolic NADPH production, either by ii) the recycling of glucose through the PPP, and/or iii) the activity of cytosolic ME, which uses glutamine carbon to form pyruvate from malate. Thus, other less explored biosynthetic pathways could affect the reducing potential in cancer cells, such as the redox sensitive biosynthesis of proline from glutamine. However, this biosynthetic pathway has not as yet been characterised as having a role in maintaining cellular redox plasticity in cancer cells.

Our results demonstrate that proline anabolism increases in response to redox stress in hypoxic environments and in conditions of pseudohypoxia experienced by cells harbouring mutations in either SDH or IDH1. An increased ratio of NADH/NAD^+ is likely to increase proline biosynthesis in order to maintain redox homeostasis by oxidising mitochondrial NADH, which would otherwise be oxidised by the ETC to ultimately reduce oxygen to water. As the activity of the ETC impacts cellular processes such as apoptosis and levels of ROS in cells, increased proline biosynthesis may therefore modulate/regulate these activities. Furthermore, use of this pathway could make more oxygen available for other biological purposes, which would benefit cells in environments where oxygen supply is limited. Our findings may therefore demonstrate a novel redox-sensitive mechanism by which mutations in metabolic enzymes promote tumorigenesis.

Other tumour suppressors and oncogenes have been shown to regulate proline metabolism. For example, oncogenic MYC stimulates glutamine-derived proline biosynthesis by coordinating the increased expression of GLS and proline biosynthetic enzymes P5C synthetase (P5CS) and the PYCRs, in addition to suppressing the enzymes involved in proline catabolism, proline dehydrogenase (PRODH) and P5C dehydrogenase (P5CDH) (Liu et al. 2012). Interestingly, PRODH, the first enzyme in proline catabolism, is regulated by tumour suppressor p53 to block cell cycle progression and induce apoptosis through the generation of mitochondrial ROS (Donald et al. 2001). As PRODH is usually down-regulated in tumours (Liu et al. 2009), the increased PYCR activity exhibited in SDH and IDH mutated cells is likely to result in production of proline, consistent with increased concentrations of

intracellular (Figure 3.12C) and extracellular (Figure 2.16B and 3.12D) proline. It may also be possible that PYCR1 is the major enzyme involved in proline biosynthesis, since PYCR2 is most product-inhibited (De Ingeniis et al. 2012). Indeed, PYCR1 gene expression is significantly increased in SDH-mutated PCC (Figure 2.17) and IDH1 LGG and GBMs (Figure 3.14C and 3.14D). Increased PYCR1 has also been identified in prostate cancer (Ernst et al. 2002), melanoma (De Ingeniis et al. 2012) and breast carcinoma (Possemato et al. 2011).

Previous reports have suggested that cells expressing mutant IDH1 are more sensitive to pharmacological inhibitors of complex I in the ETC (Grassian et al. 2014). Our results may contradict these findings, as the increased anabolism of proline observed in IDH1 mutant cells reduced NADH availability for complex I of the ETC, rendering these cells less sensitive to treatment with rotenone (Figure 3.20C). Given our results suggesting the role of increased proline biosynthesis in IDH1 mutant cells to promote redox plasticity, targeting aspects of this pathway, such as the PYCR isozymes, could be more therapeutically efficacious.

IDH1 mutations induce a "semi-pesudohypoxic" state

Consistent with these previous reports, we observe that IDH1 mutated cells maintain oxidative reactions in low oxygen environments (Grassian et al. 2014), in addition to hypoxic-like proline metabolism. Although the data are not entirely clear thus far, we suggest that the sustained oxidative phenotypes in IDH1 mutant cells in hypoxia occur as a result of blunted HIF transcriptional activity, yet the hypoxic-like biosynthesis of proline occurs as a consequence of hypoxic-like redox changes due

to the expression of the mutated IDH1 protein. How this benefits the progression of the tumour is yet unknown. It could be possible that this facilitates rapid metabolic plasticity to fluctuating regions of varying oxygen tension, which occur as a result of the unstable and chaotic organisation of the tumour-associated neovasculature, but are unsustainable for longer periods of hypoxia. Indeed, IDH mutations occur at high frequency in LGGs which lack hypoxia-induced necrosis and microvascular proliferation (Svensson et al. 2011; Rong et al. 2006). The partial lack of metabolic adaptation and inability to survive longer periods of hypoxia may account for the improved prognosis observed in these tumour types (Parsons et al. 2008).

In hypoxia, the suspected increase in mitochondrial NADH/NAD^+ is thought to arise as a result of decreased ETC activity. Whilst this may be the case for SDH deficient cells, our results show that IDH1 mutant cells retain a similar oxygen consumption rate to their wild-type counterparts in normoxia, suggesting that this putative increase in NADH/NAD^+ is influenced by pathways that deplete NAD^+ rather than affect the rate at which NADH is oxidised. Such examples include the activity of NAD^+-dependent sirtuins and/or poly ADP ribose polymerases (PARP), which may be further supported by the significant changes of nicotinamide levels detected between in wild-type and IDH1 mutant cells and tissues, as identified from the metabolomics approach (Figure 3.2 and 3.5).

The differential role of oncometabolites in HIF biology

Unlike SDH and FH deficient tumours, where the accumulation of succinate and fumarate unambiguously result in HIFα stabilisation and the subsequent

development of a pseduohypoxic phenotype, the effect of (R)-2HG production in IDH1 mutant gliomas appears to have an ambiguous yet intriguing effect. To date, it has been shown that the oncometabolites succinate and fumarate inhibit all αKG-dependent dioxygenases studied. However, opposing reports exist in the literature regarding the role of (R)-2HG, particularly in the regulation of the HIF hydroxylases (Zhao et al. 2009; Koivunen et al. 2012). Our data highlights differential stabilisation of HIF1α and HIF2α in IDH1 R132H-expressing oligodendroglioma cells, which imply that (R)-2HG differently affects HIF hydroxylase activity. Despite observable HIF1α stabilisation in IDH1 mutant cells, the presence of the IDH1 R132H mutation appears to partially compromise the metabolic adaptation to hypoxia, possibly indicative of a block in protein translation accounted for by inhibition of αKG-dependent translational hydroxylases. As αKG-dependent dioxygenases belong to a large family of hydroxylases involved in multiple biological processes, there may therefore be a plethora of differential effects caused by the accumulation of (R)-2HG, which are yet to be explored. There remains much to be derived from the role of (R)-2HG in HIF biology, which could extend to further αKG-dependent dioxygenases, and the implications for these in cancers in which IDH1 mutations are present.

APPENDICES

Publications:

Appendix 1 –

Hollinshead KE & Tennant DA. *Mitochondrial metabolic remodelling in response to genetic and environment perturbations.* Wiley Interdiscip Rev Syst Biol Med. 2016 Jul;8(4):272-85. doi: 10.1002/wsbm.1334.

Appendix 2 –

Eales KL*, **Hollinshead KE***, Tennant DA. *Hypoxia and metabolic adaptation of cancer cells.* Oncogenesis, 2016. 5: e190. doi:10.1038/oncsis.2015.50

Appendix 3 –

Hollinshead KE, Williams DS, Tennant DA, Ludwig C. Probing Cancer Cell Metabolism Using NMR Spectroscopy. Adv Exp Med Biol. 2016;899:89-111. doi: 10.1007/978-3-319-26666-4_6.

Appendix 4 –

Lussey-Lepoutre C*, **Hollinshead KE***, Ludwig C, Menara M, Morin A, Castro-Vega LJ, Parker SJ, Janin M, Martinelli C, Ottolenghi C, Metallo C, Gimenez-Roqueplo AP, Favier J, Tennant DA. *Loss of succinate dehydrogenase activity results in dependency on pyruvate carboxylation for cellular anabolism.* Nat Commun. 2015 Nov 2;6:8784. doi: 10.1038/ncomms9784.

**Joint authorship*

LIST OF REFERENCES

Adam, J. et al., 2013. A Role for Cytosolic Fumarate Hydratase in Urea Cycle Metabolism and Renal Neoplasia. *Cell Reports*, 3(5), pp.1440–1448. Available at: http://linkinghub.elsevier.com/retrieve/pii/S2211124713001733.

Adam, J. et al., 2011. Renal Cyst Formation in Fh1-Deficient Mice Is Independent of the Hif/Phd Pathway: Roles for Fumarate in KEAP1 Succination and Nrf2 Signaling. *Cancer Cell*, 20(4), pp.524–537. Available at: http://linkinghub.elsevier.com/retrieve/pii/S1535610811003540.

Adeva, M. et al., 2013. Enzymes involved in l-lactate metabolism in humans. *Mitochondrion*, 13(6), pp.615–29. Available at: http://www.ncbi.nlm.nih.gov/pubmed/24029012.

Allen, L.A. et al., 1995. Isoforms of yeast cytochrome c oxidase subunit V affect the binuclear reaction center and alter the kinetics of interaction with the isoforms of yeast cytochrome c. *The Journal of biological chemistry*, 270(1), pp.110–8. Available at: http://www.ncbi.nlm.nih.gov/pubmed/7814361.

Amar, L. et al., 2007. Succinate Dehydrogenase B Gene Mutations Predict Survival in Patients with Malignant Pheochromocytomas or Paragangliomas. *The Journal of Clinical Endocrinology & Metabolism*, 92(10), pp.3822–3828. Available at: http://press.endocrine.org/doi/abs/10.1210/jc.2007-0709.

Antoniewicz, M.R., 2013. Tandem mass spectrometry for measuring stable-isotope labeling. *Current opinion in biotechnology*, 24(1), pp.48–53. Available at: http://www.ncbi.nlm.nih.gov/pubmed/23142542.

Antoniewicz, M.R., Kelleher, J.K. & Stephanopoulos, G., 2011. Measuring deuterium enrichment of glucose hydrogen atoms by gas chromatography/mass spectrometry. *Analytical chemistry*, 83(8), pp.3211–6. Available at: http://www.ncbi.nlm.nih.gov/pubmed/21413777.

Appelhoff, R.J. et al., 2004. Differential Function of the Prolyl Hydroxylases PHD1, PHD2, and PHD3 in the Regulation of Hypoxia-inducible Factor. *Journal of Biological Chemistry*, 279(37), pp.38458–38465. Available at: http://www.jbc.org/cgi/doi/10.1074/jbc.M406026200.

Del Arco, A., Agudo, M. & Satrústegui, J., 2000. Characterization of a second member of the subfamily of calcium-binding mitochondrial carriers expressed in

human non-excitable tissues. *The Biochemical journal*, 345 Pt 3, pp.725–32. Available at: http://www.ncbi.nlm.nih.gov/pubmed/10642534.

Armitage, E.G. et al., 2015. Metabolic profiling reveals potential metabolic markers associated with Hypoxia Inducible Factor-mediated signalling in hypoxic cancer cells. *Scientific Reports*, 5, p.15649. Available at: http://www.nature.com/articles/srep15649.

Astuti, D. et al., 2001. Gene Mutations in the Succinate Dehydrogenase Subunit SDHB Cause Susceptibility to Familial Pheochromocytoma and to Familial Paraganglioma. *The American Journal of Human Genetics*, 69(1), pp.49–54. Available at: http://linkinghub.elsevier.com/retrieve/pii/S000292970761444X.

Avi-Dor, Y. et al., 1962. Fluorescence of Pyridine Nucleotides in Mitochondria. *J. Biol. Chem.*, 237, pp.2377–2383.

Balss, J. et al., 2008. Analysis of the IDH1 codon 132 mutation in brain tumors. *Acta Neuropathologica*, 116(6), pp.597–602. Available at: http://link.springer.com/10.1007/s00401-008-0455-2.

Bardella, C., El-Bahrawy, M., et al., 2011. Aberrant succination of proteins in fumarate hydratase-deficient mice and HLRCC patients is a robust biomarker of mutation status. *The Journal of Pathology*, 225(1), pp.4–11. Available at: http://doi.wiley.com/10.1002/path.2932.

Bardella, C., Pollard, P.J. & Tomlinson, I., 2011. SDH mutations in cancer. *Biochimica et Biophysica Acta (BBA) - Bioenergetics*, 1807(11), pp.1432–1443. Available at: http://linkinghub.elsevier.com/retrieve/pii/S0005272811001629.

Baysal, B.E., 2008. Clinical and molecular progress in hereditary paraganglioma. *Journal of Medical Genetics*, 45(11), pp.689–694. Available at: http://jmg.bmj.com/cgi/doi/10.1136/jmg.2008.058560.

Baysal, B.E. et al., 2000. Mutations in SDHD, a mitochondrial complex II gene, in hereditary paraganglioma. *Science (New York, N.Y.)*, 287(5454), pp.848–51. Available at: http://www.ncbi.nlm.nih.gov/pubmed/10657297.

Beiko, J. et al., 2014. IDH1 mutant malignant astrocytomas are more amenable to surgical resection and have a survival benefit associated with maximal surgical resection. *Neuro-Oncology*, 16(1), pp.81–91. Available at: http://neuro-oncology.oxfordjournals.org/cgi/doi/10.1093/neuonc/not159.

Bensaad, K. et al., 2006. TIGAR, a p53-Inducible Regulator of Glycolysis and Apoptosis. *Cell*, 126(1), pp.107–120. Available at: http://linkinghub.elsevier.com/retrieve/pii/S0092867406007628.

Berra, E., 2003. HIF prolyl-hydroxylase 2 is the key oxygen sensor setting low steady-state levels of HIF-1 in normoxia. *The EMBO Journal*, 22(16), pp.4082–4090. Available at: http://emboj.embopress.org/cgi/doi/10.1093/emboj/cdg392.

Biankin, A. V et al., 2012. Pancreatic cancer genomes reveal aberrations in axon guidance pathway genes. *Nature*, 491(7424), pp.399–405. Available at: http://www.ncbi.nlm.nih.gov/pubmed/23103869.

Birsoy, K. et al., 2015. An Essential Role of the Mitochondrial Electron Transport Chain in Cell Proliferation Is to Enable Aspartate Synthesis. *Cell*, 162(3), pp.540–551. Available at: http://linkinghub.elsevier.com/retrieve/pii/S0092867415008533.

Bishop, M.J., Everse, J. & Kaplan, N.O., 1972. Identification of lactate dehydrogenase isoenzymes by rapid kinetics. *Proceedings of the National Academy of Sciences of the United States of America*, 69(7), pp.1761–5. Available at: http://www.ncbi.nlm.nih.gov/pubmed/4340158.

Bloch, K., Biological synthesis of cholesterol. *Harvey lectures*, 48, pp.68–88. Available at: http://www.ncbi.nlm.nih.gov/pubmed/13142481.

Boedeker, C. et al., 2007. Malignant head and neck paragangliomas in SDHB mutation carriers. *Otolaryngology - Head and Neck Surgery*, 137(1), pp.126–129. Available at: http://oto.sagepub.com/lookup/doi/10.1016/j.otohns.2007.01.015.

Bralten, L.B.C. et al., 2011. IDH1 R132H decreases proliferation of glioma cell lines in vitro and in vivo. *Annals of Neurology*, 69(3), pp.455–463. Available at: http://doi.wiley.com/10.1002/ana.22390.

Brand, K., 1985. Glutamine and glucose metabolism during thymocyte proliferation. Pathways of glutamine and glutamate metabolism. *The Biochemical journal*, 228(2), pp.353–61. Available at: http://www.ncbi.nlm.nih.gov/pubmed/2861809.

Briere, J.-J., 2005. Mitochondrial succinate is instrumental for HIF1 nuclear translocation in SDHA-mutant fibroblasts under normoxic conditions. *Human Molecular Genetics*, 14(21), pp.3263–3269. Available at:

http://www.hmg.oxfordjournals.org/cgi/doi/10.1093/hmg/ddi359.

Brooks, E. et al., 2014. Identification and Characterization of Small-Molecule Inhibitors of the R132H/R132H Mutant Isocitrate Dehydrogenase 1 Homodimer and R132H/Wild-Type Heterodimer. *Journal of Biomolecular Screening*, 19(8), pp.1193–1200. Available at: http://jbx.sagepub.com/cgi/doi/10.1177/1087057114541148.

Bruick, R.K., 2001. A Conserved Family of Prolyl-4-Hydroxylases That Modify HIF. *Science*, 294(5545), pp.1337–1340. Available at: http://www.sciencemag.org/cgi/doi/10.1126/science.1066373.

Buescher, J.M. et al., 2015. A roadmap for interpreting 13C metabolite labeling patterns from cells. *Current Opinion in Biotechnology*, 34, pp.189–201. Available at: http://linkinghub.elsevier.com/retrieve/pii/S0958166915000221.

Burke, P. V et al., 1997. Effects of oxygen concentration on the expression of cytochrome c and cytochrome c oxidase genes in yeast. *The Journal of biological chemistry*, 272(23), pp.14705–12. Available at: http://www.ncbi.nlm.nih.gov/pubmed/9169434.

Burnichon, N. et al., 2011. Integrative genomic analysis reveals somatic mutations in pheochromocytoma and paraganglioma. *Human Molecular Genetics*, 20(20), pp.3974–3985. Available at: http://www.hmg.oxfordjournals.org/cgi/doi/10.1093/hmg/ddr324.

Burnichon, N. et al., 2010. SDHA is a tumor suppressor gene causing paraganglioma. *Human Molecular Genetics*, 19(15), pp.3011–3020. Available at: http://www.hmg.oxfordjournals.org/cgi/doi/10.1093/hmg/ddq206.

Cahn, R.D. et al., 1962. Nature and Development of Lactic Dehydrogenases: The two major types of this enzyme form molecular hybrids which change in makeup during development. *Science*, 136(3520), pp.962–969. Available at: http://www.sciencemag.org/cgi/doi/10.1126/science.136.3520.962.

Cairns, R.A., Harris, I.S. & Mak, T.W., 2011. Regulation of cancer cell metabolism. *Nature Reviews Cancer*, 11(2), pp.85–95. Available at: http://www.nature.com/doifinder/10.1038/nrc2981.

Cantor, J.R. & Sabatini, D.M., 2012. Cancer Cell Metabolism: One Hallmark, Many Faces. *Cancer Discovery*, 2(10), pp.881–898. Available at:

http://cancerdiscovery.aacrjournals.org/cgi/doi/10.1158/2159-8290.CD-12-0345.

Cardaci, S. et al., 2015. Pyruvate carboxylation enables growth of SDH-deficient cells by supporting aspartate biosynthesis. *Nature Cell Biology*, 17(10), pp.1317–1326. Available at: http://www.nature.com/doifinder/10.1038/ncb3233.

Castro-Vega, L.J. et al., 2015. Multi-omics analysis defines core genomic alterations in pheochromocytomas and paragangliomas. *Nature Communications*, 6, p.6044. Available at: http://www.nature.com/doifinder/10.1038/ncomms7044.

Ceccarelli, C., 2002. Crystal Structure of Porcine Mitochondrial NADP+-dependent Isocitrate Dehydrogenase Complexed with Mn2+ and Isocitrate. INSIGHTS INTO THE ENZYME MECHANISM. *Journal of Biological Chemistry*, 277(45), pp.43454–43462. Available at: http://www.jbc.org/cgi/doi/10.1074/jbc.M207306200.

Chance, B. & Baltscheffsky, H., 1958. Respiratory enzymes in oxidative phosphorylation. VII. Binding of intramitochondrial reduced pyridine nucleotide. *The Journal of biological chemistry*, 233(3), pp.736–9. Available at: http://www.ncbi.nlm.nih.gov/pubmed/13575447.

Chance, B. & Williams, G.R., 1955. Respiratory enzymes in oxidative phosphorylation. III. The steady state. *The Journal of biological chemistry*, 217(1), pp.409–27. Available at: http://www.ncbi.nlm.nih.gov/pubmed/13271404.

Chandel, N.S. et al., 1998. Mitochondrial reactive oxygen species trigger hypoxia-induced transcription. *Proceedings of the National Academy of Sciences of the United States of America*, 95(20), pp.11715–20. Available at: http://www.ncbi.nlm.nih.gov/pubmed/9751731.

Chandel, N.S. et al., 2000. Reactive Oxygen Species Generated at Mitochondrial Complex III Stabilize Hypoxia-inducible Factor-1 during Hypoxia: A MECHANISM OF O2 SENSING. *Journal of Biological Chemistry*, 275(33), pp.25130–25138. Available at: http://www.jbc.org/cgi/doi/10.1074/jbc.M001914200.

Chaneton, B. et al., 2012. Serine is a natural ligand and allosteric activator of pyruvate kinase M2. *Nature*, 491(7424), pp.458–462. Available at: http://www.nature.com/doifinder/10.1038/nature11540.

Chaturvedi, A. et al., 2013. Mutant IDH1 promotes leukemogenesis in vivo and can

be specifically targeted in human AML. *Blood*, 122(16), pp.2877–2887. Available at: http://www.bloodjournal.org/cgi/doi/10.1182/blood-2013-03-491571.

Choi, J., Grossbach, M.T. & Antoniewicz, M.R., 2012. Measuring complete isotopomer distribution of aspartate using gas chromatography/tandem mass spectrometry. *Analytical chemistry*, 84(10), pp.4628–32. Available at: http://www.ncbi.nlm.nih.gov/pubmed/22510303.

Chowdhury, R. et al., 2011. The oncometabolite 2-hydroxyglutarate inhibits histone lysine demethylases. *EMBO reports*, 12(5), pp.463–469. Available at: http://embor.embopress.org/cgi/doi/10.1038/embor.2011.43.

Collingridge, D.R. et al., 1999. Polarographic measurements of oxygen tension in human glioma and surrounding peritumoural brain tissue. *Radiotherapy and oncology : journal of the European Society for Therapeutic Radiology and Oncology*, 53(2), pp.127–31. Available at: http://www.ncbi.nlm.nih.gov/pubmed/10665789.

Commisso, C. et al., 2013. Macropinocytosis of protein is an amino acid supply route in Ras-transformed cells. *Nature*, 497(7451), pp.633–7. Available at: http://www.ncbi.nlm.nih.gov/pubmed/23665962.

Dahia, P.L.M. et al., 2005. A HIF1α Regulatory Loop Links Hypoxia and Mitochondrial Signals in Pheochromocytomas. *PLoS Genetics*, 1(1), p.e8. Available at: http://dx.plos.org/10.1371/journal.pgen.0010008.

Dahia, P.L.M., 2014. Pheochromocytoma and paraganglioma pathogenesis: learning from genetic heterogeneity. *Nature Reviews Cancer*, 14(2), pp.108–119. Available at: http://www.nature.com/doifinder/10.1038/nrc3648.

Dalziel, K., 1980. Isocitrate dehydrogenase and related oxidative decarboxylases. *FEBS Letters*, 117(S1), pp.K45–K55. Available at: http://doi.wiley.com/10.1016/0014-5793(80)80569-2.

Dang, L. et al., 2009. Cancer-associated IDH1 mutations produce 2-hydroxyglutarate. *Nature*, 462(7274), pp.739–744. Available at: http://www.nature.com/doifinder/10.1038/nature08617.

Dayan, F. et al., 2006. The Oxygen Sensor Factor-Inhibiting Hypoxia-Inducible Factor-1 Controls Expression of Distinct Genes through the Bifunctional Transcriptional Character of Hypoxia-Inducible Factor-1. *Cancer Research*,

66(7), pp.3688–3698. Available at: http://cancerres.aacrjournals.org/cgi/doi/10.1158/0008-5472.CAN-05-4564.

DeBerardinis, R.J. et al., 2007. Beyond aerobic glycolysis: Transformed cells can engage in glutamine metabolism that exceeds the requirement for protein and nucleotide synthesis. *Proceedings of the National Academy of Sciences*, 104(49), pp.19345–19350. Available at: http://www.pnas.org/cgi/doi/10.1073/pnas.0709747104.

DeBerardinis, R.J. & Cheng, T., 2010. Q's next: the diverse functions of glutamine in metabolism, cell biology and cancer. *Oncogene*, 29(3), pp.313–324. Available at: http://www.nature.com/doifinder/10.1038/onc.2009.358.

Delaglio, F. et al., 1995. NMRPipe: a multidimensional spectral processing system based on UNIX pipes. *Journal of biomolecular NMR*, 6(3), pp.277–93. Available at: http://www.ncbi.nlm.nih.gov/pubmed/8520220.

DeNicola, G.M. et al., 2015. NRF2 regulates serine biosynthesis in non–small cell lung cancer. *Nature Genetics*, 47(12), pp.1475–1481. Available at: http://www.nature.com/doifinder/10.1038/ng.3421.

Dewhirst, M.W., Cao, Y. & Moeller, B., 2008. Cycling hypoxia and free radicals regulate angiogenesis and radiotherapy response. *Nature Reviews Cancer*, 8(6), pp.425–437. Available at: http://www.nature.com/doifinder/10.1038/nrc2397.

Donald, S.P. et al., 2001. Proline oxidase, encoded by p53-induced gene-6, catalyzes the generation of proline-dependent reactive oxygen species. *Cancer research*, 61(5), pp.1810–5. Available at: http://www.ncbi.nlm.nih.gov/pubmed/11280728.

Douwes Dekker, P. et al., 2003. SDHD mutations in head and neck paragangliomas result in destabilization of complex II in the mitochondrial respiratory chain with loss of enzymatic activity and abnormal mitochondrial morphology. *The Journal of Pathology*, 201(3), pp.480–486. Available at: http://doi.wiley.com/10.1002/path.1461.

Dunn, W.B et al., 2011. Procedures for large-scale metabolic profiling of serum and plasma using gas chromatography and liquid chromatography coupled to mass spectrometry. *Nature Protocols,* 6, 1060-1083. Available at: http://doi.1038/nprot.2011.335.

Ehrismann, D. et al., 2007. Studies on the activity of the hypoxia-inducible-factor hydroxylases using an oxygen consumption assay. *Biochemical Journal*, 401(1), pp.227–234. Available at: http://biochemj.org/lookup/doi/10.1042/BJ20061151.

El-Hattab, A.W., 2016. Serine biosynthesis and transport defects. *Molecular Genetics and Metabolism*, 118(3), pp.153–159. Available at: http://linkinghub.elsevier.com/retrieve/pii/S1096719216300531.

Elstrom, R.L., 2004. Akt Stimulates Aerobic Glycolysis in Cancer Cells. *Cancer Research*, 64(11), pp.3892–3899. Available at: http://cancerres.aacrjournals.org/cgi/doi/10.1158/0008-5472.CAN-03-2904.

Epstein, A.C. et al., 2001. C. elegans EGL-9 and mammalian homologs define a family of dioxygenases that regulate HIF by prolyl hydroxylation. *Cell*, 107(1), pp.43–54. Available at: http://www.ncbi.nlm.nih.gov/pubmed/11595184.

Ernst, T. et al., 2002. Decrease and Gain of Gene Expression Are Equally Discriminatory Markers for Prostate Carcinoma. *The American Journal of Pathology*, 160(6), pp.2169–2180. Available at: http://linkinghub.elsevier.com/retrieve/pii/S0002944010611650.

Evans, S.M., 2004. Hypoxia Is Important in the Biology and Aggression of Human Glial Brain Tumors. *Clinical Cancer Research*, 10(24), pp.8177–8184. Available at: http://clincancerres.aacrjournals.org/cgi/doi/10.1158/1078-0432.CCR-04-1081.

Fan, T.W.-M. et al., 2012. Stable isotope-resolved metabolomics and applications for drug development. *Pharmacology & Therapeutics*, 133(3), pp.366–391. Available at: http://linkinghub.elsevier.com/retrieve/pii/S0163725811002300.

Fantin, V.R., St-Pierre, J. & Leder, P., 2006. Attenuation of LDH-A expression uncovers a link between glycolysis, mitochondrial physiology, and tumor maintenance. *Cancer Cell*, 9(6), pp.425–434. Available at: http://linkinghub.elsevier.com/retrieve/pii/S1535610806001450.

Fendt, S.-M. et al., 2013. Reductive glutamine metabolism is a function of the α-ketoglutarate to citrate ratio in cells. *Nature Communications*, 4. Available at: http://www.nature.com/doifinder/10.1038/ncomms3236.

Fendt, S.-M. et al., 2010. Tradeoff between enzyme and metabolite efficiency maintains metabolic homeostasis upon perturbations in enzyme capacity.

Molecular systems biology, 6, p.356. Available at: http://www.ncbi.nlm.nih.gov/pubmed/20393576.

Fernandez, C.A. et al., 1996. Correction of 13C mass isotopomer distributions for natural stable isotope abundance. *Journal of mass spectrometry : JMS*, 31(3), pp.255–62. Available at: http://www.ncbi.nlm.nih.gov/pubmed/8799277.

Figueroa, M.E. et al., 2010. Leukemic IDH1 and IDH2 mutations result in a hypermethylation phenotype, disrupt TET2 function, and impair hematopoietic differentiation. *Cancer cell*, 18(6), pp.553–67. Available at: http://www.ncbi.nlm.nih.gov/pubmed/21130701.

Filipp, F. V. et al., 2012. Reverse TCA cycle flux through isocitrate dehydrogenases 1 and 2 is required for lipogenesis in hypoxic melanoma cells. *Pigment Cell & Melanoma Research*, 25(3), pp.375–383. Available at: http://doi.wiley.com/10.1111/j.1755-148X.2012.00989.x.

Fliednerm S.M.J. et al., (2010). Metastatic Paraganglioma. *Seminars in Oncology,* 37(6), 627-637. Available at: http://doi/org/10.1053/j.seminoncol.2010.10.017.

Frezza, C. et al., 2011. Haem oxygenase is synthetically lethal with the tumour suppressor fumarate hydratase. *Nature*, 477(7363), pp.225–228. Available at: http://www.nature.com/doifinder/10.1038/nature10363.

Fujii, S. et al., 2008. Autophagy is activated in pancreatic cancer cells and correlates with poor patient outcome. *Cancer science*, 99(9), pp.1813–9. Available at: http://www.ncbi.nlm.nih.gov/pubmed/18616529.

Fukuda, R. et al., 2007. HIF-1 Regulates Cytochrome Oxidase Subunits to Optimize Efficiency of Respiration in Hypoxic Cells. *Cell*, 129(1), pp.111–122. Available at: http://linkinghub.elsevier.com/retrieve/pii/S0092867407003078.

Galliani, G. et al., 1985. Biliverdin as an electron transfer catalyst for superoxide ion in aqueous medium. *Experientia*, 41(12), pp.1559–60. Available at: http://www.ncbi.nlm.nih.gov/pubmed/3000813.

Gameiro, P.A. et al., 2013. In Vivo HIF-Mediated Reductive Carboxylation Is Regulated by Citrate Levels and Sensitizes VHL-Deficient Cells to Glutamine Deprivation. *Cell Metabolism*, 17(3), pp.372–385. Available at: http://linkinghub.elsevier.com/retrieve/pii/S1550413113000508.

Gao, P. et al., 2009. c-Myc suppression of miR-23a/b enhances mitochondrial

glutaminase expression and glutamine metabolism. *Nature*, 458(7239), pp.762–765. Available at: http://www.nature.com/doifinder/10.1038/nature07823.

Gardner, P.R., 2002. Aconitase: sensitive target and measure of superoxide. *Methods in enzymology*, 349, pp.9–23. Available at: http://www.ncbi.nlm.nih.gov/pubmed/11912933.

Gatenby, R.A. & Gillies, R.J., 2008. A microenvironmental model of carcinogenesis. *Nature reviews. Cancer*, 8(1), pp.56–61. Available at: http://www.ncbi.nlm.nih.gov/pubmed/18059462.

Gaude, E. & Frezza, C., 2014. Defects in mitochondrial metabolism and cancer. *Cancer & Metabolism*, 2(1), p.10. Available at: http://www.cancerandmetabolism.com/content/2/1/10.

Ge, W. et al., 2012. Oxygenase-catalyzed ribosome hydroxylation occurs in prokaryotes and humans. *Nature Chemical Biology*, 8(12), pp.960–962. Available at: http://www.nature.com/doifinder/10.1038/nchembio.1093.

Gerlinger, M. et al., 2012. Intratumor heterogeneity and branched evolution revealed by multiregion sequencing. *The New England journal of medicine*, 366(10), pp.883–92. Available at: http://www.ncbi.nlm.nih.gov/pubmed/22397650.

Gilbert, M.R. et al., 2014. Autophagy and oxidative stress in gliomas with IDH1 mutations. *Acta Neuropathologica*, 127(2), pp.221–233. Available at: http://link.springer.com/10.1007/s00401-013-1194-6.

Gilkes, D.M. et al., 2013. Collagen Prolyl Hydroxylases Are Essential for Breast Cancer Metastasis. *Cancer Research*, 73(11), pp.3285–3296. Available at: http://cancerres.aacrjournals.org/cgi/doi/10.1158/0008-5472.CAN-12-3963.

Gimenez-Roqueplo, A.-P. et al., 2002. Functional Consequences of a SDHB Gene Mutation in an Apparently Sporadic Pheochromocytoma. *The Journal of Clinical Endocrinology & Metabolism*, 87(10), pp.4771–4774. Available at: http://press.endocrine.org/doi/abs/10.1210/jc.2002-020525.

Gimenez-Roqueplo, A.-P. et al., 2003. Mutations in the SDHB gene are associated with extra-adrenal and/or malignant phaeochromocytomas. *Cancer research*, 63(17), pp.5615–21. Available at: http://www.ncbi.nlm.nih.gov/pubmed/14500403.

Gimenez-Roqueplo, A.-P. et al., 2001. The R22X Mutation of the SDHD Gene in

Hereditary Paraganglioma Abolishes the Enzymatic Activity of Complex II in the Mitochondrial Respiratory Chain and Activates the Hypoxia Pathway. *The American Journal of Human Genetics*, 69(6), pp.1186–1197. Available at: http://linkinghub.elsevier.com/retrieve/pii/S0002929707612488.

Ginouves, A. et al., 2008. PHDs overactivation during chronic hypoxia "desensitizes" HIF and protects cells from necrosis. *Proceedings of the National Academy of Sciences*, 105(12), pp.4745–4750. Available at: http://www.pnas.org/cgi/doi/10.1073/pnas.0705680105.

Gnaiger, E. et al., 1998. Mitochondrial oxygen affinity, respiratory flux control and excess capacity of cytochrome c oxidase. *The Journal of experimental biology*, 201(Pt 8), pp.1129–39. Available at: http://www.ncbi.nlm.nih.gov/pubmed/9510525.

Gottlieb, E. & Tomlinson, I.P.M., 2005. Mitochondrial tumour suppressors: a genetic and biochemical update. *Nature Reviews Cancer*, 5(11), pp.857–866. Available at: http://www.nature.com/doifinder/10.1038/nrc1737.

Grassian, A.R. et al., 2014. IDH1 Mutations Alter Citric Acid Cycle Metabolism and Increase Dependence on Oxidative Mitochondrial Metabolism. *Cancer Research*, 74(12), pp.3317–3331. Available at: http://cancerres.aacrjournals.org/cgi/doi/10.1158/0008-5472.CAN-14-0772-T.

Gravendeel, L.A.M. et al., 2009. Intrinsic Gene Expression Profiles of Gliomas Are a Better Predictor of Survival than Histology. *Cancer Research*, 69(23), pp.9065–9072. Available at: http://cancerres.aacrjournals.org/cgi/doi/10.1158/0008-5472.CAN-09-2307.

Greaves, M. & Maley, C.C., 2012. Clonal evolution in cancer. *Nature*, 481(7381), pp.306–13. Available at: http://www.ncbi.nlm.nih.gov/pubmed/22258609.

Groen, A.K. et al., 1982. Intracellular compartmentation and control of alanine metabolism in rat liver parenchymal cells. *European journal of biochemistry / FEBS*, 122(1), pp.87–93. Available at: http://www.ncbi.nlm.nih.gov/pubmed/7060572.

Groves, A.M. et al., 2007. Non-[18F]FDG PET in clinical oncology. *The Lancet. Oncology*, 8(9), pp.822–30. Available at: http://www.ncbi.nlm.nih.gov/pubmed/17765191.

Grubb, R.L. et al., 2007. Hereditary leiomyomatosis and renal cell cancer: a syndrome associated with an aggressive form of inherited renal cancer. *The Journal of urology*, 177(6), pp.2074-9-80. Available at: http://www.ncbi.nlm.nih.gov/pubmed/17509289.

Guaragnella, N., Giannattasio, S. & Moro, L., 2014. Mitochondrial dysfunction in cancer chemoresistance. *Biochemical Pharmacology*, 92(1), pp.62–72. Available at: http://linkinghub.elsevier.com/retrieve/pii/S0006295214004481.

Guo, J.Y. et al., 2011. Activated Ras requires autophagy to maintain oxidative metabolism and tumorigenesis. *Genes & development*, 25(5), pp.460–70. Available at: http://www.ncbi.nlm.nih.gov/pubmed/21317241.

Guppy, M., Greiner, E. & Brand, K., 1993. The role of the Crabtree effect and an endogenous fuel in the energy metabolism of resting and proliferating thymocytes. *European journal of biochemistry / FEBS*, 212(1), pp.95–9. Available at: http://www.ncbi.nlm.nih.gov/pubmed/8444168.

Guzy, R.D. et al., 2008. Loss of the SdhB, but Not the SdhA, Subunit of Complex II Triggers Reactive Oxygen Species-Dependent Hypoxia-Inducible Factor Activation and Tumorigenesis. *Molecular and Cellular Biology*, 28(2), pp.718–731. Available at: http://mcb.asm.org/cgi/doi/10.1128/MCB.01338-07.

Hanahan, D. & Weinberg, R.A., 2011. Hallmarks of Cancer: The Next Generation. *Cell*, 144(5), pp.646–674. Available at: http://linkinghub.elsevier.com/retrieve/pii/S0092867411001279.

Hanahan, D. & Weinberg, R.A., 2000. The hallmarks of cancer. *Cell*, 100(1), pp.57–70. Available at: http://www.ncbi.nlm.nih.gov/pubmed/10647931.

Hao, H.-X. et al., 2009. SDH5, a Gene Required for Flavination of Succinate Dehydrogenase, Is Mutated in Paraganglioma. *Science*, 325(5944), pp.1139–1142. Available at: http://www.sciencemag.org/cgi/doi/10.1126/science.1175689.

Hedeskov, C.J., 1968. Early effects of phytohaemagglutinin on glucose metabolism of normal human lymphocytes. *The Biochemical journal*, 110(2), pp.373–80. Available at: http://www.ncbi.nlm.nih.gov/pubmed/5726214.

Hiller, K. et al., 2009. MetaboliteDetector: Comprehensive Analysis Tool for Targeted and Nontargeted GC/MS Based Metabolome Analysis. *Analytical Chemistry*, 81(9), pp.3429–3439. Available at:

http://pubs.acs.org/doi/abs/10.1021/ac802689c.

Hosios, A. M. *et al.,* 2016. Amino acids rather than glucose account for the majority of cell mass in proliferating cells. *Dev. Cell* **36,** 540-549

Hu, C.-J. et al., 2003. Differential roles of hypoxia-inducible factor 1alpha (HIF-1alpha) and HIF-2alpha in hypoxic gene regulation. *Molecular and cellular biology*, 23(24), pp.9361–74. Available at: http://www.ncbi.nlm.nih.gov/pubmed/14645546.

Huang, J. et al., 2002. Sequence Determinants in Hypoxia-inducible Factor-1 for Hydroxylation by the Prolyl Hydroxylases PHD1, PHD2, and PHD3. *Journal of Biological Chemistry*, 277(42), pp.39792–39800. Available at: http://www.jbc.org/cgi/doi/10.1074/jbc.M206955200.

Hyberts, S.G. et al., 2007. Ultrahigh-Resolution 1 H− 13 C HSQC Spectra of Metabolite Mixtures Using Nonlinear Sampling and Forward Maximum Entropy Reconstruction. *Journal of the American Chemical Society*, 129(16), pp.5108–5116. Available at: http://pubs.acs.org/doi/abs/10.1021/ja068541x.

De Ingeniis, J. et al., 2012. Functional Specialization in Proline Biosynthesis of Melanoma E. Parker, ed. *PLoS ONE*, 7(9), p.e45190. Available at: http://dx.plos.org/10.1371/journal.pone.0045190.

Isaacs, J.S. et al., 2005. HIF overexpression correlates with biallelic loss of fumarate hydratase in renal cancer: Novel role of fumarate in regulation of HIF stability. *Cancer Cell*, 8(2), pp.143–153. Available at: http://linkinghub.elsevier.com/retrieve/pii/S1535610805002266.

Jaakkola, P. et al., 2001. Targeting of HIF-alpha to the von Hippel-Lindau Ubiquitylation Complex by O2-Regulated Prolyl Hydroxylation. *Science*, 292(5516), pp.468–472. Available at: http://www.sciencemag.org/cgi/doi/10.1126/science.1059796.

Janeway, K.A. et al., 2011. Defects in succinate dehydrogenase in gastrointestinal stromal tumors lacking KIT and PDGFRA mutations. *Proceedings of the National Academy of Sciences*, 108(1), pp.314–318. Available at: http://www.pnas.org/cgi/doi/10.1073/pnas.1009199108.

Jiang, B.H. et al., 1996. Dimerization, DNA binding, and transactivation properties of hypoxia-inducible factor 1. *The Journal of biological chemistry*, 271(30),

pp.17771–8. Available at: http://www.ncbi.nlm.nih.gov/pubmed/8663540.

Jin, G. et al., 2013. Disruption of Wild-Type IDH1 Suppresses D-2-Hydroxyglutarate Production in IDH1-Mutated Gliomas. *Cancer Research*, 73(2), pp.496–501. Available at: http://cancerres.aacrjournals.org/cgi/doi/10.1158/0008-5472.CAN-12-2852.

Jitrapakdee, S. et al., 2008. Structure, mechanism and regulation of pyruvate carboxylase. *Biochemical Journal*, 413(3), pp.369–387. Available at: http://biochemj.org/lookup/doi/10.1042/BJ20080709.

Jones, S. et al., 2008. Core signaling pathways in human pancreatic cancers revealed by global genomic analyses. *Science (New York, N.Y.)*, 321(5897), pp.1801–6. Available at: http://www.ncbi.nlm.nih.gov/pubmed/18772397.

Kamphorst, J.J. et al., 2013. Hypoxic and Ras-transformed cells support growth by scavenging unsaturated fatty acids from lysophospholipids. *Proceedings of the National Academy of Sciences*, 110(22), pp.8882–8887. Available at: http://www.pnas.org/cgi/doi/10.1073/pnas.1307237110.

Kazimierczuk, K. & Orekhov, V.Y., 2011. Accelerated NMR Spectroscopy by Using Compressed Sensing. *Angewandte Chemie International Edition*, 50(24), pp.5556–5559. Available at: http://doi.wiley.com/10.1002/anie.201100370.

Kim, D. et al., 2015. SHMT2 drives glioma cell survival in ischaemia but imposes a dependence on glycine clearance. *Nature*, 520(7547), pp.363–367. Available at: http://www.nature.com/doifinder/10.1038/nature14363.

Kim, J. et al., 2006. HIF-1-mediated expression of pyruvate dehydrogenase kinase: A metabolic switch required for cellular adaptation to hypoxia. *Cell Metabolism*, 3(3), pp.177–185. Available at: http://linkinghub.elsevier.com/retrieve/pii/S1550413106000623.

Kim, S.Y. et al., 2007. Regulation of singlet oxygen-induced apoptosis by cytosolic NADP+-dependent isocitrate dehydrogenase. *Molecular and Cellular Biochemistry*, 302(1–2), pp.27–34. Available at: http://link.springer.com/10.1007/s11010-007-9421-x.

Koek, M.M. et al., 2006. Microbial metabolomics with gas chromatography/mass spectrometry. *Analytical chemistry*, 78(4), pp.1272–81. Available at: http://www.ncbi.nlm.nih.gov/pubmed/16478122.

Koivunen, P. et al., 2004. Catalytic Properties of the Asparaginyl Hydroxylase (FIH) in the Oxygen Sensing Pathway Are Distinct from Those of Its Prolyl 4-Hydroxylases. *Journal of Biological Chemistry*, 279(11), pp.9899–9904. Available at: http://www.jbc.org/cgi/doi/10.1074/jbc.M312254200.

Koivunen, P. et al., 2012. Transformation by the (R)-enantiomer of 2-hydroxyglutarate linked to EGLN activation. *Nature*, 483(7390), pp.484–488. Available at: http://www.nature.com/doifinder/10.1038/nature10898.

Kondo, K. et al., 2002. Inhibition of HIF is necessary for tumor suppression by the von Hippel-Lindau protein. *Cancer cell*, 1(3), pp.237–46. Available at: http://www.ncbi.nlm.nih.gov/pubmed/12086860.

Kumashiro, N. et al., 2013. Targeting Pyruvate Carboxylase Reduces Gluconeogenesis and Adiposity and Improves Insulin Resistance. *Diabetes*, 62(7), pp.2183–2194. Available at: http://diabetes.diabetesjournals.org/cgi/doi/10.2337/db12-1311.

Kuwada, M. et al., 2014. Novel missense mutation in the FH gene in familial renal cell cancer patients lacking cutaneous leiomyomas. *BMC Research Notes*, 7(1), p.203. Available at: http://bmcresnotes.biomedcentral.com/articles/10.1186/1756-0500-7-203.

Lando, D., 2002. FIH-1 is an asparaginyl hydroxylase enzyme that regulates the transcriptional activity of hypoxia-inducible factor. *Genes & Development*, 16(12), pp.1466–1471. Available at: http://www.genesdev.org/cgi/doi/10.1101/gad.991402.

Latif, F. et al., 1993. Identification of the von Hippel-Lindau disease tumor suppressor gene. *Science (New York, N.Y.)*, 260(5112), pp.1317–20. Available at: http://www.ncbi.nlm.nih.gov/pubmed/8493574.

Le, A. et al., 2010. Inhibition of lactate dehydrogenase A induces oxidative stress and inhibits tumor progression. *Proceedings of the National Academy of Sciences*, 107(5), pp.2037–2042. Available at: http://www.pnas.org/cgi/doi/10.1073/pnas.0914433107.

Lee, G.Y. et al., 2014. Comparative Oncogenomics Identifies PSMB4 and SHMT2 as Potential Cancer Driver Genes. *Cancer Research*, 74(11), pp.3114–3126. Available at: http://cancerres.aacrjournals.org/cgi/doi/10.1158/0008-5472.CAN-

13-2683.

Lehtonen, H.J., 2006. Increased risk of cancer in patients with fumarate hydratase germline mutation. *Journal of Medical Genetics*, 43(6), pp.523–526. Available at: http://jmg.bmj.com/cgi/doi/10.1136/jmg.2005.036400.

Lenders, J.W.M. et al., 2014. Pheochromocytoma and Paraganglioma: An Endocrine Society Clinical Practice Guideline. *The Journal of Clinical Endocrinology & Metabolism*, 99(6), pp.1915–1942. Available at: http://press.endocrine.org/doi/abs/10.1210/jc.2014-1498.

Leonardi, R. et al., 2012. Cancer-associated Isocitrate Dehydrogenase Mutations Inactivate NADPH-dependent Reductive Carboxylation. *Journal of Biological Chemistry*, 287(18), pp.14615–14620. Available at: http://www.jbc.org/cgi/doi/10.1074/jbc.C112.353946.

Letouzé, E. et al., 2013. SDH Mutations Establish a Hypermethylator Phenotype in Paraganglioma. *Cancer Cell*, 23(6), pp.739–752. Available at: http://linkinghub.elsevier.com/retrieve/pii/S1535610813001839.

Lewis, C.A. et al., 2014. Tracing Compartmentalized NADPH Metabolism in the Cytosol and Mitochondria of Mammalian Cells. *Molecular Cell*, 55(2), pp.253–263. Available at: http://linkinghub.elsevier.com/retrieve/pii/S109727651400402X.

Liao, D. & Johnson, R.S., 2007. Hypoxia: A key regulator of angiogenesis in cancer. *Cancer and Metastasis Reviews*, 26(2), pp.281–290. Available at: http://link.springer.com/10.1007/s10555-007-9066-y.

Lin, Q., Cong, X. & Yun, Z., 2011. Differential Hypoxic Regulation of Hypoxia-Inducible Factors 1 and 2. *Molecular Cancer Research*, 9(6), pp.757–765. Available at: http://mcr.aacrjournals.org/cgi/doi/10.1158/1541-7786.MCR-11-0053.

Liu, W. et al., 2012. Reprogramming of proline and glutamine metabolism contributes to the proliferative and metabolic responses regulated by oncogenic transcription factor c-MYC. *Proceedings of the National Academy of Sciences*, 109(23), pp.8983–8988. Available at: http://www.pnas.org/cgi/doi/10.1073/pnas.1203244109.

Liu, Y. et al., 2009. Proline Oxidase Functions as a Mitochondrial Tumor Suppressor

in Human Cancers. *Cancer Research*, 69(16), pp.6414–6422. Available at: http://cancerres.aacrjournals.org/cgi/doi/10.1158/0008-5472.CAN-09-1223.

Locasale, J.W., 2013. Serine, glycine and one-carbon units: cancer metabolism in full circle. *Nature Reviews Cancer*, 13(8), pp.572–583. Available at: http://www.nature.com/doifinder/10.1038/nrc3557.

Loenarz, C. et al., 2014. Hydroxylation of the eukaryotic ribosomal decoding center affects translational accuracy. *Proceedings of the National Academy of Sciences*, 111(11), pp.4019–4024. Available at: http://www.pnas.org/cgi/doi/10.1073/pnas.1311750111.

Louis, D.N. et al., 2007. The 2007 WHO Classification of Tumours of the Central Nervous System. *Acta Neuropathologica*, 114(2), pp.97–109. Available at: http://link.springer.com/10.1007/s00401-007-0243-4.

Lu, C. et al., 2012. IDH mutation impairs histone demethylation and results in a block to cell differentiation. *Nature*, 483(7390), pp.474–8. Available at: http://www.ncbi.nlm.nih.gov/pubmed/22343901.

Ludwig, C. & Günther, U.L., 2011. MetaboLab - advanced NMR data processing and analysis for metabolomics. *BMC Bioinformatics*, 12(1), p.366. Available at: http://www.biomedcentral.com/1471-2105/12/366.

Lunt, S.Y. & Vander Heiden, M.G., 2011. Aerobic Glycolysis: Meeting the Metabolic Requirements of Cell Proliferation. *Annual Review of Cell and Developmental Biology*, 27(1), pp.441–464. Available at: http://www.annualreviews.org/doi/abs/10.1146/annurev-cellbio-092910-154237.

Luo, W. & Semenza, G.L., 2011. Pyruvate kinase M2 regulates glucose metabolism by functioning as a coactivator for hypoxia-inducible factor 1 in cancer cells. *Oncotarget*, 2(7), pp.551–556. Available at: http://oncotarget.com/abstract/299.

Lussey-Lepoutre, C. et al., 2015. Loss of succinate dehydrogenase activity results in dependency on pyruvate carboxylation for cellular anabolism. *Nature Communications*, 6, p.8784. Available at: http://www.nature.com/doifinder/10.1038/ncomms9784.

Maddocks, O.D.K. et al., 2012. Serine starvation induces stress and p53-dependent metabolic remodelling in cancer cells. *Nature*, 493(7433), pp.542–546. Available at: http://www.nature.com/doifinder/10.1038/nature11743.

Mardis, E.R. et al., 2009. Recurring Mutations Found by Sequencing an Acute Myeloid Leukemia Genome. *New England Journal of Medicine*, 361(11), pp.1058–1066. Available at: http://www.nejm.org/doi/abs/10.1056/NEJMoa0903840.

Martinez-Outschoorn, U.E. et al., 2011. Anti-estrogen resistance in breast cancer is induced by the tumor microenvironment and can be overcome by inhibiting mitochondrial function in epithelial cancer cells. *Cancer biology & therapy*, 12(10), pp.924–38. Available at: http://www.ncbi.nlm.nih.gov/pubmed/22041887.

Marusyk, A., Almendro, V. & Polyak, K., 2012. Intra-tumour heterogeneity: a looking glass for cancer? *Nature reviews. Cancer*, 12(5), pp.323–34. Available at: http://www.ncbi.nlm.nih.gov/pubmed/22513401.

Maxwell, P.H., Pugh, C.W. & Ratcliffe, P.J., 2001. The pVHL-hIF-1 system. A key mediator of oxygen homeostasis. *Advances in experimental medicine and biology*, 502, pp.365–76. Available at: http://www.ncbi.nlm.nih.gov/pubmed/11950150.

Mayers, J.R. & Vander Heiden, M.G., 2015. Famine versus feast: understanding the metabolism of tumors in vivo. *Trends in Biochemical Sciences*, 40(3), pp.130–140. Available at: http://linkinghub.elsevier.com/retrieve/pii/S0968000415000055.

Mayevsky, A., 1984. Brain NADH redox state monitored in vivo by fiber optic surface fluorometry. *Brain research*, 319(1), pp.49–68. Available at: http://www.ncbi.nlm.nih.gov/pubmed/6370376.

Mayevsky, A. & Rogatsky, G.G., 2006. Mitochondrial function in vivo evaluated by NADH fluorescence: from animal models to human studies. *AJP: Cell Physiology*, 292(2), pp.C615–C640. Available at: http://ajpcell.physiology.org/cgi/doi/10.1152/ajpcell.00249.2006.

McNeil, L.A. et al., 2002. Hypoxia-inducible factor asparaginyl hydroxylase (FIH-1) catalyses hydroxylation at the β-carbon of asparagine-803. *Biochemical Journal*, 367(3), pp.571–575. Available at: http://biochemj.org/lookup/doi/10.1042/bj20021162.

Metallo, C.M. et al., 2011. Reductive glutamine metabolism by IDH1 mediates lipogenesis under hypoxia. *Nature*. Available at:

http://www.nature.com/doifinder/10.1038/nature10602.

Metallo, C.M., Walther, J.L. & Stephanopoulos, G., 2009. Evaluation of 13C isotopic tracers for metabolic flux analysis in mammalian cells. *Journal of Biotechnology*, 144(3), pp.167–174. Available at: http://linkinghub.elsevier.com/retrieve/pii/S0168165609003009.

Moellering, R.E. et al., 2008. Acid treatment of melanoma cells selects for invasive phenotypes. *Clinical & Experimental Metastasis*, 25(4), pp.411–425. Available at: http://link.springer.com/10.1007/s10585-008-9145-7.

Molenaar, R.J. et al., 2014. The driver and passenger effects of isocitrate dehydrogenase 1 and 2 mutations in oncogenesis and survival prolongation. *Biochimica et Biophysica Acta (BBA) - Reviews on Cancer*, 1846(2), pp.326–341. Available at: http://linkinghub.elsevier.com/retrieve/pii/S0304419X14000493.

Moreno-Sánchez, R. et al., 2007. Energy metabolism in tumor cells. *FEBS Journal*, 274(6), pp.1393–1418. Available at: http://doi.wiley.com/10.1111/j.1742-4658.2007.05686.x.

Mullarky, E. et al., 2011. PHGDH amplification and altered glucose metabolism in human melanoma. *Pigment Cell & Melanoma Research*, 24(6), pp.1112–1115. Available at: http://doi.wiley.com/10.1111/j.1755-148X.2011.00919.x.

Mullen, A.R. et al., 2011. Reductive carboxylation supports growth in tumour cells with defective mitochondria. *Nature*. Available at: http://www.nature.com/doifinder/10.1038/nature10642.

Myllyharju, J., 2004. Collagens, modifying enzymes and their mutations in humans, flies and worms. *Trends in Genetics*, 20(1), pp.33–43. Available at: http://linkinghub.elsevier.com/retrieve/pii/S0168952503003196.

Nakajima, E.C. & Van Houten, B., 2013. Metabolic symbiosis in cancer: Refocusing the Warburg lens. *Molecular Carcinogenesis*, 52(5), pp.329–337. Available at: http://doi.wiley.com/10.1002/mc.21863.

Nguyen, A.D. et al., 2007. Hypoxia Stimulates Degradation of 3-Hydroxy-3-methylglutaryl-coenzyme A Reductase through Accumulation of Lanosterol and Hypoxia-Inducible Factor-mediated Induction of Insigs. *Journal of Biological Chemistry*, 282(37), pp.27436–27446. Available at:

http://www.jbc.org/cgi/doi/10.1074/jbc.M704976200.

Nicklin, P. et al., 2009. Bidirectional Transport of Amino Acids Regulates mTOR and Autophagy. *Cell*, 136(3), pp.521–534. Available at: http://linkinghub.elsevier.com/retrieve/pii/S0092867408015195.

Nickols, N.G. et al., 2007. Modulating Hypoxia-Inducible Transcription by Disrupting the HIF-1–DNA Interface. *ACS Chemical Biology*, 2(8), pp.561–571. Available at: http://pubs.acs.org/doi/abs/10.1021/cb700110z.

Nieman, K.M. et al., 2011. Adipocytes promote ovarian cancer metastasis and provide energy for rapid tumor growth. *Nature medicine*, 17(11), pp.1498–503. Available at: http://www.ncbi.nlm.nih.gov/pubmed/22037646.

Niemann S, M.U., 2000. Mutations in SDHC cause autosomal dominant paraganglioma, type 3. *Nat Genet*, 26(3), pp.268–70.

Nilsson, L.M. et al., 2012. Mouse Genetics Suggests Cell-Context Dependency for Myc-Regulated Metabolic Enzymes during Tumorigenesis B. E. Clurman, ed. *PLoS Genetics*, 8(3), p.e1002573. Available at: http://dx.plos.org/10.1371/journal.pgen.1002573.

Ohgaki, H. & Kleihues, P., 2007. Genetic Pathways to Primary and Secondary Glioblastoma. *The American Journal of Pathology*, 170(5), pp.1445–1453. Available at: http://linkinghub.elsevier.com/retrieve/pii/S0002944010613582.

Ooi, A. et al., 2011. An Antioxidant Response Phenotype Shared between Hereditary and Sporadic Type 2 Papillary Renal Cell Carcinoma. *Cancer Cell*, 20(4), pp.511–523. Available at: http://linkinghub.elsevier.com/retrieve/pii/S1535610811003199.

Orekhov, V.Y. & Jaravine, V.A., 2011. Analysis of non-uniformly sampled spectra with multi-dimensional decomposition. *Progress in Nuclear Magnetic Resonance Spectroscopy*, 59(3), pp.271–292. Available at: http://linkinghub.elsevier.com/retrieve/pii/S0079656511000161.

Palmieri, L. et al., 2001. Citrin and aralar1 are Ca(2+)-stimulated aspartate/glutamate transporters in mitochondria. *The EMBO journal*, 20(18), pp.5060–9. Available at: http://www.ncbi.nlm.nih.gov/pubmed/11566871.

Papandreou, I. et al., 2006. HIF-1 mediates adaptation to hypoxia by actively downregulating mitochondrial oxygen consumption. *Cell Metabolism*, 3(3),

pp.187–197. Available at: http://linkinghub.elsevier.com/retrieve/pii/S155041310600060X.

Parks, S.K., Chiche, J. & Pouyssegur, J., 2011. pH control mechanisms of tumor survival and growth. *Journal of cellular physiology*, 226(2), pp.299–308. Available at: http://www.ncbi.nlm.nih.gov/pubmed/20857482.

Parsons, D.W. et al., 2008. An Integrated Genomic Analysis of Human Glioblastoma Multiforme. *Science*, 321(5897), pp.1807–1812. Available at: http://www.sciencemag.org/cgi/doi/10.1126/science.1164382.

Piskounova, E. et al., 2015. Oxidative stress inhibits distant metastasis by human melanoma cells. *Nature*, 527(7577), pp.186–191. Available at: http://www.nature.com/doifinder/10.1038/nature15726.

Plouin PF, Gimenez-Roqueplo AP, B.X., COMETE, a network for the study and management of hypersecreting adrenal tumors. *Bull Acad Natl Med.*, 192((1)), p.73–82 discussion 83–5.

Pollard, P.J., 2005. Accumulation of Krebs cycle intermediates and over-expression of HIF1 in tumours which result from germline FH and SDH mutations. *Human Molecular Genetics*, 14(15), pp.2231–2239. Available at: http://www.hmg.oxfordjournals.org/cgi/doi/10.1093/hmg/ddi227.

Poschl, E., 2004. Collagen IV is essential for basement membrane stability but dispensable for initiation of its assembly during early development. *Development*, 131(7), pp.1619–1628. Available at: http://dev.biologists.org/cgi/doi/10.1242/dev.01037.

Possemato, R. et al., 2011. Functional genomics reveal that the serine synthesis pathway is essential in breast cancer. *Nature*, 476(7360), pp.346–350. Available at: http://www.nature.com/doifinder/10.1038/nature10350.

Pusch, S. et al., 2014. D-2-Hydroxyglutarate producing neo-enzymatic activity inversely correlates with frequency of the type of isocitrate dehydrogenase 1 mutations found in glioma. *Acta Neuropathologica Communications*, 2(1), p.19. Available at: http://actaneurocomms.biomedcentral.com/articles/10.1186/2051-5960-2-19.

Rajeshkumar, N. V. et al., 2015. Therapeutic Targeting of the Warburg Effect in Pancreatic Cancer Relies on an Absence of p53 Function. *Cancer Research*,

75(16), pp.3355–3364. Available at: http://cancerres.aacrjournals.org/cgi/doi/10.1158/0008-5472.CAN-15-0108.

Ratcliffe, P.J. et al., 1999. The tumor suppressor protein VHL targets hypoxia-inducible factors for oxygen-dependent proteolysis. *Nature*, 399(6733), pp.271–275. Available at: http://www.nature.com/doifinder/10.1038/20459.

Raval, R.R. et al., 2005. Contrasting Properties of Hypoxia-Inducible Factor 1 (HIF-1) and HIF-2 in von Hippel-Lindau-Associated Renal Cell Carcinoma. *Molecular and Cellular Biology*, 25(13), pp.5675–5686. Available at: http://mcb.asm.org/cgi/doi/10.1128/MCB.25.13.5675-5686.2005.

Reitman, Z.J. et al., 2011. Profiling the effects of isocitrate dehydrogenase 1 and 2 mutations on the cellular metabolome. *Proceedings of the National Academy of Sciences*, 108(8), pp.3270–3275. Available at: http://www.pnas.org/cgi/doi/10.1073/pnas.1019393108.

Rendina, A.R. et al., 2013. Mutant IDH1 Enhances the Production of 2-Hydroxyglutarate Due to Its Kinetic Mechanism. *Biochemistry*, 52(26), pp.4563–4577. Available at: http://pubs.acs.org/doi/abs/10.1021/bi400514k.

Ricketts, C. et al., 2008. Germline SDHB Mutations and Familial Renal Cell Carcinoma. *JNCI Journal of the National Cancer Institute*, 100(17), pp.1260–1262. Available at: http://jnci.oxfordjournals.org/cgi/doi/10.1093/jnci/djn254.

Robertson, P. & Fridovich, I., 1982. A reaction of the superoxide radical with tetrapyrroles. *Archives of biochemistry and biophysics*, 213(2), pp.353–7. Available at: http://www.ncbi.nlm.nih.gov/pubmed/6280613.

van Roermund, C.W.T., 1998. Peroxisomal beta -oxidation of polyunsaturated fatty acids in Saccharomyces cerevisiae: isocitrate dehydrogenase provides NADPH for reduction of double bonds at even positions. *The EMBO Journal*, 17(3), pp.677–687. Available at: http://emboj.embopress.org/cgi/doi/10.1093/emboj/17.3.677.

Rohle, D. et al., 2013. An Inhibitor of Mutant IDH1 Delays Growth and Promotes Differentiation of Glioma Cells. *Science*, 340(6132), pp.626–630. Available at: http://www.sciencemag.org/cgi/doi/10.1126/science.1236062.

Rong, Y. et al., 2006. “Pseudopalisading” necrosis in glioblastoma: a familiar morphologic feature that links vascular pathology, hypoxia, and angiogenesis.

Journal of neuropathology and experimental neurology, 65(6), pp.529–39. Available at: http://www.ncbi.nlm.nih.gov/pubmed/16783163.

Roos, D. & Loos, J.A., 1973. Changes in the carbohydrate metabolism of mitogenically stimulated human peripheral lymphocytes. II. Relative importance of glycolysis and oxidative phosphorylation on phytohaemagglutinin stimulation. *Experimental cell research*, 77(1), pp.127–35. Available at: http://www.ncbi.nlm.nih.gov/pubmed/4690164.

S, T. et al., 2012. IDH1 mutation is sufficient to establish the glioma hypermethylator phenotype. *Nature*, 483(7390), pp.479–483. Available at: http://www.nature.com/doifinder/10.1038/nature10866.

Sasaki, M. et al., 2012. D-2-hydroxyglutarate produced by mutant IDH1 perturbs collagen maturation and basement membrane function. *Genes & Development*, 26(18), pp.2038–2049. Available at: http://genesdev.cshlp.org/cgi/doi/10.1101/gad.198200.112.

Sasaki, M. et al., 2012. IDH1(R132H) mutation increases murine haematopoietic progenitors and alters epigenetics. *Nature*, 488(7413), pp.656–659. Available at: http://www.nature.com/doifinder/10.1038/nature11323.

Schimke, R.N., Collins, D.L. & Stolle, C.A., 2010. Paraganglioma, neuroblastoma, and a SDHB mutation: Resolution of a 30-year-old mystery. *American Journal of Medical Genetics Part A*, p.n/a-n/a. Available at: http://doi.wiley.com/10.1002/ajmg.a.33384.

Schodel, J. et al., 2011. High-resolution genome-wide mapping of HIF-binding sites by ChIP-seq. *Blood*, 117(23), pp.e207–e217. Available at: http://www.bloodjournal.org/cgi/doi/10.1182/blood-2010-10-314427.

Schödel, J., Mole, D.R. & Ratcliffe, P.J., 2013. Pan-genomic binding of hypoxia-inducible transcription factors. *Biological Chemistry*, 394(4). Available at: http://www.degruyter.com/view/j/bchm.2013.394.issue-4/hsz-2012-0351/hsz-2012-0351.xml.

Selak, M.A. et al., 2005. Succinate links TCA cycle dysfunction to oncogenesis by inhibiting HIF-α prolyl hydroxylase. *Cancer Cell*, 7(1), pp.77–85. Available at: http://linkinghub.elsevier.com/retrieve/pii/S153561080400368X.

Sellers, K. et al., 2015. Pyruvate carboxylase is critical for non–small-cell lung cancer

proliferation. *Journal of Clinical Investigation*, 125(2), pp.687–698. Available at: http://www.jci.org/articles/view/72873.

Semenza, G.L., 2010. Defining the role of hypoxia-inducible factor 1 in cancer biology and therapeutics. *Oncogene*, 29(5), pp.625–634. Available at: http://www.nature.com/doifinder/10.1038/onc.2009.441.

Semenza, G.L., 2012. Hypoxia-Inducible Factors in Physiology and Medicine. *Cell*, 148(3), pp.399–408. Available at: http://linkinghub.elsevier.com/retrieve/pii/S0092867412000876.

Semenza, G.L. et al., 1996. Hypoxia response elements in the aldolase A, enolase 1, and lactate dehydrogenase A gene promoters contain essential binding sites for hypoxia-inducible factor 1. *The Journal of biological chemistry*, 271(51), pp.32529–37. Available at: http://www.ncbi.nlm.nih.gov/pubmed/8955077.

Shimoda, L.A. et al., 2006. HIF-1 regulates hypoxic induction of NHE1 expression and alkalinization of intracellular pH in pulmonary arterial myocytes. *AJP: Lung Cellular and Molecular Physiology*, 291(5), pp.L941–L949. Available at: http://ajplung.physiology.org/cgi/doi/10.1152/ajplung.00528.2005.

Singleton, R.S. et al., 2014. OGFOD1 catalyzes prolyl hydroxylation of RPS23 and is involved in translation control and stress granule formation. *Proceedings of the National Academy of Sciences*, 111(11), pp.4031–4036. Available at: http://www.pnas.org/cgi/doi/10.1073/pnas.1314482111.

Sinha, K.M. et al., 2010. Regulation of the osteoblast-specific transcription factor Osterix by NO66, a Jumonji family histone demethylase. *The EMBO Journal*, 29(1), pp.68–79. Available at: http://emboj.embopress.org/cgi/doi/10.1038/emboj.2009.332.

Smith, S.A. et al., 1994. Computer Simulations in Magnetic Resonance. An Object-Oriented Programming Approach. *Journal of Magnetic Resonance, Series A*, 106(1), pp.75–105. Available at: http://linkinghub.elsevier.com/retrieve/pii/S1064185884710084.

Son, J. et al., 2013. Glutamine supports pancreatic cancer growth through a KRAS-regulated metabolic pathway. *Nature*, 496(7443), pp.101–105. Available at: http://www.nature.com/doifinder/10.1038/nature12040.

Søndergaard, K.L. et al., 2002. Expression of hypoxia-inducible factor 1alpha in

tumours of patients with glioblastoma. *Neuropathology and applied neurobiology*, 28(3), pp.210–7. Available at: http://www.ncbi.nlm.nih.gov/pubmed/12060345.

Song, B.-L., Javitt, N.B. & DeBose-Boyd, R.A., 2005. Insig-mediated degradation of HMG CoA reductase stimulated by lanosterol, an intermediate in the synthesis of cholesterol. *Cell Metabolism*, 1(3), pp.179–189. Available at: http://linkinghub.elsevier.com/retrieve/pii/S1550413105000288.

Sonveaux, P. et al., 2008. Targeting lactate-fueled respiration selectively kills hypoxic tumor cells in mice. *Journal of Clinical Investigation*. Available at: http://www.jci.org/articles/view/36843.

Sotgia, F. et al., 2011. Understanding the Warburg effect and the prognostic value of stromal caveolin-1 as a marker of a lethal tumor microenvironment. *Breast cancer research : BCR*, 13(4), p.213. Available at: http://www.ncbi.nlm.nih.gov/pubmed/21867571.

Sowter, H.M. et al., 2003. Predominant role of hypoxia-inducible transcription factor (Hif)-1alpha versus Hif-2alpha in regulation of the transcriptional response to hypoxia. *Cancer research*, 63(19), pp.6130–4. Available at: http://www.ncbi.nlm.nih.gov/pubmed/14559790.

Stanek, J. & Koźmiński, W., 2010. Iterative algorithm of discrete Fourier transform for processing randomly sampled NMR data sets. *Journal of Biomolecular NMR*, 47(1), pp.65–77. Available at: http://link.springer.com/10.1007/s10858-010-9411-2.

Sudarshan, S. et al., 2009. Fumarate Hydratase Deficiency in Renal Cancer Induces Glycolytic Addiction and Hypoxia-Inducible Transcription Factor 1 Stabilization by Glucose-Dependent Generation of Reactive Oxygen Species. *Molecular and Cellular Biology*, 29(15), pp.4080–4090. Available at: http://mcb.asm.org/cgi/doi/10.1128/MCB.00483-09.

Sullivan, L.B. et al., 2015. Supporting Aspartate Biosynthesis Is an Essential Function of Respiration in Proliferating Cells. *Cell*, 162(3), pp.552–563. Available at: http://linkinghub.elsevier.com/retrieve/pii/S0092867415008545.

Sullivan, L.B. et al., 2013. The Proto-oncometabolite Fumarate Binds Glutathione to Amplify ROS-Dependent Signaling. *Molecular Cell*, 51(2), pp.236–248. Available at: http://linkinghub.elsevier.com/retrieve/pii/S1097276513003663.

Summons, R.E. et al., 2006. Steroids, triterpenoids and molecular oxygen. *Philosophical Transactions of the Royal Society B: Biological Sciences*, 361(1470), pp.951–968. Available at: http://rstb.royalsocietypublishing.org/cgi/doi/10.1098/rstb.2006.1837.

Švastová, E. et al., 2004. Hypoxia activates the capacity of tumor-associated carbonic anhydrase IX to acidify extracellular pH. *FEBS Letters*, 577(3), pp.439–445. Available at: http://doi.wiley.com/10.1016/j.febslet.2004.10.043.

Svensson, K.J. et al., 2011. Hypoxia triggers a proangiogenic pathway involving cancer cell microvesicles and PAR-2-mediated heparin-binding EGF signaling in endothelial cells. *Proceedings of the National Academy of Sciences*, 108(32), pp.13147–13152. Available at: http://www.pnas.org/cgi/doi/10.1073/pnas.1104261108.

Talks, K.L. et al., 2000. The expression and distribution of the hypoxia-inducible factors HIF-1alpha and HIF-2alpha in normal human tissues, cancers, and tumor-associated macrophages. *The American journal of pathology*, 157(2), pp.411–21. Available at: http://www.ncbi.nlm.nih.gov/pubmed/10934146.

Tarhonskaya, H. et al., 2014. Non-enzymatic chemistry enables 2-hydroxyglutarate-mediated activation of 2-oxoglutarate oxygenases. *Nature Communications*, 5. Available at: http://www.nature.com/doifinder/10.1038/ncomms4423.

Tarpey, P.S. et al., 2013. Frequent mutation of the major cartilage collagen gene COL2A1 in chondrosarcoma. *Nature Genetics*, 45(8), pp.923–926. Available at: http://www.nature.com/doifinder/10.1038/ng.2668.

Tateishi, K. et al., 2015. Extreme Vulnerability of IDH1 Mutant Cancers to NAD+ Depletion. *Cancer Cell*, 28(6), pp.773–784. Available at: http://linkinghub.elsevier.com/retrieve/pii/S1535610815004274.

Tennant, D.A., Durán, R. V. & Gottlieb, E., 2010. Targeting metabolic transformation for cancer therapy. *Nature Reviews Cancer*, 10(4), pp.267–277. Available at: http://www.nature.com/doifinder/10.1038/nrc2817.

Ternette, N. et al., 2013. Inhibition of Mitochondrial Aconitase by Succination in Fumarate Hydratase Deficiency. *Cell Reports*, 3(3), pp.689–700. Available at: http://linkinghub.elsevier.com/retrieve/pii/S2211124713000727.

Tomlinson, I.P.M. et al., 2002. Germline mutations in FH predispose to dominantly

inherited uterine fibroids, skin leiomyomata and papillary renal cell cancer. *Nature Genetics*, 30(4), pp.406–410. Available at: http://www.nature.com/doifinder/10.1038/ng849.

Tönjes, M. et al., 2013. BCAT1 promotes cell proliferation through amino acid catabolism in gliomas carrying wild-type IDH1. *Nature Medicine*, 19(7), pp.901–908. Available at: http://www.nature.com/doifinder/10.1038/nm.3217.

Trueblood, C.E. & Poyton, R.O., 1988. Identification of REO1, a gene involved in negative regulation of COX5b and ANB1 in aerobically grown Saccharomyces cerevisiae. *Genetics*, 120(3), pp.671–80. Available at: http://www.ncbi.nlm.nih.gov/pubmed/2852136.

Tsuneoka, M. et al., 2002. A Novel Myc Target Gene, mina53, That Is Involved in Cell Proliferation. *Journal of Biological Chemistry*, 277(38), pp.35450–35459. Available at: http://www.jbc.org/cgi/doi/10.1074/jbc.M204458200.

Turcan, S. et al., 2012. IDH1 mutation is sufficient to establish the glioma hypermethylator phenotype. *Nature*, 483(7390), pp.479–83. Available at: http://www.ncbi.nlm.nih.gov/pubmed/22343889.

Ullah, M.S., Davies, A.J. & Halestrap, A.P., 2006. The Plasma Membrane Lactate Transporter MCT4, but Not MCT1, Is Up-regulated by Hypoxia through a HIF-1 -dependent Mechanism. *Journal of Biological Chemistry*, 281(14), pp.9030–9037. Available at: http://www.jbc.org/cgi/doi/10.1074/jbc.M511397200.

Vacanti, N.M. et al., 2014. Regulation of substrate utilization by the mitochondrial pyruvate carrier. *Molecular cell*, 56(3), pp.425–35. Available at: http://www.ncbi.nlm.nih.gov/pubmed/25458843.

Vaupel, P., Mayer, A. & Höckel, M., 2004. Tumor Hypoxia and Malignant Progression. In pp. 335–354. Available at: http://linkinghub.elsevier.com/retrieve/pii/S0076687904810231.

Verhaak, R.G.W. et al., 2010. Integrated Genomic Analysis Identifies Clinically Relevant Subtypes of Glioblastoma Characterized by Abnormalities in PDGFRA, IDH1, EGFR, and NF1. *Cancer Cell*, 17(1), pp.98–110. Available at: http://linkinghub.elsevier.com/retrieve/pii/S1535610809004322.

Wakimoto, H. et al., 2014. Targetable Signaling Pathway Mutations Are Associated with Malignant Phenotype in IDH-Mutant Gliomas. *Clinical Cancer Research*,

20(11), pp.2898–2909. Available at: http://clincancerres.aacrjournals.org/cgi/doi/10.1158/1078-0432.CCR-13-3052.

Wang, P. et al., 2015. Oncometabolite D-2-Hydroxyglutarate Inhibits ALKBH DNA Repair Enzymes and Sensitizes IDH Mutant Cells to Alkylating Agents. *Cell Reports*, 13(11), pp.2353–2361. Available at: http://linkinghub.elsevier.com/retrieve/pii/S2211124715013297.

Wang, T., Marquardt, C. & Foker, J., 1976. Aerobic glycolysis during lymphocyte proliferation. *Nature*, 261(5562), pp.702–5. Available at: http://www.ncbi.nlm.nih.gov/pubmed/934318.

Warburg, O., 1925. IRON, THE OXYGEN-CARRIER OF RESPIRATION-FERMENT. *Science (New York, N.Y.)*, 61(1588), pp.575–82. Available at: http://www.ncbi.nlm.nih.gov/pubmed/17837805.

Warburg, O., 1956a. On respiratory impairment in cancer cells. *Science (New York, N.Y.)*, 124(3215), pp.269–70. Available at: http://www.ncbi.nlm.nih.gov/pubmed/13351639.

Warburg, O., 1956b. On the origin of cancer cells. *Science (New York, N.Y.)*, 123(3191), pp.309–14. Available at: http://www.ncbi.nlm.nih.gov/pubmed/13298683.

Ward, P.S. et al., 2010. The Common Feature of Leukemia-Associated IDH1 and IDH2 Mutations Is a Neomorphic Enzyme Activity Converting α-Ketoglutarate to 2-Hydroxyglutarate. *Cancer Cell*, 17(3), pp.225–234. Available at: http://linkinghub.elsevier.com/retrieve/pii/S153561081000036X.

Ward, P.S. et al., 2013. The Potential for Isocitrate Dehydrogenase Mutations to Produce 2-Hydroxyglutarate Depends on Allele Specificity and Subcellular Compartmentalization. *Journal of Biological Chemistry*, 288(6), pp.3804–3815. Available at: http://www.jbc.org/cgi/doi/10.1074/jbc.M112.435495.

Watanabe, T., Nobusawa, S., et al., 2009. IDH1 Mutations Are Early Events in the Development of Astrocytomas and Oligodendrogliomas. *The American Journal of Pathology*, 174(4), pp.1149–1153. Available at: http://linkinghub.elsevier.com/retrieve/pii/S0002944010609741.

Watanabe, T., Vital, A., et al., 2009. Selective acquisition of IDH1 R132C mutations in astrocytomas associated with Li-Fraumeni syndrome. *Acta Neuropathologica*,

117(6), pp.653–656. Available at: http://link.springer.com/10.1007/s00401-009-0528-x.

Waterland, R.A. et al., 1991. The isoforms of yeast cytochrome c oxidase subunit V alter the in vivo kinetic properties of the holoenzyme. *The Journal of biological chemistry*, 266(7), pp.4180–6. Available at: http://www.ncbi.nlm.nih.gov/pubmed/1847916.

Wiesener, M.S., 2002. Widespread, hypoxia-inducible expression of HIF-2alpha in distinct cell populations of different organs. *The FASEB Journal*. Available at: http://www.fasebj.org/cgi/doi/10.1096/fj.02-0445fje.

Williams, S.C. et al., 2011. R132H-mutation of isocitrate dehydrogenase-1 is not sufficient for HIF-1α upregulation in adult glioma. *Acta Neuropathologica*, 121(2), pp.279–281. Available at: http://link.springer.com/10.1007/s00401-010-0790-y.

Wise, D.R. et al., 2011. Hypoxia promotes isocitrate dehydrogenase-dependent carboxylation of -ketoglutarate to citrate to support cell growth and viability. *Proceedings of the National Academy of Sciences*, 108(49), pp.19611–19616. Available at: http://www.pnas.org/cgi/doi/10.1073/pnas.1117773108.

Wise, D.R. et al., 2008. Myc regulates a transcriptional program that stimulates mitochondrial glutaminolysis and leads to glutamine addiction. *Proceedings of the National Academy of Sciences*, 105(48), pp.18782–18787. Available at: http://www.pnas.org/cgi/doi/10.1073/pnas.0810199105.

Wise, D.R. & Thompson, C.B., 2010. Glutamine addiction: a new therapeutic target in cancer. *Trends in Biochemical Sciences*, 35(8), pp.427–433. Available at: http://linkinghub.elsevier.com/retrieve/pii/S0968000410000915.

Wishart, D.S. et al., 2013. HMDB 3.0--The Human Metabolome Database in 2013. *Nucleic Acids Research*, 41(D1), pp.D801–D807. Available at: http://nar.oxfordjournals.org/lookup/doi/10.1093/nar/gks1065.

Wong, C.C.-L. et al., 2012. Inhibitors of hypoxia-inducible factor 1 block breast cancer metastatic niche formation and lung metastasis. *Journal of Molecular Medicine*, 90(7), pp.803–815. Available at: http://link.springer.com/10.1007/s00109-011-0855-y.

Wong, K.M., Hudson, T.J. & McPherson, J.D., 2011. Unraveling the genetics of cancer: genome sequencing and beyond. *Annual review of genomics and*

human genetics, 12, pp.407–30. Available at: http://www.ncbi.nlm.nih.gov/pubmed/21639794.

Xia J et al., 2012. MetaboAnalyst 2.0--a comprehensive server for metabolomic data analysis. *Nucleic Acids Res,* 127-33. Available at: http://doi:10.1093/nar/gks374.

Xiao, M. et al., 2012. Inhibition of -KG-dependent histone and DNA demethylases by fumarate and succinate that are accumulated in mutations of FH and SDH tumor suppressors. *Genes & Development*, 26(12), pp.1326–1338. Available at: http://genesdev.cshlp.org/cgi/doi/10.1101/gad.191056.112.

Xie, H. et al., 2014. Targeting Lactate Dehydrogenase-A Inhibits Tumorigenesis and Tumor Progression in Mouse Models of Lung Cancer and Impacts Tumor-Initiating Cells. *Cell Metabolism*, 19(5), pp.795–809. Available at: http://linkinghub.elsevier.com/retrieve/pii/S1550413114001077.

Xu, W. et al., 2011. Oncometabolite 2-hydroxyglutarate is a competitive inhibitor of α-ketoglutarate-dependent dioxygenases. *Cancer cell*, 19(1), pp.17–30. Available at: http://www.ncbi.nlm.nih.gov/pubmed/21251613.

Xu, X. et al., 2004. Structures of Human Cytosolic NADP-dependent Isocitrate Dehydrogenase Reveal a Novel Self-regulatory Mechanism of Activity. *Journal of Biological Chemistry*, 279(32), pp.33946–33957. Available at: http://www.jbc.org/cgi/doi/10.1074/jbc.M404298200.

Yan, H. et al., 2009. IDH1 and IDH2 Mutations in Gliomas. *New England Journal of Medicine*, 360(8), pp.765–773. Available at: http://www.nejm.org/doi/abs/10.1056/NEJMoa0808710.

Yang, C. et al., 2014. Glutamine oxidation maintains the TCA cycle and cell survival during impaired mitochondrial pyruvate transport. *Molecular cell*, 56(3), pp.414–24. Available at: http://www.ncbi.nlm.nih.gov/pubmed/25458842.

Yang, M., Soga, T. & Pollard, P.J., 2013. Oncometabolites: linking altered metabolism with cancer. *Journal of Clinical Investigation*, 123(9), pp.3652–3658. Available at: http://www.jci.org/articles/view/67228.

Yang, S. et al., 2011. Pancreatic cancers require autophagy for tumor growth. *Genes & development*, 25(7), pp.717–29. Available at: http://www.ncbi.nlm.nih.gov/pubmed/21406549.

Yankovskaya, V., 2003. Architecture of Succinate Dehydrogenase and Reactive

Oxygen Species Generation. *Science*, 299(5607), pp.700–704. Available at: http://www.sciencemag.org/cgi/doi/10.1126/science.1079605.

Yasuda, T. et al., 2013. DJ-1 cooperates with PYCR1 in cell protection against oxidative stress. *Biochemical and Biophysical Research Communications*, 436(2), pp.289–294. Available at: http://linkinghub.elsevier.com/retrieve/pii/S0006291X13009029.

Ye, J. et al., 2014. Serine Catabolism Regulates Mitochondrial Redox Control during Hypoxia. *Cancer Discovery*, 4(12), pp.1406–1417. Available at: http://cancerdiscovery.aacrjournals.org/cgi/doi/10.1158/2159-8290.CD-14-0250.

Yoo, H. et al., 2008. Quantifying reductive carboxylation flux of glutamine to lipid in a brown adipocyte cell line. *The Journal of biological chemistry*, 283(30), pp.20621–7. Available at: http://www.ncbi.nlm.nih.gov/pubmed/18364355.

Yoon, S. et al., 2015. Clinical Implication of Serine Metabolism-Associated Enzymes in Colon Cancer. *Oncology*, 89(6), pp.351–359. Available at: http://www.karger.com/?doi=10.1159/000439571.

Yuan, J., Bennett, B.D. & Rabinowitz, J.D., 2008. Kinetic flux profiling for quantitation of cellular metabolic fluxes. *Nature protocols*, 3(8), pp.1328–40. Available at: http://www.ncbi.nlm.nih.gov/pubmed/18714301.

Zhang, H. et al., 2008. Mitochondrial Autophagy Is an HIF-1-dependent Adaptive Metabolic Response to Hypoxia. *Journal of Biological Chemistry*, 283(16), pp.10892–10903. Available at: http://www.jbc.org/cgi/doi/10.1074/jbc.M800102200.

Zhao, S. et al., 2009. Glioma-Derived Mutations in IDH1 Dominantly Inhibit IDH1 Catalytic Activity and Induce HIF-1. *Science*, 324(5924), pp.261–265. Available at: http://www.sciencemag.org/cgi/doi/10.1126/science.1170944.

Zheng, L. et al., 2015. Fumarate induces redox-dependent senescence by modifying glutathione metabolism. *Nature Communications*, 6, p.6001. Available at: http://www.nature.com/doifinder/10.1038/ncomms7001.

Zheng, L. et al., 2013. Reversed argininosuccinate lyase activity in fumarate hydratase-deficient cancer cells. *Cancer & Metabolism*, 1(1), p.12. Available at: http://cancerandmetabolism.biomedcentral.com/articles/10.1186/2049-3002-1-12.

Zhong, H. et al., 1999. Overexpression of hypoxia-inducible factor 1alpha in common human cancers and their metastases. *Cancer research*, 59(22), pp.5830–5. Available at: http://www.ncbi.nlm.nih.gov/pubmed/10582706.

Zhuang, Q., Feng, T. & Coleman, M.L., 2015. Modifying the maker: Oxygenases target ribosome biology. *Translation*, 3(1), p.e1009331. Available at: http://www.tandfonline.com/doi/full/10.1080/21690731.2015.1009331.

Zogg, C.K., 2014. Phosphoglycerate Dehydrogenase: Potential Therapeutic Target and Putative Metabolic Oncogene. *Journal of Oncology*, 2014, pp.1–13. Available at: http://www.hindawi.com/journals/jo/2014/524101/.